NOTICE

The quality of this microform is heavily dependent upon the quality of the original thesis submitted for microfilming. Every effort has been made to ensure the highest quality of reproduction possible.

If pages are missing, contact the university which granted the degree.

Some pages may have indistinct print especially if the original pages were typed with a poor typewriter ribbon or if the university sent us an inferior photocopy.

Previously copyrighted materials (journal articles, published tests, etc.) are not filmed.

Reproduction in full or in part of this microform is governed by the Canadian Copyright Act, R.S.C. 1970, c. C-30.

AVIS

La qualité de cette microforme dépend grandement de la qualité de la thèse soumise au microfilmage. Nous avons tout fait pour assurer une qualité supérieure de reproduction.

S'il manque des pages, veuillez communiquer avec l'université qui a conféré le grade.

La qualité d'impression de certaines pages peut laisser à désirer, surtout si les pages originales ont été dactylographiées à l'aide d'un ruban usé ou si l'université nous a fait parvenir une photocopie de qualité inférieure.

Les documents qui font déjà l'objet d'un droit d'auteur (articles de revue, tests publiés, etc.) ne sont pas microfilmés.

La reproduction, même partielle, de cette microforme est soumise à la Loi canadienne sur le droit d'auteur, SRC 1970, c. C-30.

Canada

Dynamic Behaviour of Geared Rotor Systems Subjected to Internal and External Excitations

Santosh Neriya

A Thesis

in

The Department

of

Mechanical Engineering

Presented in Partial Fulfillment of the Requirements
for the Degree of Doctor of Philosophy at
Concordia University
Montréal, Québec, Canada

July 1987

ISBN 0-315-41648-3

ABSTRACT

Dynamic Behaviour of Geared Rotor Systems Subjected to Internal and External Excitations

Santosh Neriya, Ph.D.
Concordia University, 1987

The dynamic behaviour of a geared shaft system due to internal and external excitations is studied employing analytical, numerical and experimental methods. Linear time invariant models of geared rotor systems employing spur or helical gears are obtained using lumped mass or finite element discretisation procedures. The torsional-flexural coupling in spur gears and the torsional-flexural-axial- rotational coupling in helical gears are included in the analysis. The excitation to the geared shaft system arising from internal sources such as mass unbalance, geometric eccentricity or a static transmission error composed of deterministic and random components; or external sources such as random support excitations are considered. The behaviour of a spur geared train of rotors is studied including the motion coupling effects of all gear pairs. Modal analysis is used as a solution procedure to obtain the resonant frequencies, mode shapes and dynamic response to the internal and external excitations. The dynamic tooth loads are also computed. The dynamical model of the helical geared shaft system is used along with the mean stress diagram and the maximum energy of distortion theory to obtain the fatigue life of the gear

carrying shafts at critical cross sections. The regions of instability in helical geared rotor systems due to the sinusoidally varying tooth stiffness is determined using Floquet theory. A complex non-linear time varying helical geared shaft system considering the effects of non-symmetric backlash and varying tooth stiffness, subjected to deterministic and filtered white noise inputs is solved numerically using a Matrix Exponenial Technique with piecewise linearisation to obtain the mean and variance of the dynamic response. Numerical solutions were obtained for time periods much larger than the duration for individual gear rotations to confirm stability. Experimental work is carried out on a spur geared rotor system in order to validate the analytical results. The measured dynamic response shows peaks at the system natural frequenices and their gear ratio multiples as predicted analytically. Modal parameters of the system were obtained by modal testing methods and are compared with analytically obtained results.

ACKNOWLEDGEMENTS

The author is sincerely grateful to his thesis supervisor Dr. R.B. Bhat for his excellent guidance, help and encouragement during the course of this work. The guidance and support provided by the thesis co-supervisor Dr. T.S. Sankar is acknowledged with gratitude.

The author wishes to thank Mr. P. Canzano for his help in the experimental work, Ms. Nancy Nicholson and Ms. Lorraine Wibbing for their accurate typing, and Ms. Suzanne LaFontaine for preparing the excellent illustrations. Special thanks are due to Dr. S.K. Arumugam for his suggestions and guidance.

The financial support provided by the department of Mechanical Engineering of Concordia University, and the Natural Sciences and Engineering Research Council of Canada is acknowledged.

Finally, the author is grateful to his parents for their abundant moral support and understanding throughout the course of this investigation.

TABLE OF CONTENTS

LIST OF FIGURES

Figures

Figures

LIST OF TABLES

NOMENCLATURE

a_1, a_2	filter constants
A	cross sectional area of the beam element
C_a	surface factor
C_b	size factor
C_{b1}	flexural damping of the driving shaft
C_{b2}	flexural damping of the driven shaft
C_c	reliability factor
C_d	temperature factor
C_e	modifying factor for stress concentration or notch effect factor
C_f	miscellaneous effects factor
c_M, c_L	lumped torsional damping at the motor and dynamo
$\bar{c}_t$	average flexural damping of the gear tooth
$\bar{c}_{tz}$	average flexural damping of the gear tooth in the z-direction
$\bar{c}_{ty}$	average flexural damping of the gear tooth in the y-direction
$c_{x1}, c_{y1}, c_{\theta 1}, c_{\phi 1}$	lumped damping at the driving gear in the x, y, θ_x, & θ_y directions
$c_{x2}, c_{y2}, c_{\theta 2}, c_{\phi 2}$	lumped damping at the driven gear in the x, y, θ_x & θ_y directions
c_1, c_2	lumped torsional damping at the driving and driven gears
[C]	generalized damping matrix
e(t)	time dependent static transmission error

e_{av}	amplitude of the deterministic component of the static transmission error
$e_p(t)$	periodic component of e(t)
$e_r(t)$	random component of e(t)
f_{BL}	backlash function
f_s	factor of safety
F_n	force transmitted through the gears in the normal direction
F_{axa}	axial force amplitude
F_{axm}	mean axial force
$\{F\}$	generalised force vector
$\{F\}_a$	amplitude of the excitation force
$\{F\}_m$	mean component of the excitation force
$\{F\}_e$	element end forces
$\{F\}_{ea}$	element end forces due to amplitude loads
$\{F\}_{em}$	element end forces due to mean loads
$\{F\}_R$	random support excitation force
G	modulus of rigidity
[G]	gyroscopic matrix
$[H(j\omega)]$	frequency response matrix
I_1	moment of inertia of the driving gear
I_2	moment of inertia of the driven gear
I	moment of inertia of the beam element about the y or z axis
J	polar moment of inertia of the beam element
J_M	moment of inertia of the motor
J_L	moment of inertia of the dynamo
k_{bl}	flexural stiffness of the driving shaft

k_{b2} flexural stiffness of the driven shaft

k_1 torsional stiffness of the driving shaft

k_2 torsional stiffness of the driven shaft

$\bar{k}_t$ average flexural stiffness of the gear tooth

$\bar{k}_{ty}, \bar{k}_{tz}$ average flexural stiffness of the gear tooth in the y and z directions

k_{xx}, k_{yy}, k_{zz} stiffness of the rolling contact bearing in the x, y and z directions

$k_{x1}, k_{y1}, k_{\theta 1}, k_{\phi 1}$ lumped stiffness at the driving gear in the x, y, θ_x and θ_y directions.

$k_{x2}, k_{y2}, k_{\theta 2}, k_{\phi 2}$ lumped stiffness at the driven gear in the x, y, θ_x and θ_y directions.

$k(t)$ time varying tooth stiffness.

k_b geometric stress concentration factor for flexural loading.

k_{ax} geometric stress concentration factor for axial loading.

k_s geometric stress concentration factor for torsional loading.

k_T combined geometric stress concentration factor.

$[K^e]$ element stiffness matrix

$[K]$ global stiffness matrix

ℓ length of the beam element

$\bar{m}$ mass per unit length of the beam element

m_1 mass of the driving gear

m_2 mass of the driven gear

m_{t1} mass of the driving gear tooth

m_{t2} mass of the driven gear tooth

$m_x(t_i)$ mean of the x(t) process at time t_i

M_a moment amplitude

M_m mean moment

$[M]$ generalised mass matrix

$[M_t^e]$ translational mass matrix of an element

$[M_r^e]$ rotatory inertia matrix of an element

n number of gear pairs

N number of degrees of freedom of the system

$\{p_s\}_k$, $\{p_c\}_k$ principal coordinates corresponding to the k^{th} sine and cosine excitations.

P_i pole for the ith mode

P_i^* complex conjugate of P_i

$p_{xx}(t_i)$ covariance matrix of the x(t) process at time t_i

q_b notch sensitivity for flexural loading

q_s notch sensitivity for torsional loading

q_x notch sensitivity for axial loading

$\{q\}$ generalised displacement vector

$\{q\}_a$ rotor displacement vector due to alternating loads

$\{q\}_m$ rotor displacement vector due to mean loads

$\{q_s\}$ support displacement vector

$\{q_r\}$ relative displacement vector

$Q(t)$ intensity of white noise

r_1 base circle radius of the driving gear

r_2 base circle radius of the driven gear

r radius of the beam element

R_f resultant of the fatique strength reducing factors

$S_e(\omega)$ PSD of the random STE

S_{eo} endurance limit for infinite life

S'_{ef} endurance limite for finite life.

S_u ultimate tensile strength

S_y yield strength

$[S_F(\omega)]$ PSD of the random excitation force

$[S_q(\omega)]$ PSD of the response

$[S_{qr}(\omega)]$ matrix of the relative displacement PSD

$[S_{qs}(\omega)]$ matrix of the support displacement PSD

T_M input torque

T_L output torque

T_a alternating torque

T_m mean torque

T temperature, F

U_1, U_2 mass unbalance in the driving and driven gears

$w(t)$ Gaussian white noise with mean zero and strength $Q(t)$

y_1, y_2 flexural displacement in the y-direction for the driving and driven gears

y_{t1}, y_{t2} absolute displacement for the driving and driven gear teeth

z_1, z_2 flexural displacement in the z-direction for the driving and driven gears

β helix angle

$[\gamma]$ diagonal damping matrix

δ_n displacement of the gear tooth in the normal direction

$\varepsilon(t)$ static transmission error

$\varepsilon_1, \varepsilon_2$ geometrical eccentricity of the driving and driven gears

ε_{av} amplitude of the deterministic component of the static transmission error

$\varepsilon_d(t)$ deterministic component of the static transmission error.

$\varepsilon_r(t)$ random component of the static transmission error

θ_1, θ_2 rotational angle for the driving and driven gears

θ_{f1}, θ_{f2} angle between the directions of unbalance and eccentricity for the driving and driven gears

θ_M, θ_L rotational angle of the motor and dynamo

$\phi(t_{i+1}, t_i)$ state transition matrix for the internal t_i to t_{i+1}

ϕ_1, ϕ_2 rotational angle (about a gear diameter) for the driving and driven gears.

$\Phi_{\Delta F}(\omega)$ PSD of the dynamic tooth load

$[\kappa]$ diagonal stiffness matrix

λ_i ith eigenvalue

$[\mu]$ diagonal mass matrix

$\{\rho\}$ ith left eigen vector

σ_a basic alternating stress

σ_m basic mean stress

σ_{af} failure value of the alternating stress

σ_{mf} failure value of the mean stress

σ_e reduced endurance limit

$\{\sigma(t)\}$ normalized force vector

$\{\phi_i\}$ i-th right eigenvector

$[\phi]$ modal matrix formed by concatenating all $\{\phi_i\}$

$[\phi^*]$ matrix formed by concatenating all $\{\phi_i\}^*$

$\{\mathcal{F}\}$ generalised force vector

CHAPTER 1

INTRODUCTION AND LITERATURE REVIEW

1.1 GENERAL OBJECTIVES

Gear transmission is used in most of the industrial machinery to transmit power between shafts, to change speeds, change directions of motion etc. Typical uses of gear drives are in heavy-lift helicopters, industrial speed reducers, naval propulsion systems, and heavy, off-road equipment.

For the satisfactory operation of geared shaft systems, they must be designed so that the stresses in the shaft and teeth are within safe limits from the point of view of strength and fatigue. Hence, it is important to analyse and understand the complete dynamic behaviour of geared shaft systems. Further, the noise generated by the operation of geared system has been a source of concern to engineers for a long time. These high noise levels generated can cause health problems such as hearing damage in helicopter pilots [1]. The high noise levels in the lower frequency range indicate high stress levels of the components and hence, noisy gearboxes give an early indication of the impending mechanical failure [2].

Since the dynamic response of the shafts in a gearbox

is directly related to the noise generated, an accurate prediction of the dynamic response of geared rotor system becomes necessary. The actual stiffness of gear teeth is known to vary as much as 50 percent during the engagement cycle [3]. This introduces time varying stiffness coefficients, resulting in what is classically known as a Mathieu problem. Instabilities can occur as a consequence of the time varying nature of the gear mesh. Backlash between gear teeth is unavoidable in gear transmission since it is also necessary for lubricating the tooth surface and preventing teeth from getting jammed. However, backlash also results in additonal dynamic force, reduced stability, and excessive noise and vibration. The effects of backlash and time varying stiffness of the gear mesh have to be considered in the analysis of the geared rotor system.

In a gear mesh, the transmission of load from one gear to another takes place along the line of contact and there exists a coupling between the motions of the driving and driven shafts of the geared rotor system. This is known as force coupling, where the motions of one rotor produces forces in another rotor due to the presence of the gear mesh. In spur gears, there exists a coupling between the torsional and flexural motions. In a helical gear, there exists a coupling between the torsional, flexural, axial and rotational (about a gear diameter) motions. Inclusion of the coupling results in a more accurate prediction of the dynamic

response.

The excitation to the geared shaft system can come from internal and external sources. The internal sources of excitation are due to a static transmission error and unbalance in gears. The external source of excitation is through the bearing supports.

The static transmission error encompasses all the effects such as eccentric mounting, errors of manufacture, elastic deformation etc. This static transmission error could be expressed as a sum of periodic and random components. The periodic component is primarily at the frequency of tooth mesh, while the random component can be modelled as a second order Markov process which is obtained by passing a white noise through a second order linear shaping filter [16]. External excitations in the form of support excitations can be modelled as an output of a first or second order linear filter, the input to which is a Gaussian white noise.

The dynamic model of the geared rotor system must consider all the effects such as inertial effects of all components, coupling between different types of motion, tooth stiffness variation, tooth backlash, system damping etc. The system can be modelled as either a continuous system, or a system with lumped mass and springs and analyzed using

transfer matrix approach or finite element techniques. Linear equations of motion are solved by Modal analysis techniques and the numerical approach is used for a non-linear time varying model.

The state of the art in the design of geared rotors considers the torsional and flexural motions independent of each other. A simple form of static transmission error such as a sinusoidal form representing the fundamental component of the error only is considered in the design until now. Such a model is used to study the dynamic behaviour, fatigue properties and stability problems. However, in an actual geared rotor system motions in different directions are coupled due to the presence of the meshing gears with variable mesh stiffness and a complex form of backlash. Random support excitations in geared rotors has not received any attention. Hence, the objectives of the present investigation are to formulate a comprehensive model for a geared rotor system including the coupling effects between torsional, flexural, axial and rotational motions, to incorporate better models for the static transmission error considering its random nature, to study the behaviour of the system subjected to random support excitations, to study the fatigue behaviour of the gear carrying shafts and to study the stability of the system using the improved model, and finally to experimentally verify some of the theoretical predictions.

1.2 Literature Review

A review of the literature relevant to the present study is presented below.

1.2.1 Gear Dynamics

Dynamic gear tooth loads resulting from power transmission through the gear mesh are studied by several investigators. The earliest among them, Lewis [4] and Buckhingham [5] were primarily concerned with the strength of the gear teeth in order to ensure that they do not fail during operation.

Tuplin [6-7] and Reswick [8] discussed the effect of profile errors on the dynamic load. The error was modelled as a wedge introduced between two perfectly mating teeth. Johnson and Bishop [9] considered incorrect mounting as a source of error. Johnson [10] showed that with a fully-loaded precision gear, the elastic deformation was considerably greater than likely inaccuracies of manufacture.

Modal analysis methods were used by Mahalingam and Bishop [11] to determine the dynamic load of a geared shaft system when excited by a static transmission error, which encompassess all the effects such as eccentric mounting, errors of manufacture and elastic deformation. Cornell et al

[12] determined the dynamic tooth load for high contact ratio spur gears, having varying tooth pair stiffnesses using numerical techniques with piecewise linearization. Mark [13, 14] derived expressions for the mean and random components of the static transmission error. Here, the mean component had contribution due to elastic tooth deformation and intentional tooth surface modifications and the "random" component was due to machining errors. He also showed that the harmonic components of the static transmission error, occurring at the tooth meshing frequency and its integral multiples, are due to elastic tooth deformations and intentional tooth surface modifications while the harmonic components that occur at the gear rotational frequency and its integral multiples are due to machining errors. Remmers [15] described an analytical method for assessing the influence of tooth spacing errors, load, design contact ratio and profile modifications on vibration, noise and dynamic tooth loads.

The random component of the static transmission error modelled by a second order Markov process by Tobe et al. [16, 17], was obtained by passing a white noise through a second order linear filter. He varied the constants of the filter to fit the experimentally obtained autocorrelation function. A single degree of freedom model of the geared shaft system was considered. The Fokker-Planck Equation was used to solve the equations of motion of the system including

the filter to obtain the mean and variance of the dynamic loads. The effects of backlash and impact on dynamic loads was studied extensively by Wang [18, 19]. A simple 2 degree of freedom (2 DOF) model was used for the analysis. Dubowsky [20] studied the dynamic forces of one dimensional systems with clearances. Azar and Crossley [21] used this analysis to study a gear pair including the effects of impact, backlash, inertial effects of the gears and stiffness variation. A rotary model was developed by Wang [22], as opposed to the rectilinear model of Azar and Crossley, to study dynamic loads including effects of backlash, time varying stiffness and damping in the gear teeth. Nakada [23], Harris [24], Attia [25], Gregory et al [26], Utagawa et al [27], Ichimam and Hirano [28] and Kasuba and Evans [29] determined the dynamic loads due to a periodic excitation, including the effects of varying tooth stiffness. Tobe [30] also studied dynamic loads in gear teeth due to impact.

1.2.2 Dynamics of Rotors

Most of the literature cited in 1.2.1 discuss methods of accurately modelling the gear mesh. The rotor carrying the gears is at best, modelled as a massless torsional spring supported on rigid bearings and having only torsional degrees of freedom. However, in reality the rotor shaft is a continuous system with distributed mass and elasticity and is capable of vibration in all possible directions.

The shaft rotational speed coinciding with any one of its natural frequencies is termed as the critial speed of the rotor and the shaft dynamic response at these speeds is of concern. Rotors are essentially continuous systems and in simple cases they can be analysed as such. Complex rotors can be analysed by considering equivalent discrete models of systems, such as lumped parameter model and finite element model. There are different methods of analysis used to study these systems such as Direct Method, a Transfer matrix method and Modal analysis.

One of the earlier works on the prediction of critical speeds of rotors introducing a simple model was by Jeffcott [31]. In his work, the rotor system was modelled as a single mass mounted on a shaft supported on identical bearings and the resulting equations of motion were solved by the Direct method. Prohl [32] extended this method to calculate the critical speeds in flexible rotors based on a technique developed by Myklestad [33] to calculate the torsional natural frequencies of an airplane wing. Bishop and Gladwell [34] studied the behaviour of simple rotors using a lumped mass model. This rotor model was improved by Green [35] to include the gyroscopic effects on the critical speed. Eshleman and Eubanks [36] studied the effect of shaft phenomena such as axial torque, gyroscopic moments and transverse shear on critical speeds of rotor systems. Their work was basically an extension of the analysis carried out by Tondl [37]. The earliest work using tranfer matrix method

on rotor system was carried out by Myklestad [38]. He used the cantilever beam theory in his approach to formulate the point and field transfer matrices. The critical speeds and unbalance response were then determined. Modal analysis is another solution procedure which is widely used by several investigators to study the behaviour of rotor systems. Gunter et al [38] used the planar modes of the undamped rotor systems ignoring the effects of disk gyroscopics and bearing properties.

Finite element techniques are convenient to model complex rotor systems consisting of several disks. Ruhl [39] and Ruhl and Booker [40] as well as Nelson and McVaugh [41] used finite element methods to evaluate the dynamic characteristics of rotors. In their approach, the rotor was discretised into rigid disk elements, shaft elements and bearing elements. The resulting equations were solved using the Direct method. Subsequent studies by Zorzi and Nelson [42], Nelson [43] and Zorzi and Nelson [44], included the effects of internal damping, axial torque, hysteresis damping etc. in the finite element model of the rotor system.

In geared rotor system, the effect of the gear mesh also must be incorporated in the study. The critical speeds and modes of geared rotors was studied by Johnson [45], who considered a torsional model of the rotor having elastic gear teeth. Porter [46] obtained the critical speeds of torsional oscillation due to a displacement excitation. Sankar [47]

analysed the torsional vibration of branched systems like geared shaft systems using extended transfer matrix method. Mitchell [48] coupled the rotors using a modified Hibner-type transfer matrix, developed by a transfer matrix march from one gear tooth base to the other across the gear mesh.

As a part of the design procedure for a geared rotor system it is common practice to calculate the torsional critical speeds of the composite gear train and, in addition, the lateral critical speeds of the individual rotors. In this way the effect of coupling between torsional and flexural vibrations is ignored. Johnson [45] and Seireg [49] observed a change in the critical speeds and mode shapes of the rotors due to the presence of the gears. Mitchell [50] observed experimentally that the high speed branch of a gear coupled rotor system experienced large lateral vibrations at a subharmonic frequency equivalent to the low speed branch of the system. This was found to be due to torsional-lateral coupling. Lund [51] considered the force coupled vibration in a geared train of rotors. He carried out the rotor analysis for torsional and lateral vibrations separately and coupled them through impedance matching at the gear meshes. Also, he obtained the dynamic response and studied the stability of the system.

Daws [52] discussed the two forms of coupling of the torsional and flexural motions in geared shaft systems, 1)

force coupling, which Lund [51] considered in his analysis and 2) dynamic coupling. The predomimant form is the force coupling. This is due to lateral mesh forces generated by torsional oscillations of the shaft and is of order of the geometric eccentricity, ε. He showed that the dynamic coupling terms are of the order ε^2 and are due to the angular acceleration of the gears and found that the effect of coupling is significant at higher frequencies. Iida et al. [54] studied a spur geared system and calculated the response due to mass unbalance and geometric eccentricity. The geared shaft system was described as a 4 DOF lumped mass model where the driven shaft was considered flexible in bending and the driving shaft was considered rigid. The gear tooth was also considered rigid. Iwatsubo et al. [55] discussed the coupled lateral torsional vibration of a geared shaft system and obtained the response due to unbalance by the transfer matrix method. Iida and Tamura [56] also discussed the torsional-flexural coupling in spur gear systems. Iwatsubo [57] studied torsional- flexural coupling in a geared shaft system. The variation in the tooth stiffness was considered and the stability regions were obtained. The response to tooth profile correction is also obtained. Hamad and Seireg [58] obtained the whirl response of pinion gear systems on oil film bearings using phase-plane simulation. Wang [59] carried out the torsional linear and non linear transient analysis of complex gear train systems. The time varying tooth stiffness and backlash were considered and state space

techniques were used to solve the equations of motion.

Helical gears are often used in industrial applications. There exists a force coupling between the torsional, flexural, axial and rotational (about a gear diameter) motions of the helical gear pair. Kacukay [60] used a 8 DOF lumped mass model to study a pair of helical gears and obtained the response and dynamic tooth loads. Kiyono et al. [61] also studied a pair of helical gears and showed that the torsional vibration is the most important component. Kiyono et al. [62] also carried out an experimental investigation of their analysis in [61].

The stability of geared rotor systems has also recieved considerable attention in literature. A gear mesh has stiffness varying with time and this periodic variation is the source of instability in the system. Bolotin [63] studied the stability characteristics of a second order differential equation subjected to parametric excitation. This results in a Mathieu-Hill type equation which is solved to obtain the regions of instability. He showed that two solutions of identical periods bound the region of instability, and two solutions of different periods bound the region of stability. Benton and Seireg [64] used the analysis of Bolotin to study the stability of a single degree of freedom pinion gear system, when the variation of the mesh stiffness is a square wave form. The possible effects of

mesh stiffness variation on a two stage gear drive are examined by Tordion and Gauvin [65]. The instability regions of the two-stage gear drive are discussed. The width of the primary regions of instability are shown to be minimum for zero or 180^0 relative phase angles corresponding to a mesh cycle. Benton and Seireg [66] studied the effect of external excitations, system inertia, variation in mesh stiffness, contact ratio and damping in the mesh on the instability behaviour of multiple reduction geared systems. Iwatsubo [57] studied the stability of a four degree of freedom geared shaft system. A square wave variation was assumed and the equations were put in the state space form. The analysis of Bolotin [63] was used to obtain the boundaries of the stable and unstable regions. When the system equations are expressed in state space form its stability may be determined following an approach advanced by Hsu [67, 68]. He stated that the system is asymptotically stable if all the eigenvalues of the overall state transition matrix for the system (also called the Growth Matrix) have absolute values less than unity.

As discussed earlier, the sources of excitation originate from internal sources such as a static transmission error interposed between two mating teeth. This has been discussed in literature on dynamic response of geared rotors. However, the geared rotor may be subjected to external forces of excitation such as that from the supports, for instance

when on board various types of vehicles. If the support exciations are random in nature with constant power distributed over a frequency range, and one of the system natural frequencies of the geared rotor is within this range, the resulting response may be of concern. Lund [69] carried out the response spectral density analysis of rotor systems due to stationary random excitations of the base, considering excitations only in the vertical direction. Tessarzik et al. [70] analysed the turbo-rotor responses due to external random vibrations. The rotor-bearing system was treated as a linear, three mass model and the numerical results of amplitude power spectral density were obtained for the case when the vibrations were applied along the rotor axis, were found to agree with those obtained experimentally. Subbiah et al. [71] obtained the amplitude Power Spectral Density (PSD) of a simple rotor subjected to random support excitations using modal analysis methods. The excitations were assumed to be stationary and Gaussian with a white noise type of PSD.

State-space techniques can be used in the prediction of dynamic response of structures. The Matrix Exponential Technique was used by Bahar [72] to obtain the dynamic response of structures when excited by deterministic sources. He found the method was stable and accurate and it compared well with the Wilson method [73]. The Wilson method is based on introducing a simple relationship between displacement,

velocity and acceleration which may be assumed to be valid for a short increment of time, which is then used to convert simultaneous differential equations of motion into simultaneous algebraic equations. Maybeck [74] obtained expressions for the mean and variance of a system subjected to deterministic and filtered white noise inputs. Since, the static transmission error could be modelled as having deterministic and filtered white noise components, the analysis of Maybeck [74] could prove useful.

1.2.3 Fatigue Design of a Geared Rotor

The fatigue life of gear-carrying shafts are important in the design of transmission systems. Bagci [75] in his state of the art review article describes the rapid progress in the fatigue design of machine elements in the recent years. The stresses at critical sections where the failure is most likely to occur, are not obtained accurately, leading to an inaccurate fatigue design as shown in a recent study by Bagci [76]. This is because the inertial effects of the different elements in the system are ignored in determining the displacements. The damping is also neglected. The external force acting on the geared rotor system are taken as constant values. The effects of static transmission error and torsional-flexural-axial-rotational coupling that exists in helical gears are ignored.

1.2.4 Experimental work on a Geared Rotor System

Compared to the several analytical studies reported for geared rotor systems in literature, only a few experimental investigations are reported. Seireg [49] studied the effect of gear constraint on the whirl of a simply supported pinion shaft with or without overhung masses. Mitchell [50] carried out an experimental investigation of torsional-flexural coupling in spur geared rotor systems and emphasized the need for considering torsional-flexural coupling in the response calculations in geared rotor systems. Kiyono et al. [62] carried out an experimental investigation of vibration in helical gears and found that the torsional component is the most important from the vibration point of view. Iida et al. [54] obtained the dynamic response in a spur geared rotor system due to unbalance and geometric eccentricity. Kacukay [60] also obtained the dynamic response of a helical geared shaft system.

Recent developments in the measurement techniques and computing technology have led to modal testing methods for system identification. The modal testing of a structure is carried out by measuring the modal parameters such as natural frequencies, mode shapes, damping ratio, through experiments and using them in a different mathematical model called "modal model". This method provides a reliable

means of obtaining realistic physical parameters of the structure. Klosterman [77] identified the modal parameters of stationary beam structures. For the present work, a comparative study between the analytically obtained natural frequencies of the system and those obtained by modal testing procedures is carried out.

1.3 Scope of the Present Investigation

The objectives of the present investigation are:

i) To study the torsional-flexural coupling in spur geared rotor systems and also the torsional-flexural-axial-rotational coupling in helical geared rotor systems.

ii) To obtain the dynamic response of a spur and helical geared rotor system to internal excitations such as unbalance, geometric eccentricity or static transmission error. The effect of deterministic and random components of the static transmission error on the response are investigated. The effect of external excitations such as random support excitations is also determined.

iii) To obtain the fatigue life of gear carrying shafts.

iv) To study the stability of a helical geared shaft system.

v) To conduct modal testing of the geared shaft system and compare the system natural frequencies

with those obtained from the analytical studies.

In Chapter 2, the dynamic response of a spur geared shaft system employing one or more pairs of gears is presented. Lumped mass and finite element models are used in the analysis. The gear mesh effects include the effects of torsional-flexural coupling but ignore effects such as time variation in tooth stiffness and backlash in order to carry out a linear analysis to obtain the natural frequencies and mode shapes of the geared rotor system. Normal mode analysis is used to obtain the response to internal and external excitations. The sources of internal excitations are in the form of mass unbalance and geometric eccentricity or in the form of static transmission error. The static transmission error could be described in terms of deterministic and random components. The external excitations are in the form of random support excitations.

Chapter 3, presents the analysis of a helical geared shaft system and its dynamic response. For a helical gear mesh, the torsional, flexural, axial and rotational (about a gear diameter) motions are coupled. The effects of this coupling are considered in the linear model, ignoring effects such as time variation in tooth stiffness and backlash. Normal mode analysis is used to obtain the response to internal excitations in the form of a deterministic static transmission error and external random support excitations.

In Chapter 4, the fatigue design of power transmission shafts using helical gears is carried out. The dynamic model of the helical geared shaft system obtained in Chapter 3 is used to obtain the stresses at critical sections on the gear carrying shafts. The inertial effects, damping in the system and time variation in forces acting on the system, torsional-flexural-axial-rotational coupling, all previously ignored, are considered in this study. The stresses are used in evaluating the fatigue life of the critical component.

In Chapter 5, a complex helical geared shaft system is studied. The effect of torsional-flexural-axial-rotational coupling is considered as well as the effect of backlash and time varying tooth stiffness. The excitation to the geared shaft system in the form of a static transmission error is considered. The static transmisssion error is composed of two components, a deterministic component at the tooth mesh frequency and random component in the form of a filtered white noise. The filtered white noise is obtained by passing a Gaussian white noise through a linear filter. The resulting equations of motion are put in a state-space form and are solved using a Matrix Exponential Technique with piecewise linearisation.

In Chapter 6, the stability of a helical geared shaft system is studied. The tooth stiffness is considered to be made up of a mean value along with a sinusoidal variation at

the tooth mesh frequency. The effect of torsional- flexural-axial-rotational coupling is considered. The instability regions for different magnitudes of variation in tooth stiffness and damping in the system are presented.

In Chapter 7, results of experiments carried out on a spur geared rotor system are given. Firstly, the analytical response obtained from the model of Chapter 2 is compared with the measured response. The natural frequencies and the phenomena of doubling in resonant frequencies is verified. The Structural Analysis system consisting of a micro-computer with a Modal Analysis package and a FFT analyser are used to compare the system properties with those obtained from the analytical studies.

The results of the work achieved in all the chapters discussed so far are summarized in Chapter 8. Also, a discussion of the results is presented along with the recommendations for future work.

In the next Chapter, the linear response analysis of a spur geared rotor system is discussed.

CHAPTER 2

LINEAR RESPONSE ANALYSIS OF A SPUR GEARED ROTOR SYSTEM

2.1 Introduction

Spur gears are one of the most basic and widely used forms of gearing in modern technology. Noise and vibration are serious problems in power transmission systems using spur gearing, and therefore an understanding of their dynamical behaviour is very important. In this chapter, linearized equations of motion of a spur geared rotor system is analysed.

A basic spur geared shaft system can be considered as a motor driving a load through a pair of gears. The gears are mounted on flexible shafts which are supported by flexible pedestals. As a part of the design procedure for a geared rotor system, it is essential to calculate the critical speeds and predict the dynamic response due to internal or external excitations. The stress and fatigue life are then computed from the dynamic response.

In a geared rotor system, the standard design procedure is to calculate the torsional critical speeds of the composite gear train and, in addition, the bending critical speeds of the individual rotors. The assumption here is that the presence of the gear mesh would not couple the two

phenomena. This assumption however, leads to erroneous results as discussed in [51]. In a gear mesh, the torsional and flexural motions are coupled in two distinct forms i) "force coupling" and ii) "dynamic coupling". The predominant form is the "force coupling". This is due to the lateral mesh forces generated by torsional oscillations of the shaft and is of the order of the geometric eccentricity, ε. The second form of coupling is the "dynamic coupling" which occurs due to the angular acceleration of the gears. Dynamic coupling terms are of the order $\dot{\varepsilon}^2$ [52] and are therefore neglected in the present analysis.

The rotor system carrying the gears can be analysed using a lumped mass model, a finite element model or transfer matrix method. In this chapter, the rotor system is analysed using a lumped mass model and a finite element model.

The excitations coming to a geared shaft system may be from internal sources such as fluctuating torques, eccentric mounting of the gears, variation of tooth stiffness during engagement, changes in tooth profile due to elastic distortion under load and errors of manufacture. The effects of eccentric mounting, errors of manufacture, elastic deformation etc. are often lumped into a "static transmission error" [11]. External excitations are in the form of support excitations.

The stiffness of the meshing teeth varies in a periodic manner and affects both the presence and severity of gear system resonances and instabilities. Another contributing factor in the vibrations of gear systems is the tooth backlash. The tooth backlash function is non-linear because no torque is transmitted between the gears when there is loss of contact between the mating teeth. Inclusion of the time varying mesh stiffness and the tooth backlash, of course, describes the system behaviour more accurately and will be considered in chapter 5. A simple linear analysis is resorted to in this chapter in order to study the effect of torsional-flexural coupling and to determine the natural frequencies and mode shapes of the rotor. Modal analysis is used to obtain the system response in terms of the undamped normal modes of the system.

2.2 Sources of Deterministic and Random Internal Excitations

A pair of meshing gears with rigid, perfect, uniformly spaced involute teeth would transmit exactly uniform angular motion. However, when a pair of meshing rotating gears is transmitting torque, the teeth deform elastically, giving rise to a fluctuating component in the relative angular motion of the two gears. This fluctuating component is caused by the periodic variation in the stiffness of the gear mesh that is attributable to i) the periodic variation in the

numbers of teeth in contact (called contact ratio) and ii) the variation in the stiffness of the individual tooth pairs as the location of their mutual points of contact change during rotation. Furthermore, the tooth faces of real gears are designed to deviate slightly from perfect involute surfaces by providing relief at the tip and root in order to avoid high local stresses on contact. They also contain machining errors that may vary from tooth to tooth. The intentional tooth-face modifications, machining errors, wear and tooth deformations all contribute to the deviation from exact uniform relative angular motion of pairs of meshing rotating gears. The composite effect of the above contributions is described by the static transmission error [11] which may be defined as the deviation $\delta\theta$ from the angular position θ of a gear. Static transmission error of the gear is measured as a function of the angular position of the gear it meshes with, when the gear pair is transmitting a constant torque at low enough speed so that inertial effects are negligible. It is now generally recognised that the static transmission error describes the principal source of vibratory excitation of gear systems.

When a gear system is in operation at normal speed, the static transmission error of each pair of its meshing gears causes a fluctuating component in the total force transmitted between the meshing teeth (in a direction normal to the tooth surfaces). This is transmitted through the

support bearings to the gear casings, which in turn vibrates and radiates sound. Mark [13] obtained a general expression for the static transmission error and decomposed it into components attributable to elastic tooth deformations and to deviations of tooth faces from perfect involute surfaces with uniform lead and spacing. The component due to tooth face deviations is further decomposed into appropriately defined mean and random components. The harmonic components of the static transmission error that occur at integral multiples of the tooth-meshing frequency are shown to be caused by deviation of tooth faces from perfect involute surfaces and elastic tooth deformations. Harmonic components that occur at multiples of gear rotation frequencies are shown to be caused by the random components of the tooth face deviations such as machining errors.

2.3 Torsional-Flexural "Force" Coupling

As explained in Section 2.1, there exists a "force coupling" between the torsional and flexural motions in a geared shaft system. The term "coupling", means a dependence of one system motion variable on another. Thus torsional-flexural coupling means that lateral mesh forces are generated by torsional oscillation of the shaft and vice versa. Fig. 2.1 [54] shows that inclusion of this coupling makes a significant difference in the magnitude of the system natural

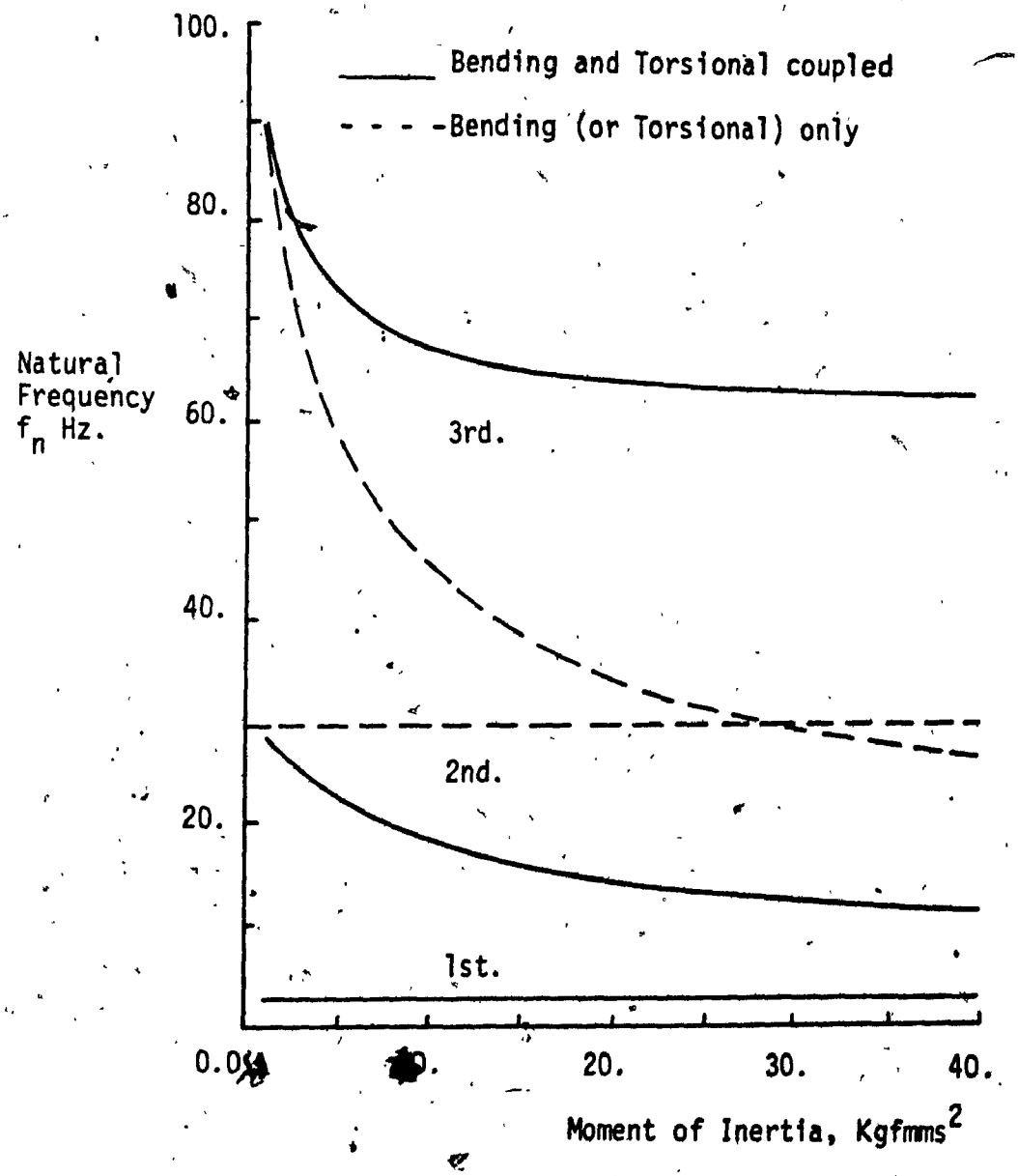

Fig. 2.1 Effect of Torsional-Flexural Coupling on the Natural Frequencies. [54]

frequencies. This will also result in a change in mode shapes, dynamic response, stress and fatigue life. Lund [51] considered such coupling in the torsional-flexural vibrations in a geared system of rotors. Here both forced vibrations caused by mesh errors and/or by mass unbalance, and free damped vibrations whose complex eigen frequencies define the damped critical speeds and stability of the rotor system are considered. Iida et al [54] studied a simple geared system including coupling in the torsional-flexural vibration and calculated the response due to mass unbalance and geometric eccentricity in the gears. In their model, they considered only the driven shaft to be flexible in bending and the driving shaft to be rigid. The flexibility of the gear teeth was also not considered in the analysis.

2.4 Lumped Mass Mathematical Model

2.4.1 Analysis

A schematic representation of a simple geared shaft system is shown in Fig. 2.2. It shows a motor of moment of inertia J_M driving a dynamo of moment of inertia J_L through gears of moment of inertia I_1 and I_2. The driving and driven gears and their relative positions are shown in Fig. 2.3. An equivalent spring mass representation for the same is shown in Fig. 2.4. The gear teeth have involute faces and $\bar{k}_t$ represents the time average tooth stiffness.

Assuming that the shafts are massless, the equations of motion for the system can be written as:

$$m_1\ddot{z}_1 + c_{b_1}\dot{z}_1 + k_{b_1}z_1 = U_1\dot{\theta}_1^2 \cos(\theta_1 + \theta_{f_1}) \tag{2.1}$$

$$m_2\ddot{z}_2 + c_{b_2}\dot{z}_2 + k_{b_2}z_2 = U_2\dot{\theta}_2^2 \cos(\theta_2 + \theta_{f_2}) \tag{2.2}$$

$$\begin{aligned} &m_1\ddot{y}_1 + c_{b_1}\dot{y}_1 + k_{b_1}y_1 \\ &\quad + \bar{c}_t(\dot{y}_1 + \varepsilon_1\omega_1 \cos\theta_1 + r_1\dot{\theta}_1 - \dot{y}_{t_1}) \\ &\quad + \bar{k}_t(y_1 + \varepsilon_1 \sin\theta_1 + r_1\theta_1 - y_{t_1}) \\ &\quad = U_1\dot{\theta}_1^2 \sin(\theta_1 + \theta_{f_1}) \end{aligned} \tag{2.3}$$

$$\begin{aligned} &m_2\ddot{y}_2 + c_{b_2}\dot{y}_2 + k_{b_2}y_2 \\ &\quad + \bar{c}_t(\dot{y}_2 + \varepsilon_2\omega_2 \cos\theta_2 + r_2\dot{\theta}_2 - \dot{y}_{t_2}) \\ &\quad + \bar{k}_t(y_2 + \varepsilon_2 \sin\theta_2 + r_2\theta_2 - y_{t_2}) \\ &\quad = U_2\dot{\theta}_2^2 \sin(\theta_2 + \theta_{f_2}) \end{aligned} \tag{2.4}$$

$$\begin{aligned} &m_{t_1}\ddot{y}_{t_1} + \bar{c}_t(\dot{y}_{t_1} - \dot{y}_1 - \varepsilon_1\omega_1 \cos\theta_1 - r_1\dot{\theta}_1) \\ &\quad + \bar{k}_t(y_{t_1} - y_1 - \varepsilon_1 \sin\theta_1 - r_1\theta_1) = -F \end{aligned} \tag{2.5}$$

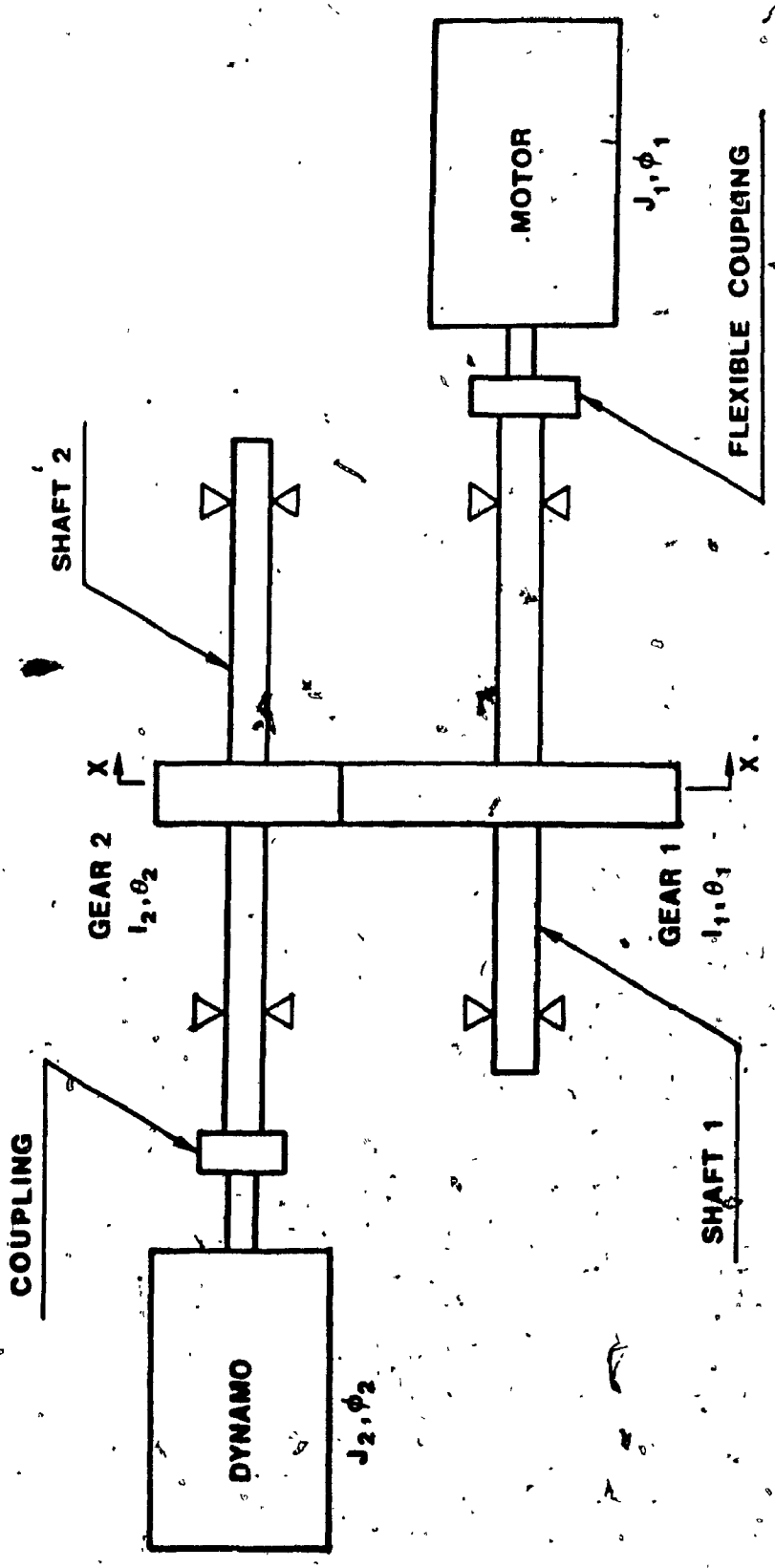

Fig. 2.2 Simple Geared Shaft System

O_1 geometric center of the driving gear

O_1' geometric center of the driven gear

O_2 center of the driving shaft when it is rotating

O_2' center of the driven shaft when it is rotating

O_3 center of the driving shaft when it is stationary

O_3' center of the driven shaft when it is stationary

ϕ pressure angle

O_2O_1 Geometric ectentricity ε_1

$O_2'O_1'$ Geometric eccentricity ε_2

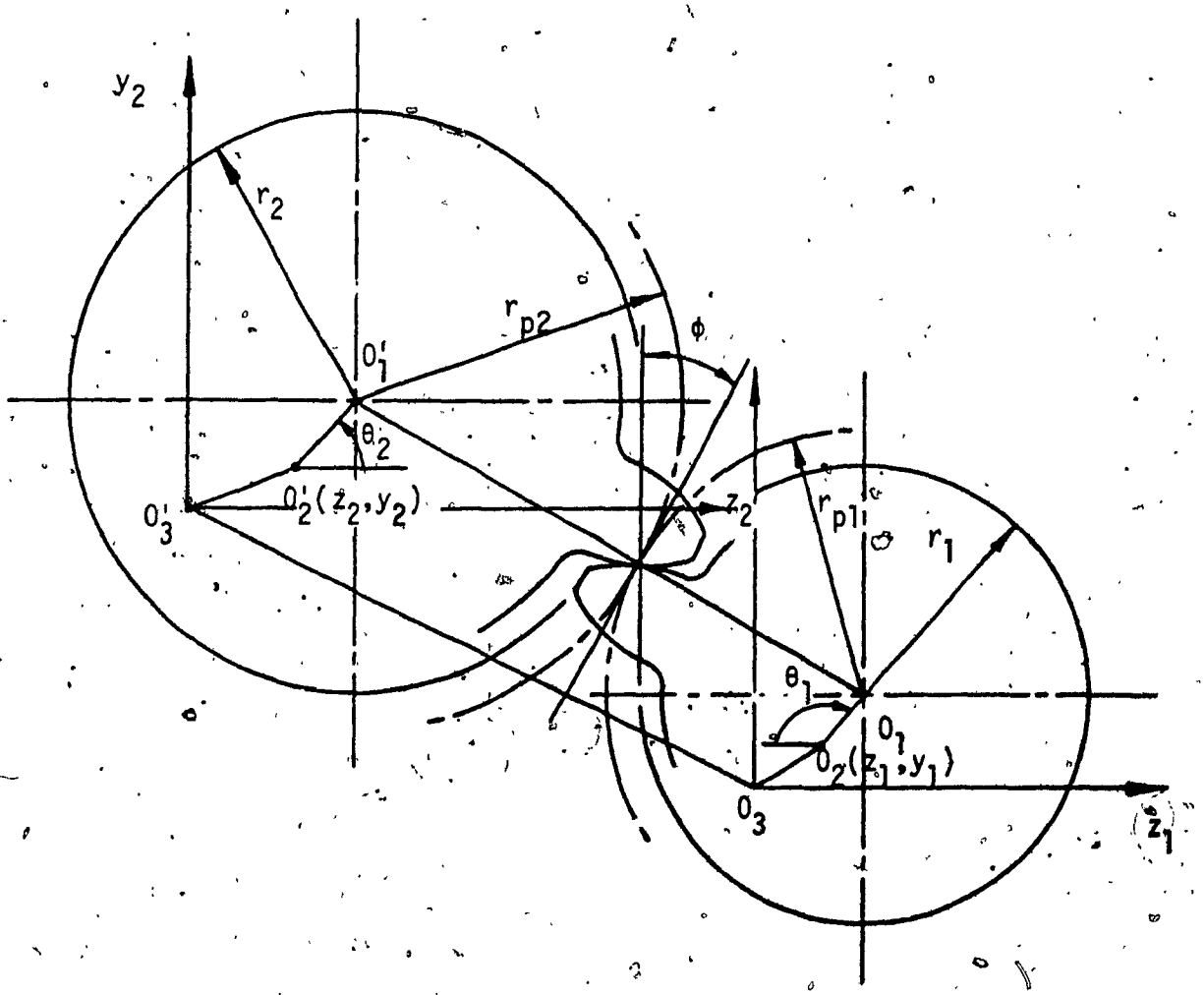

Fig. 2.3 View at the Gear Location (X-X)

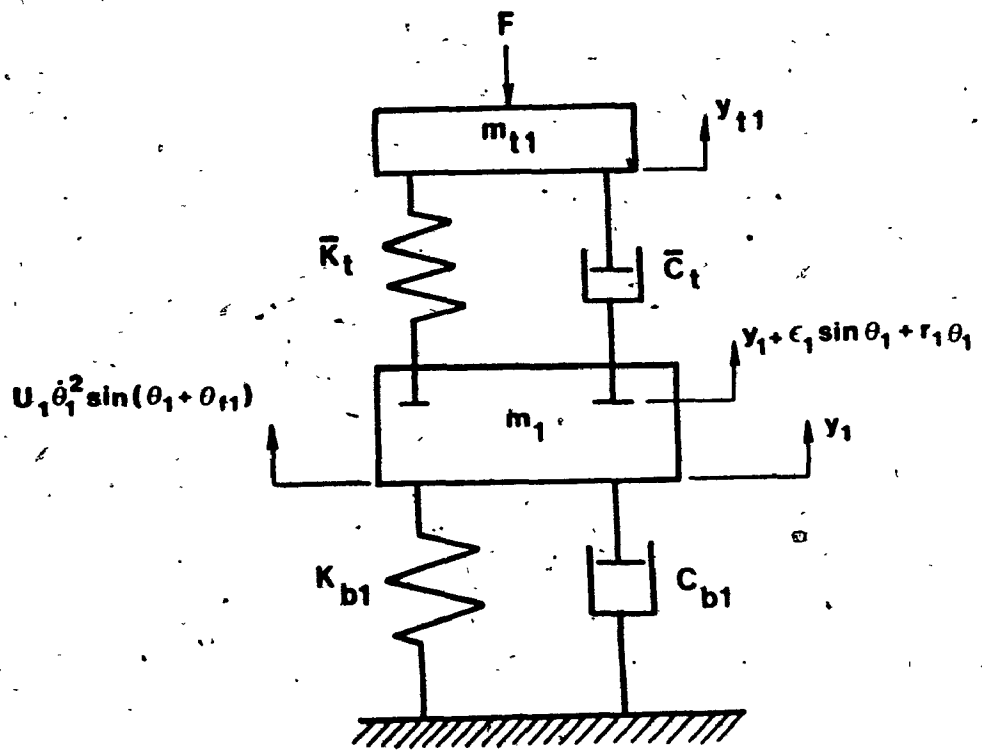

Fig. 2.4(a) Driving Gear Model

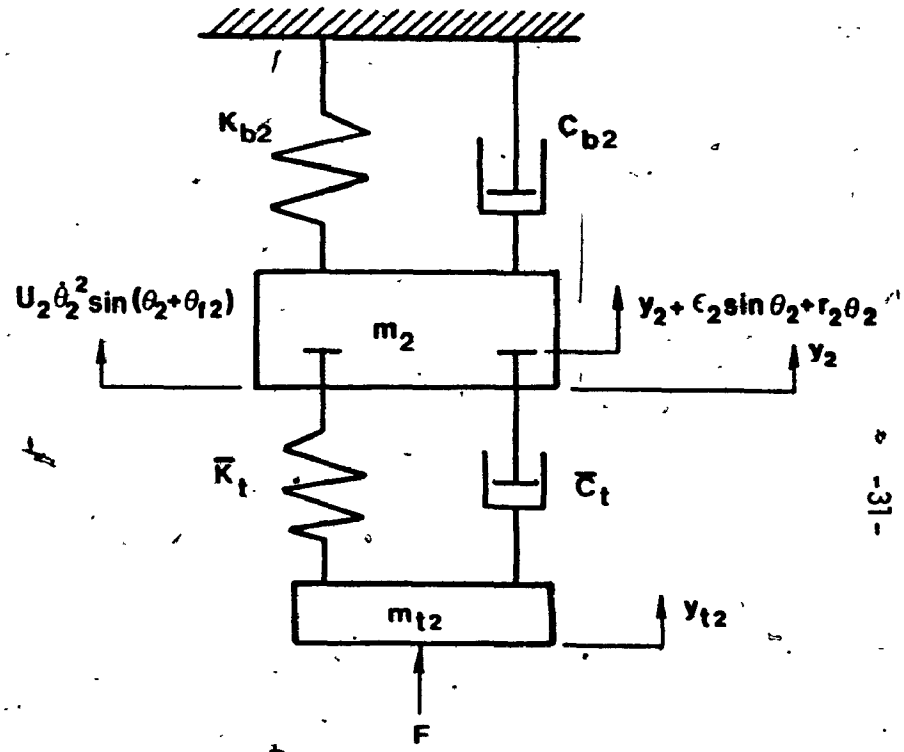

Fig. 2.4(b) Driven Gear Model

$$m_{t_2}\ddot{y}_{t_2} + \bar{c}_t(\dot{y}_{t_2} - \dot{y}_2 - \varepsilon_2\omega_2 \cos\theta_2 - r_2\dot{\theta}_2) + \bar{k}_t(y_{t_2} - y_2 - \varepsilon_2 \sin\theta_2 - r_2\theta_2) = F \tag{2.6}$$

$$I_1\ddot{\theta}_1 + k_1(\theta_1 - \theta_M) + \bar{c}_t(\dot{y}_1 + \varepsilon_1\omega_1 \cos\theta_1 + r_1\dot{\theta}_1 - \dot{y}_{t_1})(r_1 + \varepsilon_1 \cos\theta_1) + \bar{k}_t(y_1 + \varepsilon_1 \sin\theta_1 + r_1\theta_1 - y_{t_1})(r_1 + \varepsilon_1 \cos\theta_1) + c_1\dot{\theta}_1 = 0 \tag{2.7}$$

$$I_2\ddot{\theta}_2 + k_2(\theta_2 - \theta_L) + c_t(\dot{y}_2 + \varepsilon_2\omega_2 \cos\dot{\theta}_2 + r_2\dot{\theta}_2 - \dot{y}_{t_2})(r_2 + \varepsilon_2 \cos\theta_2) + \bar{k}_t(y_2 + \varepsilon_2 \sin\theta_2 + r_2\theta_2 - y_{t_2})(r_2 + \varepsilon_2 \cos\theta_2) + c_2\dot{\theta}_2 = 0 \tag{2.8}$$

$$J_M\ddot{\theta}_M + k_1(\theta_M - \theta_1) - T_M = 0 \tag{2.9}$$

$$J_L\ddot{\theta}_L + k_2(\theta_L - \theta_2) + T_L = 0 \tag{2.10}$$

The condition for the mating teeth to remain in contact is

$$y_{t1} = y_{t2} \tag{2.11}$$

Expressing all the variables in terms of their respective mean values and variations about the mean,

$$
\begin{aligned}
y_1 &= y_{10} + \Delta y_1 & \theta_1 &= \theta_{10} + \omega_1 t + \Delta\theta_1 \\
y_2 &= y_{20} + \Delta y_2 & \theta_2 &= \theta_{20} + \omega_2 t + \Delta\theta_2 \\
y_t &= y_{t_0} + \Delta y_t & \theta_M &= \theta_{M_0} + \omega_1 t + \Delta\theta_M \\
T_M &= T_{M_0} - c_M \Delta\dot{\theta}_M & \theta_L &= \theta_{L_0} + \omega_2 t + \Delta\theta_L \\
T_L &= T_{L_0} - c_L \Delta\dot{\theta}_L & F &= F_0 + \Delta F
\end{aligned}
\qquad (2.12)
$$

where θ_{10}, θ_{20}, θ_{M_0} and θ_{L_0} are initial angular positions.

Since only the flexural displacement in the y-direction is coupled with torsion, equations of motion in z-direction will not be considered in the subsequent analysis. Substituting the mean and variation about the mean of all the variables given in equation (2.12) into the equations of motion (2.3 - 2.10) and after considerable manipulation and simplifcation by ignoring terms involving squares and higher powers of small quantities, the equations of motion involving the quantities varying about the mean value can be written in the following matrix form:

$$[M]\{\ddot{q}\} + [C]\{\dot{q}\} + [K]\{q\} = \{F\} \qquad (2.13)$$

where the generalized displacement vector $\{q\}$ is:

$$\{q\} = [\Delta y_1, \Delta y_2, \Delta y_t, \Delta\theta_M, \Delta\theta_1, \Delta\theta_2, \Delta\theta_L]^T \qquad (2.14)$$

The matrices [M], [C] and [K] referred to in Eq. (2.13) are given by

$$[M] = \begin{bmatrix} m_1 & 0 & 0 & 0 & 0 & 0 & 0 \\ 0 & m_2 & 0 & 0 & 0 & 0 & 0 \\ 0 & 0 & m_{t_1}+m_{t_2} & 0 & 0 & 0 & 0 \\ 0 & 0 & 0 & J_M & 0 & 0 & 0 \\ 0 & 0 & 0 & 0 & I_1 & 0 & 0 \\ 0 & 0 & 0 & 0 & 0 & I_2 & 0 \\ 0 & 0 & 0 & 0 & 0 & 0 & J_L \end{bmatrix} \tag{2.15a}$$

$$[K] = \begin{bmatrix} k_{b_1}+\bar{k}_t & 0 & -\bar{k}_t & 0 & \bar{k}_t r_1 & 0 & 0 \\ 0 & k_b+\bar{k}_t & -\bar{k}_t & 0 & 0 & \bar{k}_t r_2 & 0 \\ -\bar{k}_t & -\bar{k}_t & 2\bar{k}_t & 0 & -\bar{k}_t r_1 & -\bar{k}_t r_2 & 0 \\ 0 & 0 & 0 & k_1 & -k_1 & 0 & 0 \\ \bar{k}_t r_1 & 0 & -\bar{k}_t r_1 & -k_1 & k_1+\bar{k}_t r_1^2 & 0 & 0 \\ 0 & \bar{k}_t r_2 & -\bar{k}_t r_2 & 0 & 0 & k_2+\bar{k}_t r_2^2 & -k_2 \\ 0 & 0 & 0 & 0 & 0 & -k_2 & k_2 \end{bmatrix} \tag{2.15b}$$

$$[C]=\begin{bmatrix} c_{b_1}+\bar{c}_t & 0 & -\bar{c}_t & 0 & \bar{c}_t r_1 & 0 & 0 \\ 0 & c_{b_2}+\bar{c}_t & -\bar{c}_t & 0 & 0 & \bar{c}_t r_2 & 0 \\ -\bar{c}_t & -\bar{c}_t & 2\bar{c}_t & 0 & -\bar{c}_t r_1 & -\bar{c}_t r_2 & 0 \\ 0 & 0 & 0 & c_M & 0 & 0 & 0 \\ \bar{c}_t r_1 & 0 & -\bar{c}_t r_1 & 0 & c_1+\bar{c}_t r_1^2 & 0 & 0 \\ 0 & \bar{c}_t r_2 & -\bar{c}_t r_2 & 0 & 0 & c_2+\bar{c}_t r_2^2 & 0 \\ 0 & 0 & 0 & 0 & 0 & 0 & -c_L \end{bmatrix} \tag{2:15c}$$

and

$$\{F\}=\begin{Bmatrix} -\bar{c}_t \varepsilon_1 \omega_1 \cos(\omega_1 t + \theta_{10}) - \bar{k}_t \varepsilon_1 \sin(\omega_1 t + \theta_{10}) \\ \quad + U_1 \omega_1^2 \sin(\omega_1 t + \theta_{10} + \theta_{f1}) \\ -\bar{c}_t \varepsilon_2 \omega_2 \cos(\omega_2 t + \theta_{20}) - \bar{k}_t \varepsilon_2 \sin(\omega_2 t + \theta_{20}) \\ \quad + U_2 \omega_2^2 \sin(\omega_2 t + \theta_{20} + \theta_{f2}) \\ \bar{c}_t \{\varepsilon_2 \omega_2 \cos(\omega_2 t + \theta_{20}) + \varepsilon_1 \omega_1 \cos(\omega_1 t \\ \quad + \bar{k}_t \{\varepsilon_2 \sin(\omega_2 t + \theta_{20}) + \varepsilon_1 \sin(\omega_1 t + \theta_{10})\} \\ 0 \\ -\bar{c}_t r_1 \varepsilon_1 \omega_1 \cos(\theta_{10} + \omega_1 t) - F_0 \varepsilon_1 \cos(\theta_{10} + \omega_1 t) \\ \quad - \bar{k}_t r_1 \varepsilon_1 \sin(\theta_{10} + \omega_1 t) \\ -\bar{c}_t r_2 \varepsilon_2 \omega_2 \cos(\theta_{20} + \omega_2 t) + F_0 \varepsilon_2 \cos(\theta_{20} + \omega_2 t) \\ \quad - \bar{k}_t r_2 \varepsilon_2 \sin(\theta_{20} + \omega_2 t) \\ 0 \end{Bmatrix} \tag{2.15d}$$

where θ_{f1} and θ_{f2} are angle between directions of mass unbalance and geometrical eccentricity.

The expression for the dynamic tooth load ΔF, is obtained as

$$\Delta F = m_{t1}\Delta\ddot{y}_t + \bar{c}_t(\Delta\dot{y}_t - \Delta\dot{y}_1 - \varepsilon_1\omega_1\cos(\omega_1 t + \theta_{10}) - r_1\Delta\dot{\theta}_1) + \bar{k}_t(\Delta y_t - \Delta y_1 - \varepsilon_1\sin(\omega_1 t + \theta_{10}) - r_1\Delta\theta_1) \quad (2.16)$$

2.4.2 Dynamic Response using Modal Analysis

The linear equations of motion described by Eq. (2.13) are coupled. In order to obtain the system dynamic response, the original equations of motion are transformed into an independent set of equations by use of the undamped or damped modes. This procedure is called modal analysis. When the damping matrix in Eq. (2.13) can be expressed as a linear combination of the mass and stiffness matrix (which are both symmetric), the undamped modes are used to uncouple the equations of motion and the procedure is called normal mode analysis, which is used in this section. Complex modal analysis using damped modes to uncouple the equations of motion is discussed in section 2.7. In the present analysis modal damping is used, to account for system damping.

The homogeneous part of equation (2.13) neglecting damping, is given by,

$$[M]\{\ddot{q}\} + [K]\{q\} = \{0\} \tag{2.17}$$

which is solved to obtain the eigen values λ_i and eigen-vectors $\{\phi_i\}$ of the undamped system.

An inspection of the force vector $\{F\}$ in equation (2.15d) shows that the excitation consists of frequencies ω_1 and ω_2 corresponding to the speeds of driving and driven shafts. The force vector $\{F\}$ can be expressed as the sum of sine and cosine components, involving the two frequencies ω_1 and ω_2 as,

$$\{F\} = \{F_s\}_1 \sin \omega_1 t + \{F_s\}_2 \sin \omega_2 t + \{F_c\}_1 \cos \omega_1 t + \{F_c\}_2 \cos \omega_2 t \tag{2.18}$$

where θ_{10}, θ_{20}, θ_{f1} and θ_{f2} have been assumed to be zero.

The corresponding response also can be expressed involving the two frequencies as

$$\{q\} = \{q_s\}_1 \sin \omega_1 t + \{q_s\}_2 \sin \omega_2 t + \{q_c\}_1 \cos \omega_1 t + \{q_c\}_2 \cos \omega_2 t \tag{2.19}$$

Using equations (2.18) and (2.19), equation (2.13) can be written as four separate equations.

$$[M]\{\ddot{q}_s\}_k + [C]\{\dot{q}_s\}_k + [K]\{q_s\}_k = \{F_s\}_k \qquad (2.20)$$
$$[M]\{\ddot{q}_c\}_k + [C]\{\dot{q}_c\}_k + [K]\{q_c\}_k = \{F_c\}_k \; ; k = 1,2$$

Expressing the response $\{q\}$ in terms of the modal coordinates $\{p\}$ as

$$\{q_s\}_k = [\phi]\{p_s\}_k \qquad (2.21)$$
$$\{q_c\}_k = [\phi]\{p_c\}_k \; ; \; k = 1,2$$

where $[\phi]$ is the modal matrix formed by concatenating the eigen vectors $\{\phi_i\}$, and $\{p_s\}_k$ and $\{p_c\}_k$, are the principal coordinate vectors corresponding to the sine and cosine components. Using equations (2.21) in equation (2.20) and premultiplying by $[\phi]^T$ results in uncoupled equations in the modal coordinates of the form,

$$\mu_i(\ddot{p}_{si})_k + \gamma_i(\dot{p}_{si})_k + \kappa_i(p_{si})_k = (\sigma_{si})_k \qquad (2.22)$$
$$\mu_i(\ddot{p}_{ci})_k + \gamma_i(\dot{p}_{ci})_k + \kappa_i(p_{ci})_k = (\sigma_{ci})_k$$
$$\text{where } k = 1,2$$
$$i = 1,2\ldots7$$

where μ_i and κ_i are the elements of diagonal matrices $[\mu]$ and $[\kappa]$ given by

$$[\mu] = [\phi]^T[M][\phi]$$
$$[\kappa] = [\phi]^T[K][\phi]$$

and γ_i is the equivalent damping coefficient in each mode. $(\sigma_{si})_k$ and $(\sigma_{ci})_k$ are the elements of the generalized force vectors $\{\sigma_s\}_k$ and $\{\sigma_c\}_k$, given by

$$\{\sigma_s\}_k = [\phi]^T\{F_s\}_k$$
$$\{\sigma_c\}_k = [\phi]^T\{F_c\}_k; \qquad k = 1,2$$

The solution of equation (2.22) yields,

$$(p_{si})_k = \frac{(\sigma_{si})_k}{(-\omega_k^2 \mu_i + \kappa_i) + j(\gamma_i \omega_k)} \qquad (2.23)$$

$$(p_{ci})_k = \frac{(\sigma_{ci})_k}{(-\omega_k^2 \mu_i + \kappa_i) + j(\gamma_i \omega_k)};$$

$$k = 1,2$$
$$i = 1,2,\ldots 7$$

Using equations (2.23), (2.21) and (2.19) we obtain the system dynamic response $\{q\}$. The dynamic tooth load ΔF is calculated by using equation (2.16). Since the response involves two frequencies ω_1 and ω_2, the total response has the form

$$\begin{aligned} q_j &= q_{1j} \sin(\omega_1 t + \psi_{1j}) + q_{2j} \sin(\omega_2 t + \psi_{2j}) \qquad (2.24) \\ &= q_{1j} \sin \lambda_1 + q_{2j} \sin \lambda_2 \\ &= (q_{1j} + q_{2j}) \sin\left(\frac{\lambda_1 + \lambda_2}{2}\right) \cos\left(\frac{\lambda_1 - \lambda_2}{2}\right) \\ &\quad + (q_{1j} - q_{2j}) \cos\left(\frac{\lambda_1 + \lambda_2}{2}\right) \sin\left(\frac{\lambda_1 - \lambda_2}{2}\right) \end{aligned}$$

Hence, the response is an amplitude modulated harmonic phenomenon. If ω_1 and ω_2 are close to each other, this will result in beats.

2.4.3 Numerical Results

The details of the geared shaft system used to obtain the numerical results are given in Table 2.1. The maximum

TABLE 2.1

Details of the Geared Rotor System

I_1	3.12×10^{-2} Kgm^2
I_2	6.53×10^{-3} Kgm^2
J_1	4.78×10^{-1} Kgm^2
J_2	5.71×10^{-1} Kgm^2
k_{b1}, k_{b2}	2.04×10^{5} N/m
$\bar{k}_t$	2.55×10^{9} N/m
k_1	1.17×10^{2} Nm/rad
k_2	2.88×10^{3} Nm/rad
m_1	16.96 kg
m_2	5.65 kg
m_{t1}, m_{t2}	4.9×10^{-3} kg
r_1	0.1015 m
r_2	0.0564 m
$\varepsilon_1, \varepsilon_2$	120 μm (variable)
U_1, U_2	2.8×10^{-4} kgm (variable)

value of the dynamic response obtained from equation (2.24) are illustrated in Figs. 2.5 and 2.6 and the maximum dynamic tooth loads obtained from equation (2.16) are shown in Figs. 2.7 - 2.10. In the present investigation one percent of the critical damping is used in all the modes. The dynamic responses are plotted against the frequency of rotation of the driven shaft ω_2. This representation also facilitates comparison of present results with those presented in [54]. Responses are presented up to 100 Hz which includes only the first five natural frequencies of the system, since the other two natural frequencies are much higher in the range. The system natural frequencies are given in Table 2.2 where the natural frequencies of the system considered in [54] are also given for comparison.

The dynamic response of the driven shaft, Δy_2, is plotted in Fig. 2.5 against the frequency of rotation of the driven shaft, for nominal values of ε_1, U_1 and U_2 and for different values of ε_2. A comparison of Δy_2 response with that presented in [54] was attempted. However, no information about damping in the system is given in [54] and in the frequency range for which the results are presented, there is only one response peak which compares satisfactorily with the present results. It is interesting to note in Fig. 2.5 that when the excitation frequency is related to the system natural frequency through the gear ratio, the system

TABLE 2.2

Natural Frequencies Hz

Mode No.	Present System	System of Ref. [54]
1	zero	zero
2	2.65	2.7
3	16.14	24.6
4	25.37	77.3
5	79	-
6	5806.43	-
7	1.13×10^5	-

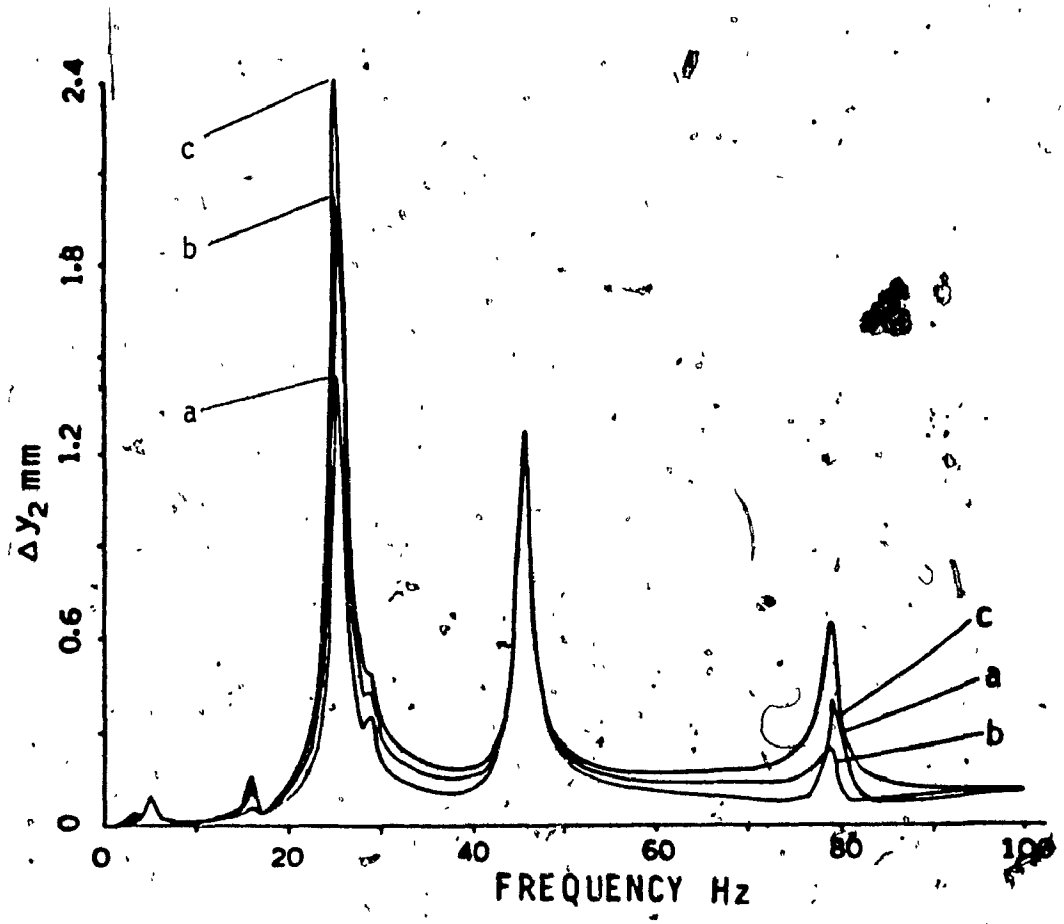

Fig. 2.5 Dynamic response of the driven shaft, Δy_2, against frequency of rotation of the driven shaft.
(U_1 = 2.8 x 10^{-4}kgm, U_2 = 2.8 x 10^{-4}kgm, ε_1 = 120 μm,
(a) ε_2 = 20 μm, (b) ε_2 = 80 μm, (c) ε_2 = 120 μm)

experiences resonance. This is the reason for the peaks occuring at 4.77 Hz, 29 Hz and 45.66 Hz. The Δy_2 response increases with eccentricity of the driven gear, ε_2. The response is very high at 25.37 Hz since the corresponding mode is predominantly the flexural mode of the driven shaft. The response is also significant at 45.66 Hz since, the driving side is exciting the system at its natural frequency of 25.37 Hz.

The flexural response of the driving shaft is shown in Fig. 2.6. The natural frequency corresponding to the flexure of the driving shaft is 16.14 Hz. The response is predominant at this frequency and at 29 Hz which are related by the gear ratio. The response at 29 Hz is higher compared to that at 16.14 Hz, since the plot is against the frequency of rotation of the driven shaft, ω_2, and the driving shaft is subjected to excitation at 16.14 Hz when the driven shaft rotates at 29 Hz. For nominal value of ε_1, U_1 and U_2 the response increases with increasing eccentricity of the driven gear.

The dynamic tooth load ΔF, is plotted against the frequency of rotation of the driven shaft in Fig. 2.7. The unbalance U_1 and U_2 and the geometrical eccentricity in the driving gear ε_1 are kept at nominal values and the curves are plotted for different values of ε_2. It is seen that the

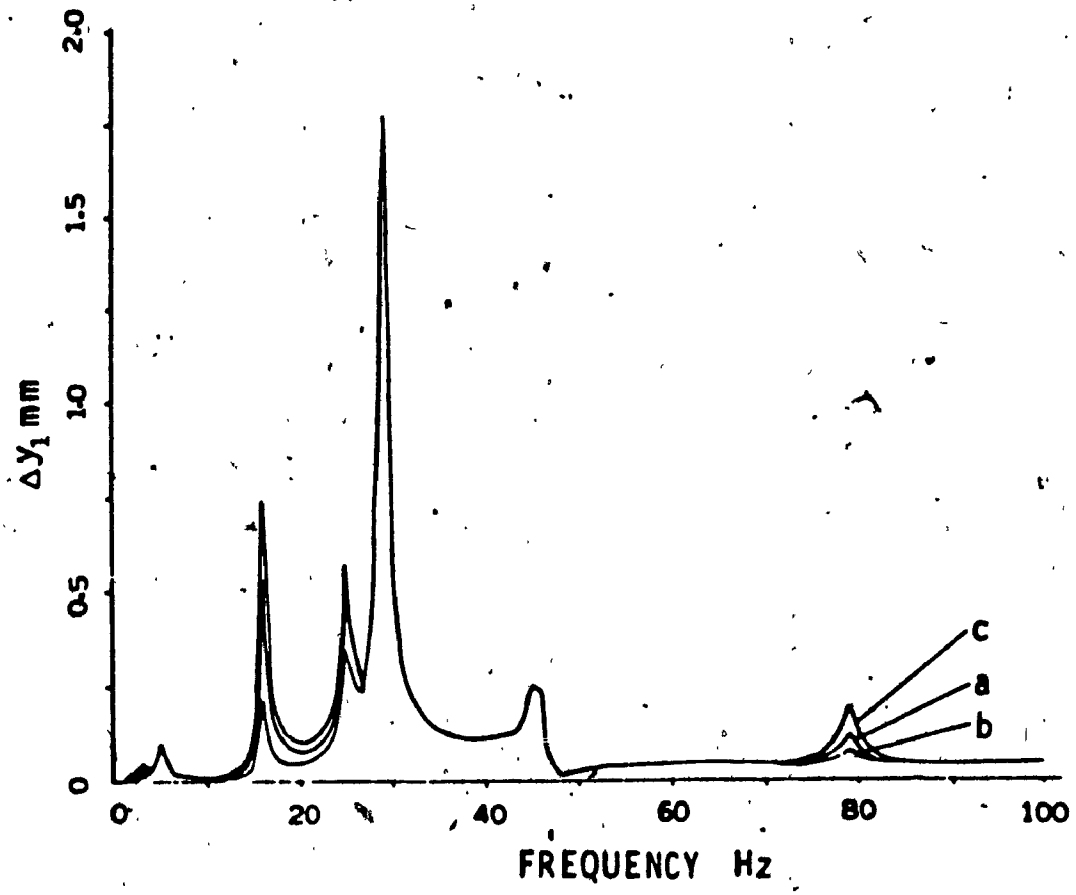

Fig. 2.6 Dynamic response of the driving shaft, Δy_1, against frequency of rotation of the driven shaft
($U_1 = 2.8 \times 10^{-4}$kgm, $U_2 = 2.8 \times 10^{-4}$kgm, $\varepsilon_1 = 120$ μm,
(a) $\varepsilon_2 = 20$ μm, (b) $\varepsilon_2 = 80$ μm, (c) $\varepsilon_2 = 120$ μm)

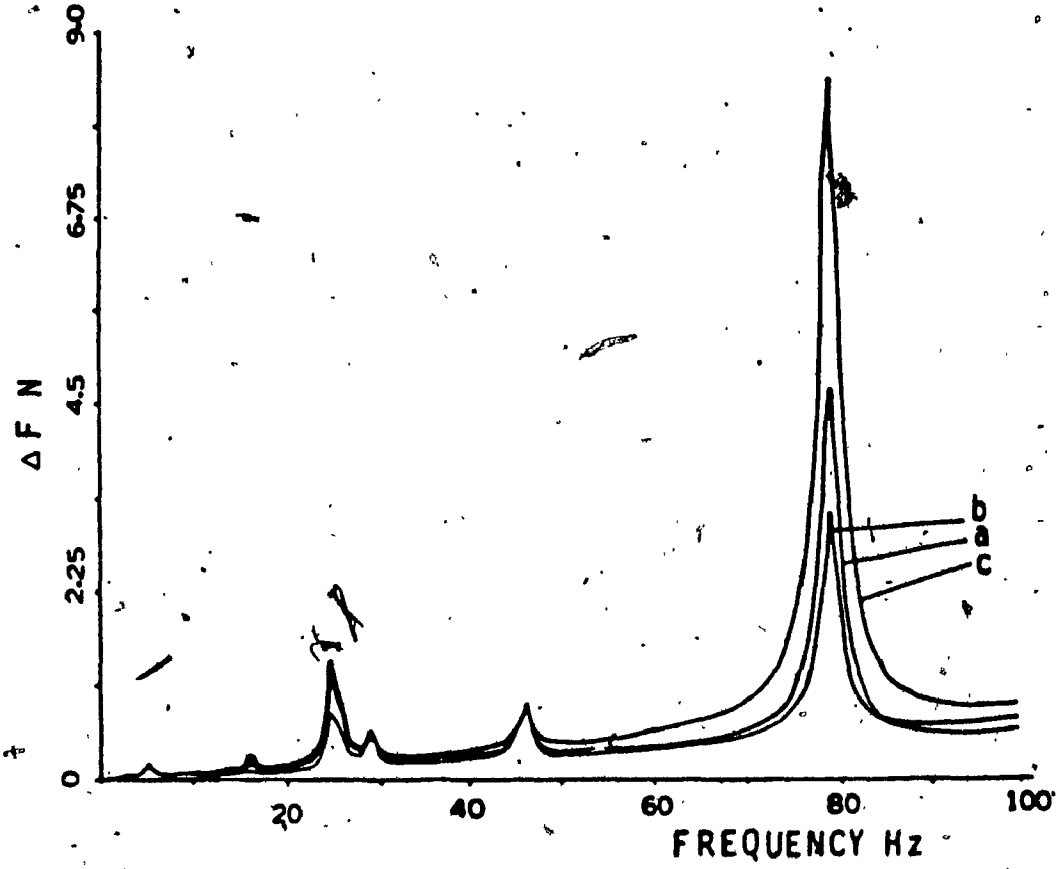

Fig. 2.7 Dynamic tooth load against frequency of rotation of the driven shaft.

($U_1 = 2.8 \times 10^{-4}$kgm, $U_2 = 2.8 \times 10^{-4}$kgm, $\varepsilon_1 = 120$ μm, (a) $\varepsilon_2 = 20$ μm, (b) $\varepsilon_2 = 80$ μm, (c) $\varepsilon_2 = 120$ μm)

dynamic response exhibits the most significant peak at 79 Hz, which corresponds to the fifth natural frequency.

The dynamic tooth load ΔF, is plotted against the frequency of rotation of the driven shaft in Fig. 2.8. The unbalance U_I and geometrical eccentricities ε_1 and ε_2 are kept at nominal values and the curves are plotted for different values of U_2. Again, the dynamic force exhibits a significant peak at 79 Hz.

The dynamic tooth load ΔF, is plotted against the frequency of rotation of the driven shaft in Fig. 2.9. The unbalances U_1 and U_2 and the geometrical eccentricity ε_2, are kept at nominal values and the curves are plotted for different values of ε_1. The dynamic force still exhibits a significant peak at 79 Hz.

The variation of dynamic tooth load against the frequency of rotation of the driven shaft is shown in Fig. 2.10 for nominal values of U_2, ε_1 and ε_2 and for different values of U_1. The peak dynamic tooth load occurs again at 79 Hz. The variation of the dynamic tooth load with U_1 is negligible.

In all the above cases, the dynamic tooth load has a maximum only at 79 Hz which is the system natural frequency

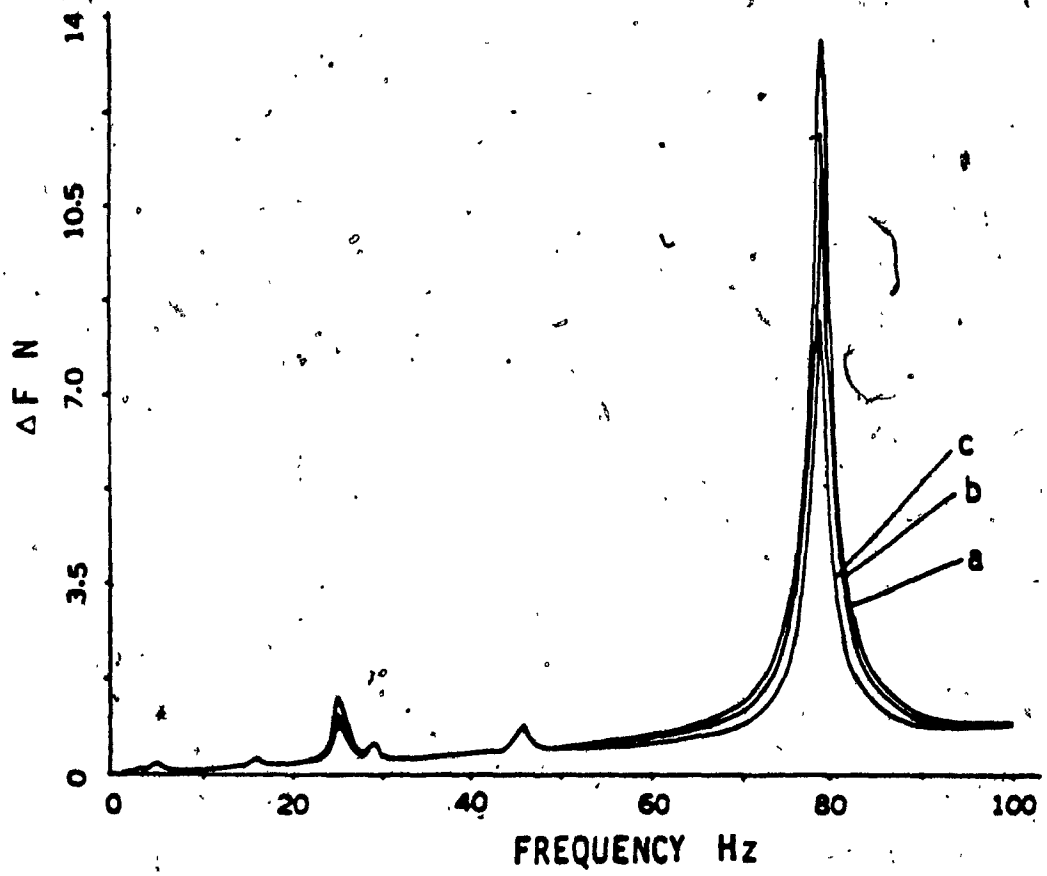

Fig. 2.8 Dynamic tooth load against frequency of rotation of the driven shaft

(U_1 = 2.8 x 10^{-4}kgm, ε_1 = 120 μm, ε_2 = 120 μm,

(a) U_2 = 0.78 x 10^{-4}kgm, (b) U_2 = 1.47 x 10^{-4}kgm,

(c) U_2 = 2.8 x 10^{-4}kgm)

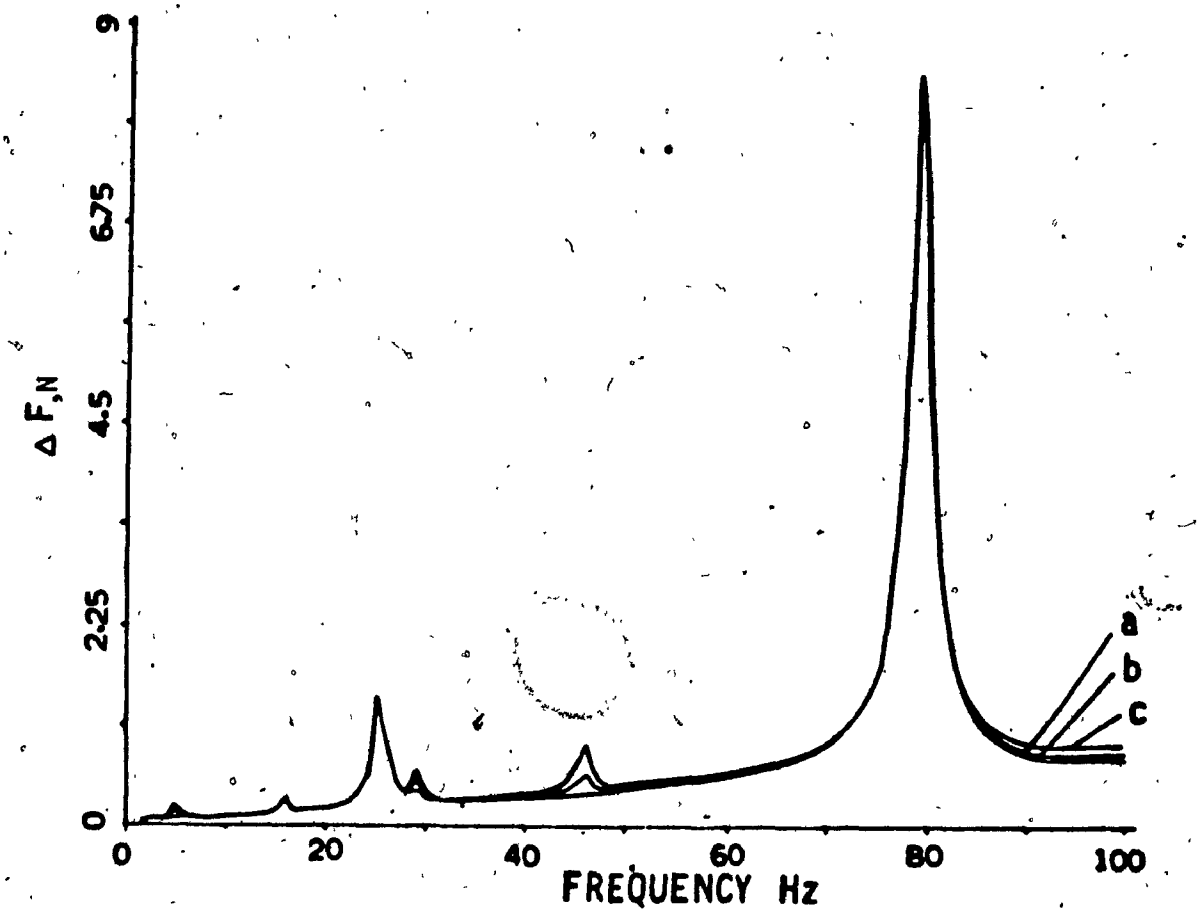

Fig. 2.9 Dynamic tooth load against the frequency of rotation of the driven shaft

(U_1 = 2.8 x 10^{-4}kgm, U_2 = 2.8 x 10^{-4}kgm, ε_2 = 120 μm,

(a) ε_1 = 20 μm, (b) ε_1 = 80 μm, (c) ε_1 = 120 μm)

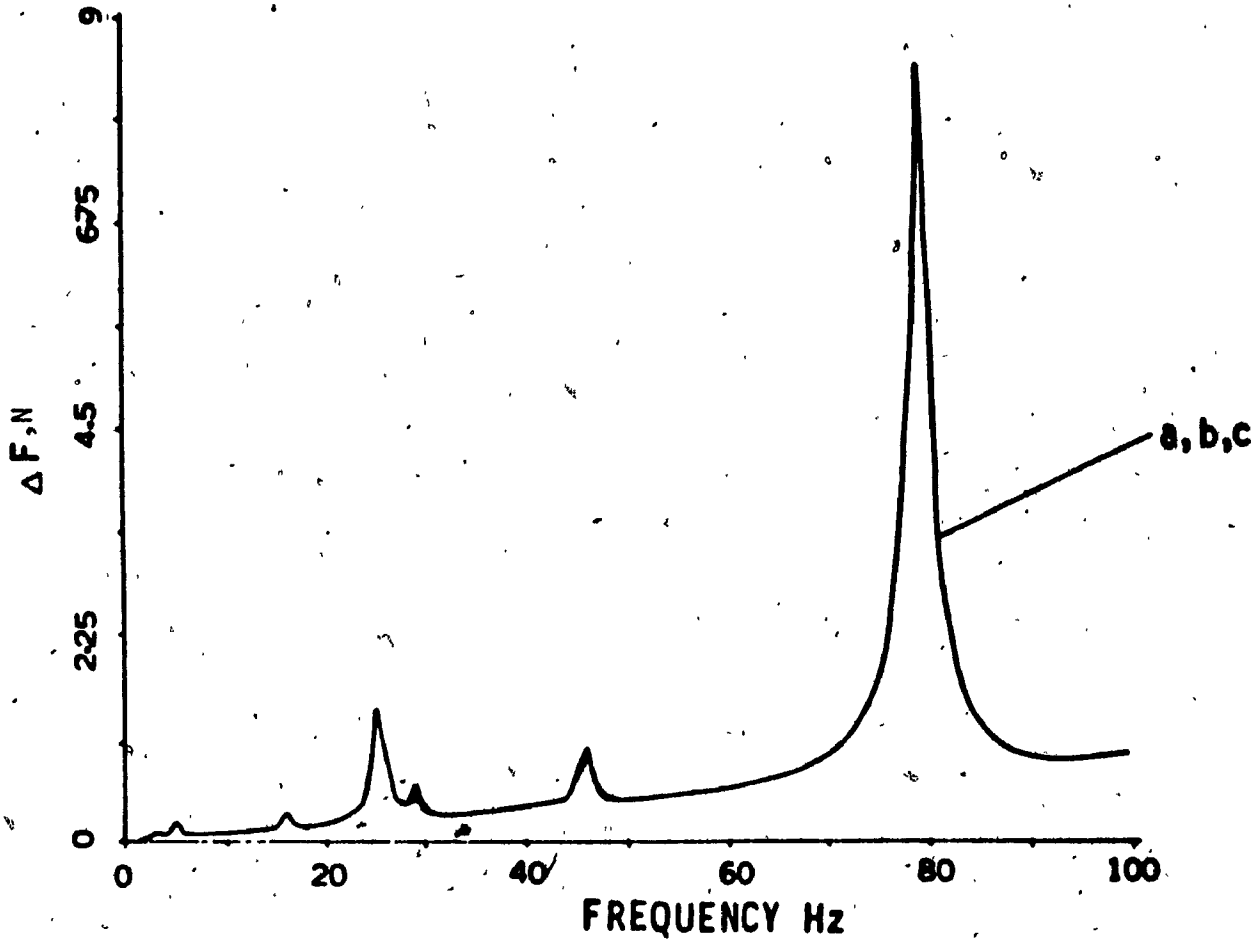

Fig. 2.10 Dynamic tooth load against the frequency of rotation of the driven shaft

($U_2 = 2.8 \times 10^{-4}$kgm, $\varepsilon_1 = 120$ μm, $\varepsilon_2 = 120$ μm,

(a) $U_1 = 0.78 \times 10^{-4}$kgm, (b) $U_1 = 1.47 \times 10^{-4}$kgm,

(c) $U_1 = 2.8 \times 10^{-4}$kgm)

corresponding to a predominantly torsional mode. However, the dynamic responses Δy_1 and Δy_2 exhibit maximum values at other system natural frequencies also. The torsional responses of the driving and driven shafts at the gear locations also exhibit peaks at all the system natural frequencies. One possible explanation for the dynamic tooth load having a peak at 79 Hz only is that the effect of dynamic responses at other natural frequencies are nullified due to their mutual phase relations. The dynamic tooth load is significant only at the torsional resonance in the system, and the coupling between the torsional and flexural vibrations does not change this behaviour.

2.5 Application of the Finite Element Method

The Finite Element method has been recognized as one of the well established and convenient tools for structural analysis by engineers and applied scientists. It is basically a discretisation procedure. Here a complex structure is regarded as a finite assemblage of discrete elements, where every such element is a continuous structural member. By requiring that the displacement be compatible and the inertial forces be in balance at certain points shared by several elements, the entire structure is compelled to act as one entity.

2.5.1 Analysis

A typical rotor shaft beam element is illustrated in Fig. 2.11. Each element has 2 nodes and each node has six degrees of freedom which include translation and rotation about the three mutually perpendicular axes x, y, and z. Przemeniecki [88] derived the mass and stiffness matrices for such a beam element. The effects of elastic bending energy translational kinetic energy and rotatory inertia are included in the analysis.

The undamped equations of motion for a beam element are given by:

$$\{[M_t^e] + [M_r^e]\}\ \ddot{q}_e + [K^e]\ \{q_e\} = \{F_e\}$$

where $\{q_e\} = \{x_1, y_1, z_1, \theta_{x1}, \theta_{y1}, \theta_{z1},$
$x_2, y_2, z_2, \theta_{x2}, \theta_{y2}, \theta_{z2}\}^T$

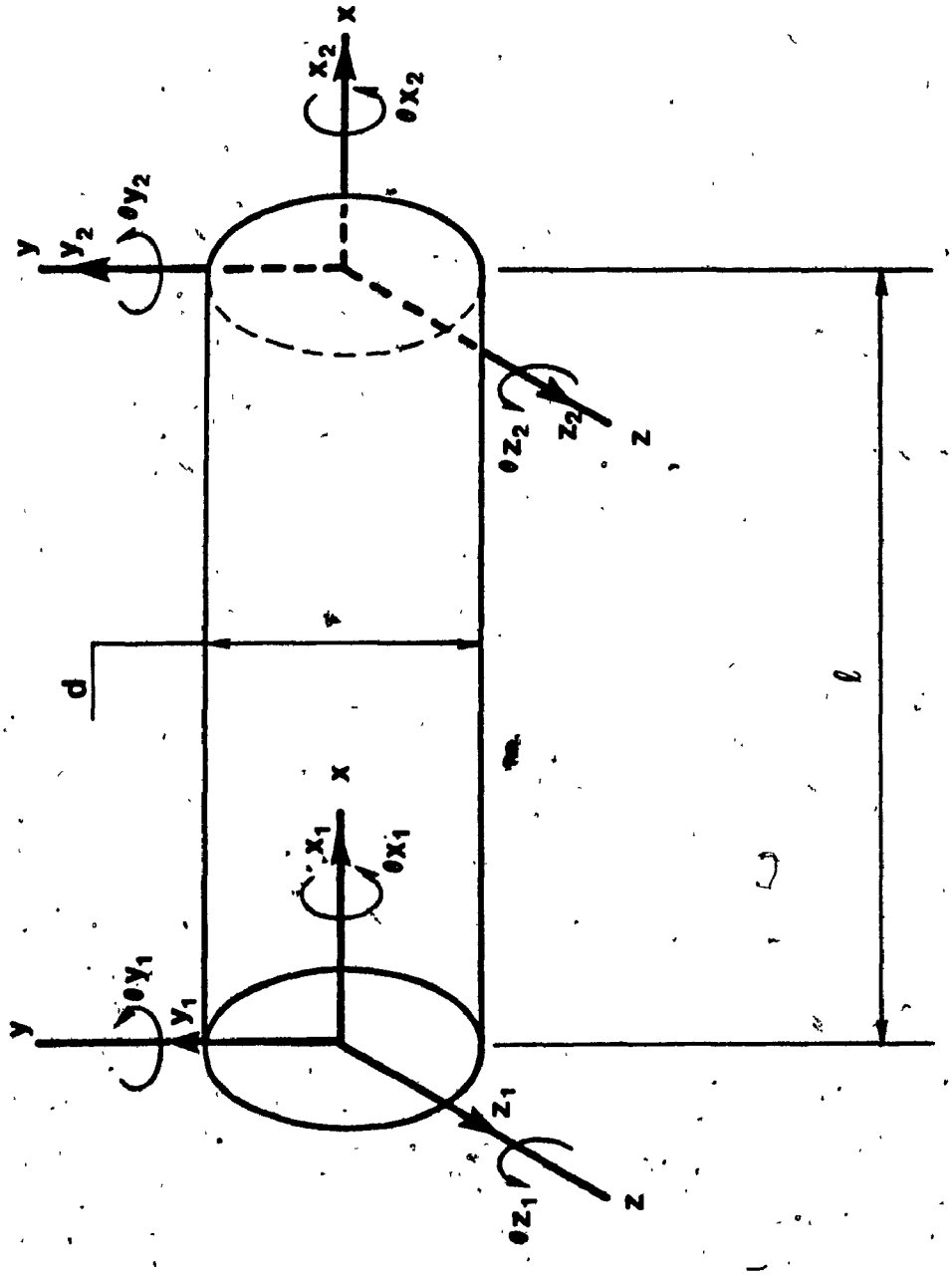

Fig. 2.11 Typical beam element

The works of Ruhl [39] and Ruhl and Booker [40] are the first examples of studies using finite elements in rotor dynamics. Ruhl's finite element includes only elastic bending energy and translational kinetic energy, while the effects of rotatory inertia, gyroscopic moments, shear deformations, axial load and internal damping have been neglected. The effects can be quite significant for some configurations as indicated by several investigators referenced in [86]. Thorkildsen [87] included the effects of rotatory inertia and gyroscopic moments. Several other investigators like Nelson and McVaugh [41] studied similar problems by including different effects. The work of Zorzi and Nelson [42] was a generalization of [41] by the inclusion of internal damping. Nelson [43] utilised Timoshenko beam theory to establish the shape function. He derived the system matrices including the effects of rotatory inertia, gyroscopic moments, axial load and shear deformations.

The finite elements used to model the geared rotor in this study will initially include the effects of elastic bending energy, translational kinetic energy and rotatory inertia. The gyroscopic terms make the system non symmetric and are neglected in order to carry out a simple normal mode analysis. Later, in section 2.7, a complex modal analysis using a biorthogonality relation is carried out including the skew symmertic gyroscopic terms.

and,

$$[M_t^e] = \frac{\bar{m}\ell}{420}$$

140											
	156										
		156									
			$\frac{140J}{A}$								
		-22ℓ		$4\ell^2$							
	22ℓ				$4\ell^2$						
70						140					
	54				13ℓ		156				
		54		-13ℓ				156			
			$\frac{70J}{A}$						$\frac{140J}{A}$		
		-13ℓ		$-3\ell^2$				22ℓ		$4\ell^2$	
	-13ℓ				$-3\ell^2$		-22ℓ				$4\ell^2$

Symmetric

(2.25a)

and,

$$[M_r^e] = \frac{\bar{m}r^2}{120}$$

0											
0	36										
0	0	36									
0	0	0	0								
0	0	-3ℓ	0	$4\ell^2$							
0	3ℓ	0	0	0	$4\ell^2$						
0	0	0	0	0	0	0					
0	-36	0	0	0	-3ℓ	0	36				
0	0	-36	0	3ℓ	0	0	0	36			
0	0	0	0	0	0	0	0	0	0		
0	0	-3ℓ	0	$-\ell^2$	0	0	0	3ℓ	0	$4\ell^2$	
0	3ℓ	0	0	0	$-\ell^2$	0	-3ℓ	0	0	0	$4\ell^2$

Symmetric

(2.25b)

and,

$$[K^e] = \begin{bmatrix}
\frac{EA}{\ell} & & & & & & & & & & & \\
 & \frac{12EI}{\ell^3} & & & & & & & & & & \\
 & & \frac{12EI}{\ell^3} & & & & & & & & & \\
 & & & \frac{GJ}{\ell} & & & & & & & & \\
 & & \frac{-6EI}{\ell^2} & & \frac{4EI}{\ell} & & & & & & & \\
 & \frac{6}{\ell} & & & & \frac{4EI_z}{\ell} & & & & & & \\
-\frac{EA}{\ell} & & & & & & \frac{EA}{\ell} & & & & & \\
 & -\frac{12EI}{\ell^3} & & & & -\frac{6EI}{\ell^2} & & \frac{12EI}{\ell^3} & & & & \\
 & & -\frac{12EI}{\ell^3} & & \frac{6EI}{\ell^2} & & & & \frac{12EI}{\ell^3} & & & \\
 & & & -\frac{GJ}{\ell} & & & & & & \frac{GJ}{\ell} & & \\
 & & -\frac{6EI_y}{\ell^2} & & \frac{2EI}{\ell} & & & & \frac{6EI}{\ell^2} & & \frac{4EI}{\ell} & \\
 & \frac{6EI_z}{\ell^2} & & & & \frac{2EI}{\ell} & & -\frac{6EI}{\ell^2} & & & & \frac{4EI}{\ell}
\end{bmatrix}$$

Symmetric

(2.25c)

The procedure to carry out finite element vibration analysis of the geared shaft system is as follows,

1) Discretise the shafts carrying the gears by beam finite elements.

2) Assemble the elements to form the global mass and stiffness matrices.

3) Introduce the concentrated masses and inertias into the appropriate locations in the global mass matrix.

4) Introduce the terms arising from the coupling between the torsional and flexural motions obtained from Equation (2.15b) into the global stiffness matrix.

$$\begin{Bmatrix} y_1 \\ y_2 \\ y_t \\ \theta_1 \\ \theta_2 \end{Bmatrix} \rightarrow \begin{bmatrix} \bar{k}_t & 0 & -\bar{k}_t & \bar{k}_t r_1 & 0 \\ 0 & \bar{k}_t & -\bar{k}_t & 0 & \bar{k}_t r_2 \\ -\bar{k}_t & -\bar{k}_t & 2\bar{k}_t & -\bar{k}_t r_1 & -\bar{k}_t r_2 \\ \bar{k}_t r_1 & 0 & -\bar{k}_t r_1 & \bar{k}_t r_1^2 & 0 \\ 0 & \bar{k}_t r_2 & -\bar{k}_t r_2 & 0 & \bar{k}_t r_2^2 \end{bmatrix} \quad (2.26)$$

Also introduce the rolling contact bearing stiffness.

5) Obtain the global force vector from Equation (2.15d).

$$
\begin{bmatrix} F_{y1} \\ F_{z1} \\ F_{y2} \\ F_{z2} \\ F_{yt} \\ F_{\theta 1} \\ F_{\theta 2} \end{bmatrix}
\rightarrow
\begin{Bmatrix}
-\bar{c}_t \varepsilon_1 \omega_1 \cos(\omega_1 t + \theta_{10}) - \bar{k}_t \varepsilon_1 \sin(\omega_1 t + \theta_{10}) \\
\quad + U_1 \omega_1^2 \sin(\omega_1 t + \theta_{10} + \theta_{f_1}) \\
\hline
U_1 \omega_1^2 \cos(\omega_1 t + \theta_{10} + \theta_{f_1}) \\
\hline
-\bar{c}_t \varepsilon_2 \omega_2 \cos(\omega_2 t + \theta_{20}) - \bar{k}_t \varepsilon_2 \sin(\omega_2 t + \theta_{20}) \\
\quad + U_2 \omega_2^2 \sin(\omega_2 t + \theta_{20} + \theta_{f_2}) \\
\hline
U_2 \omega_2^2 \cos(\omega_2 t + \theta_{20} + \theta_{f_2}) \\
\hline
\bar{c}_t \{\varepsilon_2 \omega_2 \cos(\omega_2 t + \theta_{20}) + \varepsilon_1 \omega_1 \cos(\omega_1 t + \theta_{10})\} \\
\quad + \bar{k}_t \{\varepsilon_2 \sin(\omega_2 t + \theta_{20}) + \varepsilon_1 \sin(\omega_1 t + \theta_{10})\} \\
\hline
-\bar{c}_t r_1 \varepsilon_1 \omega_1 \cos(\theta_{10} + \omega_1 t) - F_0 \varepsilon_1 \cos(\theta_{10} + \omega_1 t) \\
\quad - \bar{k}_t r_1 \varepsilon_1 \sin(\theta_{10} + \omega_1 t) \\
\hline
-\bar{c}_t r_2 \varepsilon_2 \omega_2 \cos(\theta_{20} + \omega_2 t) + F_0 \varepsilon_2 \cos(\theta_{20} + \omega_2 t) \\
\quad - \bar{k}_t r_2 \varepsilon_2 \sin(\theta_{20} + \omega_2 t)
\end{Bmatrix}
\tag{2.27}
$$

6) Compute the natural frequency, mode shapes and dynamic response according to the Modal Analysis procedure described in section 2.4.2.

2.5.2 Numerical Results

The details of the geared shaft system used to obtain the numerical results are given in Table 2.3. The pedestals are assumed to be flexible in both y and z directions and the stiffnesses along these directions are denoted by k_{yy} and k_{zz} respectively. A finite element discretisation of a simple geared shaft system considered in Fig. 2.2 is shown in Fig. 2.12. The driving and driven shafts are divided into beam element 1 to 6 as shown. Each node of the system has 5 degrees of freedom excluding motion in the axial direction. The contact point of the mating gear teeth has one DOF on the z direction which accounts for tooth flexibility. The details of the beam elements comprising the finite element model are given in Table 2.4. The system natural frequencies and their gear ratio multiples in the range 0-80 Hz are given in Table 2.5. The zero natural frequency corresponds to a torsional rigid body mode.

The time domain response at two individual frequencies are plotted in Fig. 2.13 and Fig. 2.14. Fig. 2.13(a) shows the time domain response at the driven gear location at a frequency of 37 Hz which is very close to a system natural frequency. Fig. 2.13(b) shows the same at the driving gear location. Fig. 2.14(a) shows the time domain response at the driven gear location at a frequency of 50 Hz which is

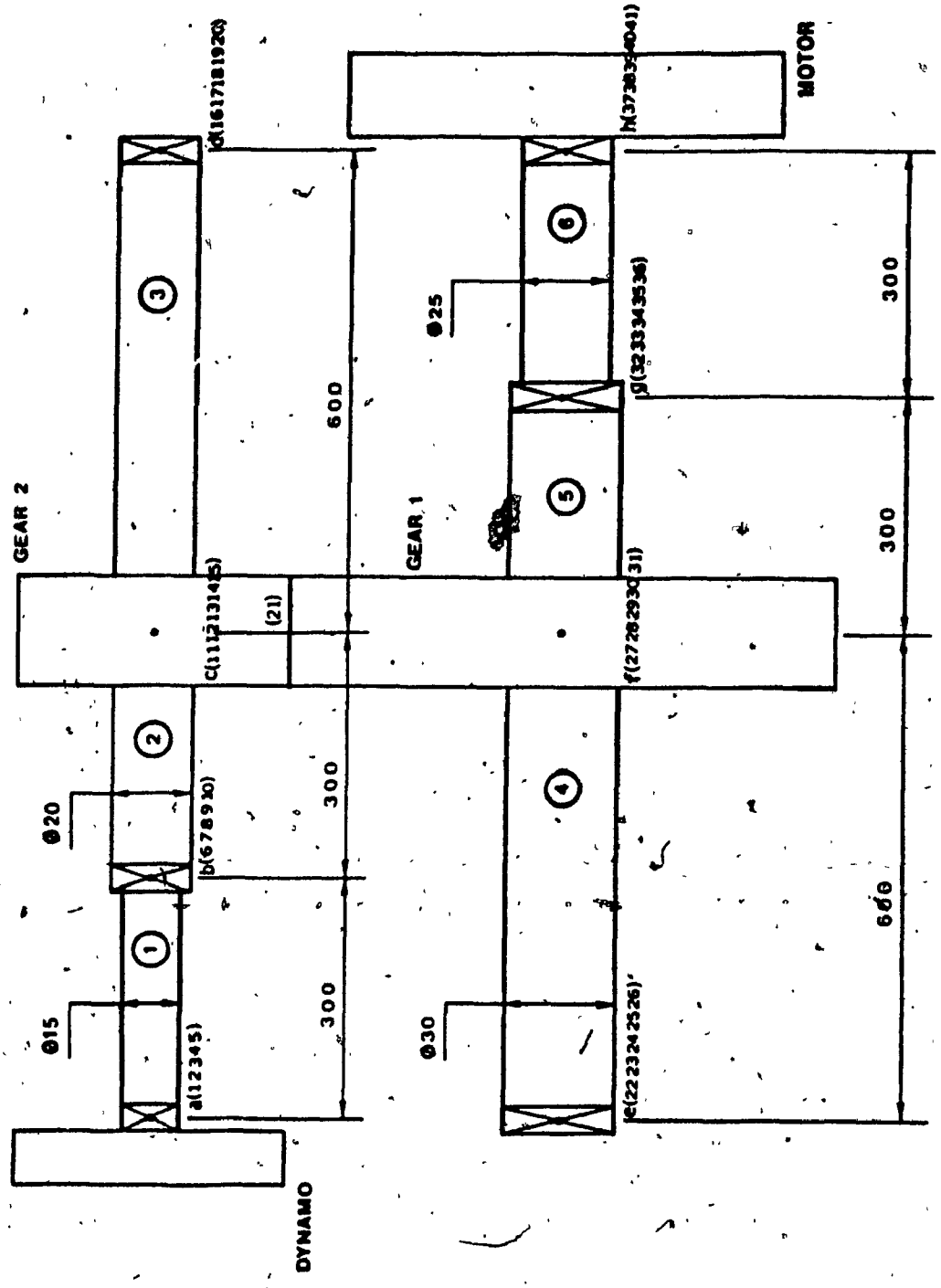

Fig. 2.12 Geared shaft system and its finite element discretisation.

TABLE 2.3

Details of the Geared Rotor System

E	1.96×10^{11} N/m^2
G	7.84×10^{10} N/m^2
I_1	3.0×10^{-2} kgm^3
I_2	6.28×10^{-3} kgm^2
J_1	4.59×10^{-1} kgm^2
J_2	5.49×10^{-1} kgm^2
$\bar{k}_t$	2.45×10^{9} N/m
k_{yy}	8.83×10^{8} N/m
k_{zz}	8.83×10^{8} N/m
m_1	16.96 kg
m_2	5.65 kg
m_{t1} , m_{t2}	4.9×10^{-3} kg
r_1	0.1 m
r_2	0.05 m
ε_1 , ε_2	120×10^{-3} m (variable)
U_1 , U_2	2.8×10^{-4} kgm (variable)

TABLE 2.4

Details of the Rotor Elements

Element No.	Length ℓ, m	Diameter d mm	Mass per unit length — m kg/m
1	0.3	0.015	1.41
2	0.3	0.020	2.51
3	0.6	0.020	2.51
4	0.6	0.030	5.655
5	0.3	0.030	5.655
6	0.3	0.025	3.93

TABLE 2.5

System Natural Frequencies and their Gear Ratio Multiples in the Range 0 - 80 Hz

Mode No.	System Natural Frequency	System Natural Frequency x Gear Ratio (= 2.)
1	zero	zero
2	7.78	15.56
3	21.27	42.54
4	22.96	45.92
5	29.22	58.44
6	35.46	70.92
7	36.57	73.14
8	44.09	--
9	71.39	--
10	71.57	--
11	72.24	--

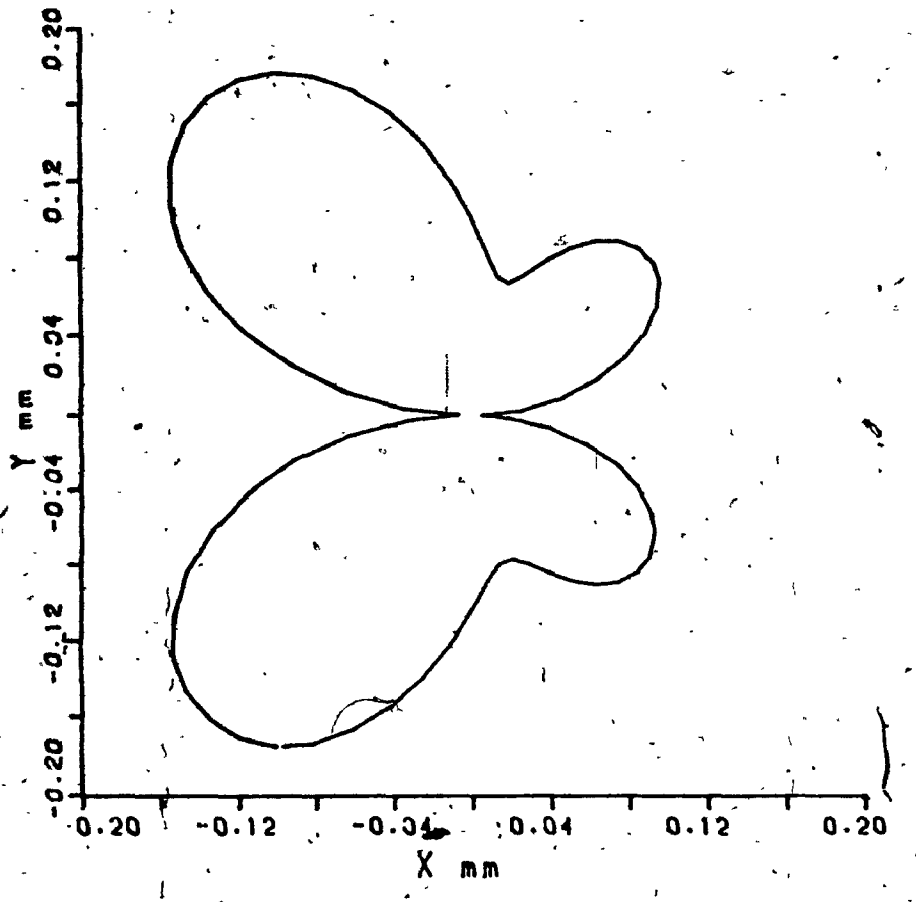

a) Driven Gear Location

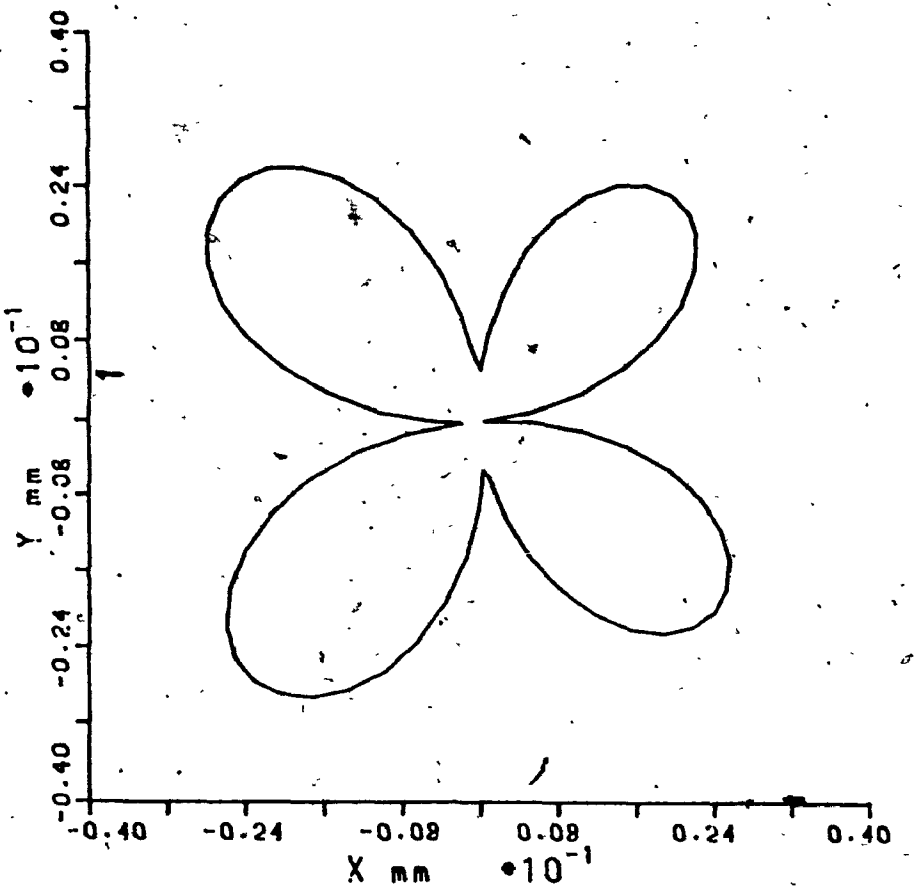

b) Driving Gear Location

Fig. 2.13 Time Domain Response at 38 Hz.

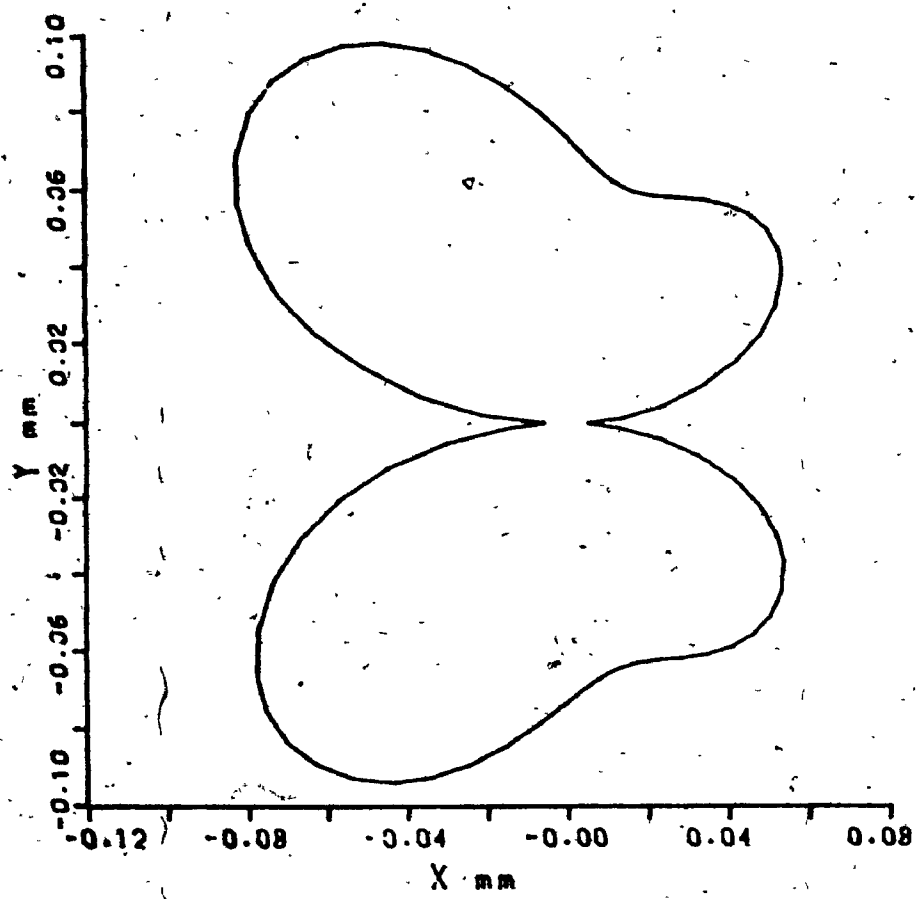

a) Driven Gear Location

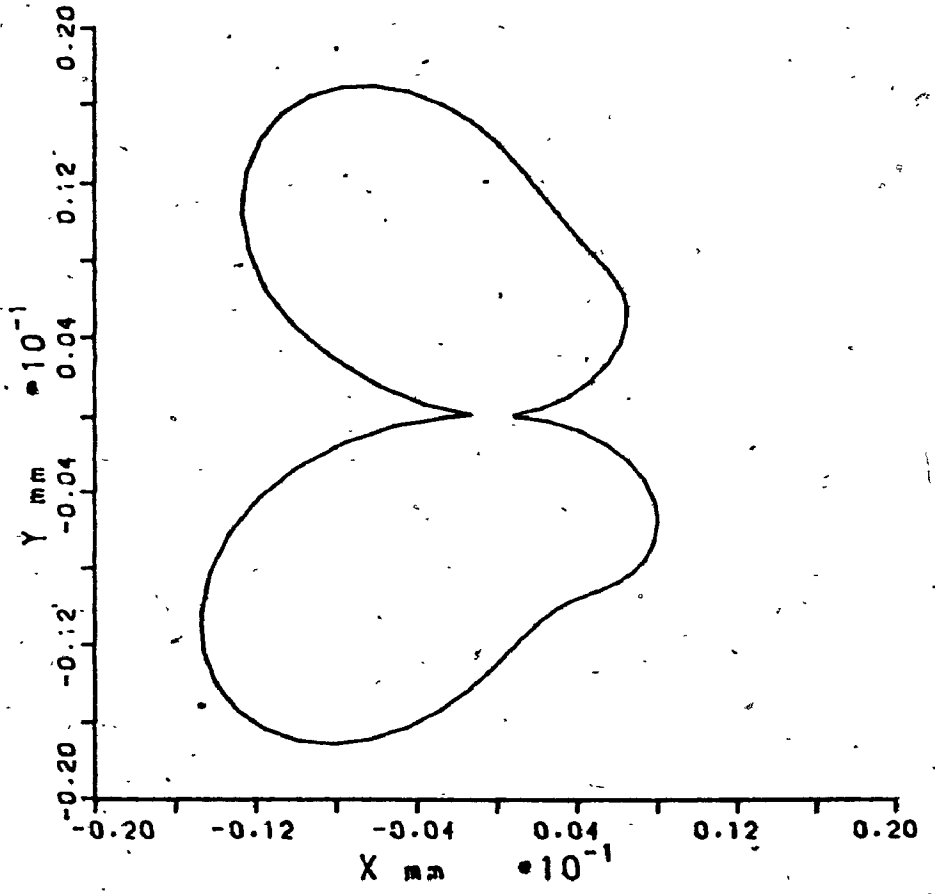

b) Driving Gear Location

Fig. 2.14 Time Domain Response at 50 Hz.

away from a system natural frequency. Fig. 2.14(b) shows the same at the driving gear location.

The frequency domain response is plotted for the flexural responses at the gear locations. Fig. 2.15 shows the response in the z direction at the driven gear location. The system shows peak responses at the system natural frequencies corresponding to modes 2, 4, 6 and 8, and also at the frequencies related to the modes 2, 4 and 6 by the gear ratio (Table 2.5). The natural frequency of mode 8 when multiplied by the gear ratio is found to be outside the frequency range of interest. Three cases corresponding to varying unbalance and eccentricity are plotted.

The response in the z direction at the driving gear location is shown in Fig. 2.16. The system shows peak responses at the system natural frequencies corresponding to modes 2, 4, 6 and 8, and also at frequencies related to the modes 2, 4, and 6 by the gear ratio (Table 2.5). The natural frequency of mode 8 when multiplied by the gear ratio is found to be outside the frequency range of interest. Three cases corresponding to varying unbalance and eccentricity are plotted.

2.6 Extension to a Geared Train of Rotors

The finite element formulation offers great ease in

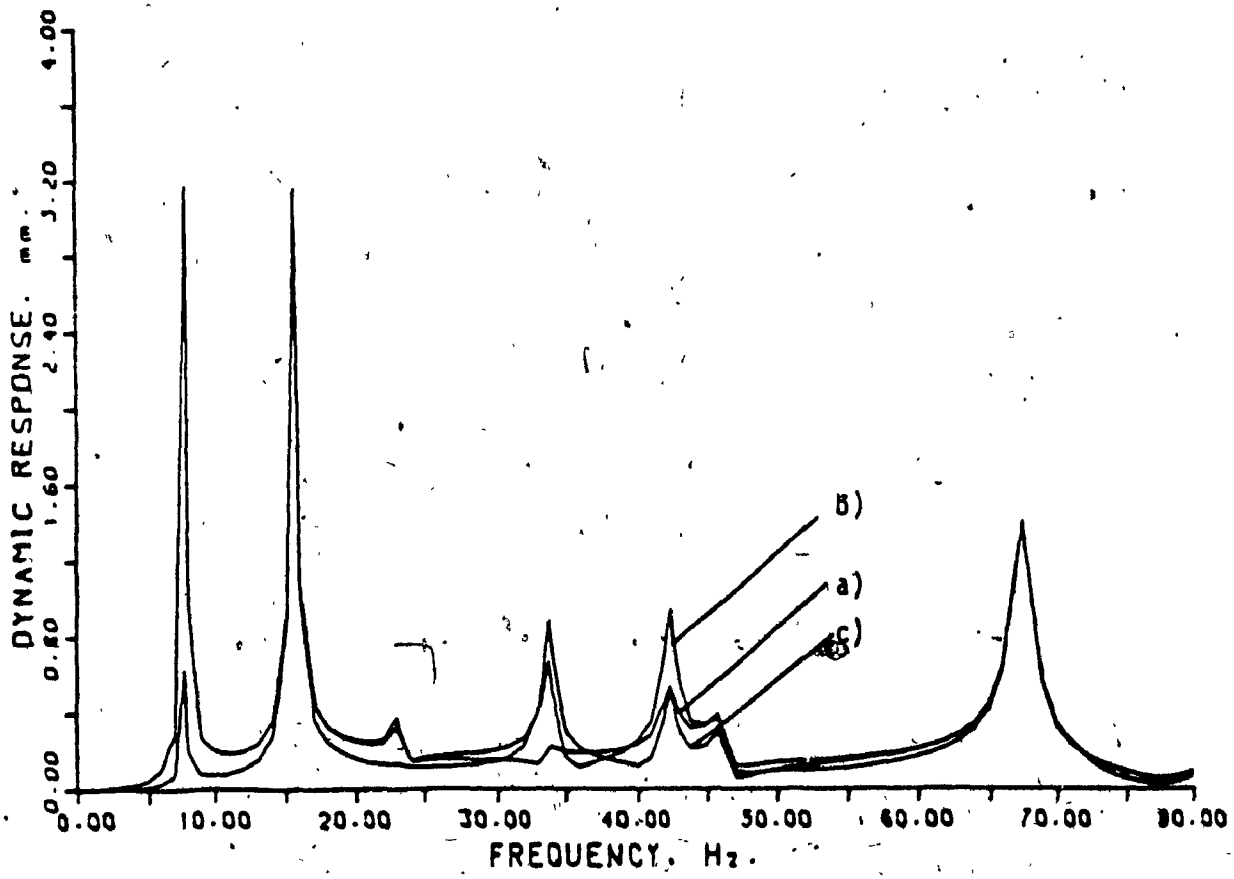

Fig. 2.15 Frequency domain response in the z direction at the driven gear location (DOF #12)

a) ε_1 = 120 μm, ε_2 = 20 μm, U_1 = 2.8×10^{-4}kgm, U_2 = 2.8×10^{-4}kgm

b) ε_1 = 120 μm, ε_2 = 120 μm, U_1 = 2.8×10^{-4}kgm, U_2 = 0.78×10^{-4}kgm

c) ε_1 = 120 μm, ε_2 = 120 μm, U_1 = 2.8×10^{-4}kgm, U_2 = 2.8×10^{-4}kgm

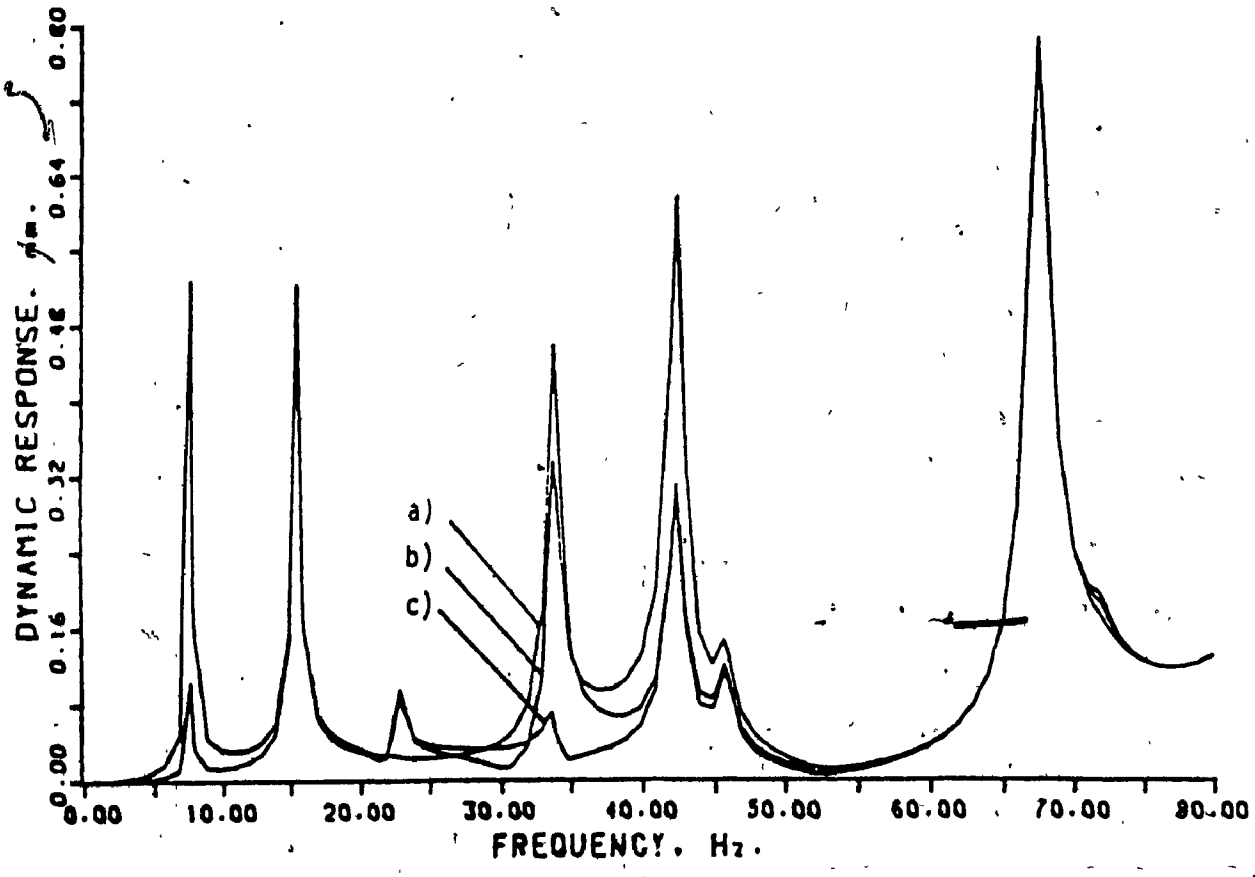

Fig. 2.16. Frequency domain response in the z direction at the driving gear location (DOF #28)

(a) ε_1 = 120 μm, ε_2 = 20 μm, $U_1 = 2.8 \times 10^{-4}$kgm, $U_2 = 2.8 \times 10^{-4}$kgm

b) ε_1 = 120 μm, ε_2 = 120 μm, $U_1 = 2.8 \times 10^{-4}$kgm, $U_2 = 0.78 \times 10^{-4}$kgm

c) ε_1 = 120 μm, ε_2 = 120 μm, $U_1 = 2.8 \times 10^{-4}$kgm, $U_2 = 2.8 \times 10^{-4}$kgm

extending the analysis of 2.5.1 to a geared train of rotors.

2.6.1 Analysis

A schematic representation of a geared train of rotors is shown in Fig. 2.17. A sectional view x-x at the ith gear pair location [see Fig. 2.17] is shown in Fig. 2.18 and it shows the relative positions of the driving and driven gears. O_1 and O_1' represent the geometric centers of the driving and driven shafts when they are rotating and O_3 and O_3' represent the centers of the driving and driven shafts when they are stationary. There exists a coupling between the translational motion of the gear center y, z; and the rotational motion of the gear θ. At the gear location they correspond to the flexural motion of the shaft carrying the gear and its torsional motion . Fig. 2.19(a) shows the spring mass representation for the driving gear of the jth gear pair. The mass of the driving gear tooth is denoted by m_{tlj}. The coordinates y_{tlj} and z_{tlj} describe the gear tooth motion. The time average stiffness and damping of the gear tooth in the y and z directions are denoted by $\bar{k}_{tyj}$, $\bar{k}_{tzj}$, $\bar{c}_{tyj}$, and $\bar{c}_{tzj}$ respectively. k_{blj} and c_{blj} denote the stiffness and damping of the shaft carrying the driving gear. The driven gear for the jth gear pair is similarly modelled and is shown in Fig. 2.19(b). The dynamical equations of

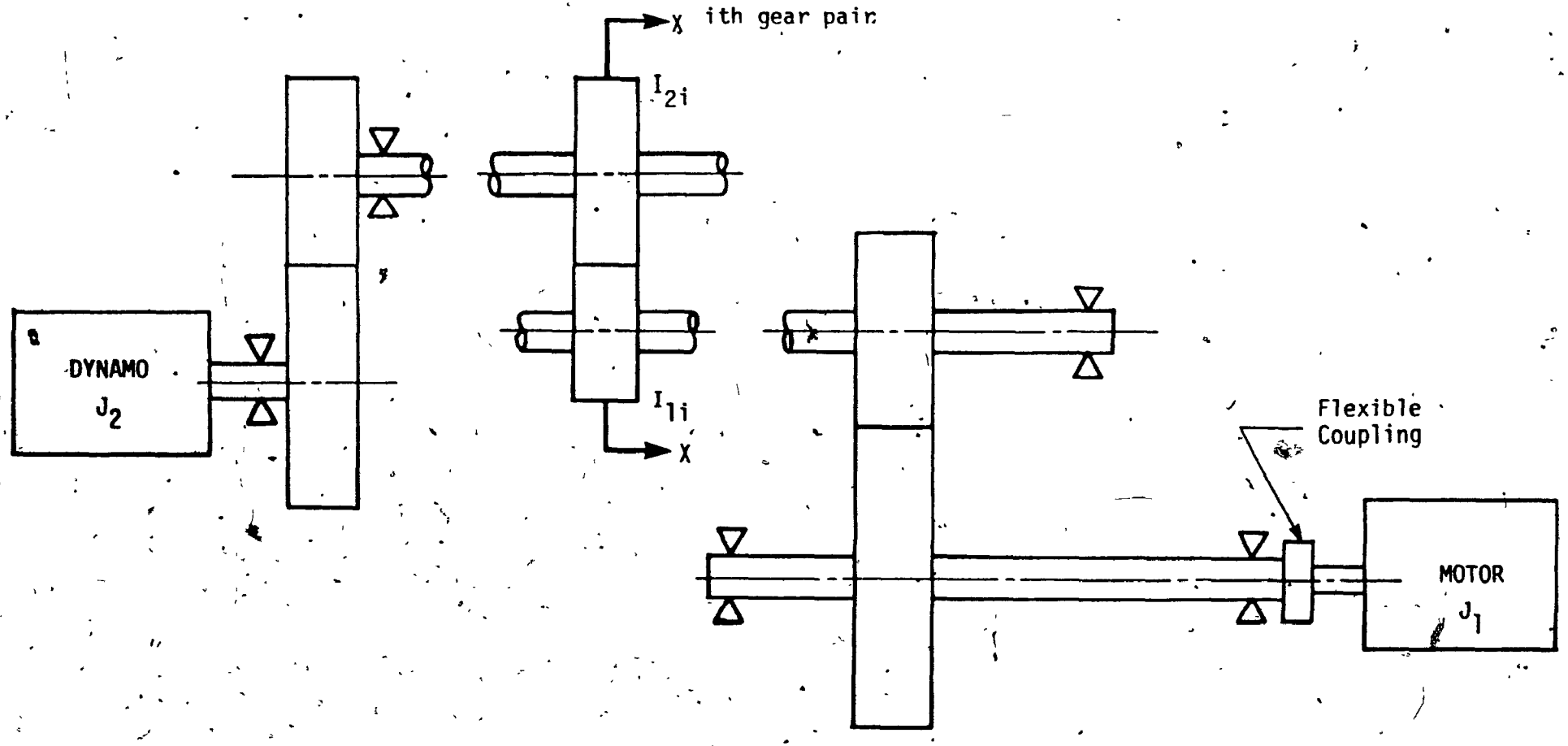

Fig. 2.17 Geared Train of Rotors

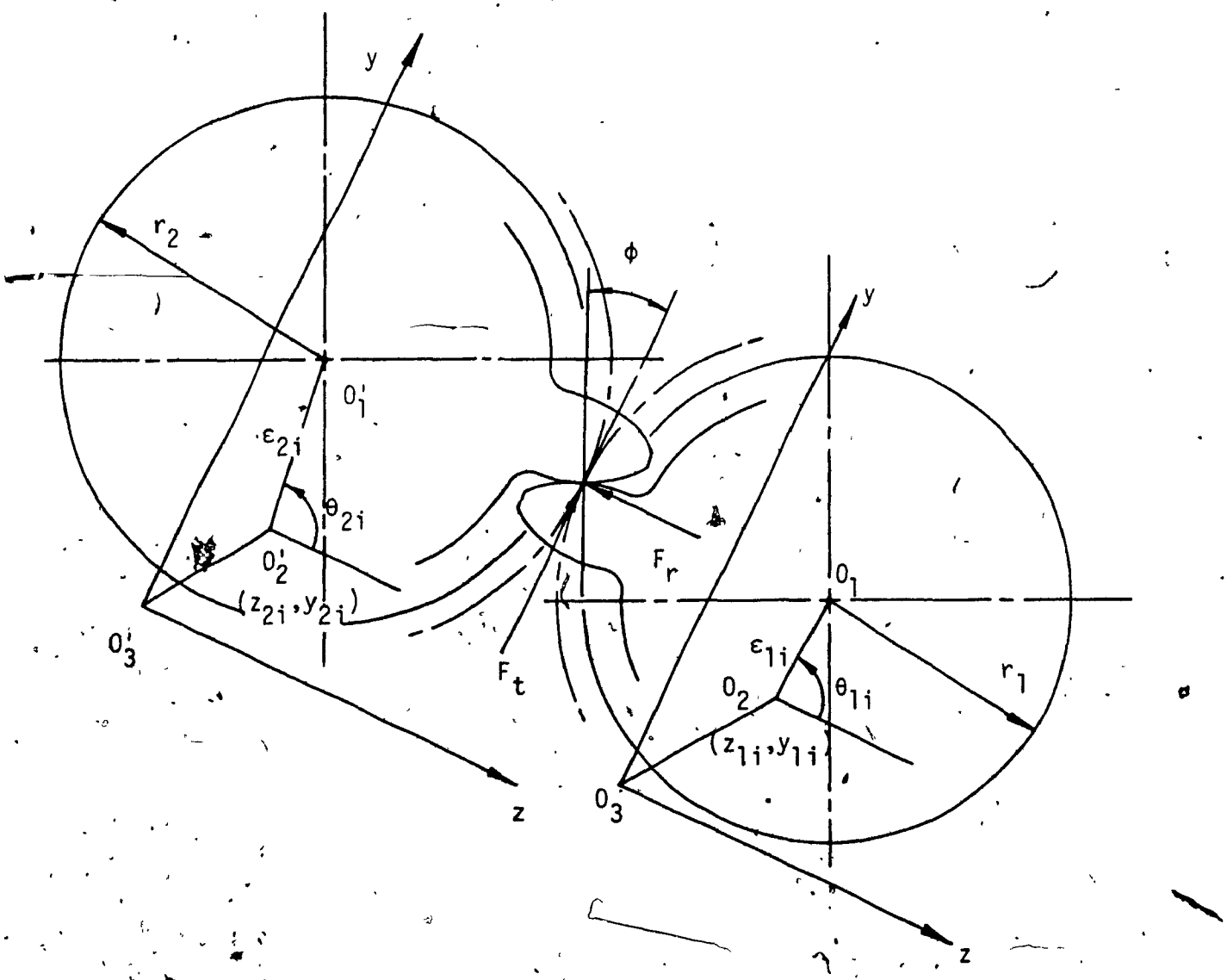

Fig. 2.18 -View at the ith gear pair location

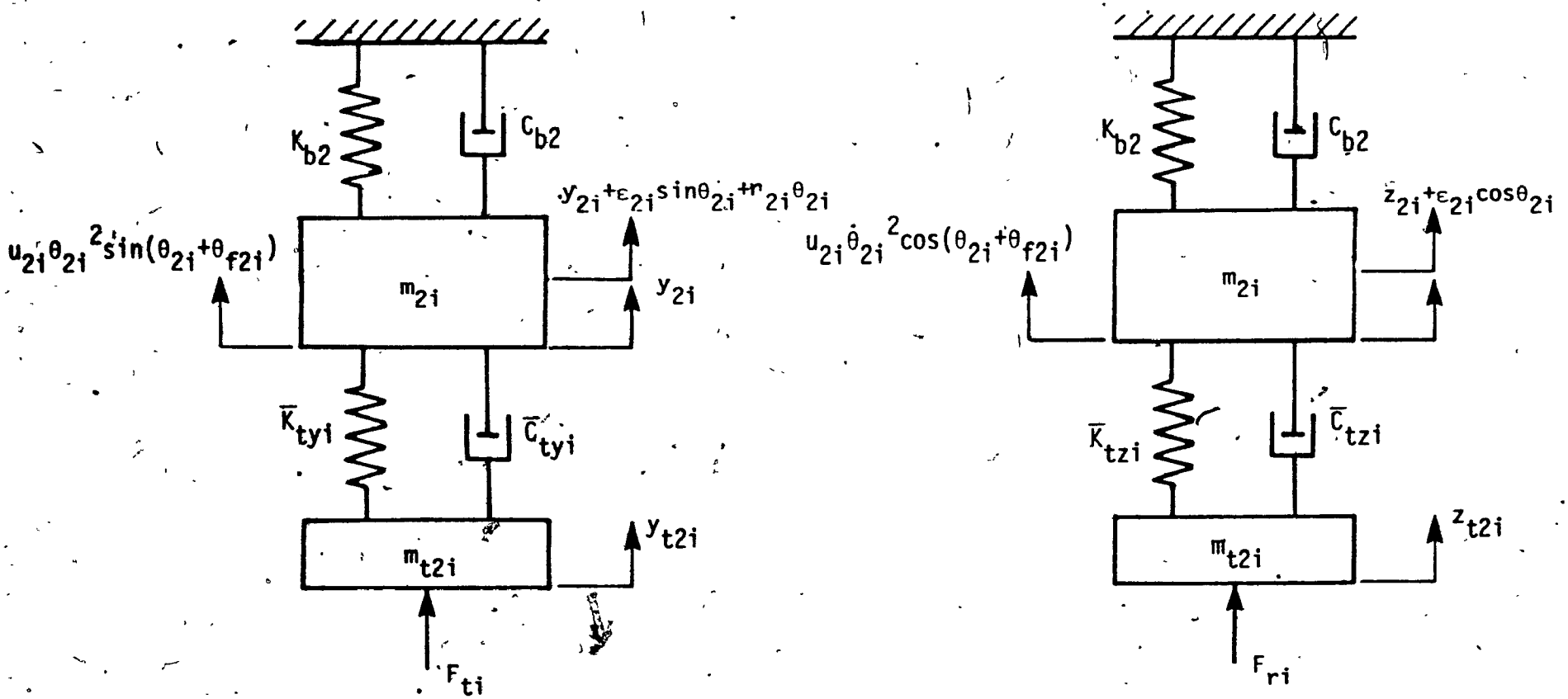

Fig. 2.19(a) Driven gear model in the y and z direction for the i th gear pair.

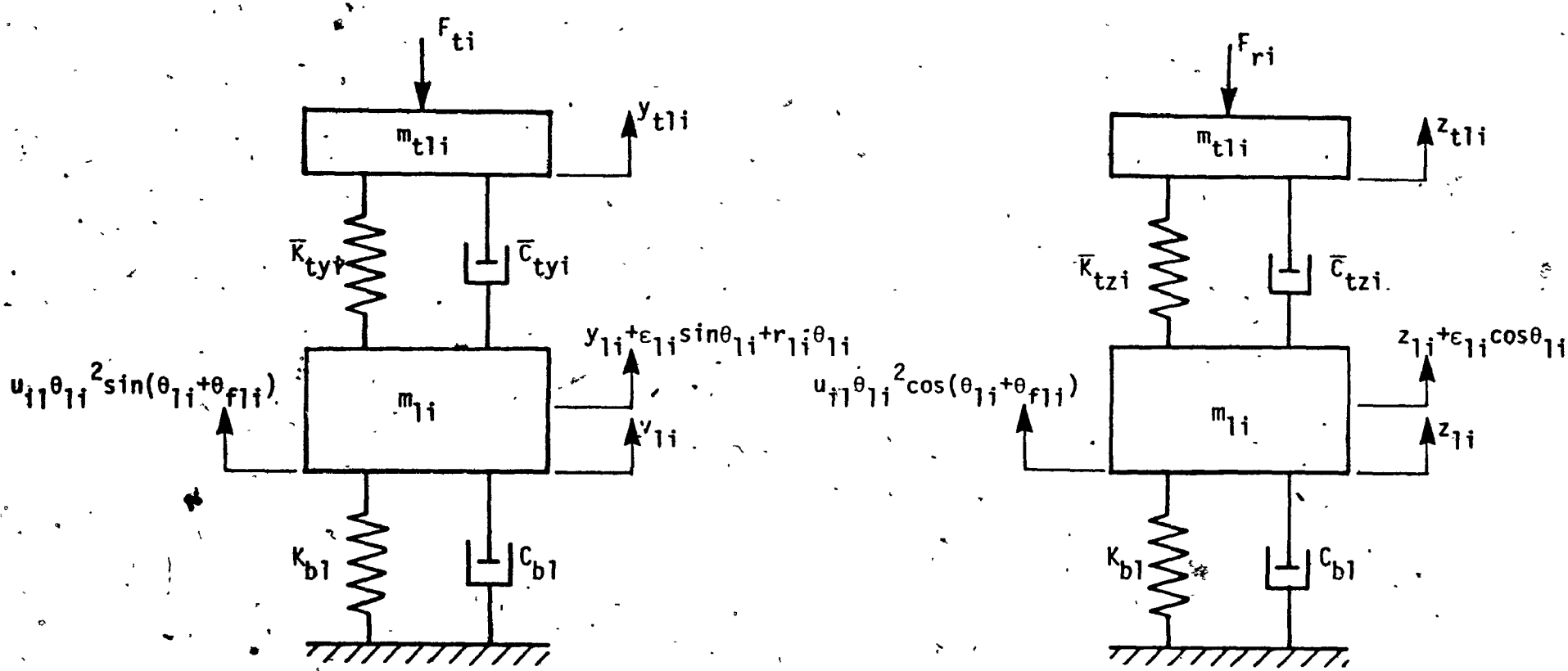

Fig. 2.19(b) Driving gear model in the y and z directions for the i th gear pair.

motion for a gear pair are derived following the approach in section 2.4.1 and they are,

$$m_{1j}\ddot{z}_{1j}+c_{b1j}\dot{z}_{1j}+k_{b1j}z_{1j} + \bar{k}_{tzj}(z_{1j}+\varepsilon_{1j}\cos\theta_{1j}-z_{t1j}) + \bar{c}_{tzj}(\dot{z}_{1j}-\varepsilon_{1j}\omega_{1j}\sin\theta_{1j}-\dot{z}_{t1j}) = U_{1j}\dot{\theta}_{1j}^{2}\cos(\theta_{1j}+\theta_{f1j}) \quad (2.28)$$

$$m_{2j}\ddot{z}_{2j}+c_{b2j}\dot{z}_{2j}+k_{b2j}z_{2j}+\bar{k}_{tzj}(z_{2j}+\varepsilon_{2j}\cos\theta_{2j}-z_{t2j}) + \bar{c}_{tzj}(\dot{z}_{2j}-\varepsilon_{2j}\omega_{2j}\sin\theta_{2j}-\dot{z}_{t2j}) = U_{2j}\dot{\theta}_{2j}^{2}\cos(\theta_{2j}+\theta_{f2j}) \quad (2.29)$$

$$m_{1j}\ddot{y}_{1j}+c_{b1j}\dot{y}_{1j}+k_{b1j}y_{1j} + \bar{c}_{tyj}(\dot{y}_{1j}+\varepsilon_{1j}\omega_{1j}\cos\theta_{1j}+r_{1j}\dot{\theta}_{1j}-\dot{y}_{t1j}) + \bar{k}_{tyj}(y_{1j}+\varepsilon_{1j}\sin\theta_{1j}+r_{1j}\theta_{1j}-y_{t1j}) = U_{1j}\dot{\theta}_{1j}^{2}\sin(\theta_{1j}+\theta_{f1j}) \quad (2.30)$$

$$m_{2j}\ddot{y}_{2j}+c_{b2j}\dot{y}_{2j}+k_{b2j}y_{2j} + \bar{c}_{tyj}(\dot{y}_{2j}+\varepsilon_{2j}\omega_{2j}\cos\theta_{2j}+r_{2j}\dot{\theta}_{2j}-\dot{y}_{t2j}) + \bar{k}_{tyj}(y_{2j}+\varepsilon_{2j}\sin\theta_{2j}+r_{2j}\theta_{2j}-y_{t2j}) = U_{2j}\dot{\theta}_{2j}^{2}\sin(\theta_{2j}+\theta_{f2j}) \quad (2.31)$$

$$m_{t1j}\ddot{z}_{t1j}+\bar{c}_{tzj}(\dot{z}_{t1j}-\dot{z}_{1j}+\varepsilon_{1j}\omega_{1j}\sin\theta_{1j}) + \bar{k}_{tzj}(z_{t1j}-z_{1j}\varepsilon_{1j}\cos\theta_{1j})=-F_{rj} \quad (2.32)$$

$$m_{t2j}\ddot{z}_{t2j}+\bar{c}_{tzj}(\dot{z}_{t2j}-\dot{z}_{2j}+\varepsilon_{2j}\omega_{2j}\sin\theta_{2j}) + \bar{k}_{tzj}(z_{t2j}-z_{2j}-\varepsilon_{2j}\cos\theta_{2j})=F_{rj} \quad (2.33)$$

$$m_{t1j}\ddot{y}_{t1j}+\bar{c}_{tyj}(\dot{y}_{t1j}-\dot{y}_{1j}-\varepsilon_{1j}\omega_{1j}\cos\theta_{1j}-r_{1j}\dot{\theta}_{1j})$$
$$+\bar{k}_{tyj}(y_{t1j}-y_{1j}-\varepsilon_{1j}\sin\theta_{1j}-r_{1j}\theta_{1j})=-F_{tj} \qquad (2.34)$$

$$m_{t2j}\ddot{y}_{t2j}+\bar{c}_{tyj}(\dot{y}_{t2j}-\dot{y}_{2j}-\varepsilon_{2j}\omega_{2j}\cos\theta_{2j}-r_{2j}\dot{\theta}_{2j})$$
$$+\bar{k}_{tyj}(y_{t2j}-y_{2j}-\varepsilon_{2j}\sin\theta_{2j}-r_{2j}\theta_{2j})=F_{tj} \qquad (2.35)$$

$$I_{1j}\ddot{\theta}_{1j}+k_{1j}(\theta_{1j}-\theta_M)+$$
$$\bar{c}_{tyj}(\dot{y}_{1j}+\varepsilon_{1j}\omega_{1j}\cos\theta_{1j}+r_{1j}\dot{\theta}_{1j}-\dot{y}_{t1j})(r_{1j}+\varepsilon_{1j}\cos\theta_{1j})$$
$$+\bar{k}_{tyj}(y_{1j}+\varepsilon_{1j}\sin\theta_{1j}+r_{1j}\theta_{1j}-y_{t1j})(r_{1j}+\varepsilon_{1j}\cos\theta_{1j})$$
$$+c_{1j}\dot{\theta}_{1j}=0 \qquad (2.36)$$

$$I_{2j}\ddot{\theta}_{2j}+k_{2j}(\theta_{2j}-\theta_L)$$
$$+\bar{c}_{tyj}(\dot{y}_{2j}+\varepsilon_{2j}\omega_{2j}\cos\theta_{2j}+r_{2j}\dot{\theta}_{2j}-\dot{y}_{t2j})(r_{2j}+\varepsilon_{2j}\cos\theta_{2j})$$
$$+\bar{k}_{tyj}(y_{2j}+\varepsilon_{2j}\sin\theta_{2j}+r_{2j}\theta_{2j}-y_{t2j})(r_{2j}+\varepsilon_{2j}\cos\theta_{2j})$$
$$+c_{2j}\dot{\theta}_{2j}=0 \qquad (2.37)$$

The condition that the mating teeth remain in contact is given by:

$$y_{t1j}=y_{t2j}$$
$$z_{t1j}=z_{t2j} \qquad (2.38)$$

The equations of motion are simplified and put in a matrix form, from which we obtain the stiffness terms coupling the torsional and flexural motions and also the forces occuring at a gear pair.

a. Stiffness Matrix

$$\begin{Bmatrix} z_{tj} \\ y_{tj} \\ z_{1j} \\ z_{2j} \\ y_{1j} \\ y_{2j} \\ \theta_{1j} \\ \theta_{2j} \end{Bmatrix} \rightarrow \begin{bmatrix} 2\bar{k}_{tzj} & 0 & -\bar{k}_{tzj} & -\bar{k}_{tzj} & 0 & 0 & 0 & 0 \\ 0 & 2\bar{k}_{tyj} & 0 & 0 & -\bar{k}_{tyj} & -\bar{k}_{tyj} & -\bar{k}_{tyj}r_{1j} & -\bar{k}_{tyj}r_{2j} \\ -\bar{k}_{tzi} & 0 & \bar{k}_{tzj} & 0 & 0 & 0 & 0 & 0 \\ -\bar{k}_{tzj} & 0 & 0 & \bar{k}_{tzj} & 0 & 0 & 0 & 0 \\ 0 & -\bar{k}_{tyj} & 0 & 0 & \bar{k}_{tyj} & 0 & \bar{k}_{tyj}r_{1j} & 0 \\ 0 & -k_{tyj} & 0 & 0 & 0 & k_{tyj} & 0 & \bar{k}_{tyi}r_{2j} \\ 0 & -\bar{k}_{tyj}r_{1j} & 0 & 0 & \bar{k}_{tyj}r_{1j} & -0 & \bar{k}_{tyj}r_{1j}^2 & 0 \\ 0 & -\bar{k}_{tzj}r_{2j} & 0 & 0 & 0 & \bar{k}_{tyj}r_{2j} & 0 & \bar{k}_{tyj}r_{2j}^2 \end{bmatrix} \quad (2.39)$$

b. Force Vector

$$
\begin{bmatrix} z_{tj} \\ y_{tj} \\ z_{1j} \\ z_{2j} \\ y_{1j} \\ y_{2j} \\ \theta_{1j} \\ \theta_{2j} \end{bmatrix}
\rightarrow
\begin{bmatrix}
-\bar{c}_{tzj}\varepsilon_{2j}\omega_{2j}\sin(\omega_{2j}t+\theta_{2oj})-\bar{c}_{tzj}\varepsilon_{1j}\omega_{j}\sin(\omega_{1j}t+\theta_{1oj}) \\
+\bar{k}_{tzj}\varepsilon_{2j}\cos(\omega_{2j}t+\theta_{2oj})+\bar{k}_{tzj}\varepsilon_{1j}\cos(\omega_{1j}t+\theta_{1oj}) \\
\hline
\bar{c}_{tyj}\varepsilon_{2j}\omega_{2j}\cos(\omega_{2j}t+\theta_{2oj})+\bar{c}_{tzj}\varepsilon_{1j}\omega_{1j}\cos(\omega_{1j}t+\theta_{1oj}) \\
+\bar{k}_{tyj}\varepsilon_{2j}\sin(\omega_{2j}t+\theta_{2oj})+\bar{k}_{tyj}\varepsilon_{1j}\sin(\omega_{1j}t+\theta_{1oj}) \\
\hline
-\bar{k}_{tzj}\varepsilon_{1j}\cos(\omega_{1j}t+\theta_{1oj})+\bar{c}_{tzj}\varepsilon_{1j}\omega_{1j}\sin(\omega_{1j}t+\theta_{1oj}) \\
+U_{1j}\omega_{1j}^{2}\cos(\omega_{1j}t+\theta_{1oj}+\theta_{f1j}) \\
\hline
-\bar{k}_{tzj}\varepsilon_{2j}\cos(\omega_{2j}t+\theta_{2oj})+\bar{c}_{tzj}\varepsilon_{2j}\omega_{2j}\sin(\omega_{2j}t+\theta_{2oj}) \\
+U_{2j}\omega_{2j}^{2}\cos(\omega_{2j}t+\theta_{2oj}+\theta_{f2j}) \\
\hline
-\bar{c}_{tyj}\varepsilon_{1j}\omega_{1j}\cos(\omega_{1j}t+\theta_{1oj})-\bar{k}_{tyj}\varepsilon_{1j}\sin(\omega_{1j}t+\theta_{1oj}) \\
+U_{1j}\omega_{1j}^{2}\sin(\omega_{1j}t+\theta_{1oj}+\theta_{f1j}) \\
\hline
-\bar{c}_{tyj}\varepsilon_{2j}\omega_{2j}\cos(\omega_{2j}t+\theta_{2oj})-\bar{k}_{tyj}\varepsilon_{2j}\sin(\omega_{2j}t+\theta_{2oj}) \\
+U_{2j}\omega_{2j}^{2}\sin(\omega_{2j}t+\theta_{2oj}+\theta_{f2j}) \\
\hline
-\bar{c}_{tyj}r_{1j}\varepsilon_{1j}\omega_{1j}\cos(\omega_{1j}t+\theta_{1oj}) \\
-\bar{k}_{tyj}r_{1j}\varepsilon_{1j}\sin(\omega_{1j}t+\theta_{1oj}) \\
-F_{oj}\cos\alpha\varepsilon_{1j}\sin(\omega_{1j}t+\theta_{1oj}) \\
\hline
-c_{tyj}r_{2j}\varepsilon_{2j}\omega_{2j}\cos(\omega_{2j}t+\theta_{2oj}) \\
-\bar{k}_{tyj}r_{2j}\varepsilon_{2j}\sin(\omega_{2j}t+\theta_{2oj}) \\
+F_{oj}\cos\alpha\varepsilon_{2j}\sin(\omega_{2j}t+\theta_{2oj})
\end{bmatrix}
\tag{2.40}
$$

The finite element analysis follows the same procedure as described in section 2.5.1.

The equations of motion of the system can now be written as

$$[M]\{\ddot{q}\} + [C]\{\dot{q}\} + [K]\{q\} = \{F\} \qquad (2.41)$$

The homogenous form of Eq. 2.41 neglecting damping is given by

$$[M]\{\ddot{q}\} + [K]\{q\} = \{0\}$$

and is solved to obtain the eigenvalues λ_i and the eigenvectors $\{\psi_i\}$ of the undamped system.

The force vector $\{F\}$ in Eq. (2.41) has the excitation consisting of frequencies ω_{1j} corresponding to the driving gear in the jth gear pair and ω_{2j} corresponding to the driven gear of the same gear pair. The force vector $\{F\}$ can be expressed as the sum of the sine and cosine components involving all the excitation frequencies as

$$\{F\} = \sum_{j=1}^{n} [\{F_{s1}\}_j \sin \omega_{1j}t + \{F_{s2}\}_j \sin \omega_{2j}t + \{F_{c1}\}_j \cos \omega_{1j}t + \{F_{c2}\}_j \cos \omega_{2j}t] \qquad (2.42)$$

where θ_{1oj}, θ_{2oj}, θ_{f1j} and θ_{f2j}, $j = 1, 2, 3 \ldots n$; have been assumed to be zero. The corresponding response also can be expressed in a form involving all the excitation frequencies as

$$\{q\} = \sum_{j=1}^{n} [\{q_{s1}\}_j \sin \omega_{1j}t + \{q_{s2}\}_j \sin \omega_{2j}t + \{q_{c1}\}_j \cos \omega_{1j}t + \{q_{c2}\}_j \cos \omega_{2j}t] \qquad (2.43)$$

Using Eq. (2.42) and (2.43), Eq. (2.41) can be written as

$$
\begin{aligned}
[M]\{\ddot{q}_{s1}\}_j + [C]\{\dot{q}_{s1}\}_j + [K]\{q_{s1}\}_j &= \{F_{s1}\}_j \\
[M]\{\ddot{q}_{s2}\}_j + [C]\{\dot{q}_{s2}\}_j + [K]\{q_{s2}\}_j &= \{F_{s2}\}_j \\
[M]\{\ddot{q}_{c1}\}_j + [C]\{\dot{q}_{c1}\}_j + [K]\{q_{c1}\}_j &= \{F_{c1}\}_j \\
[M]\{\ddot{q}_{c2}\}_j + [C]\{\dot{q}_{c2}\}_j + [K]\{q_{c2}\}_j &= \{F_{c2}\}_j \\
j = 1,2,\ldots n
\end{aligned}
\tag{2.44}
$$

Expressing the response $\{q\}$ in terms of the modal coordinates $\{p\}$ as

$$
\begin{aligned}
\{q_{s1}\}_j &= [\phi]\{p_{s1}\}_j \\
\{q_{s2}\}_j &= [\phi]\{p_{s2}\}_j \\
\{q_{c1}\}_j &= [\phi]\{p_{c1}\}_j \\
\{q_{c2}\}_j &= [\phi]\{p_{c2}\}_j \\
j &= 1,2, \ldots n
\end{aligned}
\tag{2.45}
$$

where $[\phi]$ is the modal matrix formed by using the eigenvector $\{\phi_i\}$, and $\{p_{s1}\}_j$, $\{p_{s2}\}_j$, $\{p_{c1}\}_j$ and $\{p_{c2}\}_j$ are the principal coordinate vectors corresponding to the j th gear pair. Using Eq. 2.45 in Eq. 2.44 and premultiplying by $[\phi]^T$ results in uncoupled equations in the modal coordinates of the form

$$
\begin{aligned}
\mu_i(\ddot{p}_{s1i})_j + \gamma_i(\dot{p}_{s1i})_j + \kappa_i(p_{s1i})_j &= (\sigma_{s1i})_j \\
\mu_i(\ddot{p}_{s2i})_j + \gamma_i(\dot{p}_{s2i})_j + \kappa_i(p_{s2i})_j &= (\sigma_{s2i})_j \\
\mu_i(\ddot{p}_{c1i})_j + \gamma_i(\dot{p}_{c1i})_j + \kappa_i(p_{c1i})_j &= (\sigma_{c1i})_j \\
\mu_i(\ddot{p}_{c2i})_j + \gamma_i(\dot{p}_{c2i})_j + \kappa_i(p_{c2i})_j &= (\sigma_{c2i})_j \\
\text{where } i = 1,2, \ldots N \text{ and } j &= 1,2,3 \ldots n
\end{aligned}
\tag{2.46}
$$

where μ_i and κ_i are the elements of diagonal matrices $[\mu]$ and $[\kappa]$ given by

$$[\mu] = [\tilde{\phi}]^T [M] [\phi]$$
$$[\kappa] = [\phi]^T [K] [\phi]$$

and γ_i and the equivalent damping coefficient in each mode. $(\sigma_{s1i})_j$, $(\sigma_{s2i})_j$, $(\sigma_{c1i})_j$ and $(\sigma_{c2i})_j$ are the elements of the generalized force vectors $\{\sigma_{s1}\}_j$, $\{\sigma_{s2}\}_j$, $\{\sigma_{c1}\}_j$ and $\{\sigma_{c2}\}_j$ given by

$$\{\sigma_{s1}\}_j = [\phi]^T \{F_{s1}\}_j$$
$$\{\sigma_{s2}\}_j = [\phi]^T \{F_{s2}\}_j$$
$$\{\sigma_{c1}\}_j = [\phi]^T \{F_{c1}\}_j$$
$$\{\sigma_{c2}\}_j = [\phi]^T \{F_{c2}\}_j$$
$$j = 1,2 \ldots n$$

The solution of Eq. (2.40) yields

$$(p_{s1i})_j = \frac{(\sigma_{s1i})_j}{(\omega_j^2 \mu_i + \kappa_i) + j'(\gamma_i \omega_j)}$$
$$(p_{s2i})_j = \frac{(\sigma_{s2i})_j}{(\omega_j^2 \mu_i + \kappa_i) + j'(\gamma_i \omega_j)}$$
$$(p_{c1i})_j = \frac{(\sigma_{c1i})_j}{(\omega_j^2 \mu_i + \kappa_i) + j'(\gamma_i \omega_j)}$$
$$(p_{c2i})_j = \frac{(\sigma_{c2i})_j}{(\omega_j^2 \mu_i + \kappa_i) + j'(\gamma_i \omega_j)} \qquad (2.47)$$

where $j' = \sqrt{-1}$, $i = 1,2, \ldots N$

$j = 1,2, \ldots n$

Using Eq. (2.47), (2.45) and (2.43) we can obtain the system dynamic response $\{q\}$.

2.6.2 Numerical Results

A geared train of rotors employing two pairs of gears is used to obtain the numerical results. The details of this system are given in Table 2.6. The pedestals are assumed to be flexible in both y and z directions and the stiffnesses along these directions are denoted by k_{yy} and k_{zz} respectively. The finite element discretization of the above system is shown in Fig. 2.20. The shafts are divided into beam elements 1 to 7 and the ten nodes of the system are denoted by a to j. The details of the beam elements are given in Table 2.7. The system natural frequencies and their two gear ratio multiples in the range 0 - 80 Hz are given in Table 2.8. The zero natural frequency corresponds to a torsional rigid body mode.

The frequency domain flexural response in the y direction at the driving gear location of the first gear pair (DOF #40) is shown in Fig. 2.21. The abscissa is frequency of rotation of the driven gear of the first gear pair (Gear 2). The system shows peak response at the system natural frequency and also at the frequencies which are gear ratio multiples of the system natural frequency. For example, when gear 2 rotates at 7.2 Hz which corresponds to a system natural frequency, the system experiences resonance. Now when the gear 2 rotates at 3.6 Hz the shaft carrying gear 4 rotates at 7.2 Hz which corresponds to a system natural frequency and the system experiences large flexural

TABLE 2.6

Details of the Rotor System under Study

E	1.96×10^{11} N/m^2
G	7.84×10^{10} N/m^2
I_{11}, I_{12}	0.03 kgm^2
I_{21}, I_{22}	0.0063 kgm^2
J_1	4.59×10^{-1} kgm^2
J_2	5.49×10^{-1} kg m^2
$\bar{k}_{ty}$	2.06×10^{9} N/m
$\bar{k}_{tz}$	2.60×10^{12} N/m
k_{yy}	9.6×10^{8} N/m
k_{zz}	9.6×10^{8} N/m
m_{11}, m_{12}	17.64 kg
m_{21}, m_{22}	5.88 kg
$(m_{t1})_i, (m_{t1})_i$ $(i = 1,2$	4.9×10^{-3} kg
r_{11}, r_{12}	0.1 m
r_{21}, r_{22}	0.05 m
$\epsilon_{1i}, \epsilon_{2i}$ $(i = 1,2)$	120×10^{-3} m
U_{1i}, U_{2i} $(i = 1,2)$	2.8×10^{-4} kgm (variable)

TABLE 2.7

Details of the Rotor Elements

Element No.	Length m	Diameter m	Mass per unit length m kg/m
1	0.35	0.020	2.51
2	0.3	0.015	1.41
3	0.3	0.020	2.51
4	0.6	0.020	2.51
5	0.6	0.030	5.655
6	0.3	0.030	5.655
7	0.3	0.025	3.93

TABLE 2.8

System Natural Frequencies and their Gear Ratio Multiples 0 - 80 Hz

$G_A = r_{11}/r_{21} = 2$; $G_B = r_{22}/r_{12} = 0.5$

Mode No.	System Natural Frequency Hz	S x G_A Hz	S x G_B Hz
1	zero	zero	zero
2	7.2	14.4	3.6
3	32.21	64.42	16.11
4	34.72	69.44	17.36
5	34.72	69.44	17.36
6	35.33	70.66	17.67
7	40.82		20.41
8	69.60		34.8
9	71.39		35.7
10	71.62		35.81
11			43.0
12			49.68
13			49.71

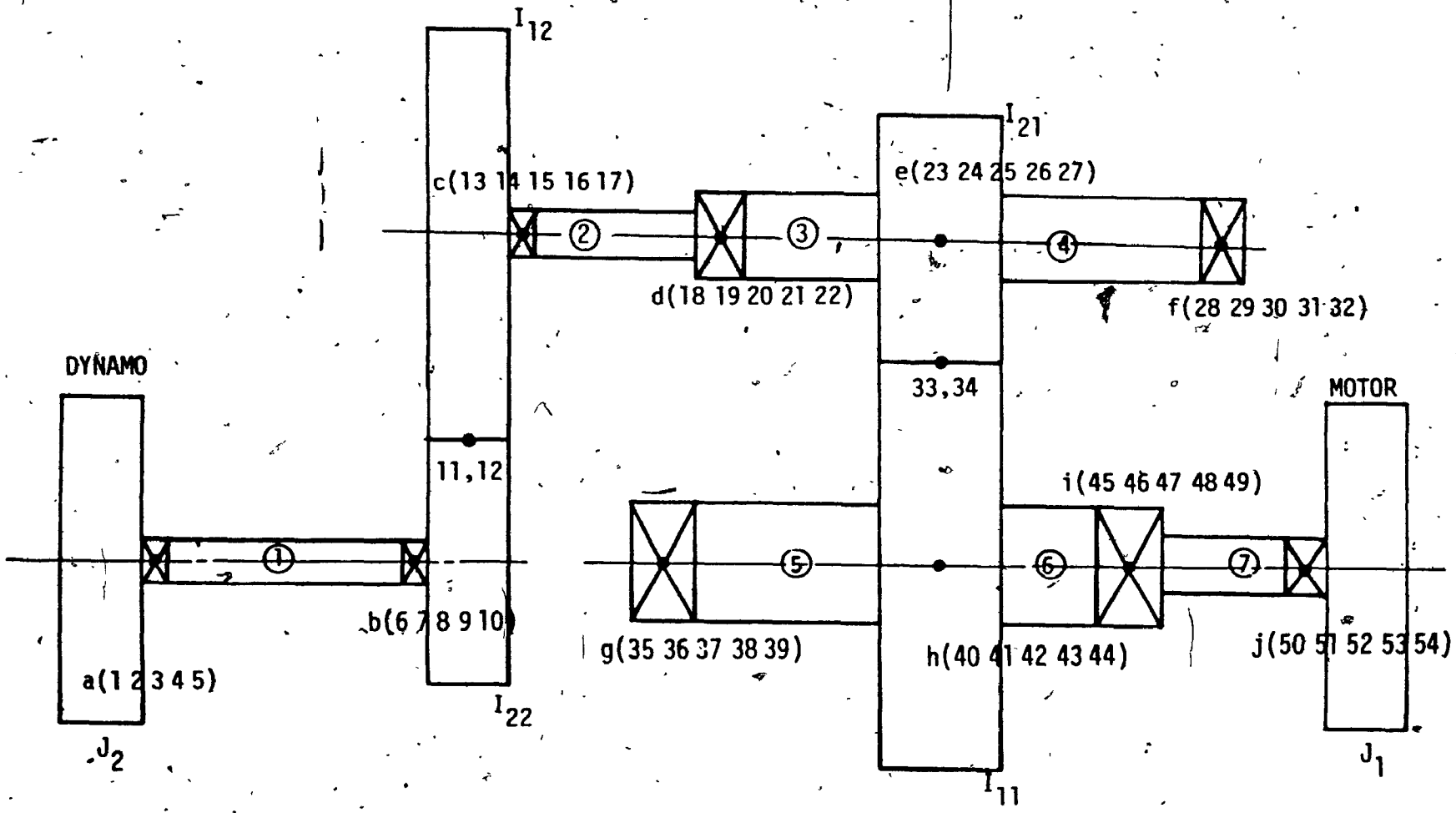

Fig. 2.20 Finite element discretisation of the geared train of rotors having two pairs of gears.

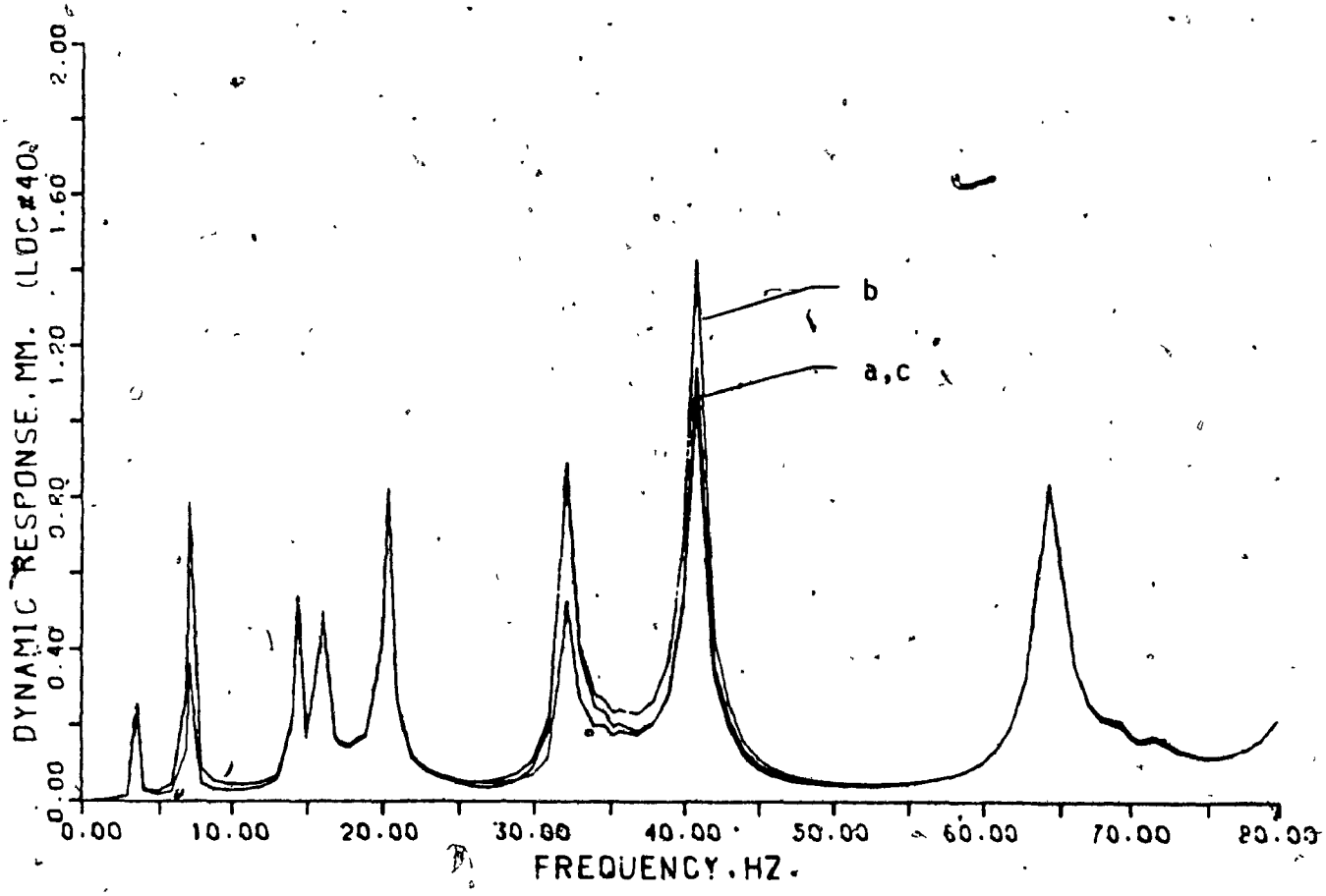

Fig. 2.21 : Frequency domain flexural response in the y direction at the driving gear location (DOF #40) of the first gear pair.

$\varepsilon_{11} = 120\ \mu m = \varepsilon_{12} = \varepsilon_{22}$; $U_{11} = 2.8 \times 10^{-4}$ kgm $= U_{12} = U_{22}$

a) $\varepsilon_{21} = 20\ \mu m$, $U_{21} = 2.8 \times 10^{-4}$ kgm

b) $\varepsilon_{21} = 120\ \mu m$, $U_{21} = .8 \times 10^{-4}$ kgm

c) $\varepsilon_{21} = 120\ \mu m$, $U_{21} = 2.8 \times 10^{-4}$ kgm

vibrations. Similarly when gear 2 rotates at 14.4 Hz, the shaft carrying gear 1 rotates at 7.2 Hz causing resonance. Some of the system natural frequencies and their gear ratio multiples are not excited because the generalized force corresponding to that mode is zero. Three cases are plotted for varying mass unbalance and geometrical eccentricity in the gears.

A similar behaviour is seen in Fig. 2.22 where the frequency domain flexural response in the y direction at the driven gear location of the first gear pair (DOF #23) is plotted. The plot of response is against the frequency of rotation of the gear 2. As in the previous case, the system experiences resonance not only at the system natural frequencies but also at both the gear ratio multiples. Some of the system natural frequencies and their gear ratio multiples are not excited because the generalized force corresponding to that mode is zero. Three cases corresponding to varying unbalance and eccentricity are plotted.

2.7 Complex Modal Analysis

The equations of motion for a damped N degree of freedom system can be written as

$$[M]_{NxN}\{\ddot{q}\}_{Nx1} + [C]_{NxN}\{\dot{q}\}_{Nx1} + [K]_{NxN}\{q\}_{Nx1} = \{F\}_{Nx1}$$

In addition to the effective forces due to viscous damping

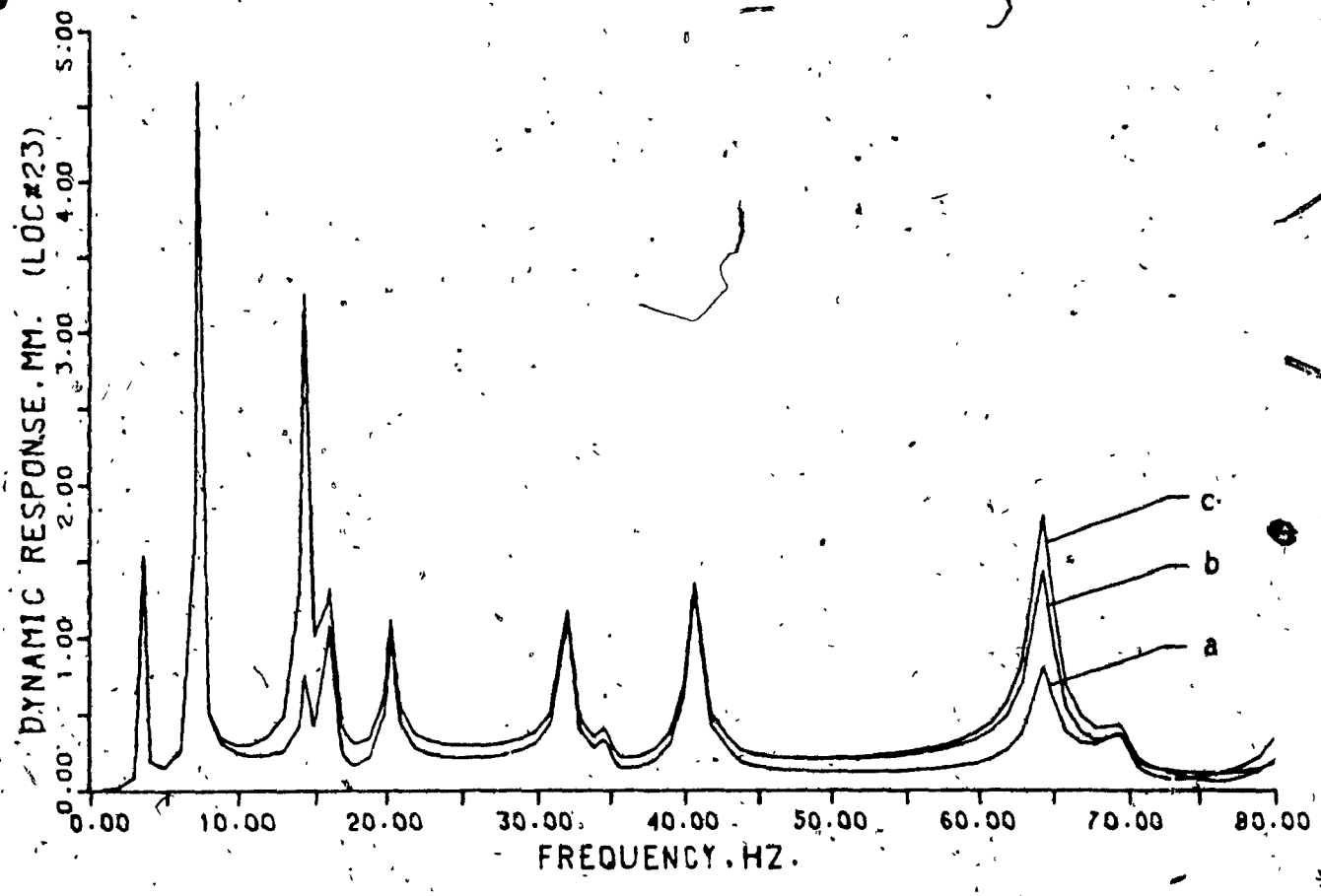

Fig. 2.22 : Frequency domain flexural response in the y direction at the driven gear location (DOF #23) of the first gear pair

$\varepsilon_{21} = 120\ \mu m = \varepsilon_{12} = \varepsilon_{22}$; $U_{21} = 2.8 \times 10^{-4}$ kgm $= U_{12} = U_{22}$

a) $\varepsilon_{11} = 20\ \mu m$, $U_{11} = 2.8 \times 10^{-4}$ kgm

b) $\varepsilon_{11} = 120\ \mu m$, $U_{11} = 0.8 \times 10^{-4}$ kgm

c) $\varepsilon_{11} = 120\ \mu m$, $U_{11} = 2.8 \times 10^{-4}$ kgm

and elastic forces, gyroscopic forces also act on a spinning structure. The effect of the gyroscopic forces on a rotating geared shaft system can be represented by a gyroscopic matrix $[G]_{NxN}$.

The equations of motion of a system including the gyroscopic effects can be written as

$$[M]\{\ddot{q}\} + [C+G]\{\dot{q}\} + [K]\{q\} = \{F\} \qquad (2.48)$$

In the analysis so far, the damping in the system was in the form of a modal damping which is a form of proportional damping, where the damping matrix can be expressed as a linear combination of the mass and stiffness matrices (both of which are symmetric). Hence normal mode analysis employing undamped modes could be used to uncouple the equations of motion.

However, when the gyroscopic effects are considered the problem becomes more complicated. This is because the gyroscopic matrix [G] is skew symmetric in nature and hence, a normal mode analysis is not possible.

2.7.1 Analysis

Expressing Eq. (2.48) of order N as 2N first-order equations we get

$$\left[\begin{array}{c|c} [M] & [0] \\ \hline [0] & [K] \end{array}\right] \begin{Bmatrix} \ddot{q} \\ \dot{q} \end{Bmatrix} + \left[\begin{array}{c|c} [C+G] & [K] \\ \hline -[K] & [0] \end{array}\right] \begin{Bmatrix} \dot{q} \\ q \end{Bmatrix} = \begin{Bmatrix} F \\ 0 \end{Bmatrix} \qquad (2.49)$$

This can be written as,

$$[m]\ \{\dot{x}\} + [k]\ \{x\} = \{f\} \qquad (2.50)$$

where $[m] = \left[\begin{array}{c|c} [M] & [0] \\ \hline [0] & [K] \end{array}\right]$

$$[k] = \left[\begin{array}{c|c} [C+G] & [K] \\ \hline -[K] & [0] \end{array}\right]$$

Meirovitch [89] discusses the case when [m] is postive definite and [k] is skew symmeteric. The eigenvalue problem defined by these two matrices was reduced to an eigenvalue problem defined by two real symmetric matrices of order N x N possessing real solutions.

In the present study, the matrix [m] is not positive definite, because of the presence of the rigid body mode and therefore the above analysis cannot be used. Hence a complex modal analysis employing biorthogonality relations is carried out. Biorthogonality relations is the orthogonality relation between the eigenvectors of the original system (right eigenvectors) and the corresponding vectors of the adjoint system (left eigenvectors). The adjoint system is obtained by transposing the system matrices in the original system.

The homogeneous form of Eq. (2.50).

$$[m]\ \{\dot{x}\} + [k]\ \{x\} = \{0\} \qquad (2.51)$$

is solved to obtain the complex eigenvalues λ_i and complex right eigenvectors $\{\phi_i\}$ of the system. Taking the transpose of the system matrices [m] and [k] and writing down an

equation similar to (2.51) we get

$$[m]^T \{\dot{x}\} + [k]^T \{x\} = \{0\} \qquad (2.52)$$

This equation is solved to obtain the eigenvalues λ_i and left eigenvectors $\{\rho_i\}$ of the system. Note that the eigenvalues λ_i are same for both the systems.

The original system coordinates $\{x\}$ are transformed to modal coordinates $\{p\}$ by the transformation

$$\{x\} = [\phi] \{p\} \qquad (2.53)$$

where $[\phi]$ is the modal matrix formed by concatenating the right eigenvectros $\{\phi_i\}$. Substituting this in Eq. (2.50) we get

$$[m] [\phi] \{\dot{p}\} + [k] [\phi] \{p\} = \{f\}$$

Multiplying throughout by $[\rho]^T$, which is the transpose of the matrix formed by concatenating all the left eigenvectors $\{\rho_i\}$ we get

$$[\rho]^T[m][\phi]\{\dot{p}\} + [\rho]^T[k][\phi]\{p\} = [\rho]^T\{f\} \qquad (2.54)$$

Using the biorthogonality property,

$$[\rho]^T [m] [\phi] = [\mu]$$

$$[\rho]^T [k] [\phi] = [\kappa]$$

Eq. (2.54) can be written as

$$[\mu] \{\dot{p}\} + [\kappa] \{p\} = \{\mathcal{F}\} \qquad (2.55)$$

The solution to which is

$$p_i(t) = \frac{\mathcal{F}_i(t)}{\kappa_i + j\omega\mu_i} \qquad i = 1,2.....2N$$

Substituting this in Eq. 2.53 we can obtain the dynamic response $\{x\}$.

2.7.2 Numerical Results

A simple geared shaft system considered in Fig. 2.2 is discretised using finite beam elements as shown in Fig. 2.23. The driving and driven shafts are both divided into beam elements 1 to 4 as shown. Each node of the system has 5 degrees of freedom excluding motion in the axial direction. The contact point of the mating gear teeth has one DOF in the z direction which accounts for tooth flexibility. As seen in Fig. 2.23, the supports are assumed to be rigid. The details of the beam elements comprising the finite element model are given in Table 2.9. The other details such as masses of the gears are as given in Table 2.3. The complex eigenvalues of the system vary with the rotational speed of the shaft and consist of a real component which accounts for the damping and an imaginary component which is a measure of the frequency. The system natural frequency when the driven shaft is rotating at 3000 rpm is given in Table 2.10.

The flexural response at the driven gear in the z direction (DOF #5) against the speed of rotation of the driven gear is shown in Fig. 2.24. The system seems to show resonance at some of the natural frequencies and their gear ratio multiples. A similar behaviour is seen in Fig. 2.25. When the flexural response at the driving gear in the z direction (DOF #17) is plotted against the speed of rotation of the driven gear.

TABLE 2.9

Details of the Rotor Elements

Element No.	Length m	Diameter m	Mass per unit length $\bar{m}$ Kg/m
1	0.3	0.02	2.51
2	0.6	0.02	2.51
3	0.6	0.03	5.655
4	0.3	0.03	5.655

TABLE 2.10

System Natural Frequency 0-80 Hz when the Driven Shaft Rotates at 3000 rpm

1	0.0
2	2.97
3	10.8
4	16.67
5	24.7
6	44.0
7	52.76
8	66.84

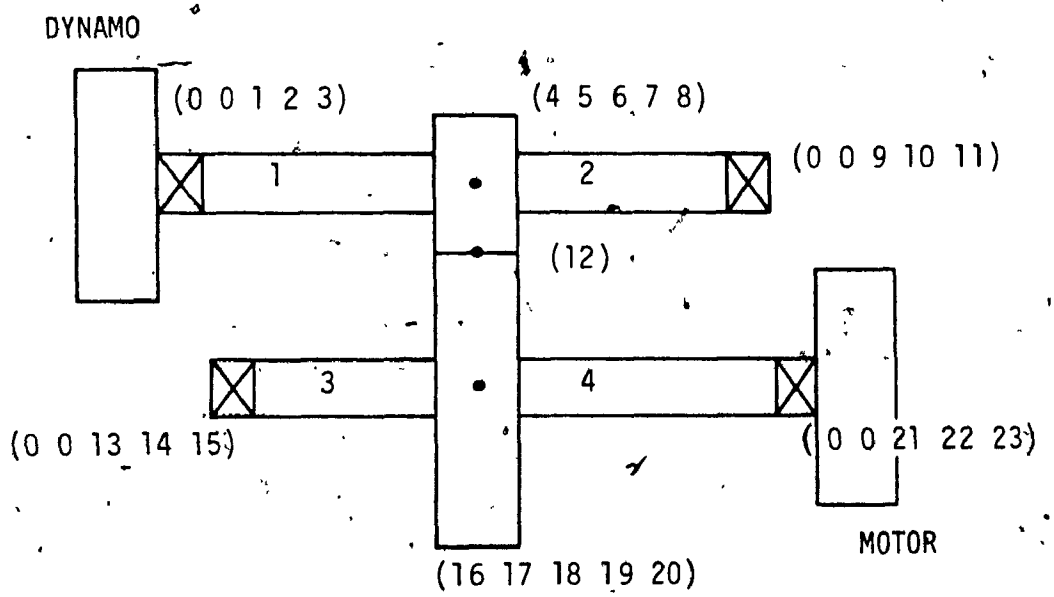

Fig. 2.23. Geared shaft system and its finite element discretisation

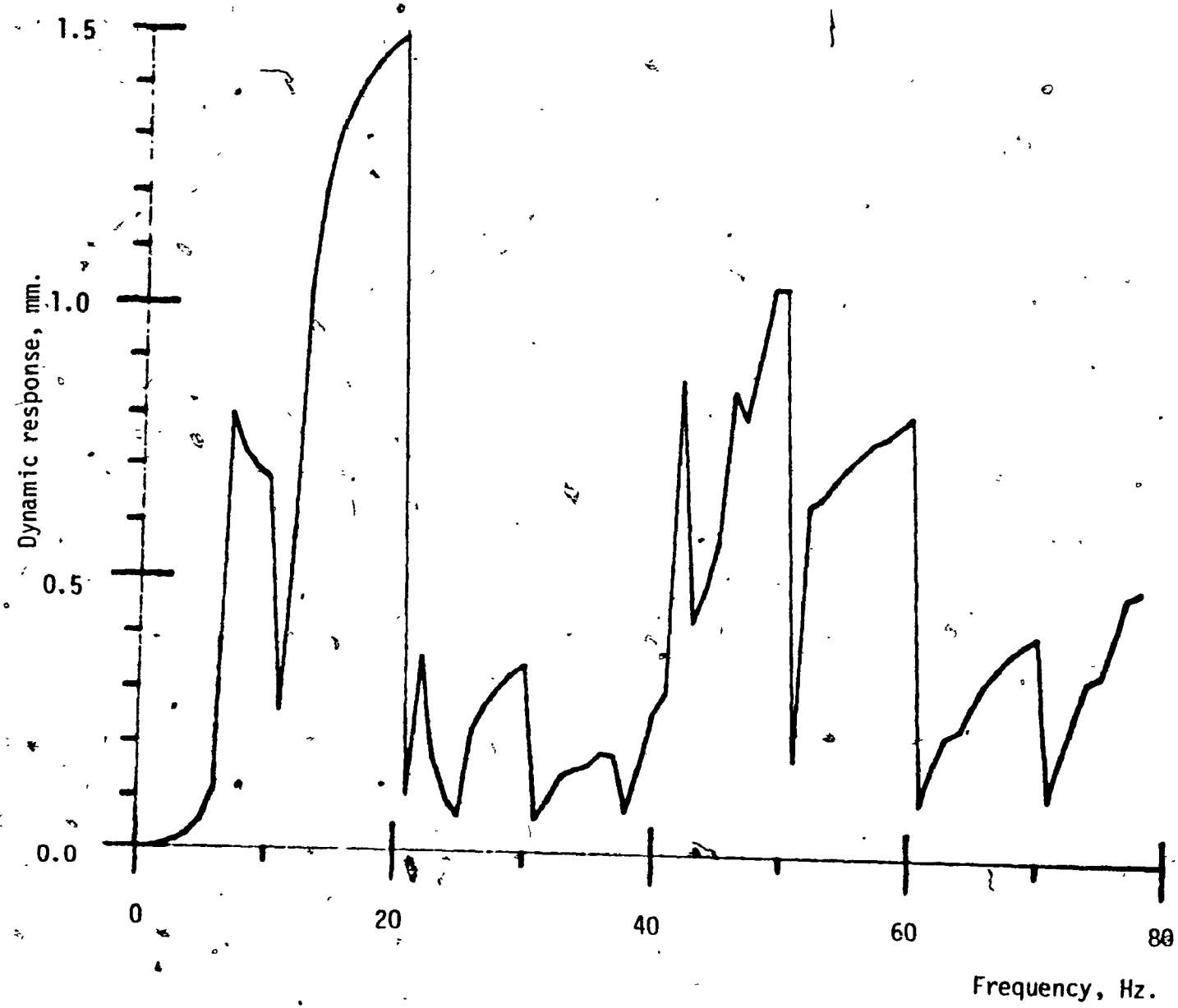

Fig. 2.24 Flexural response at the driven gear in the z direction (DOF #15) against the speed of rotation of the driven gear.

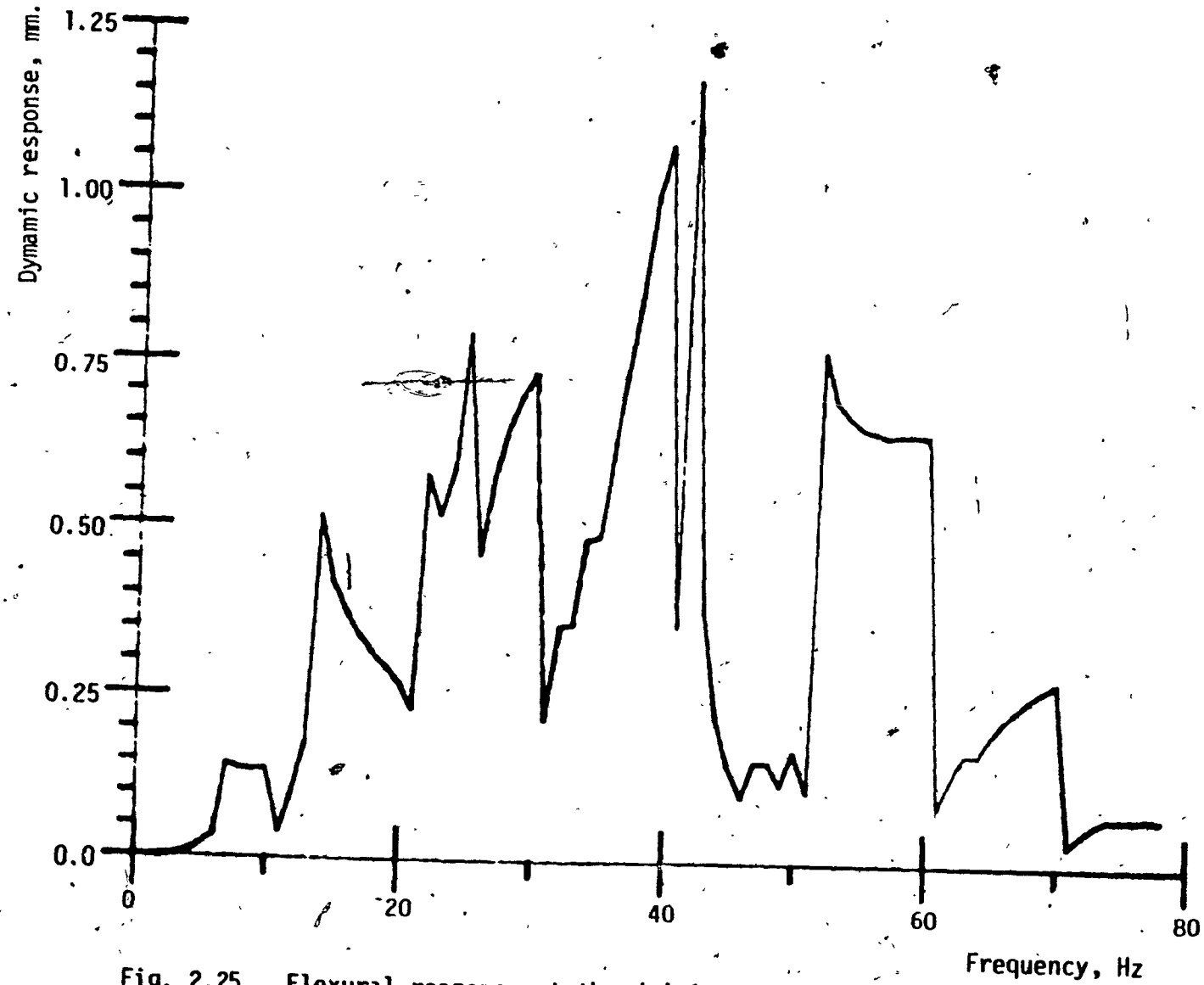

Fig. 2.25 Flexural response at the driving gear in the z direction (DOF #17) against the speed of rotation of the driven gear.

The results of the analysis in this section have the expected behaviour, showing peaks at the system natural frequencies and frequencies related to them thorough gear ratio.

2.8 The Effect of Random Static Transmission Error

As discussed in section 2.2, it is now generally recognised that the static transmission error describes the principal source of internal excitation of gear systems.

Tuplin [6] and Reswick [8] studied the excitation of a geared shaft system by profile errors. They treated the profile error as a transient excitation. During the meshing of gear wheels, the entry of the high tooth, for instance, was regarded as the introduction of a thin wedge between two perfect teeth. The dynamic loads were then estimated. Mahalingam and Bishop [11] determined the dynamic tooth load due to excitation in the form of a wedge simulating the static transmission error, periodically introduced between two perfectly mating teeth. A harmonic analysis of the static transmission curve showed that a significant component of the excitation has the frequency of tooth mesh. Mark [13] and Tobe et al. [16] decomposed the static transmission error into mean and random components. Tobe et al. [16] also studied the effect of the random component on the dynamic tooth load of a geared shaft system which was described by a simple SDOF model.

2.8.1 Analysis

In this section, the dynamic response and tooth load of a geared shaft system modelled in section 2.4.1 driven by the random component of the static transmission error is studied.

The dynamical equations of motion for the geared shaft system described in section 2.4.1 are given by Equations (2.3) - (2.10).

The STE, e(t), is composed of deterministic components $e_p(t)$ and random components $e_r(t)$ given by

$$e(t) = e_p(t) + e_r(t)$$

and is introduced in the form of a wedge between two perfectly mating teeth, as shown in Fig. 2.26. The condition that the meshing teeth are always in contact is expressed as

$$y_{t1} + e(t) = y_{t2} \tag{2.56}$$

Using (2.56) in (2.3) - (2.10) and following the same procedure described in section 2.4, the equations of motion can be written as:

$$[M]\{\ddot{q}\} + [C]\{\dot{q}\} + [K]\{q\} = \{F\} \tag{2.57}$$

where the generalised displacement vector is given by

$$\{q\} = [\Delta y_1, \Delta y_2, \Delta y_t, \Delta\theta_M, \Delta\theta_1, \Delta\theta_2, \Delta\theta_L] \tag{2.58}$$

The matrices [M], [C] and [K] are described by Equations (2.15a), (2.15b) and (2.15c).

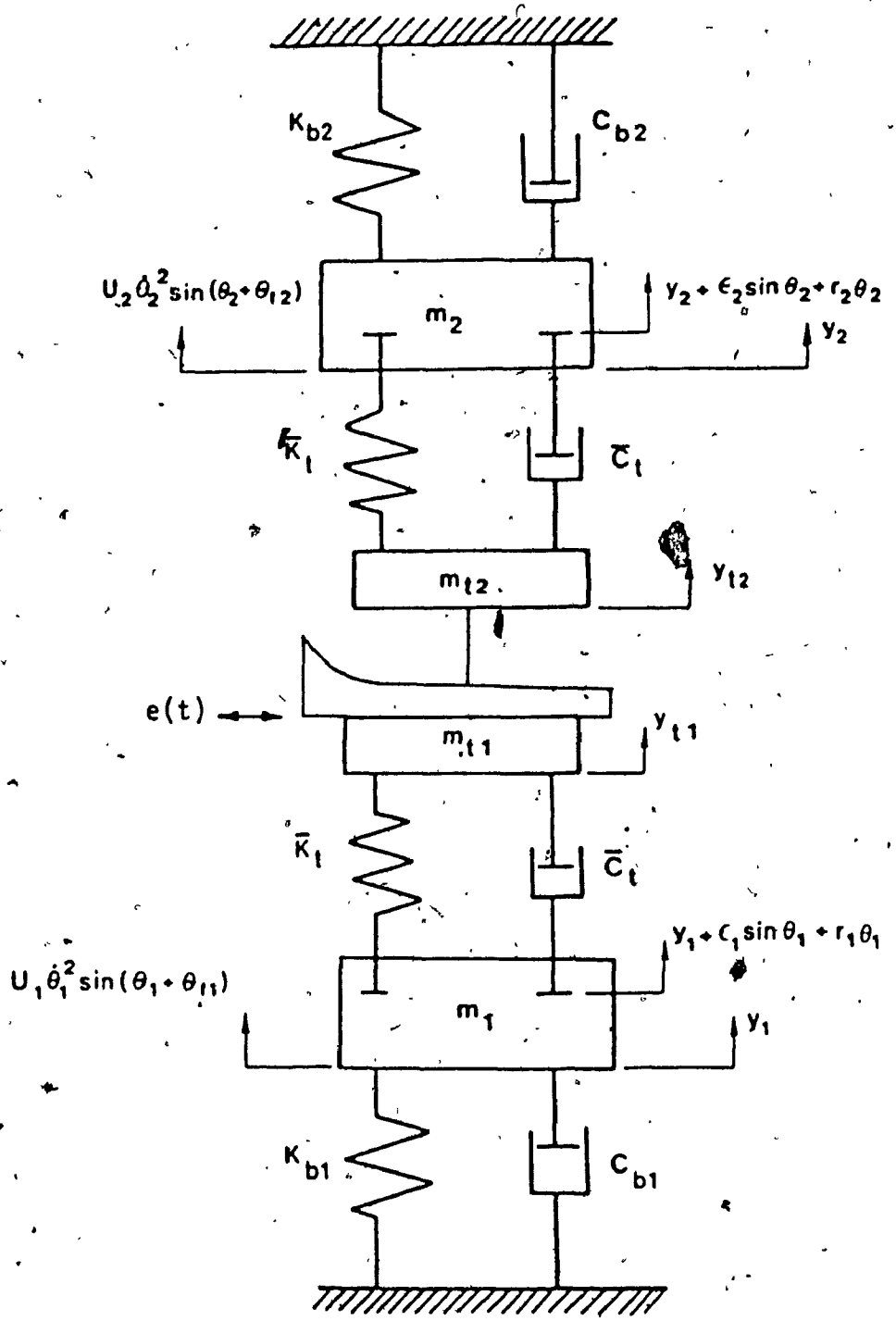

Fig. 2.26 Mathematical Model of the Gear Pair

The generalised force vector $\{F\}$ is expressed as:

$$\{F\} = \{F\}_D + \{F\}_R$$

where $\{F\}_D =$

$$\begin{bmatrix}
\bar{c}_t \varepsilon_1 \omega_1 \cos(\omega_1 t + \theta_{10}) - \bar{k}_t \varepsilon_1 \sin(\omega_1 t + \theta_{10}) \\
\quad + U_1 \omega_1^2 \sin(\omega_1 t + \theta_{10} + \theta_{f1}) \\
\hline
-\bar{c}_t \varepsilon_2 \omega_2 \cos(\omega_2 t + \theta_{20}) - \bar{k}_t \varepsilon_2 \sin(\omega_2 t + \theta_{20}) \\
\quad + U_2 \omega_2^2 \sin(\omega_2 t + \theta_{20} + \theta_{f2}) \\
\quad + \bar{k}_t e_p(t) + \bar{c}_t \dot{e}_p(t) \\
\hline
\bar{c}_t \{\varepsilon_2 \omega_2 \cos(\omega_2 t + \theta_{20}) + \varepsilon_1 \omega_1 \cos(\omega_1 t + \theta_{10})\} \\
\quad + \bar{k}_t \{\varepsilon_2 \sin(\omega_2 t + \theta_{20}) + \varepsilon_1 \sin(\omega_1 t + \theta_{10})\} \\
\quad - (m_{t2} \ddot{e}_p(t) + \bar{c}_t e_p(t) + \bar{k}_t e_p(t)) \\
\hline
0 \\
\hline
-\bar{c}_t r_1 \varepsilon_1 \omega_1 \cos(\theta_{10} + \omega_1 t) - F_0 \varepsilon_1 \cos(\theta_{10} + \omega_1 t) \\
\quad - \bar{k}_t r_1 \varepsilon_1 \sin(\theta_{10} + \omega_1 t) \\
\hline
-\bar{c}_t r_2 \varepsilon_2 \omega_2 \cos(\theta_{20} + \omega_2 t) + F_0 \varepsilon_2 \cos(\theta_{20} + \omega_2 t) \\
\quad - \bar{k}_t r_2 \varepsilon_2 \sin(\theta_{20} + \omega_2 t) \\
\quad + \bar{c}_t r_2 \dot{e}_p(t) + \bar{k}_t r_2 e_p(t)
\end{bmatrix}$$

The response of the geared shaft system to the force $\{F\}_D$ can be obtained by expressing $e_p(t)$ in terms of its Fourier

series expansion and solving;

$$[M]\{\ddot{q}\} + [C]\{\dot{q}\} + [K]\{q\} = \{F\}_R$$

Hereafter, the system response to the random part of the STE will only be considered.

Now $$\{F\}_R = \begin{Bmatrix} 0 \\ \bar{k}_t\, e_r(t) + \bar{c}_t \dot{e}_r(t) \\ (m_{t_2} \ddot{e}_r(t) + \bar{c}_t \dot{e}_r(t) + \bar{k}_t e_r(t)) \\ 0 \\ 0 \\ \bar{c}_t r_2 \dot{e}_r(t) + \bar{k}_t r_2 e_r(t) \\ 0 \end{Bmatrix}$$

The PSD of the response due to random STE can be found by considering the equation

$$[M]\{\ddot{q}\} + [C]\{\dot{q}\} + [K]\{q\} = \{F\}_R \qquad (2.59)$$

The homogeneous part of equation (2.59) neglecting damping is given by,

$$[M]\{\ddot{q}\} + [K]\{q\} = \{0\}$$

and is solved to obtain the eigenvalues λ_i and eigenvectors $\{\phi_i\}$ of the system.

Express $\{q\} = [\phi]\{p\}$

where $[\phi]$ is the modal matrix.

Using this equation in (2.59) and premultiplying by $[\phi]^T$, we get,

$$[\mu]\{\ddot{p}\} + [\gamma]\{\dot{p}\} + [\kappa]\{p\} = \{\sigma(t)\} \tag{2.60}$$

where

$$[\mu] = [\phi]^T[M][\phi]$$

$$[\kappa] = [\phi]^T[K][\phi]$$

and $$\{\sigma(t)\} = [\phi]^T\{F\}_R$$

and γ_i are elements of $[\gamma]$ and denotes the equivalent damping coefficient in each mode.

The modal response can be obtained from (2.60) as

$$\{p(t)\} = [H(\omega)]\{\sigma(t)\}$$

where

$$H_i(\omega) = \frac{1}{(\kappa_i - \mu_i\omega^2) + j(2\zeta_i\omega_i\mu_i\omega)} \tag{2.61}$$

$$j = \sqrt{-1}$$

The PSD of the response to the random STE is obtained as,

$$[S_q(\omega)] = [\phi][H(j\omega)][\phi]^T[S_F(\omega)][\phi][H(-j\omega)]^T[\phi]^T \tag{2.62}$$

where $[S_F(\omega)]$ is the PSD of the excitation force.

Expressing $$\{F\}_R = \{\underline{F}\}\, e_r(t) \tag{2.63}$$

the PSD of the excitation force is

$$[S_F(\omega)] = [\{\underline{F}\}\{\underline{F}\}^T]\, S_e(\omega) \qquad (2.64)$$

where $S_e(\omega)$ is the PSD of the random STE. Tobe et al. [16] modelled the random component of the STE, $e_r(t)$ as an output of a second order linear filter, the input to which is a Gaussian white noise, $w(t)$ of intensity S_0

The filter equation is

$$\ddot{e}_r(t) + a_1 \dot{e}_r(t) + a_2 e_r(t) = w(t) \qquad (2.65)$$

Tobe and Sato [16] obtained the constants of the filter, a_1 and a_2, by matching the autocorrelation of the filter response to that experimentally obtained. The details of the filter are given in Table 2.11. Since the filter is a linear dynamic system, the PSD of the random STE, $S_e(\omega)$ is given by

$$S_e(\omega) = |H_f(j\omega)|^2 S_0 \qquad (2.66)$$

where

$H_f(j\omega)$ = transfer function of the filter

$$= \frac{1}{(a_2-\omega^2) + j\, a_1 \omega} \qquad (2.67)$$

The expression for the dynamic tooth load ΔF is given in Equation (2.16).

$$\Delta F(t) = m_{t1}\, \ddot{\Delta y}_{t1} + \bar{c}_t(\dot{\Delta y}_t - \dot{\Delta y}_1 - \varepsilon_1 \omega_1 \cos(\omega_1 t + \theta_{10}) - r_1 \dot{\Delta\theta}_1) + \bar{k}_t\,(\Delta y_{t1} - \Delta y_1 - \varepsilon_1 \sin(\omega_1 t + \theta_{10}) - r_1 \Delta\theta_1) \qquad (2.68)$$

In order to evaluate the PSD of the dynamic tooth load, take the Fourier Transform of Eq. (2.68),

$$\Delta F(\omega) = (m_{t_1}\omega^2 - \bar{c}_t i\omega - \bar{k}_t)\,\Delta y_{t_1}(\omega) + (\bar{c}_t i\omega + \bar{k}_t)\,\Delta y_1(\omega) + (\bar{c}_t r_1 i\omega + \bar{k}_t r_1)\,\Delta\theta_1(\omega)$$

$$= A(\omega)\,\Delta y_{t_1}(\omega) + B(\omega)\,\Delta y_1(\omega) + C(\omega)\,\Delta\theta_1(\omega)$$

$$= \lfloor A(\omega)\ B(\omega)\ C(\omega)\rfloor \begin{Bmatrix} \Delta y_{t_1}(\omega) \\ \Delta y_1(\omega) \\ \Delta\theta_1(\omega) \end{Bmatrix} \qquad (2.69)$$

The PSD of the dynamic tooth load is defined as

$$\Phi_{\Delta F} = \lim_{T\to\infty} \frac{1}{T} |\Delta F(\omega)|^2 \quad /$$

Hence,

$$\Phi_{\Delta F} = \{T\}\,[S_v]\,\{T^*\}^T \qquad (2.70)$$

where $\{T\} = \lfloor A(\omega)\ B(\omega)\ C(\omega)\rfloor$ (2.71)

and $[S_v] = \begin{bmatrix} \Phi_{\Delta y_{t_1}\Delta y_{t_1}} & \Phi_{\Delta y_{t_1}\Delta y_1} & \Phi_{\Delta y_{t_1}\Delta\theta_1} \\ \Phi_{\Delta y_1\Delta y_{t_1}} & \Phi_{\Delta y_1\Delta y_1} & \Phi_{\Delta y_1\Delta\theta_1} \\ \Phi_{\Delta\theta_1\Delta y_{t_1}} & \Phi_{\Delta\theta_1\Delta y_1} & \Phi_{\Delta\theta_1\Delta\theta_1} \end{bmatrix}$ (2.72)

Define $\{v\} = \{\Delta y_{t_1}\ \Delta y_1\ \Delta\theta_1\}^T$ which is related to the dynamic tooth load and $\{w\} = \{\Delta y_2\ \Delta\theta_m\ \Delta\theta_2\ \Delta\theta_L\}^T$ Then, $\{q\}$ in Eq. (2.58) can be expressed as

$$\{q\} = [\alpha]\,\{z\} \qquad (2.73)$$

where $[\alpha]$ is the transformation matrix (see Appendix I) and

$$\{z\} = \begin{Bmatrix} \{v\} \\ \{w\} \end{Bmatrix} \qquad (2.74)$$

Eq. (2.73) gives

$$\{z\} = [\alpha]^{-1} \{q\} \tag{2.75}$$

Let $[\beta] = [\alpha]^{-1}$

Therefore $\{z\} = [\beta]\{q\}$

Partitioning $[\beta]$ using (2.74),

$$\frac{\{v\}}{\{w\}} = \frac{[\beta_1]}{[\beta_2]} \{q\}$$

$$= \frac{[\beta_1]\ \{q\}}{[\beta_2]\ \{q\}} \tag{2.76}$$

Then, $\{v\} = [\beta_1]\ \{q\}$ (2.77)

and $[S_v]$ in Eq. (2.70) is given by,

$$[S_v] = [\beta_1]\ [S_q]\ [\beta_1]^T \tag{2.78}$$

Using Eq. (2.78) and (2.62), Eq. (2.70) is rewritten as,

$$\Phi_{\Delta F} = \{T\}\ [\beta_1]\ [\phi]\ [H(j\omega)]\ [\phi]^T$$
$$x\ [S_F(\omega)]\ [\phi]\ [H(-j\omega)]^T\ [\phi]^T\ [\beta_1]^T\ \{T^*\}^T \tag{2.79}$$

where $[S_F(\omega)]$ is defined by Equations (2.64) and (2.66).

2.8.2 Numerical Results

The details of the geared shaft system used to obtain the numerical results are given in Table 2.11. The natural frequencies of the system are given in Table 2.12.

TABLE 2.11

Details of the Rotor System

a_1	0.11
a_2	0.102
$\bar{c}_t$	10.0 Ns/m
I_1	0.031 kgm^2
I_2	0.0064 kgm^2
J_1	0.46 kgm^2
J_2	0.56 kgm^2
k_{b_1}	1.77×10^6 N/m
k_{b_2}	3.49×10^5 N/m
$\bar{k}_t$	2×10^9 N/m
k_1	1.1×10^4 Nm/rad
k_2	2.1×10^3 Nm/rad
m_1	16.95 kg
m_2	5.65 kg
m_{t_1}, m_{t_2}	4.9×10^{-3} kg
r_1	0.1015 m
r_2	0.0564 m
S_0	0.332×10^{-6} m^2/s^3
ζ_i	0.01

TABLE 2.12

System Natural Frequencies (Hz)

1	0.0
2	10.56
3	47.35
4	59.88
5	94.36
6	0.5195×10^4
7	0.1018×10^6

TABLE 2.13

Filter Details

Order	Governing Equation	$\lvert H(j\omega) \rvert^2$
First	$\alpha \dot{Y} + Y = X$	$\frac{1}{1 + \alpha^2\omega^2}$
Second	$\alpha\ddot{Y} + \beta\dot{Y} + Y = X$	$\frac{1}{(1 - \alpha\ \omega^2)^2 + (\beta\omega)^2}$

$\alpha = \beta = 1.0$
$X(t)$ = input

$Y(t)$ = output

The PSD of the flexural response in the y-direction at the driving gear location is shown in Fig. 2.27. The system experiences peak response at the system natural frequencies is the frequency range. The peak responses at the higher modes are lower because of the effect of the linear shaping filter. The peak response is seen in the second mode (10.56 Hz) and corresponds to about 3.16×10^{-13} m^2/Hz. Fig. 2.28 shows the PSD of the flexural response in the y-direction at the driven gear location. The behaviour is similar to that at the driving gear. The peak response is observed in the second mode and corresponds to about 1×10^{-11} m^2/Hz. This response is larger than that at the driving gear.

The PSD of the torsional response at the driving gear locations is shown in Fig. 2.29. The system experiences peak response at the system natural frequencies in the range of interest. The maximum response is observed in the first mode and corresponds to 1.77×10^{-9} rad^2/Hz. The response is very high at around 0.05 Hz and corresponds to the resonance at the filter natural frequency. The PSD of the torsional response at the driven gear location is shown in Fig. 2.30. The behaviour is similar to the plots 2.27 to 2.29. The peak response is observed in the second mode and corresponds to 1.77×10^{-11} rad^2/Hz. It is observed that the flexural response is larger at the driven gear location as compared to the driving gear location, while the torsional response is larger at the driving gear location as compared to the driven gear location.

The PSD of the dynamic tooth load due to a random transmission error is shown in Fig. 2.31. The dynamic tooth load has peaks at the system natural frequencies. This is as expected, because the dynamic tooth load depends on the flexural and torsional responses which experience large magnitudes at the system natural frequencies. The maximum dynamic tooth load is observed in the second mode and corresponds to 1.07 N^2/Hz.

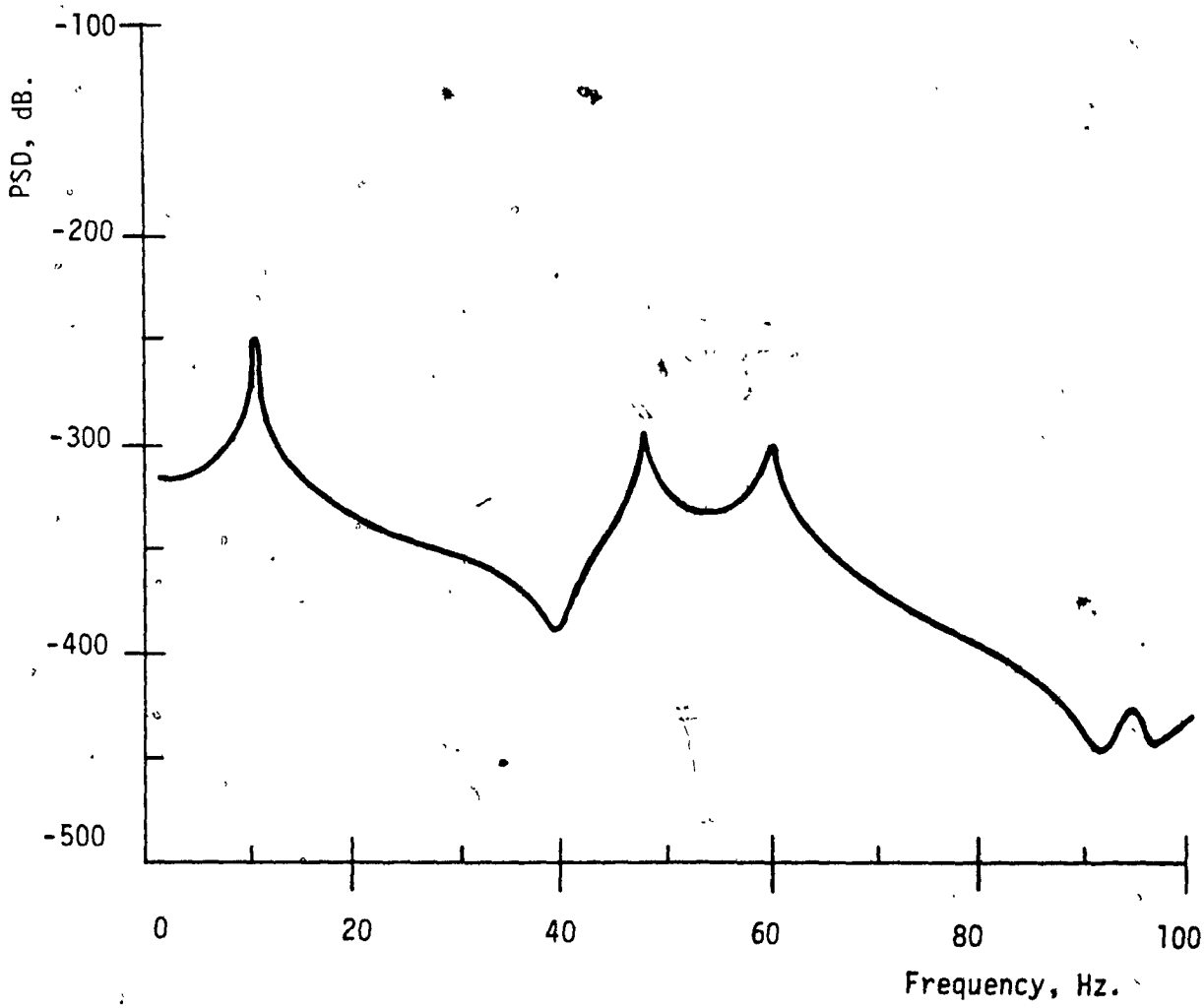

Fig. 2.27 Normalised PSD of response in the y direction at the driving gear location against the frequency of excitation.

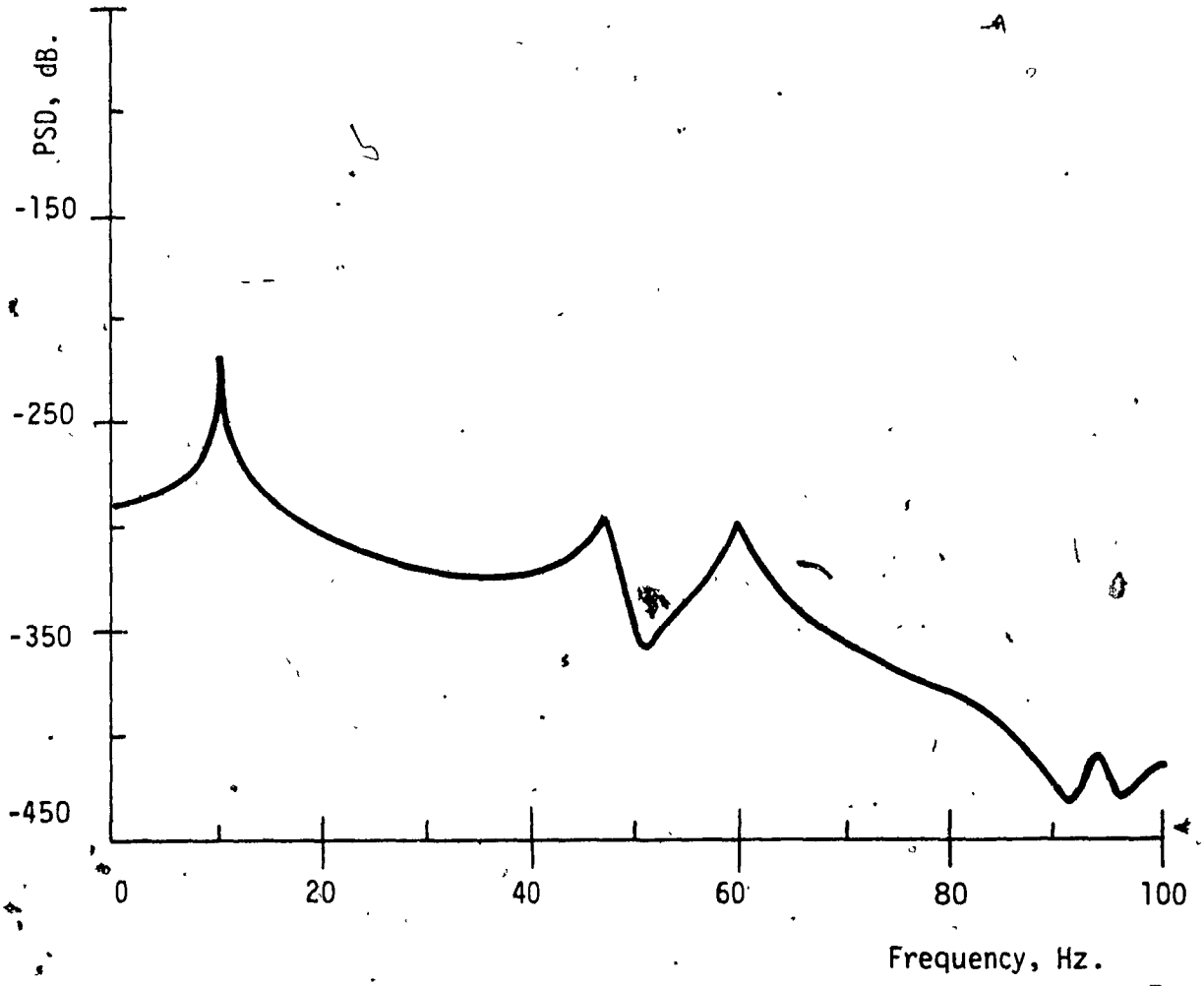

Fig. 2.28 Normalised PSD of response in the y direction at the driven gear location against the frequency of excitation.

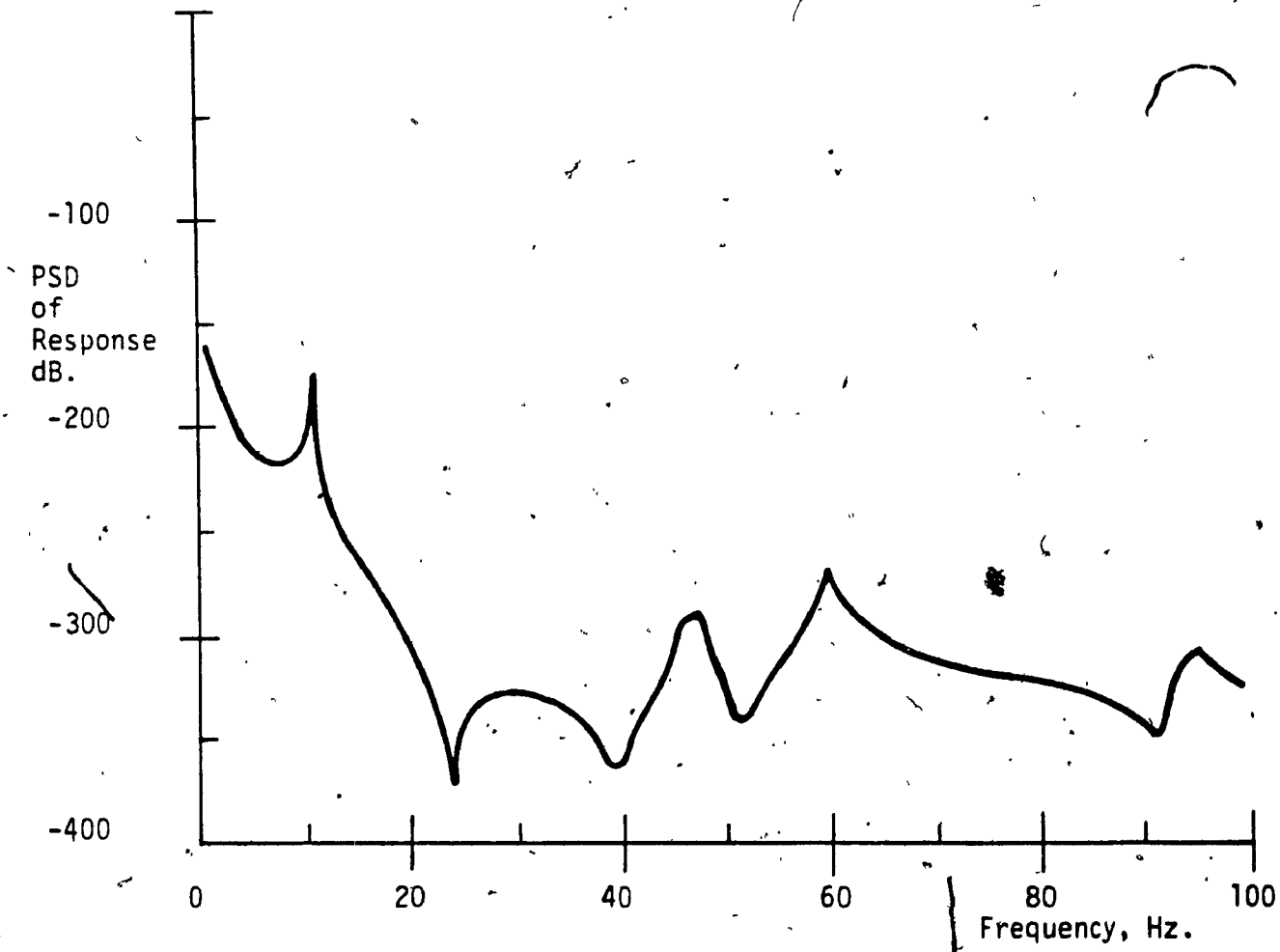

Fig. 2.29 Normalised PSD of response in the θ direction at the driving gear location against the frequency of excitation.

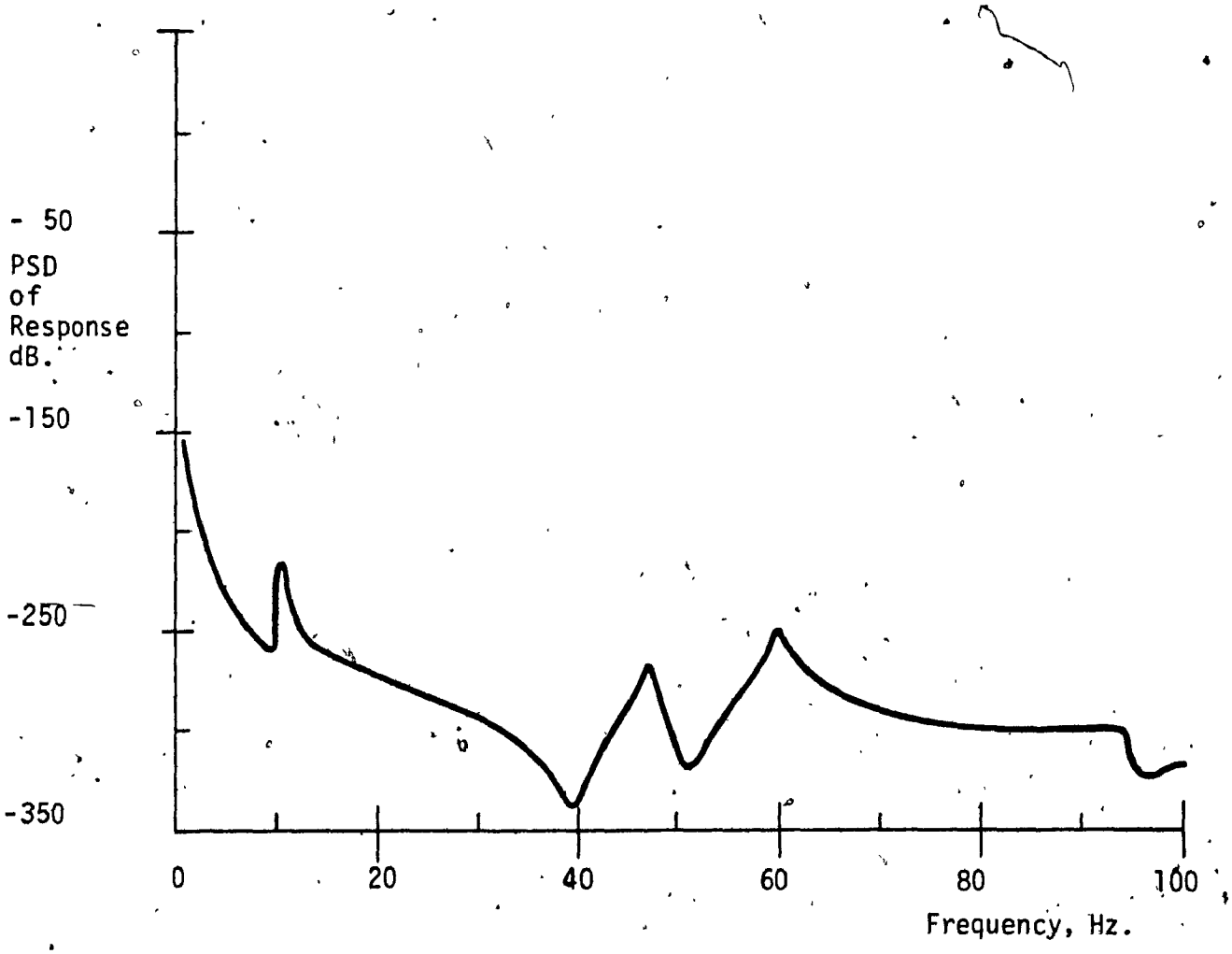

Fig. 2.30 Normalised PSD of response in the θ direction at the driven gear location against the frequency of excitation.

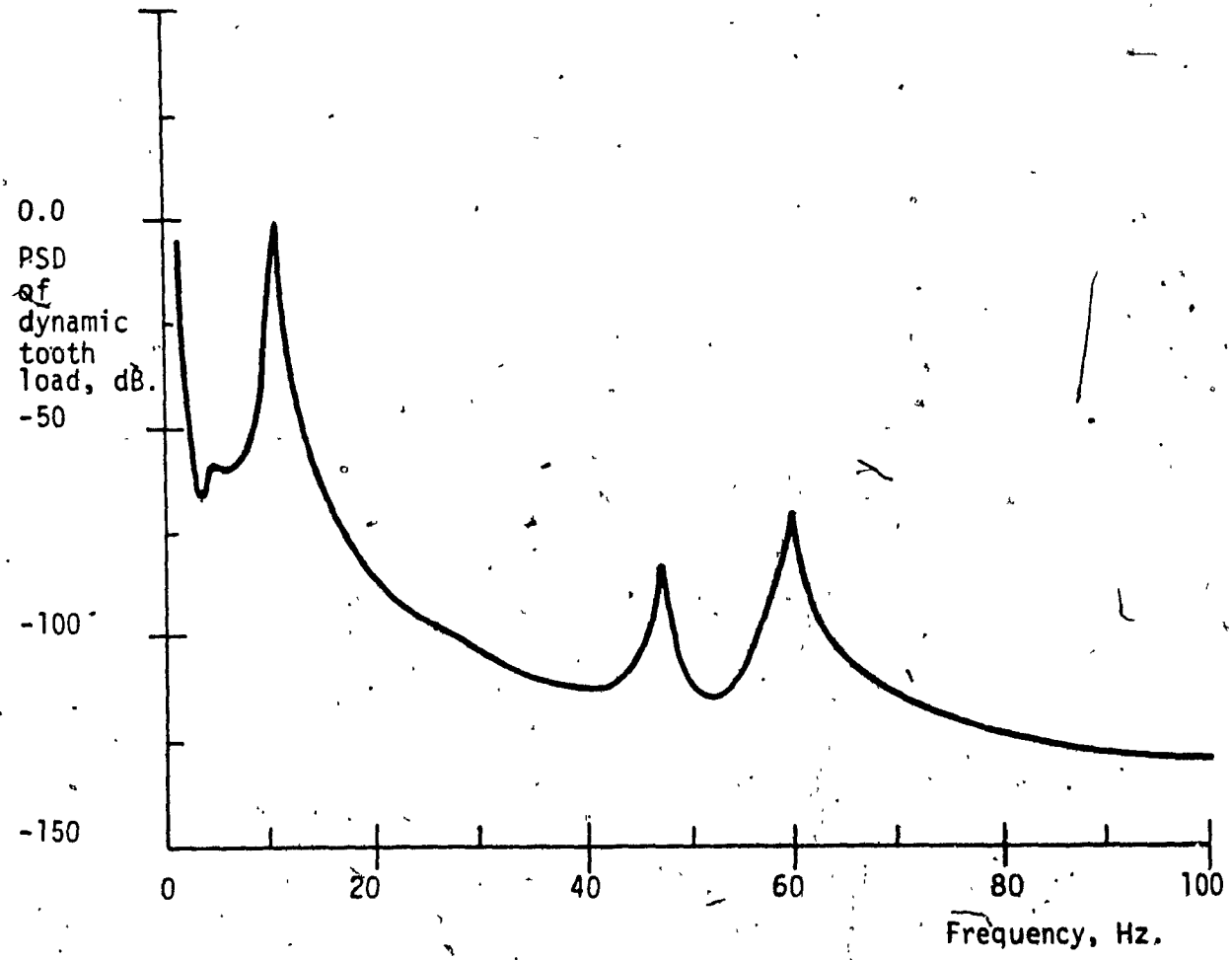

Fig. 2.31 Normalised PSD of dynamic tooth load against the frequency of excitation

2.9 Random Support Excitations Applied to a Geared Train of Rotors

In a geared rotor, some of the sources of excitation are mass unbalance, geometric eccentricity and errors of manufacture, all of which originate in the gear pair itself. However, the geared rotor system may also be subject to external forms of excitation such as that from the supports, for instance when onboard various types of vehicles. If the support excitations are random in nature with considerable power distributed over a frequency range, the system will respond at those frequencies. Moreover, if one of the system natural frequencies of the geared rotor coincides with the excitation frequencies, the resulting response may be of concern.

Several investigators have studied rotors subjected to random support excitations. Lund [69] carried out response spectral density analysis of rotor systems due to stationary random excitations of the base, considering excitations only in the vertical direction. Tessarzik et al. [70] analysed the turbo rotor responses due to external random vibrations. The rotor-bearing system was treated as a linear, three mass model and experimental results were found to compare well with calculation of amplitude spectral density for the case where the vibrations were applied along the rotor axis. Subbiah et al. [71] obtained the amplitude PSD of a simple

rotor supported on fluid film bearings subjected to random support excitation using modal analysis methods. The excitations are assumed to be stationary and Gaussian with a white noise type of PSD.

2.9.1 Analysis

In this section, a geared train of rotors studied in section 2.6 is subjected to random support excitations. The equation of motion for a N degree of freedom geared train of rotors subjected to random support excitation $\{F\}_R$ can be expressed as;

$$[M]\{\ddot{q}_r\} + [C]\{\dot{q}_r\} + [K]\{q_r\} = \{F\}_R \qquad (2.80)$$

where [M], [C] and [K] are exactly as described in Equation (2.41).

where $\{q\}$ = generalised rotor displacement vector

$\{q_s\}$ = support displacement vector

$\{q_r\} = \{q - q_s\}$, is the relative displacement vector.

and $$\{F\}_R = -[M]\{\ddot{q}_s\} \qquad (2.81)$$

The homogeneous form of Eq. (2.80) neglecting damping is solved to obtain the eigen values λ_i and eigen vectors $\{\phi_i\}$ of the system.

The response $\{q_r\}$ may be expressed in terms of the modal coordinates $\{p\}$ as

$$\{q_r\} = [\phi]\{p\} \tag{2.82}$$

where $[\phi]$ is the modal matrix formed using the eigenvector $\{\psi_i\}$.

Using Eq. (2.82) in (2.80) and premultiplying by $[\phi]^T$ we get,

$$[\mu]\{\ddot{p}\} + [\gamma]\{\dot{p}\} + [\kappa]\{p\} = \{\sigma(t)\} \tag{2.83}$$

where $[\mu] = [\phi]^T [M] [\phi]$

$[\kappa] = [\phi]^T [K] [\phi]$

$\{\sigma(t)\} = [\phi]^T \{F\}_R$

Now $$\{p(t)\} = [H(\omega)]\{\sigma(t)\} \tag{2.84}$$

where $$H_i(\omega) = \frac{1}{(\kappa_i - \mu_i \omega^2) + j(2\zeta_i \omega_i \mu_i \omega)} \tag{2.85}$$

and ζ_i is the modal damping ratio.

The PSD matrix of the response can be obtained as

$$[S_{qr}(\omega)] = [\phi][H(j\omega)][\phi]^T [S_F(\omega)][\phi][H(-j\omega)]^T [\phi]^T \tag{2.86}$$

The PSD matrix of the random excitation force $[S_F(\omega)]$ can be expressed in terms of the PSD matrix of the displacement support excitation $[S_{qs}(\omega)]$ as

$$[S_F(\omega)] = \omega^4 [M] [S_{qs}(\omega)] [M]^T \quad (2.87)$$

The displacement support excitation is assumed as the output of a linear filter, the input to which is an excitation in the vertical direction only. This excitation is an uncorrelated Gaussian stationary process with a white noise type of PSD.

2.9.2 Numerical Results

A geared train of rotors similar to that in section 2.6.2 is considered for this study. The details of the linear filter are given in Table 2.13.

The normalized PSD of relative amplitude in the y direction at the driven gear location is shown in Fig. 2.32. The base excitation is assumed to be the output of a first order linear filter, the input to which is an uncorrelated white noise type of PSD only in the vertical direction, and this is plotted on the x axis. The PSD plot shows peak response at modes 2, 3 and 7. There is also a peak response observed midway between the modes 8 and 9. The maximum response is seen in mode 8 and corresponds to about 0.1 m^2/Hz.

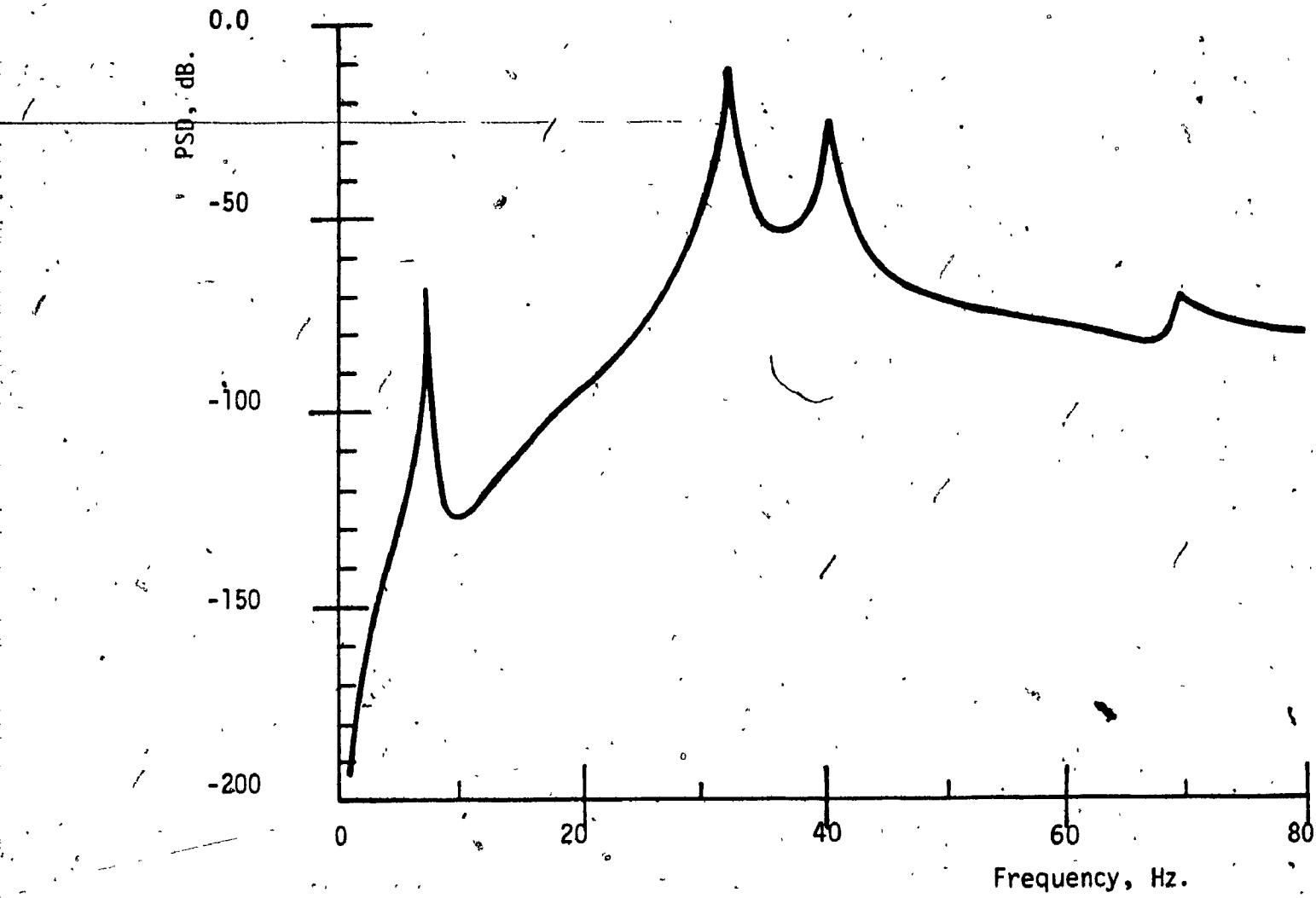

Fig. 2.32 Normalised PSD of relative amplitude in the y direction at the driven gear location (DOF #23) against the frequency of excitation. First order filter used.

A PSD plot similar to Fig. 2.32, using a second order filter is shown in Fig. 2.33. The behavior of the response is the same as in Fig. 2.32, however, the magnitude is lower for all modes.

The normalized PSD of relative amplitude in the y direction at the driving gear location is shown in Fig. 2.34. The base excitation is assumed to be the output of a first order linear filter, the input to which is an uncorrelated white noise type of PSD in the vertical direction. The PSD plot shows peak response at modes 2, 3, 7 and 10. The maximum PSD response of about 0.1 m^2/Hz which is observed at the driven gear (Fig. 2.31) is found to be higher than the driving gear at the first mode and comparable at the other modes.

A PSD plot similar to Fig. 2.34 using a second order filter is shown in Fig. 2.35. The behavior of the response is the same as in Fig. 2.34, but the magnitude is lower for all the modes.

The normalized PSD of relative amplitude in the y direction at the bearing locations (DOF #50 and #45) is shown in Figures 2.36 and 2.37. The base excitation is assumed to be the output of a first order linear filter, the input to

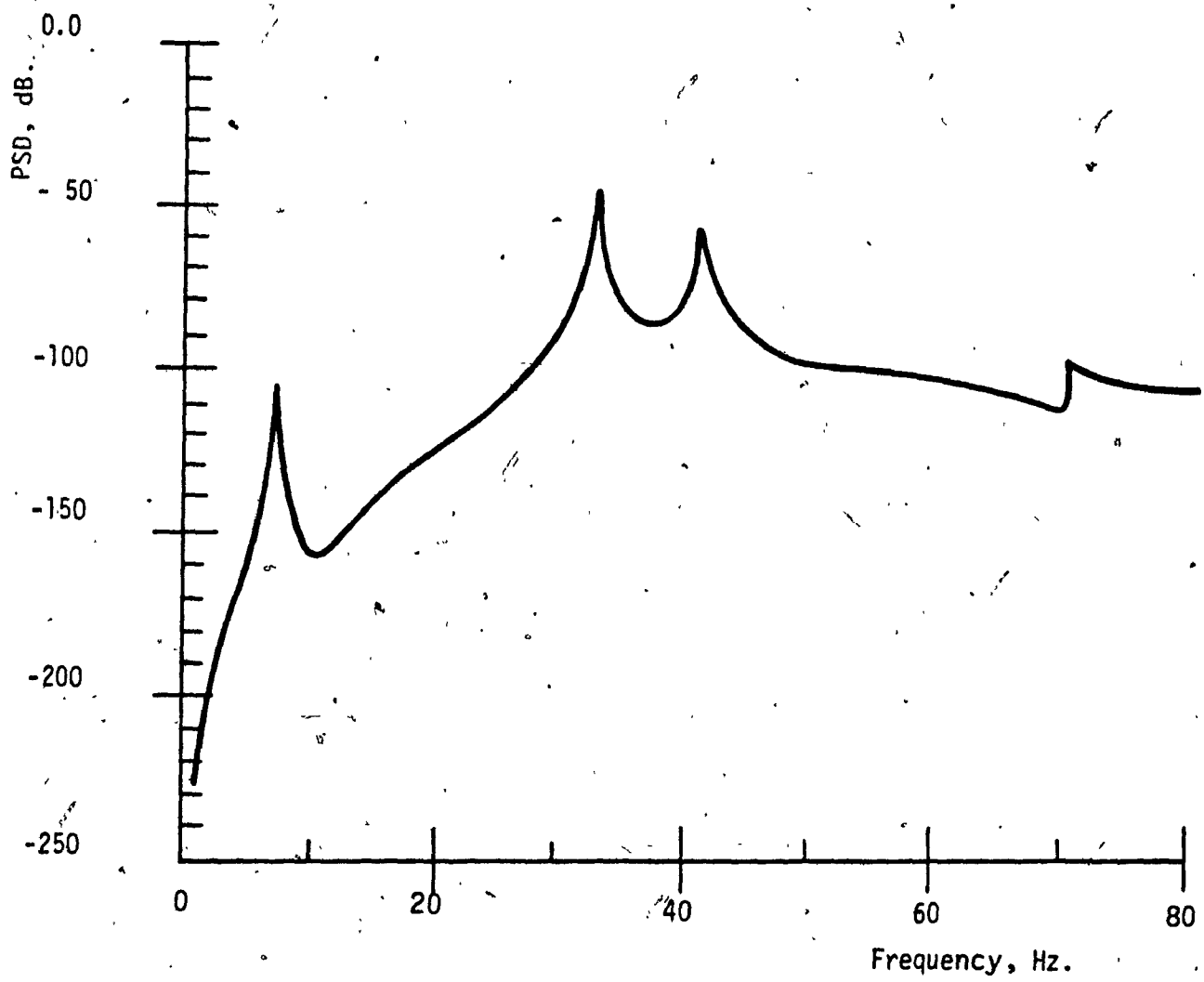

Fig. 2.33 Normalised PSD of relative amplitude in the y direction at the driven gear location (DOF #23) against the frequency of excitation. Second order filter used.

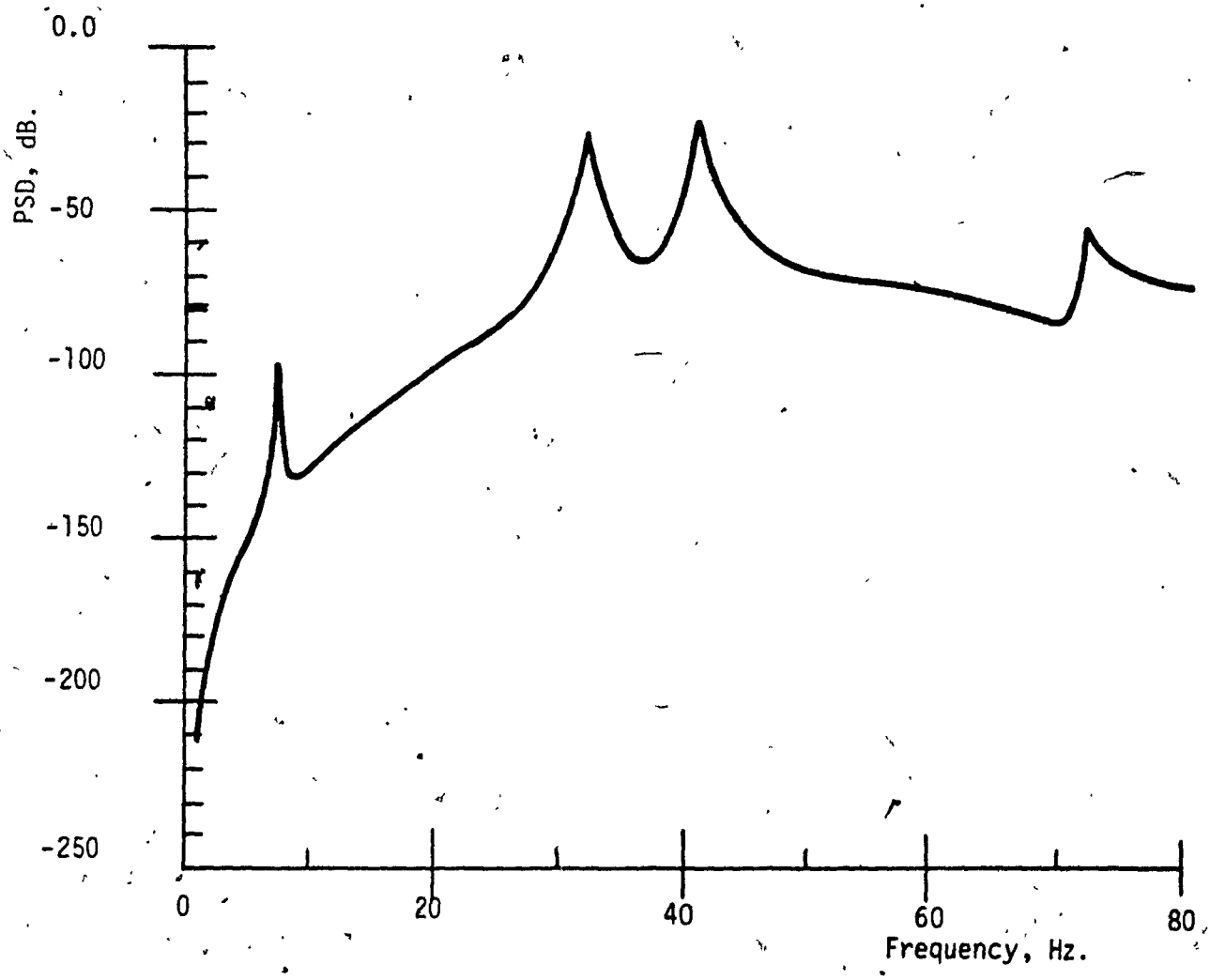

Fig. 2.34 Normalised PSD of relative amplitude in the y direction at the driving gear location (DOF #40) against the frequency of excitation. First order filter used.

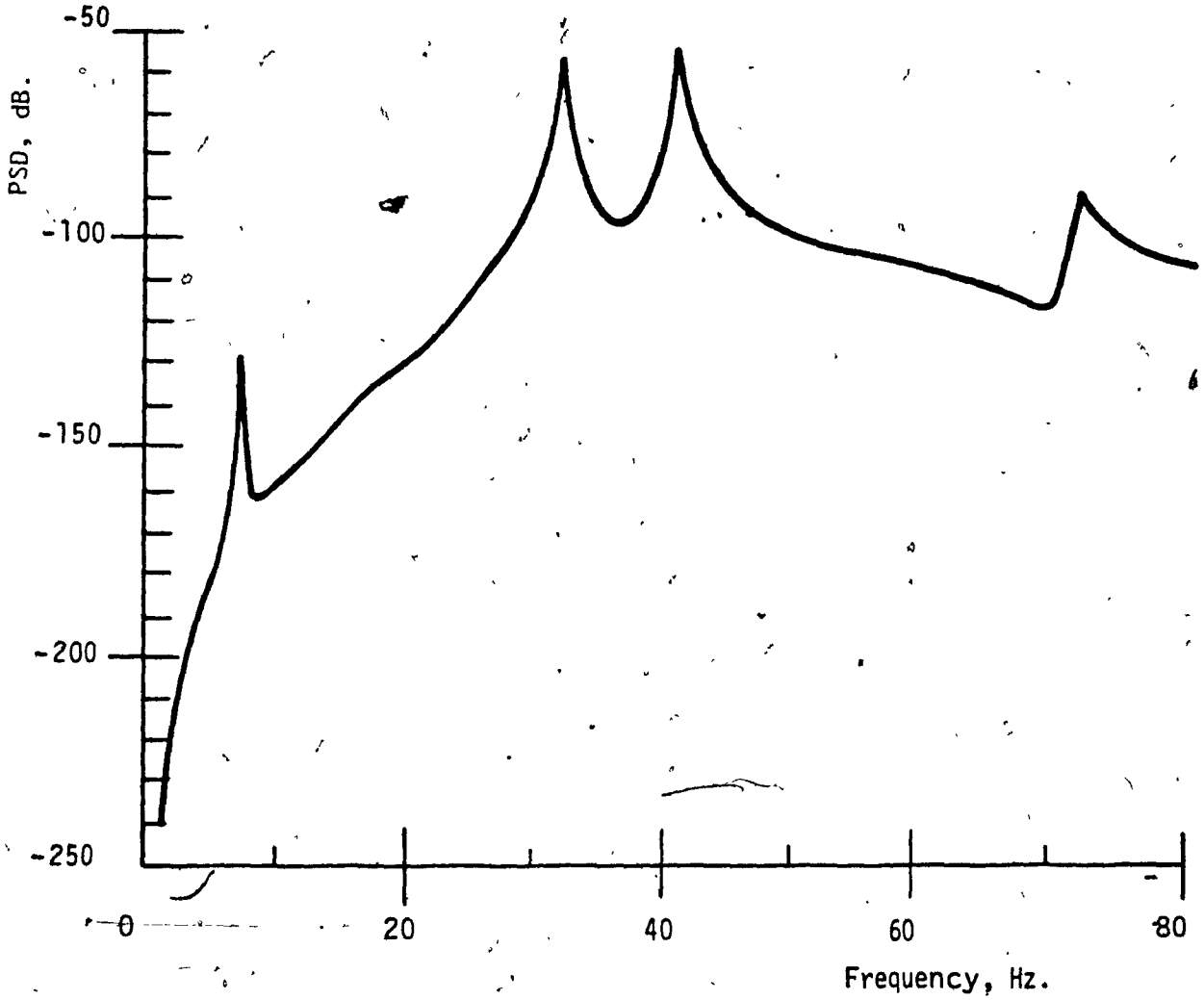

Fig. 2.35 Normalised PSD of relative amplitude in the y direction at the driving gear location (DOF #40) against the frequency of excitation. Second order filter used.

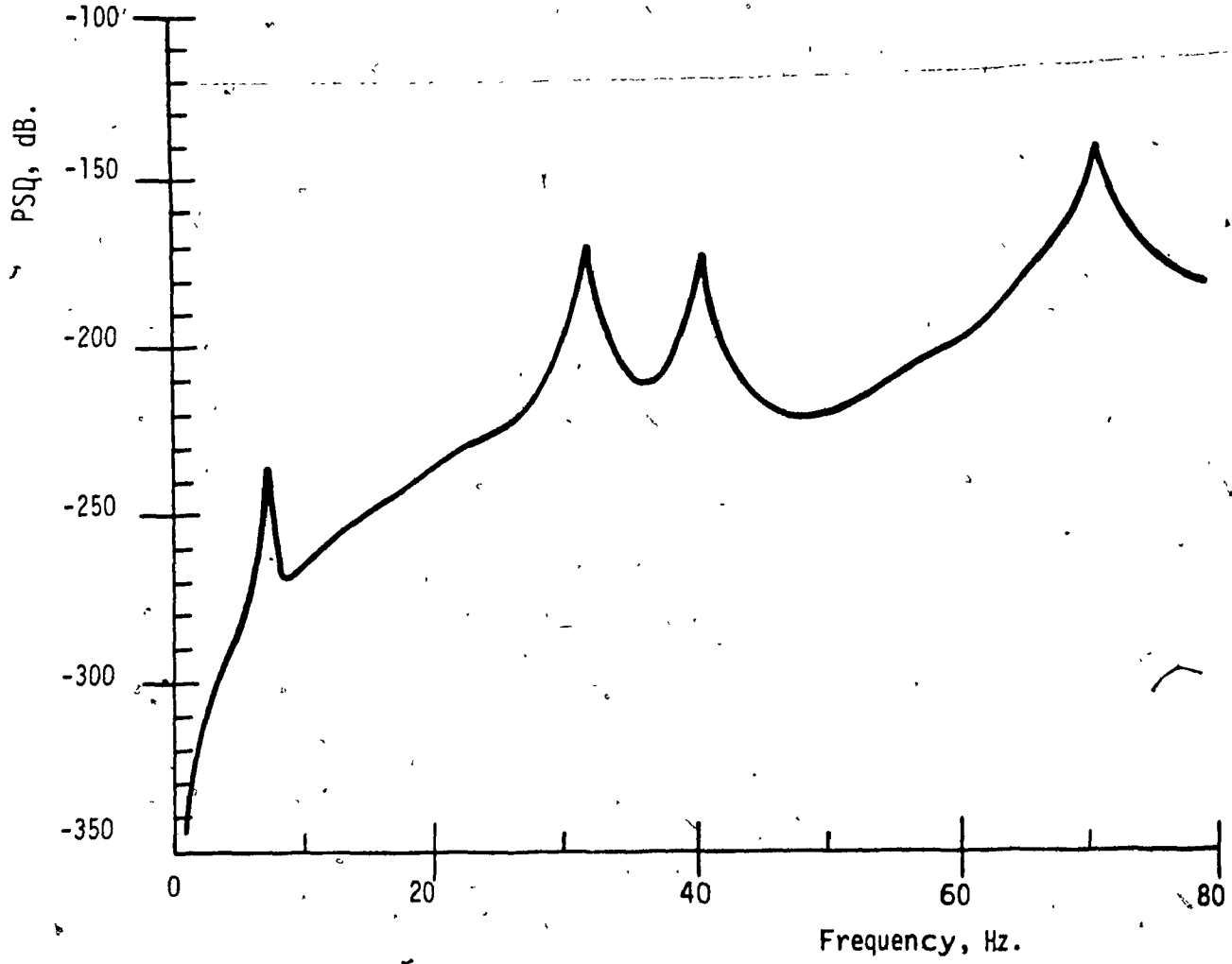

Fig. 2.36 Normalised PSD of relative amplitude in the y direction at the bearing location (DOF #50) against the frequency of excitation. First order filter used.

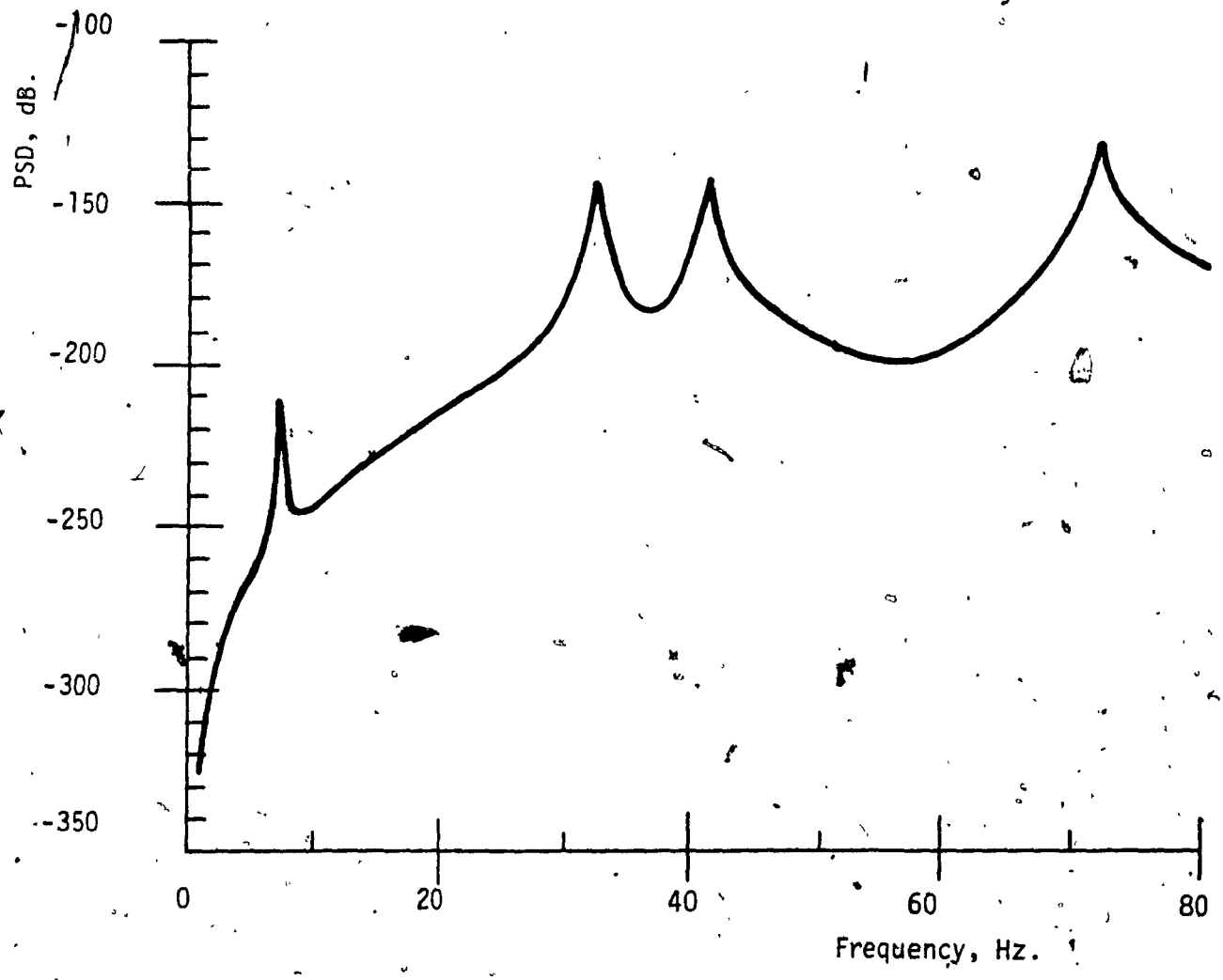

Fig. 2.37 Normalised PSD of relative amplitude in the y direction at the bearing location (DOF #45) against the frequency of excitation. First order filter used.

which is an uncorrelated white noise type of PSD in the vertical direction. The responses are as expected, much smaller than the response at the gear locations. The maximum response is observed at the 10th mode (71.59 Hz) and this corresponds to about 3.1×10^{-8} m^2/Hz.

2.10 Summary

In this chapter, the dynamic response of a spur geared shaft system employing one or more pairs of gears subjected to internal or external excitations is obtained using modal analysis methods.

Firstly, a simple geared shaft system is considered consisting of a motor driving a dynamo through a pair of gears. A lumped mass mathematical model is developed considering the coupling between torsion and flexure. The effect of backlash and time varying mesh stiffness are neglected. The dynamic response and the dynamic tooth load are obtained when the geared shaft system is subjected to excitations in the form of mass unbalance and geometric eccentricity. Normal mode analysis is used to compute the response. The system is found to exhibit large responses not only at the system natural frequencies but also at its gear ratio multiples. Later, finite beam elements are used to model the geared shaft system. The effects of coupling which were obtained from the previous analysis were introduced into

the finite element model. The response to mass unbalance and geometric eccentricity was obtained by normal mode analysis. The doubling in the number of system resonance peaks was observed once again. The orbit diagrams were also obtained. The finite element model was then extended to a geared train of rotors. The dynamic response of such a system when excited by mass unbalance and geometric eccentricity is obtained by normal mode analysis. It is seen that a system having n natural frequencies and p pairs of gears experiences np number of peak responses. Further, finite elements, considering skew symmetric gyroscopic terms are also used to model the geared rotor system and complex modal analysis employing biorthogonality relations is used to obtain the system response.

The composite effects of tooth face modifications, machining errors and wear and tooth deformations are described by the static transmission error which represents the primary source of vibratory excitation in a geared shaft system. The static transmission error may be separated into deterministic and random components. The effect of the random component of the static transmission error, modelled as a filtered white noise, on the response and dynamic loads is studied. Lastly, the effects of external excitations such as support excitations on the dynamic response of the geared train of rotors is also studied. Support excitations occur for instance onboard moving

vehicles and is modelled as the output of a linear filter, the input to which is an uncorrelated stationary Gaussian process with a white noise type of PSD. Results are presented for the response at the gear and bearing locations.

In the next chapter, the linear response analysis of a helical geared rotor system is considered.

CHAPTER 3

LINEAR RESPONSE ANAYSIS OF A HELICAL GEARED ROTOR SYSTEM

3.1 Introduction

In the previous chapter, a spur geared rotor system was analyzed. The dynamic response of a spur geared rotor system employing one or more pairs of gears subjected to internal or external excitations was obtained using modal analysis methods. This chapter deals with the response analysis of helical geared rotor systems.

If a number of spur gears formed from thin plates are assembled with a small angular displacement between the teeth, the stepped gear of Fig. 3.1 results. A helical gear can be considered the limiting case or a stepped gear as the thickness of the plates and the angular displacements are made progressively smaller. A typical example of a pair of helical gears is given by Fig. 3.2. Because of the helix angle there will be end thrust on the shafts of helical gears, which must be provided for in the design of the bearings. End thrust can be eliminated by cutting a right hand spiral over one half of the face, and using a left-hand spiral for the other half. These are called herringbone gears and is illustrated in Fig. 3.2. The helix angle as

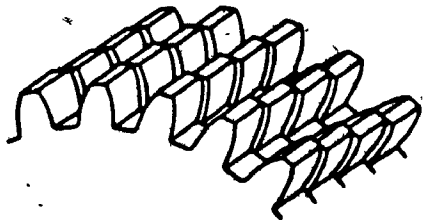

Fig. 3.1 Stepped gears. Helical gears result if the plates are made progressively thinner.

(From Spotts, M.F., Design of Machine Elements, Prentice-Hall, 1985).

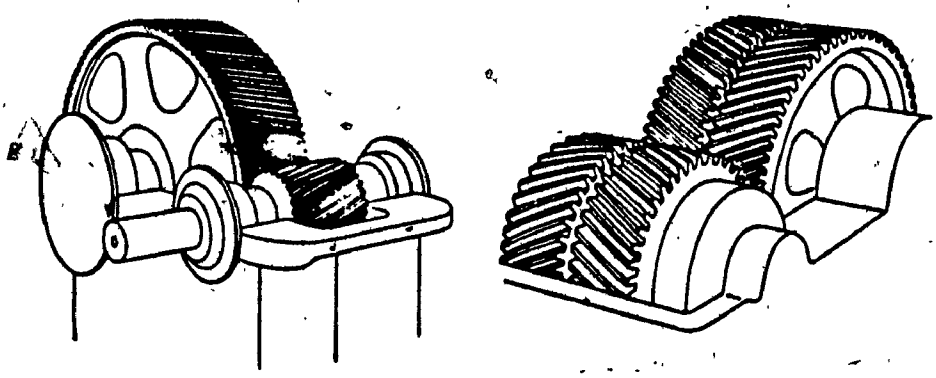

Fig. 3.2 A pair of helical gears, herringbone gears

(From Spotts, M.F., Design of Machine Elements, Prentice-Hall, 1985).

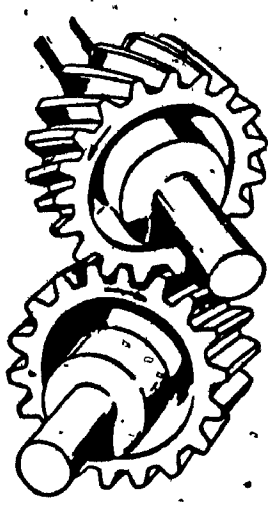

Fig. 3.4 Helical gears on nonparallel shafts. (From Spotts, M.F., Design of Machine Elements).

illustrated in Fig. 3.3 usually varies from 15^0 to 30^0 for helical gears and from 23^0 to 30^0 or even 45^0 for herringbone gears.

Gears with helical teeth possess certain inherent advantages. More teeth are in contact simultaneously, and the load is transferred gradually and uniformly as successive teeth come into engagement. Helical gears thus operate more smoothly and carry larger loads at higher speeds than spur gears. The line of contact extends diagonally across the face of mating teeth. Since more teeth are in contact, undercutting causes little trouble in helical gearing.

Helical gears can also be used for transmitting power between non-parallel shafts as shown in Fig. 3.4. When used in this way, the teeth have only point contact, which does not shift axially along the teeth during operation. Such gears are used only for the transmission of relatively small loads.

3.2 Torsional-Flexural-Axial-Rotational "Force" Coupling

In section 2.3 we discussed the torsional-flexural "Force" coupling that exists between the torsional and flexural motions of a shaft carrying spur gears.

In a rotor system consisting of parallel shafts coupled by helical gears, this "Force" coupling is more

complex than that for spur gears. Here, the torsional, flexural, axial and rotational (about a diameter) motions of the shafts at the gear locations are coupled because of the helix angle, measured between an element of the tooth at the pitch cylinder and the center line of the shaft. Thus the natural frequencies and dynamic response of the rotor system coupled by helical gears will be different from that carrying spur gears. Kacukay [60] used a 8 DOF model to study a pair of helical gears and obtained the response and dynamic tooth loads. Kiyono et al. [61, 62] also studied a pair of helical gears and showed that the torsional component of vibration is the most important.

3.3 Lumped Mass Model

Let us consider a simple helical geared shaft system which is schematically represented in Fig. 3.5. It shows a motor of moment of inertia J_M driving a dynamo of moment of inertia J_L through a pair of helical gears. I_1 and I_2 denote the moment of interia of the driving and driven gears. There exists a "force" coupling between the motions in the axial-(x), flexural-(y), torsional-(θ) and rotational (about a gear diameter)-(ϕ) directions of the shafts at the gear locations, as shown in Fig. 3.3.

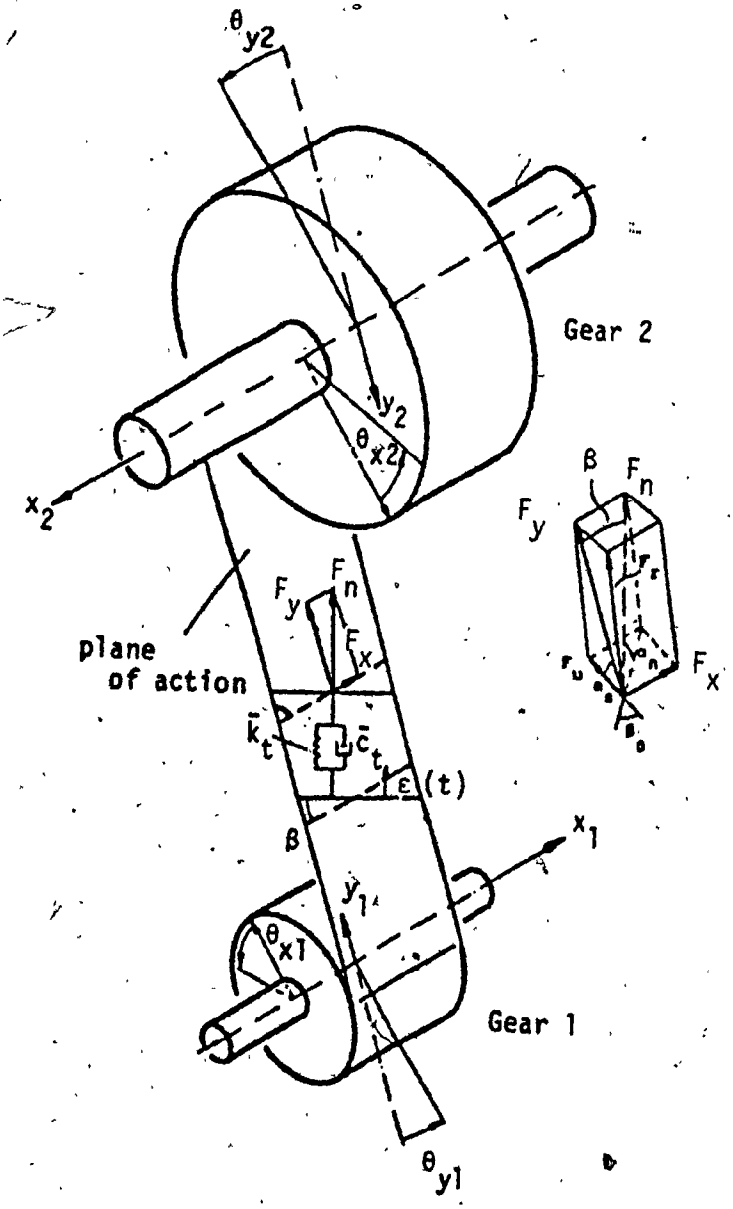

Fig. 3.3 A Pair of Helical Gears in Mesh

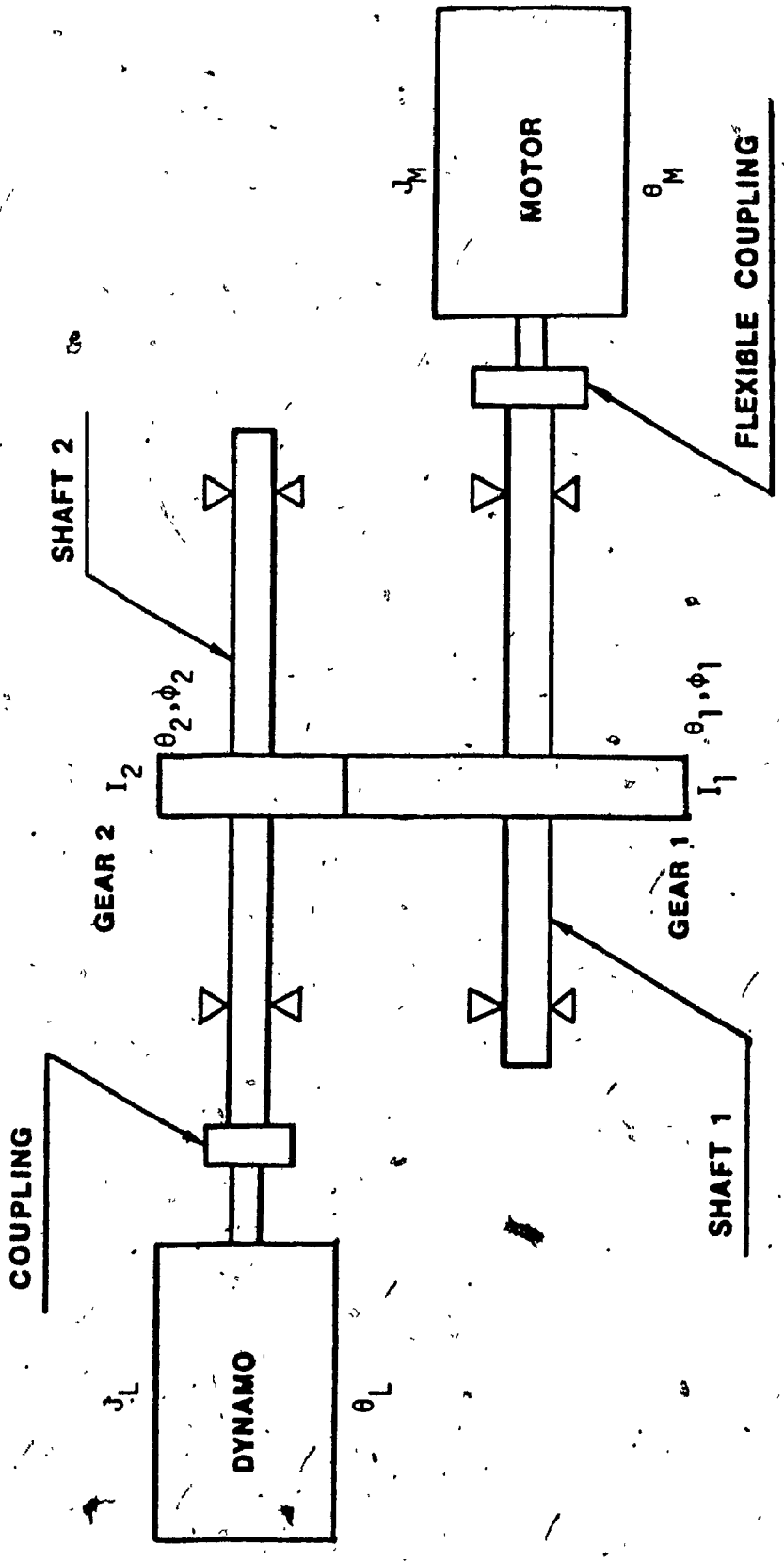

Fig. 3.5 A Simple Helical Geared Shaft System

The excitation to the helical geared rotor system can come from internal sources such a static transmission error, or from external sources such as support excitations.

The equations of motion are derived for a simple helical geared shaft system described by Fig. 3.5, when excited by a static transmission error $\varepsilon(t)$ introduced between the two mating teeth as shown in Fig. 3.3.

$$m_1 \ddot{y}_1 + k_{y1} y_1 + c_{y1} \dot{y}_1 + \bar{k}_t \delta_n \cos\beta + \bar{c}_t \dot{\delta}_n \cos\beta = [\bar{k}_t \varepsilon(t) + \bar{c}_t \dot{\varepsilon}(t)] \cos\beta \qquad (3.1)$$

$$m_2 \ddot{y}_2 + k_{y2} y_2 + c_{y2} \dot{y}_2 + \bar{k}_t \delta_n \cos\beta + \bar{c}_t \dot{\delta}_n \cos\beta = [\bar{k}_t \varepsilon(t) + \bar{c}_t \dot{\varepsilon}(t)] \cos\beta \qquad (3.2)$$

$$I_1 \ddot{\theta}_1 + k_{\theta 1}(\theta_1 - \theta_M) + c_{\theta 1} \dot{\theta}_1 + \bar{k}_t \delta_n r_1 \cos\beta + \bar{c}_t \dot{\delta}_n r_1 \cos\beta = [\bar{k}_t \varepsilon(t) + \bar{c}_t \dot{\varepsilon}(t)] r_1 \cos\beta \qquad (3.3)$$

$$I_2 \ddot{\theta}_2 + k_{\theta 2}(\theta_2 - \theta_L) + c_{\theta 2} \dot{\theta}_2 + \bar{k}_t \delta_n r_2 \cos\beta + \bar{c}_t \dot{\delta}_n r_2 \cos\beta = [\bar{k}_t \varepsilon(t) + c_t \dot{\varepsilon}(t)] r_2 \cos\beta \qquad (3.4)$$

$$m_1 \ddot{x}_1 + c_{x1} \dot{x}_1 + k_{x1} x_1 + \bar{k}_t \delta_n \sin\beta + \bar{c}_t \dot{\delta}_n \sin\beta = [\bar{k}_t \varepsilon(t) + \bar{c}_t \dot{\varepsilon}(t)] \sin\beta \qquad (3.5)$$

$$m_2 \ddot{x}_2 + c_{x2} \dot{x}_2 + k_{x2} x_2 + \bar{k}_t \delta_n \sin\beta + \bar{c}_t \dot{\delta}_n \sin\beta = [\bar{k}_t \varepsilon(t) + \bar{c}_t \dot{\varepsilon}(t)] \sin\beta \qquad (3.6)$$

$$(\frac{I_1}{2}) \ddot{\phi}_1 + k_{\phi 1} \phi_1 + c_{\phi 1} \dot{\phi}_1 + \bar{k}_t \delta_n r_1 \sin\beta + \bar{c}_t \dot{\delta}_n r_1 \sin\beta = [\bar{k}_t \varepsilon(t) + \bar{c}_t \dot{\varepsilon}(t)] r_1 \sin\beta \qquad (3.7)$$

$$(\frac{I_2}{2}) \ddot{\phi}_2 + k_{\phi 2} \phi_2 + c_{\phi 2} \dot{\phi}_2 + \bar{k}_t \delta_n r_2 \sin\beta + \bar{c}_t \dot{\delta}_n r_2 \sin\beta = [\bar{k}_t \varepsilon(t) + \bar{c}_t \dot{\varepsilon}(t)] r_2 \sin\beta \qquad (3.8)$$

$$J_M \ddot{\theta}_M + k_{\theta 1}(\theta_M - \theta_1) + c_M \dot{\theta}_M = T_M \qquad (3.9)$$

$$J_L \ddot{\theta}_L + k_{\theta 2}(\theta_L - \theta_2) + c_L \dot{\theta}_L = -T_L \qquad (3.10)$$

The displacement normal to the tooth surface, δ_n, couples the axial, flexural, torsional and rotational (about a gear diameter) motions of the two shafts at the driving and driven gear locations, and is given by

$$\delta_n = (y_1 + y_2 + r_1 \theta_1 + r_2 \theta_2) \cos\beta + (x_1 + x_2 + r_1 \phi_1 + r_2 \phi_2) \sin\beta \qquad (3.11)$$

3.4 Finite Element Model

The application of finite element method in solving a rotor system carrying spur gears to obtain the natural frequencies, mode shapes and dynamic response has already been discussed in 2.5.1. The same procedure will be used here, for the helical geared rotor. After assembling the mass and stiffness matrices, the effects of torsional-flexural-axial-rotational coupling, obtained from simplifying Eq. (3.1) to (3.10) using (3.11), are introduced into the appropriate locations. This coupling can be represented as:

Stiffness Matrix

$$\begin{Bmatrix} y_1 \\ y_2 \\ \theta_1 \\ \theta_2 \\ x_1 \\ x_2 \\ \phi_1 \\ \phi_2 \end{Bmatrix} \xrightarrow{\bar{k}_t} \begin{bmatrix} A_1 & A_2 & A_1r_1 & A_1r_2 & A_2 & A_2 & A_2r_1 & A_2r_2 \\ & A_1 & A_1r_1 & A_1r_2 & A_2 & A_2 & A_2r_1 & A_2r_2 \\ & & A_1r_1^2 & A_1r_1r_2 & A_2r_1 & A_2r_1 & A_2r_1^2 & A_2r_1r_2 \\ & & & A_1r_2^2 & A_2r_2 & A_2r_2 & A_2r_1r_2 & A_2r_2^2 \\ & & & & A_3 & A_3 & A_3r_1 & A_3r_2 \\ & & & & & A_3 & A_3r_1 & A_3r_2 \\ & & & & & & A_3r_1^2 & A_3r_1r_2 \\ & & & & & & & A_3r_2^2 \end{bmatrix}$$

Symmetric

where $A_1 = \cos^2 \beta$, $A_2 = \cos \beta \sin \beta$

$A_3 = \sin^2 \beta$

3.5 Dynamic Response due to Excitation by a Static Transmission Error

After the finite element model has been obtained, the dynamic response due to internal excitations such as that of a static transmission error is studied. The forces acting on the gear are described below and are introduced into the finite element model of appropriate locations, to obtain the global force vector.

Force Vector

$$\begin{Bmatrix} y_1 \\ y_2 \\ \theta_1 \\ \theta_2 \\ x_1 \\ x_2 \\ \phi_1 \\ \phi_2 \end{Bmatrix} \rightarrow A \begin{Bmatrix} \cos\beta \\ \cos\beta \\ \cos\beta\ r_1 \\ \cos\beta\ r_2 \\ \sin\beta \\ \sin\beta \\ \sin\beta\ r_1 \\ \sin\beta\ r_2 \end{Bmatrix}$$

where $A = \bar{k}_t\ \varepsilon(t) + \bar{c}_t\ \dot{\varepsilon}(t)$

A harmonic analysis of the static transmission error curve shows that a significant component of the excitation has the frequency of tooth mesh, Ω_r [11]. If $\varepsilon(t) = e_{av} \sin \Omega_r t$ where e_{av} = magnitude of the static transmission error, m.

Then $A = |A| \sin(\Omega_r t + \phi)$

where $|A| = e_{av} \sqrt{(\bar{k}_t)^2 + (\bar{c}_t \Omega_r)^2}$

$$\phi = \tan^{-1}\left(\frac{\bar{c}_t \Omega_r}{\bar{k}_t}\right)$$

3.5.1 Analysis

If the global mass, stiffness, and damping matrices are denoted by [M] [K] and [C] respectively, the equations of motion can be written as

$$[M]\{\ddot{q}\} + [C]\{\dot{q}\} + [K]\{q\} = \{F\} \qquad (3.12)$$

where $\{F\}$ represents the global force vector. Gyroscopic effects are neglected as in Section 2.5 and therefore a normal mode analysis is used to solve the equations of motion. The homogeneous form of Eq. (3.12) neglecting damping is given by

$$[M]\{\ddot{q}\} + [K]\{q\} = 0$$

and is solved to obtain the eigenvalues λ_j and the eigen vectors $\{\phi_j\}$ of the system.

Expressing the response $\{q\}$ in terms of the modal coordinates $\{p\}$ as

$$\{q\} = [\phi]\{p\} \qquad (3.13)$$

where $[\phi]$ is the modal matrix formed by using eigenvector $\{\phi_j\}$. Using (3.13) in (3.12) and premultiplying by $[\phi]^T$ results in uncoupled equations in the modal coordinates of the form

$$[\mu]\{\ddot{p}\} + [\gamma]\{\dot{p}\} + [\kappa]\{p\} = \{\sigma\} \qquad (3.14)$$

where $[\mu] = [\phi]^T [M] [\phi]$

$[\kappa] = [\phi]^T [K] [\phi]$

$[\sigma] = [\phi]^T \{F\}$

where γ_j are element of $[\gamma]$ and denote the equivalent damping coefficient in each mode.

The solution of (3.14) yields

$$p_i = \frac{\sigma_i}{(-\omega^2 \mu_i + \kappa_i) + j'(\gamma_i \omega)} \qquad (3.15)$$

where $j' = \sqrt{-1}$

$i = 1, 2, \ldots N$

Using (3.15) in (3.13) we can obtain the system dynamic response $\{q\}$.

3.5.2 Numerical Results

The details of the geared shaft used to obtain the numerical results are given in Table 3.1. The pedestals are assumed to be flexible in the x,y, and z directions. A finite element discretisation of the geared shaft system considered for the numerical example is shown in Fig. 3.6. Each of the elements has two nodes, and each node has 6 DOF-3 translations and 3 rotations. The details of the beam elements are given in Table 3.2. The system natural frequencies in the range 0-100 Hz are given in Table 3.3. The zero natural frequency corresponds to a torsional rigid body mode.

Frequency domain flexural response in the y direction at the driven gear location (DOF #6) is shown in Fig. 3.7. The abscissa is frequency of rotation of the driven gear. There are 50 teeth on the driven gear. The system shows peak response at the system natural frequencies in the operating

TABLE 3.1

Details of the Rotor System Under Study

E	2.0×10^{11} N/m^2
G	0.8×10^{11} N/m^2
I_1	0.08485 kg m^2
I_2	0.01142 kg m^2
J_m	0.459 kg m^2
J_L	0.02148 kg m^2
$\bar{k}_t$	2.0×10^9 N/m
k_{xx}	8.0×10^9 N/m
k_{yy}, k_{zz}	8.0×10^8 N/m
m_1	11.36 kg
m_2	6.13 kg
r_1	0.1 m
r_2	0.05 m
e_{rav}	6×10^{-4} m (variable)
β	10°

TABLE 3.2

Details of the Rotor Elements

Element No.	Length, m	Diameter, m	Mass per Unit Length kg/m
1	0.5	0.02	2.51
2	0.6	0.02	2.51
3	0.5	0.03	5.665
4	0.6	0.03	5.665

TABLE 3.3

System Natural Frequencies 0-100 Hz

Mode No.	System Natural Frequency, Hz
1	zero
2	22.84
3	42.73
4	62.43
5	70.95

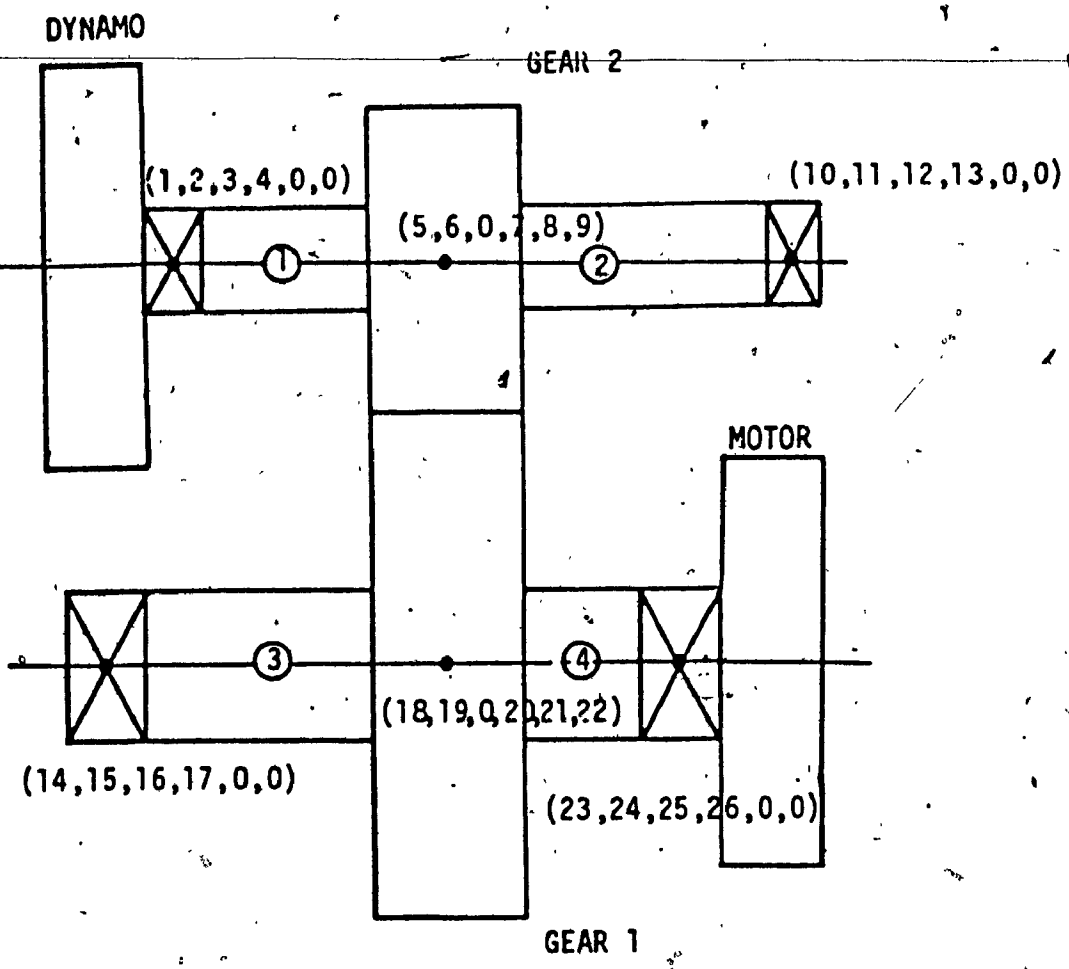

Fig. 3.6 Finite Element Discretisation of the Helical Geared Shaft System

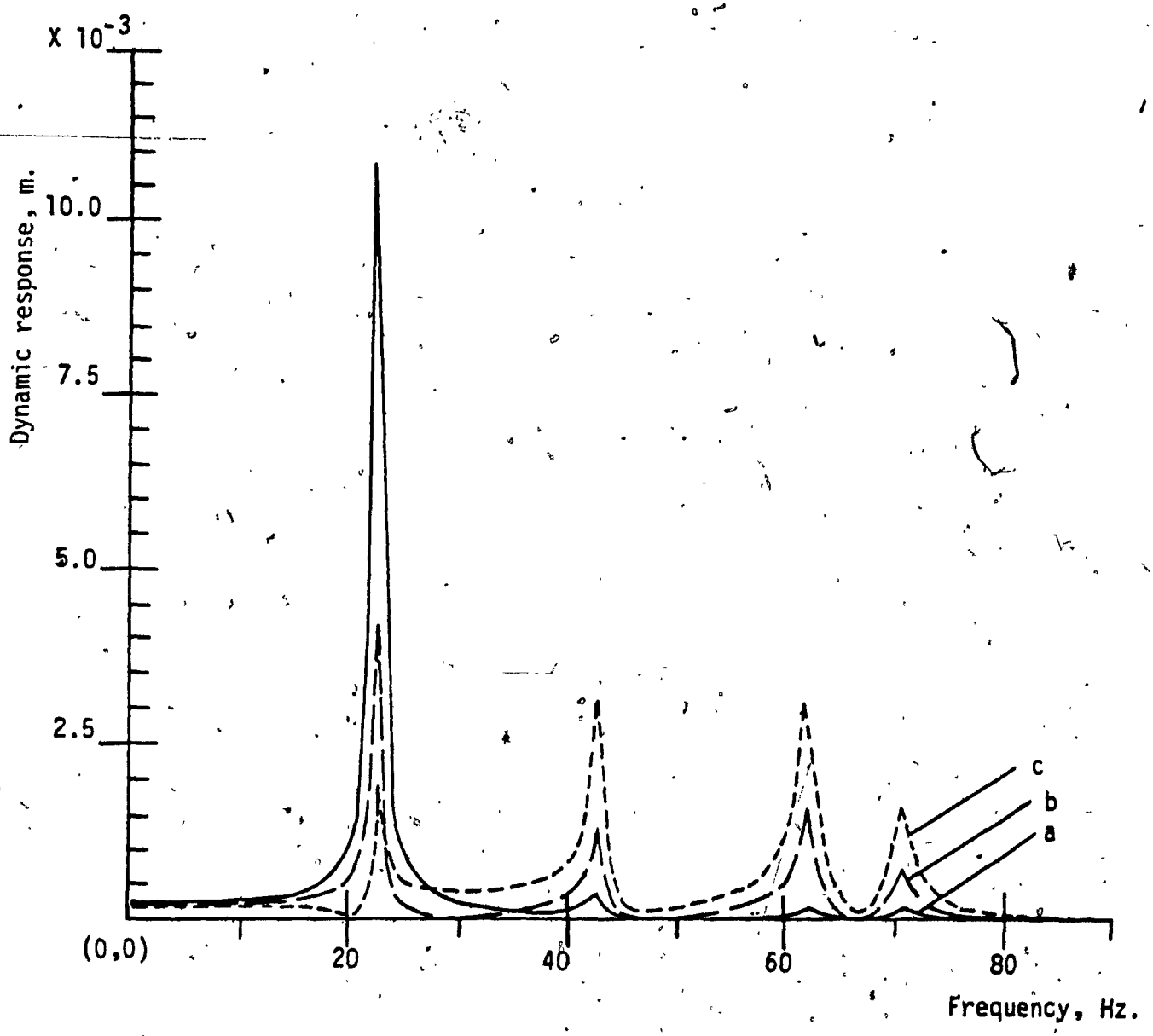

Fig. 3.7 Flexural response at the driven gear location in the y direction (DOF #6) against the frequency of rotation of the driven gear

a) $e_{av} = 2 \times 10^{-4}$ m. b) $e_{av} = 6 \times 10^{-4}$ m.

c) $e_{av} = 1 \times 10^{-3}$ m.

range. Three cases are plotted for varying magnitudes of the static transmission error. It is observed that as the magnitude of the static transmission error is increased the response decreases for the 2nd mode but increases for modes 3, 4 and 5.

The frequency domain flexural response in the y direction at the driving gear location (DOF #19) is shown in Fig. 3.8. The abscissa is frequency of rotation of the driven gear. The system shows peak response at the system natural frequenices in the operating range. Three cases are plotted for varying magnitudes of the static transmission error. It is observed that as the magnitude of the error is increased, the response decreases for the 2nd mode but increases for modes 3, 4 and 5. The response at the driving shaft is found to be smaller in magnitude to that of the driven shaft.

3.6 The Effect of Random Support Excitations

As discussed in 2.9, the excitation to a geared shaft system may be from external souces such as support excitations. Support excitations are in general random in nature and response can be obtained using a statistical analysis.

The finite element model of a helical geared shaft system described by Eq. (3.12) is used to study the system

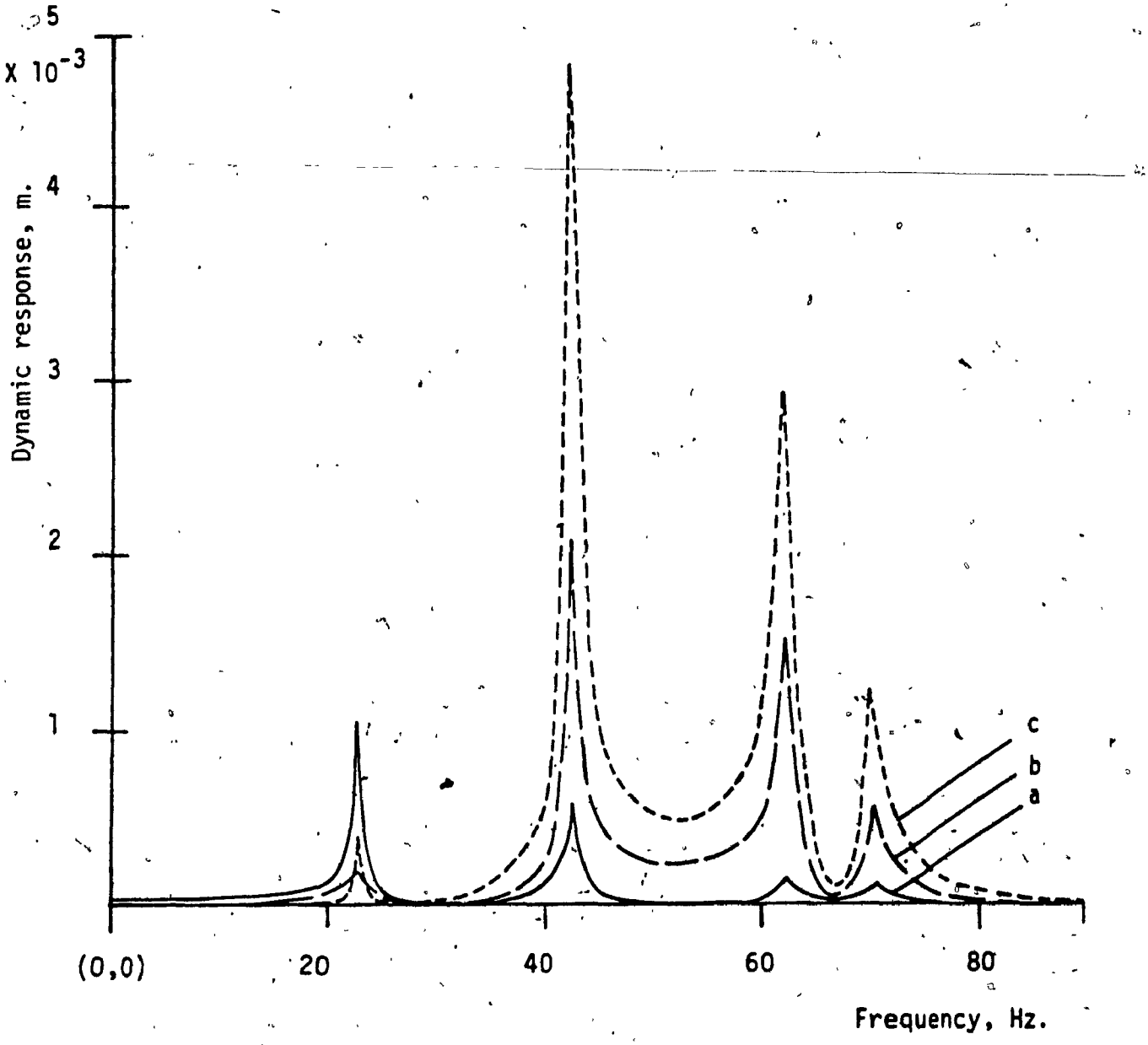

Fig. 3.8 Flexural response at the driving gear location in the y direction (DOF #19) against the frequency of rotation of the driven gear

a) $e_{av} = 2 \times 10^{-4}$ m. b) $e_{av} = 6 \times 10^{-4}$ m.

c) $e_{av} = 1 \times 10^{-3}$ m.

response due to Random Support Excitations.

3.6.1 Analysis

The equations of motion for a N degree of freedom geared shaft system subjected to support excitations can be expressed as

$$[M]\{\ddot{q}_r\} + [C]\{\dot{q}_r\} + [K]\{q_r\} = \{F\}_R \qquad (3.16)$$

where [M], [C] and [K] are described by Eq. (3.12)

$\{q\}$ = generalised rotor displacement vector

$\{q_s\}$ = support displacement vector

$\{q_r\} = \{q - q_s\}$, is the relative displacement vector.

and $$\{F\}_R = -[M]\{\ddot{q}_s\} \qquad (3.17)$$

Following the analysis as described in Section 2.9.1, the PSD matrix of the relative displacement can be obtained as given by Eq. (2.86) as,

$$[S_{qr}(\omega)] = [\phi][H(j\omega)][\phi]^T [S_F(\omega)] \times [H(-j\omega)]^T [\phi]^T \qquad (3.18)$$

where $[\phi]$ = undamped modal matrix.

and $[H(j\omega)]$ = frequency response function.

The PSD matrix of the random excitation force $[S_F(\omega)]$ can be expressed in terms of the PSD matrix of the displacement support excitation $[S_{qs}(\omega)]$ as

$$[S_F(\omega)] = \omega^4 \ [M] \ [S_{qs}(\omega)] \ [M]^T \qquad (3.19)$$

The displacement support excitation is assumed as the output of a linear filter, the input to which is an excitation in the vertical direction only. This excitation is an uncorrelated Gaussian stationary process with a white noise type of PSD.

3.6.2 Numerical Results

The details of the helical geared shaft system used to obtain the numerical results are given in Table 3.1. The pedestals through which the support excitations are transmitted to the geared rotor system are assumed to be flexible in the x, y, and z directions. A finite element discretisation of the geared shaft system considered for the numerical example is shown in Fig. 3.6. The details of the beam elements are given in Table 3.2. The system natural frequencies in the range 0-100 Hz are given in Table 3.3.

The geared rotor system is subjected to a displacement type of support excitations which is the output of a filter, the input to which is a Gaussian, stationary random process with a white noise type of PSD. This excitation is assumed to be in the vertical direction only and the excitations through the supports are assumed to be uncorrelated. The PSD of the response process is then obtained using a statistical analysis. The details of the linear filter are given in Table 2.13.

The normalized PSD of relative amplitude in the y direction at the driven gear location (DOF #6) is shown in Fig. 3.9. The base excitation is assumed to be the output of a first order linear filter, the input to which is an uncorrelated white noise type of PSD only in the vertical direction, and this is plotted on the x axis. The PSD plots shows peak response at all the elastic modes within the frequency range. The maximum response is seen at modes 2 and 3 and is about 3.16×10^{-3} m^2/Hz.

A PSD plot similar to that in Fig. 3.9 using a second order filter is shown in Fig. 3.10. The behavior of the response is the same as in Fig. 3.9 but the magnitude is lower for all modes. The maximum response is found to be around 3.16×10^{-5} m^2/Hz.

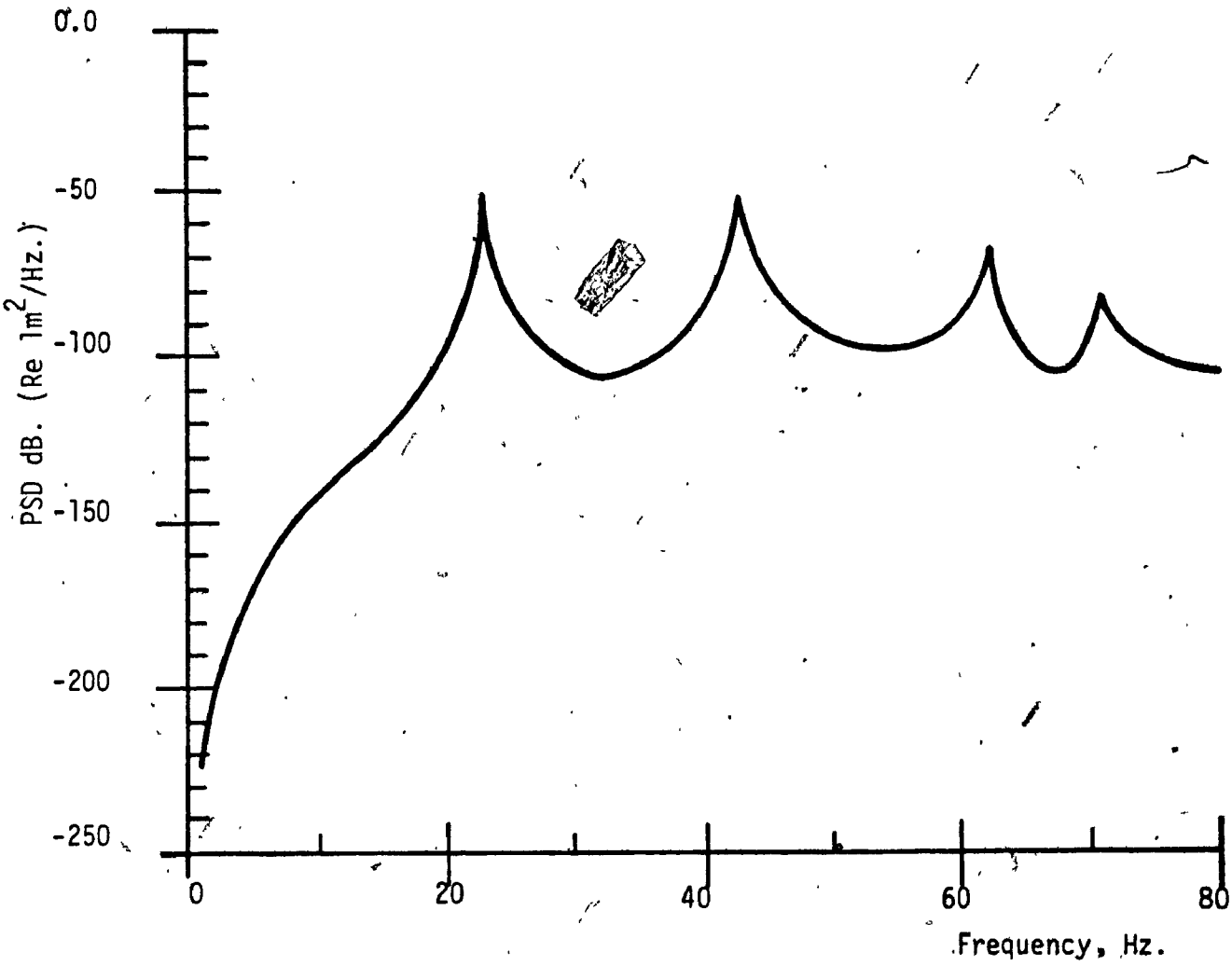

Fig. 3.9 Normalized PSD of relative amplitude in the y direction at the driven gear location (DOF #6) against the frequency of excitation. First order filter used.

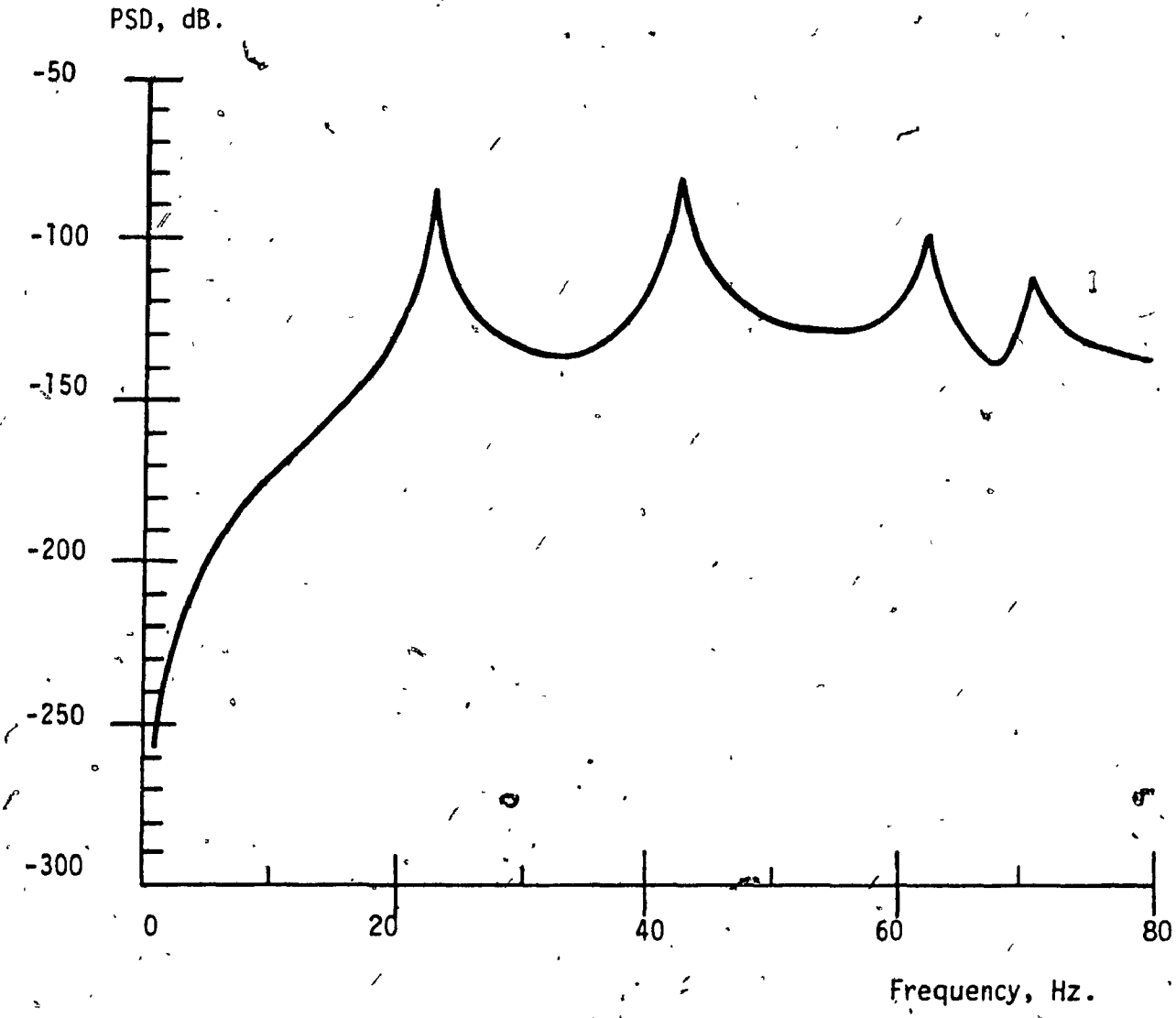

Fig. 3.10 Normalized PSD of relative amplitude in the y direction at the driven gear location (DOF #6) against the frequency of excitation. Second order filter used.

The normalized PSD of relative amplitude in the y direction at the driving gear location (DOF #19) is shown in Fig. 3.11. The base excitation is assumed to be the output of a first order linear filter, the input to which is an uncorrelated white noise type of PSD in the vertical direction. The PSD plot shows peak response at all the elastic modes within the frequency range. The maximum response is observed in the 3rd mode and corresponds to about 3.16×10^{-3} m^2/Hz.

A PSD plot similar to that in Fig. 3.11 using a second order filter is shown in Fig. 3.12. The behavior of the response is the same as in Fig. 3.11, but the magnitude is lower for all the modes. The maximum response is found to be around 1.78×10^{-4} m^2/Hz.

The normalized PSD of relative amplitude in the y direction at the bearing locations (DOF #2 and #24) is shown in Figures 3.13 and 3.14. The base excitation is assumed to be the output of a first order linear filter, the input to which is an uncorrelated white noise type of PSD in the vertical direction. The responses are as expected, much smaller than the response at the gear locations. The behaviour of the response for the bearing location (DOF #2) on the driven shaft is the same as that for the driven gear location (Fig. 3.9 & 3.10), but the maximum response is 1×10^{-10} m^2/Hz.

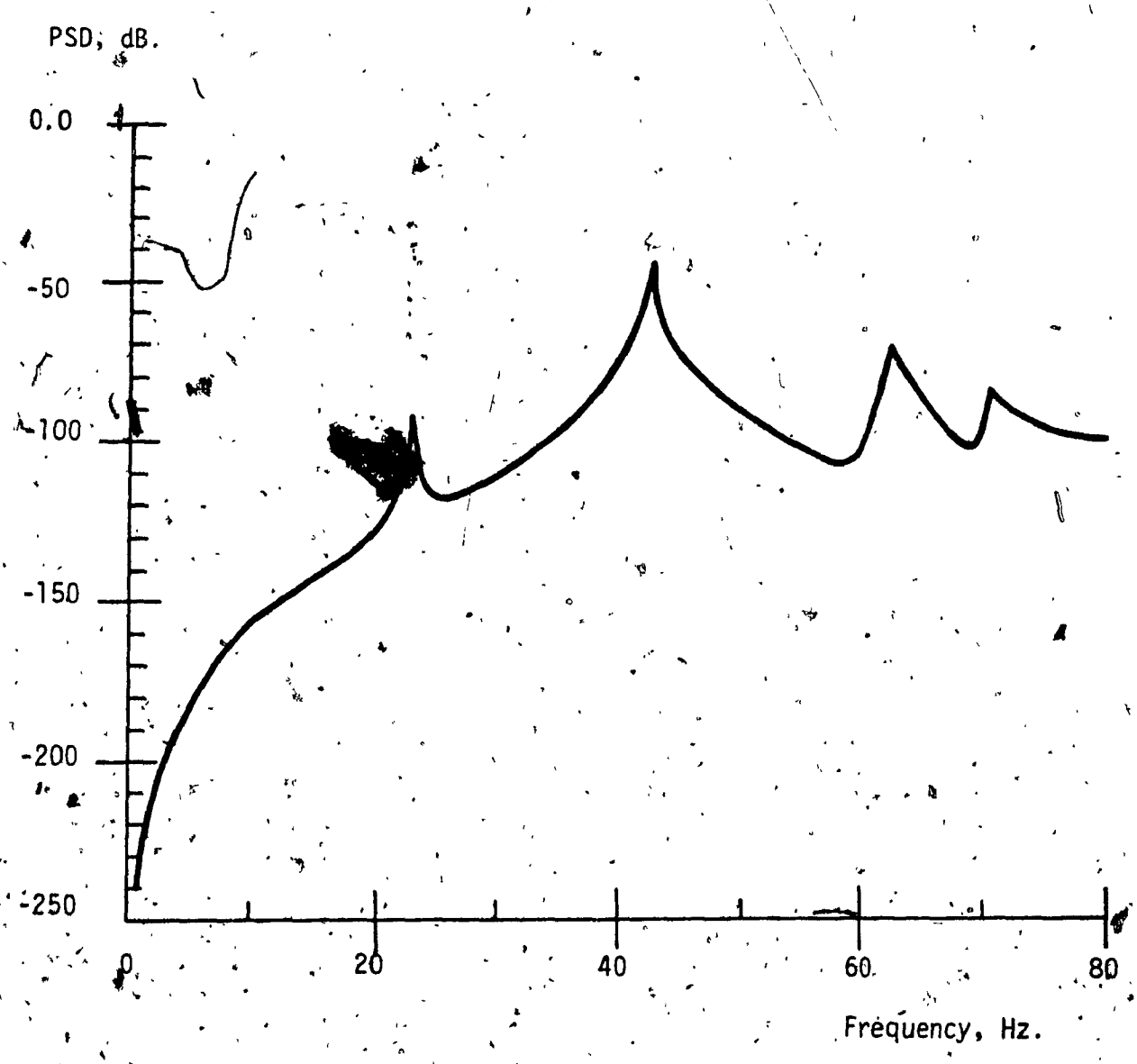

Fig. 3.11 Normalized PSD of relative amplitude in the y direction at the driving gear location (DOF #19) against the frequency of excitation. First order filter used.

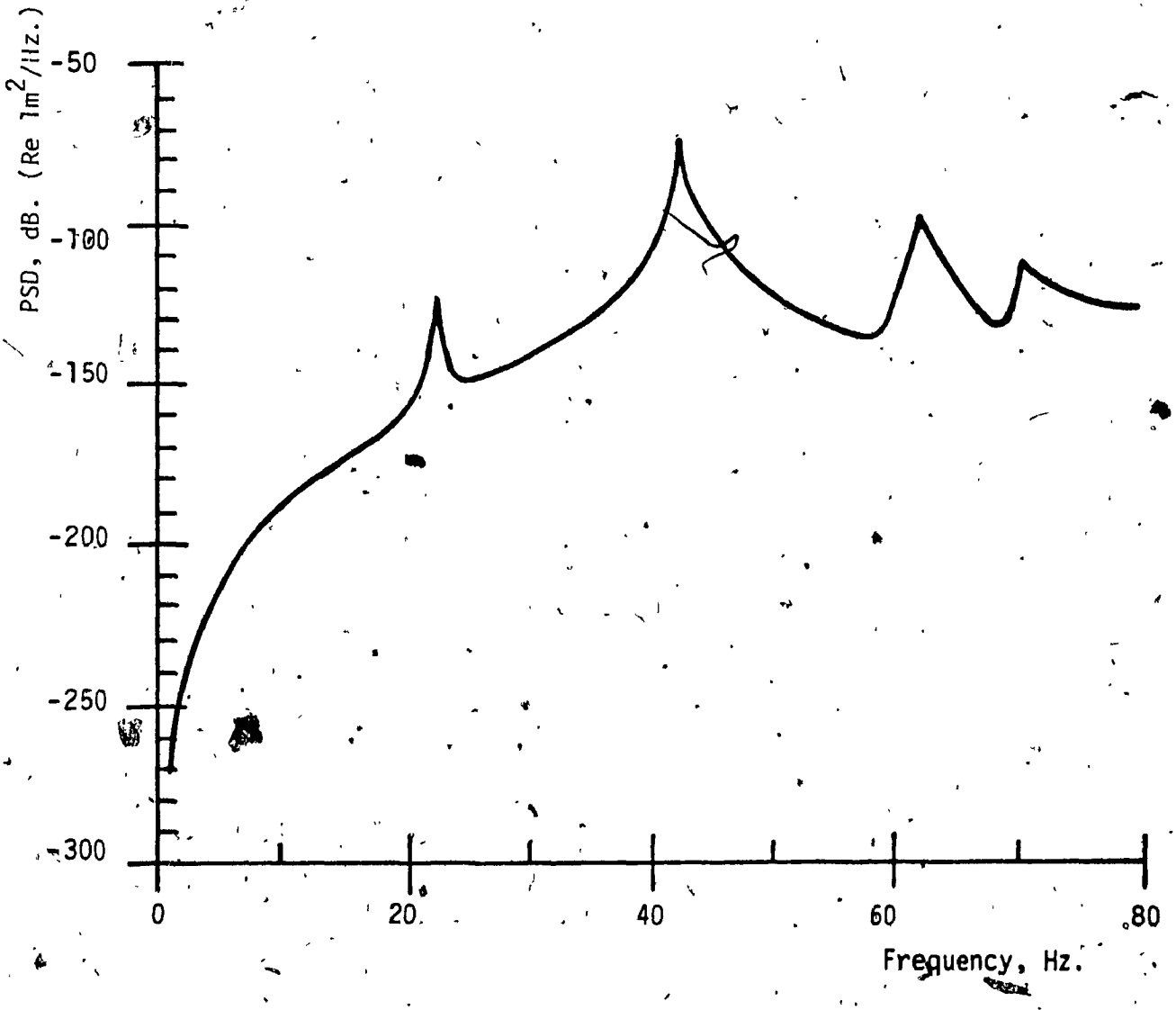

Fig. 3.12 Normalized PSD of relative amplitude in the y direction at the driving gear location (DOF #19) against the frequency of excitation. Second order filter used.

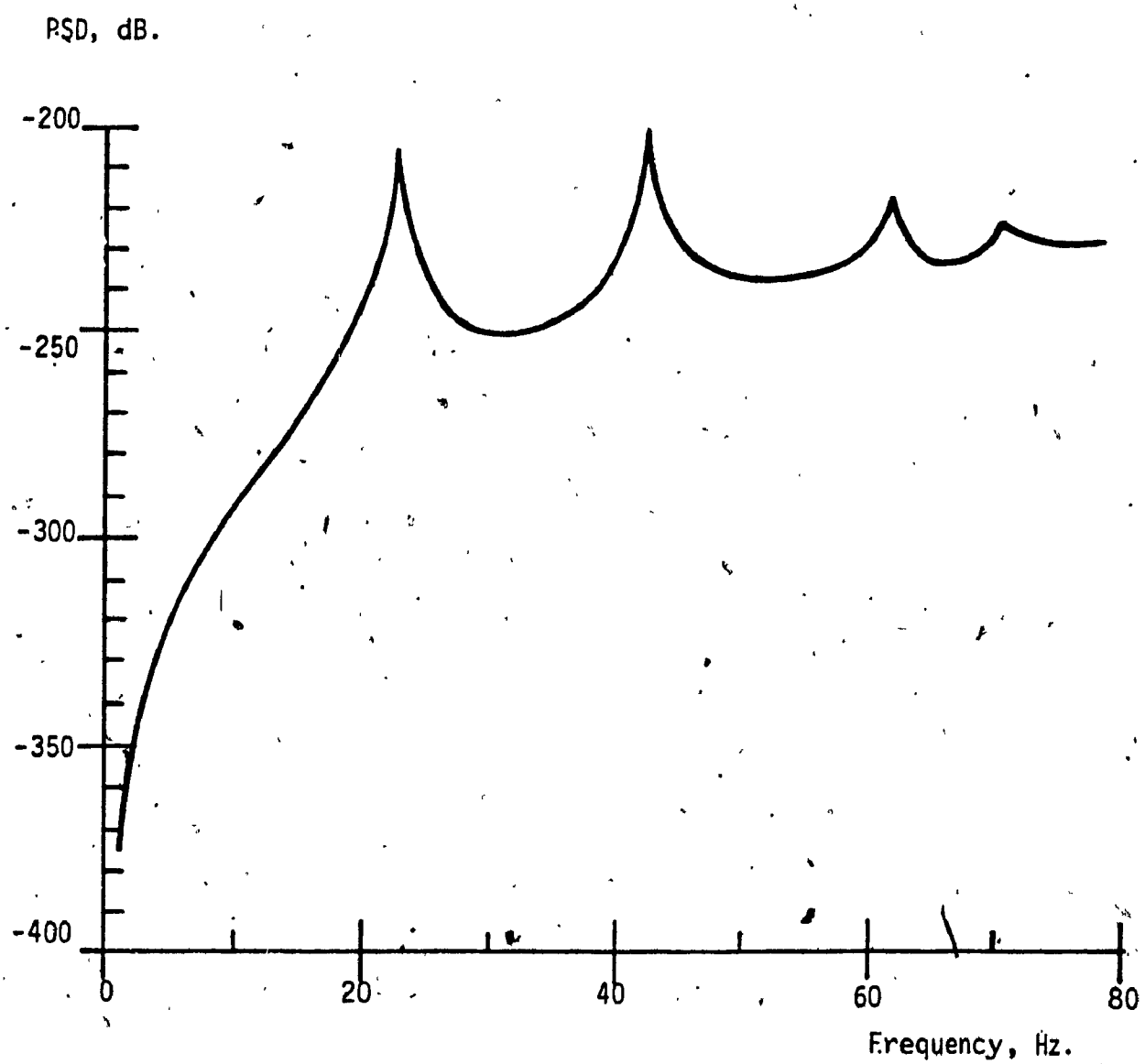

Fig. 3.13 Normalized PSD of relative amplitude in the y direction at the bearing location (DOF #2) against the frequency of excitation. First order filter used.

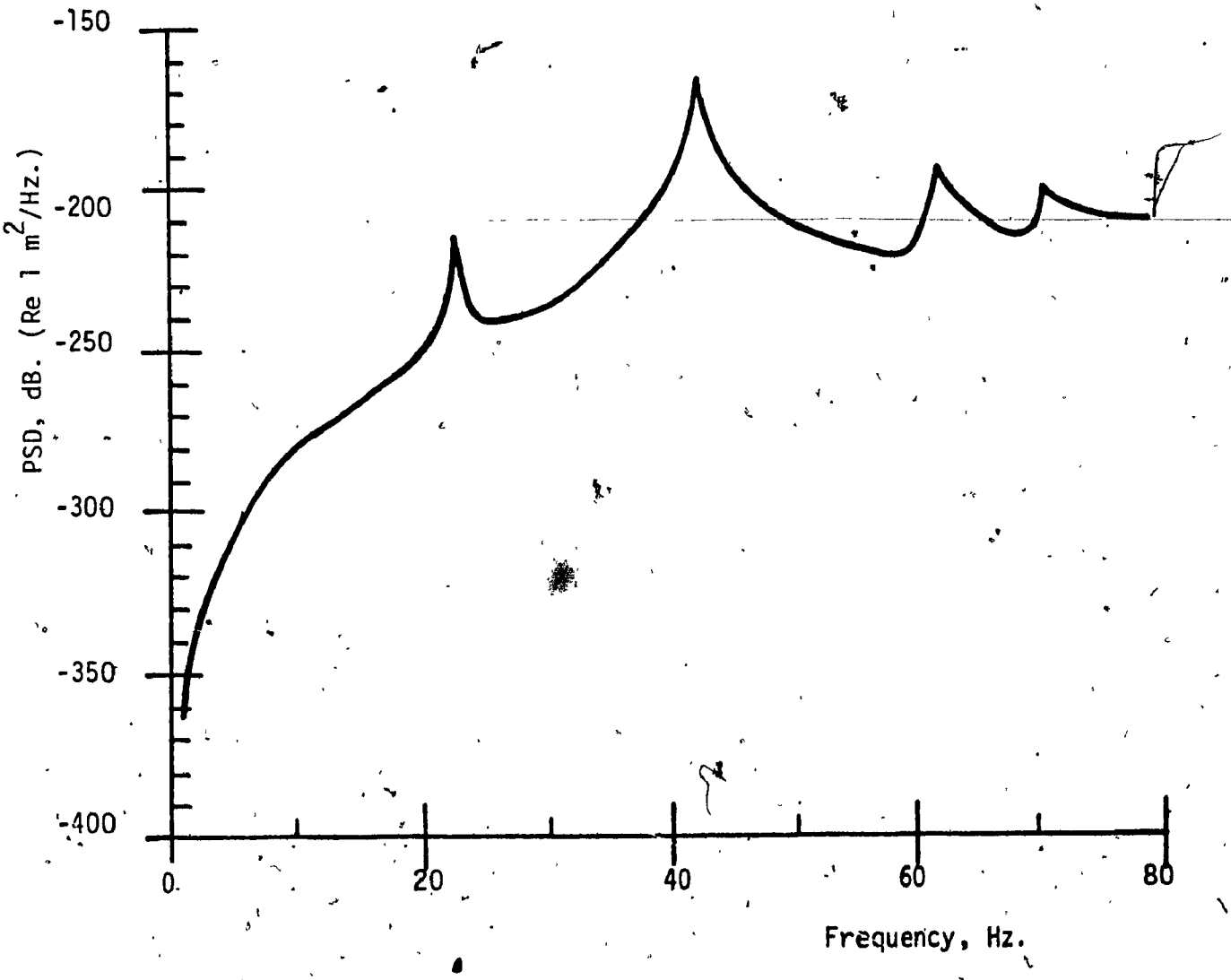

Fig. 3.14 Normalized PSD of relative amplitude in the y direction at the bearing location (DOF #24) against the frequency of excitation. First order filter used.

The behaviour of the response for the bearing locations (DOF #24) on the driving shaft is the same as that for the driving gear location (Fig. 3.11 & 3.12) but the maximum response is 1.78×10^{-7} m^2/Hz.

3.7 Summary

In this chapter, the dynamic response of a helical geared shaft system subjected to internal or external excitations is obtained using modal analysis methods.

The dynamic analysis of a helical geared shaft system is more complicated than a spur geared system because the torsional, flexural axial and rotational (about a gear diameter) motions of the shaft at the gear locations are coupled. In order to obtain these coupling terms, a simple model of a geared shaft system is considered. This system consists of a motor driving a dynamo through a pair of helical gears. The effects of backlash and time varying mesh stiffness are neglected. These coupling terms, once identified are introduced into the finite element model of a rotor system consisting of two parallel shafts mounted on elastic rolling element bearings. The internal source of excitation is considered first in the form of a static transmission error which is interposed between two mating teeth. The response is obtained at the gear locations using normal mode analysis. The static transmission error, as described in Chapter 2, is the composite

effect of tooth face modifications, machining errors and wear and tooth deformations, and represents the primary source of excitation in geared shaft systems.

Further, the effect of external excitations such as support excitations on the dynamic response of a helical geared shaft system is also studied. Support excitations occur for instance, on board moving vehicles and is modelled as the output of a linear filter, the input to which is an uncorrelated stationary Gaussian process with a white noise type of PSD. Results are presented for the response at the gear and bearing locations.

The following chapter discusses the fatigue behaviour of geared rotors.

CHAPTER 4

Fatigue Behaviour of Helical Geared Rotors

4.1 Introduction

Working stresses that have been determined from the ultimate or yield point values of the material using a factor of safety give safe and reliable results only for static loading. In Chapter 3, a simple helical geared shaft system was analysed to obtain the dynamic response of the shafts carrying the gears. In this Chapter, the fatigue behaviour of geared rotor systems is considered. Since most of the geared rotors transmitting heavy loads use helical gears, here the fatigue behaviour of helical gear carrying shafts only are studied. Results for spur gears may be obtained by considering them as a special case of helical gears. Failure of the shaft due to repetetious application of cyclic stresses for several number of cycles, well below the yield stress in the material is termed as fatigue failure. Such a failure is quite abrupt and resembles a brittle fracture. When the structure is acted upon by cyclic stresses only, fatigue life may be obtained using the S-N diagram for the material. In geared rotor systems, the fluctuating stresses are superimposed over a mean stress and in such cases fatigue life may be obtained by using a mean stress diagram.

4.2 Basic Mean and Alternating Stresses

In general, a geared shaft system is loaded to experience basic mean stresses σ'_m in addition to the basic alternating stresses σ'_a at different critical cross sections. A typical critical cross section is shown in Fig. 4.1. Let it be subjected to a non-rotating flexural moment $\bar{M} = M_m + M_a \sin \omega t$, torsional moment $\bar{T} = T_m + T_a \sin \omega t$ and axial force $\bar{F}_{ax} = F_{axm} + F_{axa} \sin \omega t$, all of which are acting in phase, where the subscripts m and a denote mean and alternating components. ω is the angular velocity of the shaft. Using the maximum energy of distortion theory, which is the most reliable strength theory [76], the basic alternating and basic mean stresses on the surface of the critical cross section are,

$$\sigma'_a = \frac{32}{\pi d^3} \sqrt{(M_a + M_m + \frac{dF_{axa}}{8})^2 + \frac{3}{4} T_a^2} \qquad (4.1)$$

$$\sigma'_m = \frac{32}{\pi d^3} \sqrt{(\frac{dF_{axm}}{8})^2 + \frac{3}{4} T_m^2} \qquad (4.2)$$

At a critical cross section of the shaft having a change in diameter, d is not known. Bagci [76] describes an iterative procedure to include the effect of axial forces $\bar{F}_{ax}$.

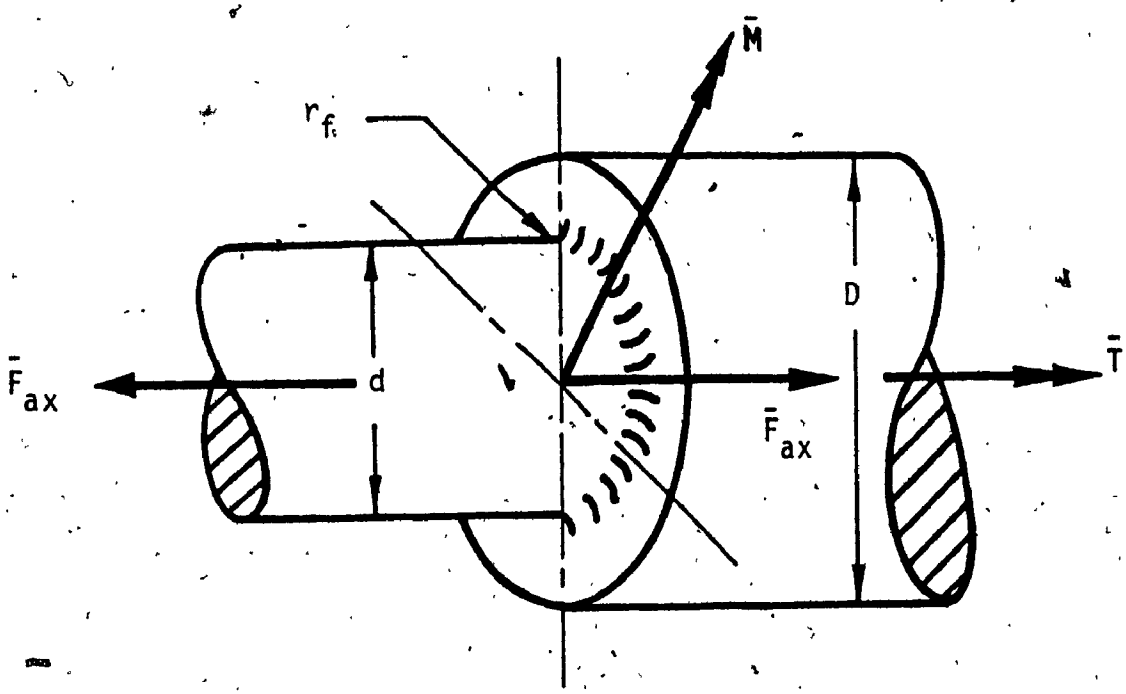

Fig. 4.1 Loading at a critical shaft section having notch due to shoulder [78]

4.3 Fatigue Design Equation

The design equation used to synthesise the shaft for fatigue life or to determine its fatigue life is

$$\sigma'_a = \sigma_{af} / f_s \tag{4.3}$$

$$\sigma'_m = \sigma_{mf} / f_s \tag{4.4}$$

where σ_{af} is the endurance limit in the presence of mean stress, σ_{mf} is the mean stress and f_s is the factors of safety.

The equation (4.3) and (4.4) are used to determine the fatigue life of a critical cross section for specified values of f_s and reliability level. They could also be used to determine the smallest factor of safety with the dimensions given for the fatigue life and reliability levels specified.

4.4 Mean Stress Diagram

A mean stress diagram is used to relate σ'_a and σ'_m at each section. Several forms of the mean stress diagram have been used since Gerber's second order relationship [90],

$$\sigma_{af} = \sigma'_e \left[1 - \left(\frac{\sigma_{mf}}{S_u}\right)^2 \right] \tag{4.5}$$

where σ'_e = endurance limit for the material.

S_u = ultimate strength of the material.

Other mean stress diagrams have been given by Goodman [91] and Soderberg [92] (see Fig. 4.2). Bagci [78] proposed a new relationship between σ'_a and σ'_m,

$$\sigma_{af} = \sigma_e \left[1 - \left(\frac{\sigma_{mf}}{S_y}\right)^4\right] \tag{4.6}$$

where S_y is the yield strength of the shaft material as determined by a test specimen of diameter 0.3 in. and σ_e is the reduced endurance limit given by,

$$\sigma_e = R_f \, S'_{ef} \tag{4.7}$$

where R_f = resultant of the fatigue strength reducing factors.

The endurance limit for a rotating-beam specimen, S'_{ef}, is given by the S-N diagram,

$$S_{ef'} = S_{eo} \qquad N > 10^6 \tag{4.8}$$

where N is the number of stress cycles, S_{eo} is the endurance limit of the material for infinite life as determined by standard test specimen of diameter 0.3 in.

Now,

$$\log S'_{ef} = - a \log N + b \quad , \; 10^3 < N < 10^6 \tag{4.9}$$

and

$$S'_{ef} = \left[1 - \frac{(1-h)}{10^3} N\right] S_u \quad , \; N < 10^3 \tag{4.10}$$

$$m = \sigma_a'/\sigma_m'$$

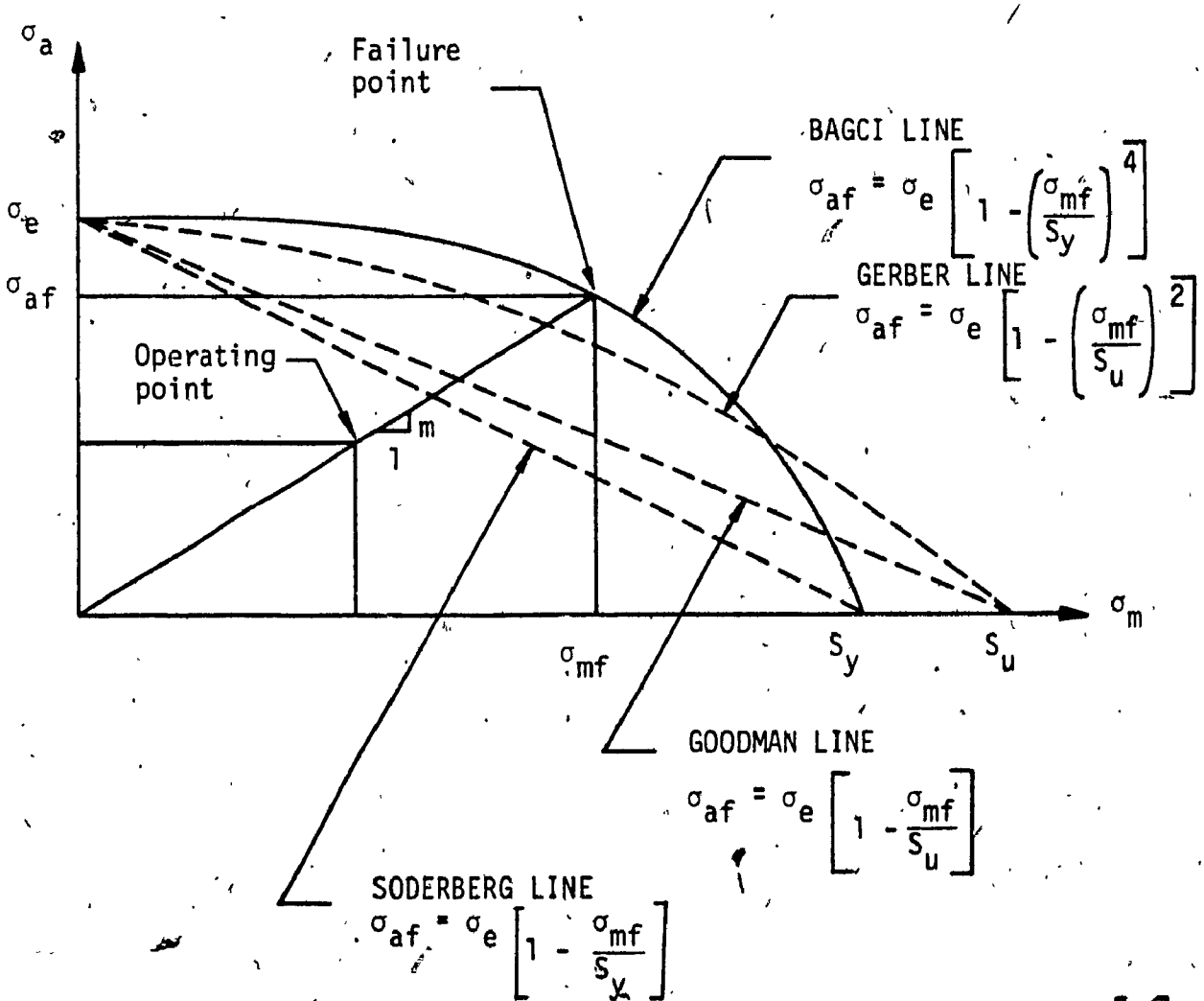

Fig. 4.2 The old and new forms of the mean stress diagram [78]

where,

$$a = \frac{1}{3} \log (h S_u / S_{eo}) \qquad (4.11a)$$

$$b = \log [(h S_u)^2 / S_{eo}] \qquad (4.11b)$$

where h is a constant ≈ 0.9 for carbon steels and S_u is the ultimate strength of the shaft material as determined by the standard test specimen of diameter 0.3 in. and S_{eo} is generally approximated by

$$S_{eo} = k S_u \qquad (4.12)$$

where k ≈ 0.5 for wrought steels and k ≈ 0.4 for cast steels. S_{eo} is also given by another result based on experimental data,

$$S_{eo} = 40 + 0.25 (S_u - 80) \qquad (4.13)$$

where S_{eo} and S_u are both in ksi.

4.5 Endurance Limit Modifying Factors

The endurance limit σ_e in Eq. (4.7) is a reduced endurance limit, which may be considerably smaller than the endurance limit S'_{ef} of a rotating beam specimen. The difference may be explained by employing a variety of modifying factors, each of which accounts for a separate effect, which are combined into a single factor R_f defined by,

$$R_f = C_a C_b C_c C_d C_e C_f \qquad (4.14)$$

where C_a = surface factor

C_b = size factor

C_c = reliability factor

C_d = temperature factor

C_e = modifying factor for stress concentration or notch effect factor

C_f = miscellaneous - effects factor

Shigley [93] gives an account of the factors mentioned above.

Fig. 4.3 gives surface modification factors for steel, depending upon the quality of finish and the tensile strength.

The rotating-beam test gives the endurance limit for a specimen 0.30 in. in diameter. When specimens of larger size are tested it is found that the endurance limit is lower. This fact is taken into account by the size factor given for bending, torsion and axial loading as,

$$C_b = \begin{cases} 1 & d \leq 0.3 \text{ in.} \\ 0.85 & 0.3 \leq d \leq 2 \text{ in.} \\ 0.75 & d \leq 2 \text{ in.} \end{cases} \qquad (4.15)$$

The reliability factor C_c is given by,

$$C_c = 1 - 0.08\, Z_R \qquad (4.16)$$

where Z_R is the standardized variable corresponding to the desired reliability R and is given in Table 4.1.

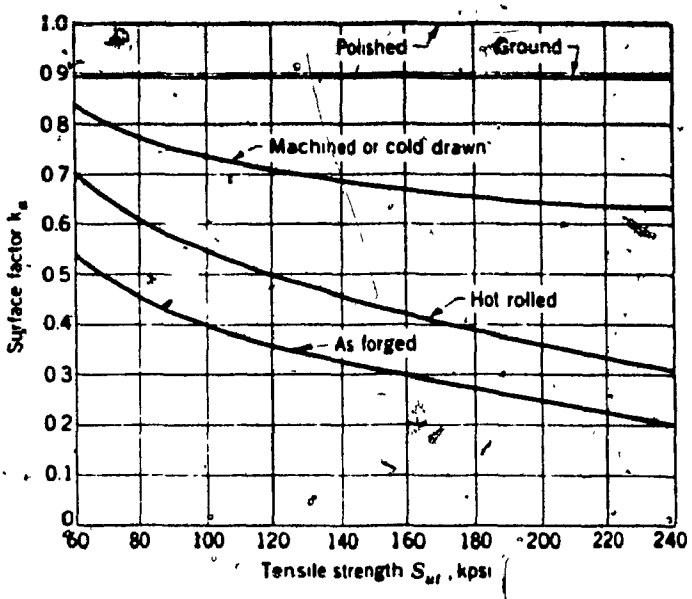

Fig. 4.3 Surface finish modifications for steel

(Figs. 4.3 to 4.5 from Shigley, J.E., Mechanical Engineering Design, McGraw-Hill).

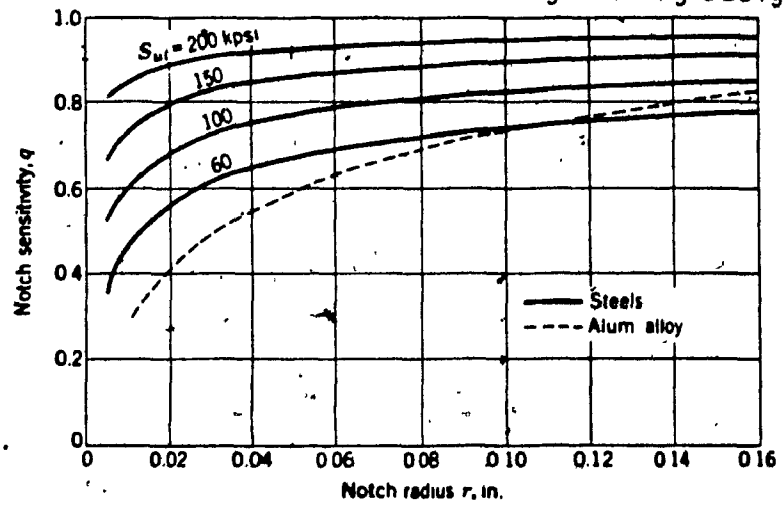

Fig. 4.4 Notch sensitivity charts for steels and 2024-T wrought aluminum alloys subjected to reversed bending or reversed axial loads (Use r = 0.16 in. if r > 0.16 in.)

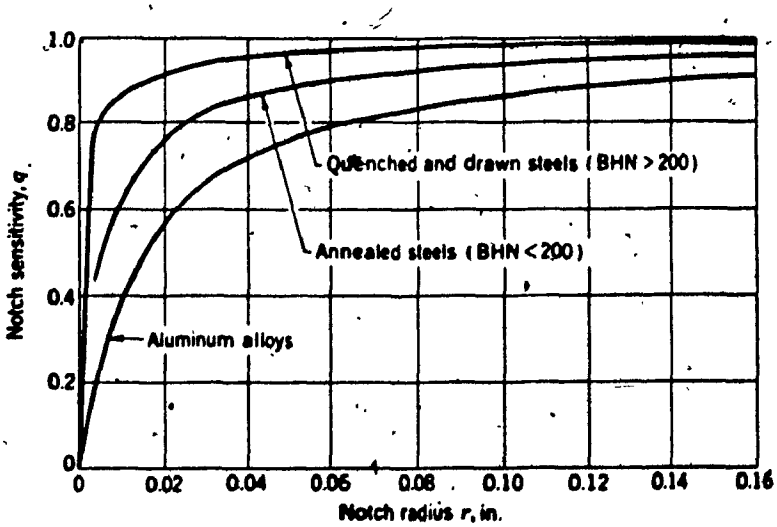

Fig. 4.5 Notch sensitivity curves for materials in reversed torsion (Use r = 0.16 in. if r > 0.16 in.)

Table 4.1

Reliability Factors C_c Corresponding to an 8 percent Standard Deviation of the Endurance Limit.

Reliability R	Standardized variable z_R	Reliability factor C_c
50	0	1.000
90	1.645	0.868
95	1.960	0.843
99	2.575	0.794
99.9	3.291	0.737
99.99	3.891	0.689

The temperature factor C_d is given by

$$C_d = \frac{620}{460 + T} \quad , \; T > 160^0 \text{ F}$$
$$= 1 \quad , \; T < 160^0 \text{ F} \qquad (4.17)$$

The notch effect factor C_e is given by

$$C_e = \frac{1}{1 + q_b (K_T - 1)} \qquad (4.18)$$

where q_b is the notch sensitivity at the critical section for flexural loading and is given by,

$$q_b = [1+0.11628(\frac{S_u}{100} - 1)] \; [0.86-326(0.25-r_f)^{(4+\frac{S_u}{100})}] \qquad (4.19)$$

where S_u is in k_{si} and r_f is in inches. The notch sensitivity for axial loading, q_x is also given by the above formula (4.19). Fig. 4.4 shows the notch sensitivity for steels and Aluminum alloys subjected to reversed bending and reversed axial loads. Fig. 4.5 shows the notch sensitivities for reversed torsion, q_s. k_T in Eq. (4.18) is the combined geometric stress concentration factor given by,

$$K_T = \frac{\sqrt{[(M_m+M_a)k_b+\frac{d}{8}(F_{axa}+F_{axm})k_{ax}\frac{q_x}{q_b}]^2+\frac{3}{4}[(T_a+T_m)k_s\frac{q_s}{q_b}]^2}}{\sqrt{[M_m+M_a+\frac{d}{8}(F_{axa}+F_{axm})]^2+\frac{3}{4}(T_a+T_m)^2}} \qquad (4.20)$$

where k_b, k_{ax} and k_s are geometric stress concentration factors for flexural, axial and torsional loading, whose numerical values can be found in Shigley [93].

The miscellanceous effects factor C_f may be due to residual stresses, corrosion or plating.

4.6 Dynamic Model of the Helical Geared Shaft System

In section 4.2, the basic mean and alternating stresses were defined in terms of the mean and alternating components of the flexural moment, torque and axial force. These basic stresses have to be obtained at the critical sections of the shafts in the geared rotor system in order to design for fatigue.

In a recent paper, Bagci [76], obtained the stresses at these critical sections using an inaccurate system model, leading to an inaccurate fatigue design. This is because the displacement of the rotors comprising the geared rotor system (which are related to stresses), are obtained by ignoring the inertial effects of the different elements. The damping in the system is also neglected. The external forces acting on the geared rotor system are taken as constant values although the analysis is carried out for a loading consisting of mean and alternating components. It is well known that in geared rotor systems, the principal source of vibratory excitation is the static transmission error [13] which to a first approximation be modelled as a sinusoidal variation at the

tooth meshing frequency [11]. In helical geared shaft systems there exists a torsional-flexural-axial-rotational coupling (section 3.4). This as well as the static transmission error are neglected in [76].

In chapter 3, the dynamic analysis of a simple helical geared shaft system was carried out. The torsional-flexural-axial-diametral coupling was considered and the dynamic response was obtained when excited by a static transmission error interposed between two perfect meshing teeth. A finite element model was used to discretise the system, which will prove to be convenient in determining the mean and alternating stresses at critical sections. The same model is used for the fatigue analysis, as shown in Fig. 4.6 including the mean components of the excitation force. The equations of motion are,

$$[M]\{\ddot{q}\} + [C]\{\dot{q}\} + [K]\{q\} = \{F\} \qquad (4.21)$$

where [M], [K] and [C] represent the mass, stiffness and damping matrices defined in Section 3.5. The excitation force vector $\{F\}$ can be expressed as,

$$\{F\} = \{F\}_m + \{F\}_a \qquad (4.22)$$

where $\{F\}_m$ denotes the mean component and $\{F\}_a$ denotes the alternating components of the excitation force and are given in Appendix II.

The response to $\{F\}_a$ was obtained in Section 3.5.1. Let us denote it as $\{q\}_a$. The response to $\{F\}_m$ can be obtained in a similar manner. Let us denote it as $\{q\}_m$. Then the total response $\{q\}_t$ can be expressed as

$$\{q\}_t = \{q\}_m + \{q\}_a \tag{4.23}$$

These are all global displacements from which the elemental displacements could be easily determined. Let $\{q\}_{em}$ and $\{q\}_{ea}$ denote the displacement vector for a representative element due to mean loading and alternating loading respectively. The element end force $\{F\}_e$ are related to the element displacements $\{q\}_e$ by,

$$\{F\}_e = [K]_e \{q\}_e \tag{4.24}$$

where $[K]_e$ is the element stiffness matrix. The mean and alternating components of the element end forces are given by

$$\{F\}_{em} = [K]_e \{q\}_{em}$$
$$\{F\}_{ea} = [K]_e \{q\}_{ea} \tag{4.25}$$

At each node, the vector $\{F\}_{em}$ is defined as,

$$\{F\}_{em} = \{F_{xm} F_{ym} F_{zm} F_{\theta xm} F_{\theta ym} F_{\theta zm}\}^T \tag{4.26}$$

Similarly,

$$\{F\}_{ea} = \{F_{xa} F_{ya} F_{za} F_{\theta xa} F_{\theta ya} F_{\theta za}\}^T \tag{4.27}$$

From (4.26) and (4.27), the mean and alternating components of the moment M_m and M_a are given by

$$M_m = \sqrt{(F_{\theta y})_m^2 + (F_{\theta z})_m^2}$$
$$M_a = \sqrt{(F_{\theta y})_a^2 + (F_{\theta z})_a^2} \tag{4.28}$$

Similarly, the mean and alternating components of the torque T_m and T_a are given by

$$T_m = (F_{\theta x})_m$$
$$T_a = (F_{\theta x})_a \qquad (4.29)$$

The effects of axial force can be considered as explained in Section 4.2, but for simplicity is neglected in the present analysis.

4.7 Numerical Results

The details of the geared shaft system used in the present study are given in Table 4.2. The pedestals are assumed to be flexible in the x, y and z directions. A finite element discretisation of the geared shaft system considered is shown in Fig. 4.6. The details of the beam elements are given in Table 3.2. Each of the elements has two nodes and each node has 6 DOF - 3 translations and 3 rotations.

The shaft is made of AISI 4340 cold drawn steel having $S_u = 7.6 \times 10^8$ N/m^2 and $S_y = 6.48 \times 10^8$ N/m^2. The surface finish factor C_a, the size factor C_b and the reliability factor C_c for 90% reliability are given by Section 4.5 as 0.72, 0.85 and 0.868.

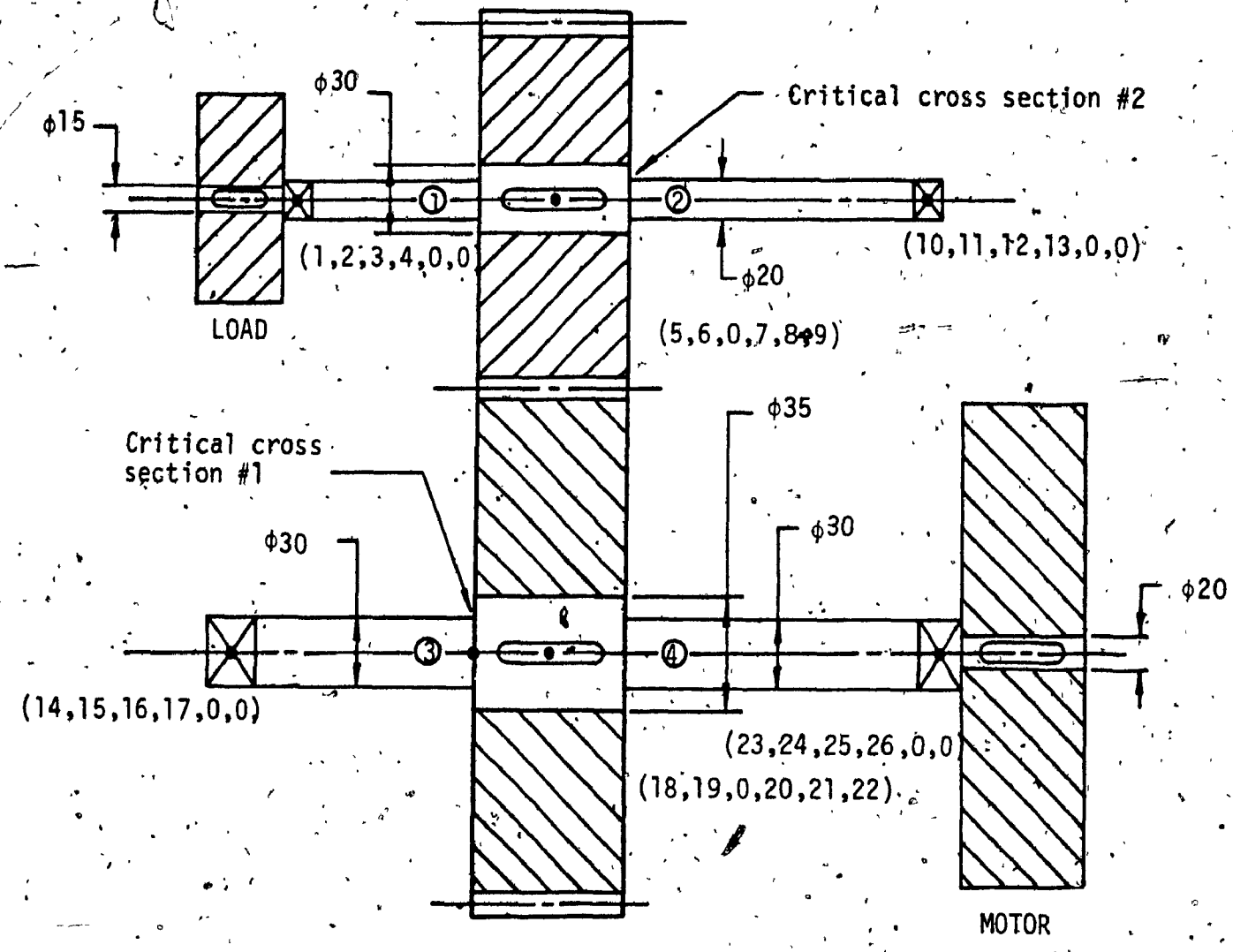

Fig. 4.6 Helical geared shaft system

The temperature factor C_d is taken as unity. The effects of axial loading are neglected for simplicity. The values of K_b and K_s as well as q_s in Eq. (4.20) are obtained from [77]. The value of q_b is calculated from Eq. (4.19), Eq. (4.20) and Eq. (4.18) are then used to compute the notch effect factor C_e. σ_e is then calculated from Eq. (4.7) and subsequently σ_{af} is calculated from Eq. (4.6). σ'_a is calculated using Eq. (4.1). The speed of the driven shaft is maintained at 3000 rpm and the number of teeth on the driven gear are assumed to be 30. The input torque is taken to be 35,62 Nm/rad.

The factor of safety is calculated from Eq. (4.3) for the data above. The first case is when the amplitude of the static transmission error is taken to be 0.1×10^{-3}m. The results at the critical cross section (#1) on the driving gear and that on the driven gear (#2) are:

#1 $\sigma'_{a1} = 0.1514 \times 10^8$ N/m^2, $\sigma'_{m1} = 0.6452 \times 10^1$ N/m^2

$\sigma_{af1} = 1.38 \times 10^8$ N/m^2

#2 $\sigma'_{a2} = 0.1127 \times 10^8$ N/m^2, $\sigma'_{m2} = 0.2769 \times 10^5$ N/m^2

$\sigma_{af2} = 1.31 \times 10^8$ N/m^2

This yields a factor of safety of 9.11 for the critical section #1 and a value of 11.62 for critical section #2.

Table 4.2

Details of the Rotor System Under Study

E	2.0×10^{11} N/m^2
G	0.8×10^{11} N/m^2
I_1	0.08485 kg m^2
I_2	0.01142 kg m^2
J_m	0.459 kg m^2
J_L	0.02148 kg m^2
$\bar{k}_t$	1.0×10^8 N/m
k_{xx}	8.0×10^9 N/m
k_{yy}, k_{zz}	8.0×10^8 N/m
m_1	11.36 kg
m_2	6.13 kg
r_1	0.1 m
r_2	0.05 m
e_{av}	5×10^{-4} m (variable)
β	10°
T_m	35.62 Nm/rad

When the magnitude of the static transmission error, e_{av} is increased to 0.5×10^{-3} m, the results are:

#1 $\sigma'_{a1} = .7567 \times 10^8$ N/m^2, $\sigma'_{m1} = 0.6452 \times 10^1$ N/m^2

$\sigma_{af1} = 1.38 \times 10^8$ N/m^2

#2 $\sigma'_{a2} = 0.555 \times 10^8$ N/m^2, $\sigma'_{m2} = 0.2769 \times 10^5$ N/m^2

$\sigma_{af2} = 1.31 \times 10^8$ N/m^2

This yields a factor of safety of 1.82 for critical section #1 and 2.36 for critical section #2. Both the designs are thus safe.

4.8 Summary

Usually, fatigue analysis of power transmission shafts are carried out by assuming loading which may not be accurate in terms of magnitude and variation, resulting in an overdesign or underdesign. In this chapter, a dynamic model of a helical geared shaft system including effects such as inertia of the elements, damping, torsional-flexural-axial-rotational coupling is considered. The basic mean and alternating stresses are obtained at critical cross sections on the shafts. The failure values of the mean and alternating stresses are obtained from a new form of the mean stress diagram. The failure values are then compared to the basic values to obtain the factor of safety and calculate the life for a given reliability.

In the following chapter, simulation studies on a nonlinear time varying helical geared shaft system subjected to deterministic and filtered white noise inputs are carried out.

CHAPTER 5

Simulation Studies on a Non-Linear Time Varying Helical Geared Shaft System Subjected to Determinsitic and Filtered White Noise Inputs

5.1 Introduction

In chapter 3, the steady state vibration of a helical geared shaft system was studied. The mathematical model considered the effects of torsional-flexural-axial coupling. The excitation to the geared shaft system was in the form of a static transmission error with a harmonic variation at the tooth meshing frequency. The rotor natural frequencies and mode shapes were determined and the dynamic response was obtained using modal analysis methods. The model used was linear and did not consider the effects of the time varying tooth stiffness and backlash.

A better estimate of the dynamic response can be obtained by considering the time varying tooth stiffness and backlash. The static transmission error not only contains a deterministic component but also a random component. This random component can be modelled as the output of a linear filter, the input to which is a Gaussian white noise [16], and this is a good approximation. The resulting equations are time varying and non-linear (because of the backlash).

The equations are put in state space form and solved numerically using the matrix exponential technique. Piecewise linearisation is used in the simulation to obtain the mean and variance of the dynamic response.

5.2 The Mathematical Model

A simple helical geared shaft system is schematically represented in Fig. 3.5. It shows a motor of moment of inertia J_M driving a dynamo of moment of inertia J_L through a pair of helical gears. I_1 and I_2 denote the moment of inertia of the driving and driven gears. As discussed in chapter 3, there exists a "force" coupling between the motions in the axial (x), flexural (y), torsional (θ) and rotational (ϕ) [about a gear diameter] directions of the shafts at the gear locations as shown in Fig. 5.1. The tooth stiffness is time varying and is represented by k(t). The excitation to the geared shaft system is in the form of a static transmission error, $\varepsilon(t)$, interposed between two perfect mating teeth.

If we consider a lumped mass model of the geared system shown in Fig. 3.5 using the gear pair model shown in Fig. 5.1, we can write the equations of motion as,

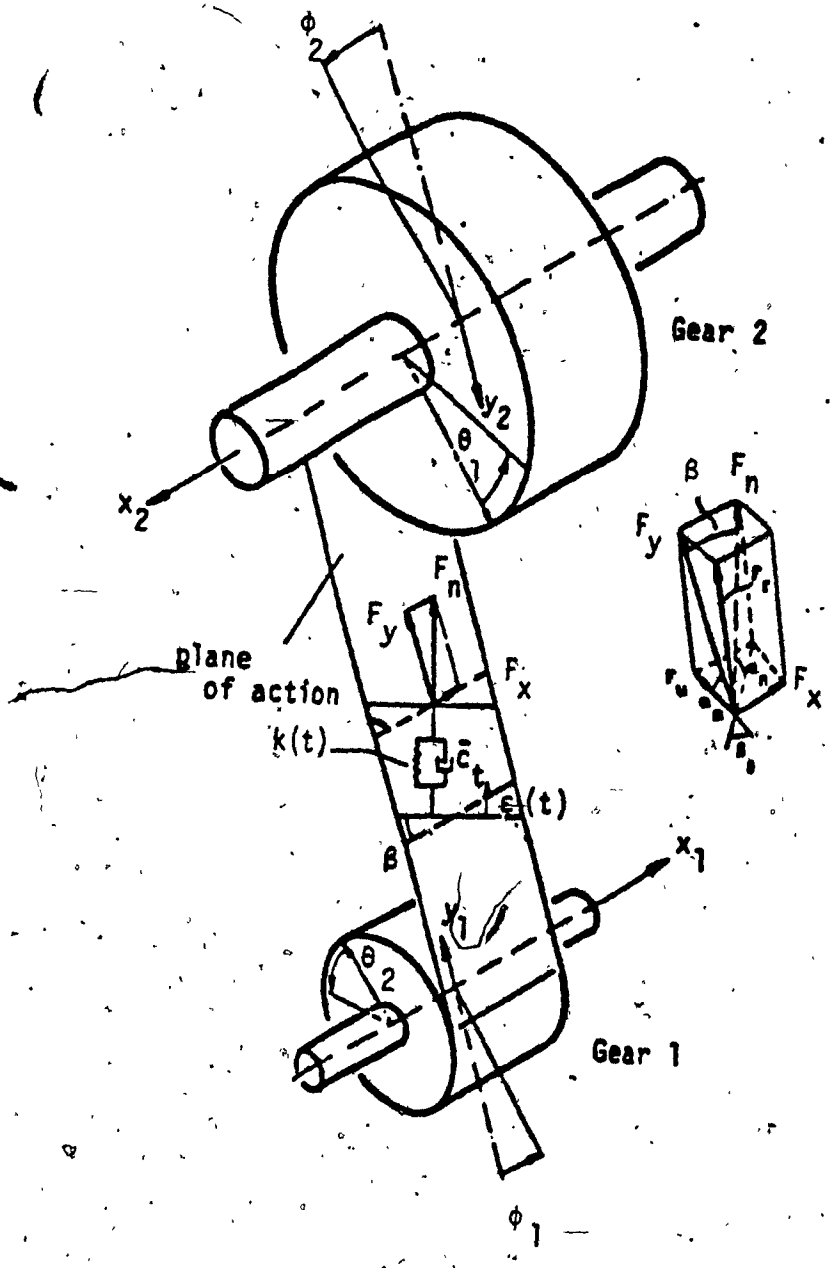

Fig. 5.1 A Pair of Helical Gears in Mesh

$$m_1 \ddot{y}_1 + k_{y1} y_1 + c_{y1} \dot{y}_1 + k(t)\, \delta_n \cos\beta + \bar{c}_t\, \dot{\delta}_n \cos\beta = [k(t)\, \varepsilon(t) + \bar{c}_t\, \dot{\varepsilon}(t)] \cos\beta \qquad (5.1)$$

$$m_2 \ddot{y}_2 + k_{y2} y_2 + c_{y2} \dot{y}_2 + k(t)\, \delta_n \cos\beta + \bar{c}_t\, \dot{\delta}_n \cos\beta = [k(t)\, \varepsilon(t) + \bar{c}_t\, \dot{\varepsilon}(t)] \cos\beta \qquad (5.2)$$

$$I_1 \ddot{\theta}_1 + k_{\theta 1}(\theta_1 - \theta_M) + c_{\theta 1}\, \dot{\theta}_1 + k(t)\, \delta_n\, r_1 \cos\beta + \bar{c}_t\, \dot{\delta}_n\, r_1 \cos\beta = [k(t)\varepsilon(t) + \bar{c}_t\, \dot{\varepsilon}(t)]\, r_1 \cos\beta + T_M \qquad (5.3)$$

$$I_2 \ddot{\theta}_2 + k_{\theta 2}(\theta_2 - \theta_L) + c_{\theta 2}\, \dot{\theta}_2 + k(t)\, \delta_n\, r_2 \cos\beta + \bar{c}_t\, \dot{\delta}_n\, r_2 \cos\beta = [k(t)\, \varepsilon(t) + c_t\, \dot{\varepsilon}(t)]\, r_2 \cos\beta - T_L \qquad (5.4)$$

$$m_1 \ddot{x}_1 + c_{x1}\, \dot{x}_1 + k_{x1}\, \dot{x}_1 + k(t)\, \delta_n \sin\beta + \bar{c}_t\, \dot{\delta}_n \sin\beta = [k(t)\varepsilon(t) + \bar{c}_t\, \dot{\varepsilon}(t)] \sin\beta \qquad (5.5)$$

$$m_2 \ddot{x}_2 + c_{x2}\, \dot{x}_2 + k_{x2}\, \dot{x}_2 + k(t)\, \delta_n \sin\beta + \bar{c}_t\, \dot{\delta}_n \sin\beta = [k(t)\varepsilon(t) + \bar{c}_t\, \dot{\varepsilon}(t)] \sin\beta \qquad (5.6)$$

$$\left(\frac{I_1}{2}\right) \ddot{\phi}_1 + k_{\phi 1}\, \phi_1 + c_{\phi 1}\, \dot{\phi}_1 + k(t)\, \delta_n\, r_1 \sin\beta + \bar{c}_t\, \dot{\delta}_n\, r_1 \sin\beta = [k(t)\, \varepsilon(t) + \bar{c}_t\, \dot{\varepsilon}(t)]\, r_1 \sin\beta \qquad (5.7)$$

$$\left(\frac{I_2}{2}\right)\ddot{\phi}_2 + k_{\phi 2}\,\phi_2 + c_{\phi 2}\,\dot{\phi}_2 + k(t)\,\delta_n\,r_2 \sin\beta + \bar{c}_t\,\dot{\delta}_n\,r_2 \sin\beta = \left[k(t)\,\varepsilon(t) + \bar{c}_t\,\dot{\varepsilon}(t)\right] r_2 \sin\beta \qquad (5.8)$$

The displacement of the gear tooth in the normal direction,

$$\delta_n = (y_1 + y_2 + r_1\,\theta_1 + r_2\,\theta_2)\cos\beta + (x_1 + x_2 + r_1\,\phi_1 + r_2\,\phi_2)\sin\beta \qquad (5.9)$$

Simplifying Eq. (5.1-5.8) using (5.9) and normalizing, gives,

$$\{\ddot{z}\} + [C]\{\dot{z}\} + [K]\{z\} = \{f(t)\} \qquad (5.10)$$

where the generalized coordinate vector is given by

$$\{z\} = \{y_1,\ y_2,\ \theta_1,\ \theta_2,\ x_1,\ x_2,\ \phi_1,\ \phi_2\}^T$$

The equations of motion described by Eq. (5.10) are recast into the state space form using, $\{\dot{X}\} = \begin{Bmatrix} \dot{z} \\ \ddot{z} \end{Bmatrix}$ in order to predict the dynamic response using the matrix exponential method, which will be discussed later. Thus,

$$\{\dot{X}\} = \left[\begin{array}{c|c} 0 & I \\ \hline -K & -C \end{array}\right] \{X\} + \begin{Bmatrix} 0 \\ f(t) \end{Bmatrix} \qquad (5.11)$$

The matrices [K] and [C] are given in the Appendix III.

5.3 Torsional-Flexural-Axial-Rotational Coupling

As disoussed earlier there exists a "force" coupling between the torsional, flexural, axial and rotational (about a gear diameter) motions of gear pair. The matrix [K] in Eq. (5.10) gives the stiffness terms coupling the gear motions:

$$\begin{Bmatrix} y_1 \\ y_2 \\ \theta_1 \\ \theta_2 \\ x_1 \\ x_2 \\ \phi_1 \\ \phi_2 \end{Bmatrix} \xrightarrow{k(t)} \begin{bmatrix} A_1 & A_2 & A_1 r_1 & A_1 r_2 & A_2 & A_2 & A_2 r_1 & A_2 r_2 \\ & A_1 & A_1 r_1 & A_1 r_2 & A_2 & A_2 & A_2 r_1 & A_2 r_2 \\ & & A_1 r_1^2 & A_1 r_1 r_2 & A_2 r_1 & A_2 r_1 & A_2 r_1^2 & A_2 r_1 r_2 \\ & & & A_1 r_2^2 & A_2 r_2 & A_2 r_2 & A_2 r_1 r_2 & A_2 r_2^2 \\ & & & & A_3 & A_3 & A_3 r_1 & A_3 r_2 \\ & & & & & A_3 & A_3 r_1 & A_3 r_2 \\ & & & & & & A_3 r_1^2 & A_3 r_1 r_2 \\ & & & & & & & A_3 r_2^2 \end{bmatrix}$$

Symmetric

where $A_1 = \cos^2 \beta$

$A_2 = \cos \beta \sin \beta$

$A_3 = \sin^2 \beta$

5.4 Time Varying Tooth Stiffness

The gear mesh is a variable stiffness element and this affects both the presence and severity of gear system resonances and instabilities. Benton and Seireg [66] modelled the gear mesh stiffness in the form of rectangular, square and sinusoidal waves. These approximations are generally considered due to the difficulty of accurately predicting the actual pattern of the stiffnes variation in practical situations. It is difficult to account for profile errors, variation in contact length, shaft misalignment and deflections, deformation of the wheel body and load distribution. Methods predicting mesh stiffness variation under idealised practical conditions have been considered by Seireg and Houser [96] and can be used for a more accurate evaluation of gear system dynamics. In this thesis, a mesh stiffness variation k(t), as shown in Fig. 5.3 is used [16] and is introduced into the equations of motion (5.1 - 5.8) of the helical geared shaft system.

5.5 Effect of Static Transmission Error

A pair of meshing gears with rigid, perfect, uniformly spaced involute teeth would transmit exactly uniform angular motion. However, the intentional tooth-face modifications, machining errors and wear and tooth deformations all contribute to the deviation from exact uniform relative angular

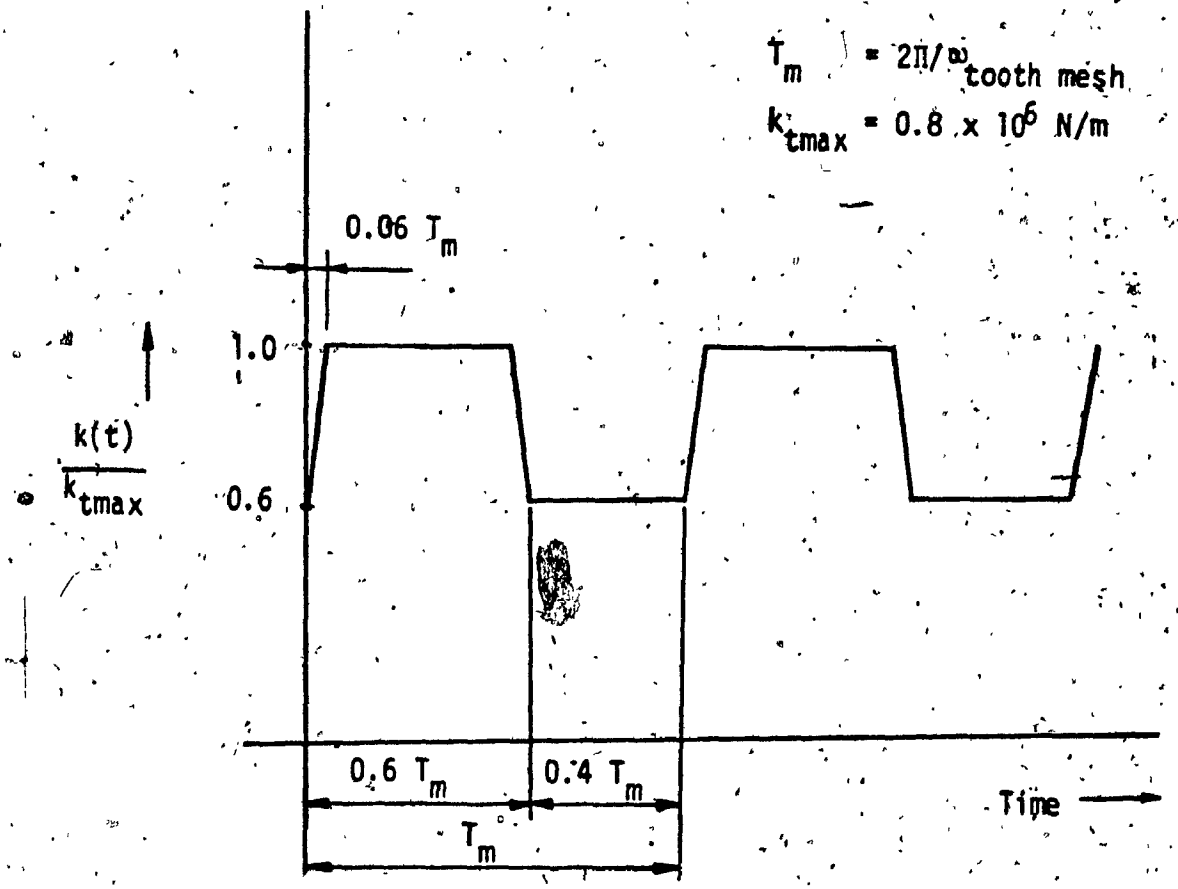

Fig. 5.2 Variation of tooth stiffness with time [16]

motion of a pair of meshing rotating gears. The composite effect of the above contributions is described by the static transmission error, and is generally recognized as a principal source of vibratory excitation of gear systems. Mark [13] obtained a general expression for the static transmission error and decomposed it into mean and random components. Let the static transmission error (STE), $\varepsilon(t)$, be expressed as,

$$\varepsilon(t) = \varepsilon_d(t) + \varepsilon_r(t) \tag{5.12}$$

where $\varepsilon_d(t)$ = deterministic component

$\varepsilon_r(t)$ = random component

The helical geared shaft system is thus driven by deterministic and random inputs, as can be seen by substituting Eq. (5.12) into $\{f(t)\}$ in Eq. (5.11).

A harmonic analysis of the static transmission error curve often shows that a significant component of excitation has the frequency of tooth mesh, Ω_r [11]. Thus, the deterministic component of the STE can be expressed as,

$$\varepsilon_d(t) = \varepsilon_{av} \sin \Omega_r t \tag{5.13}$$

A linear dynamic system acts like a filter when excited by white noise. The response (output) is called a "filtered white noise". The random component of the static transmission error, $\varepsilon_r(t)$ in Eq. (5.12) is represented by a "filtered white noise" which is obtained by passing a white noise

through a second order linear shaping filter [16,98,99]. The shaping filter equation is given by,

$$\ddot{\varepsilon}_r(t) + a_1 \dot{\varepsilon}_r(t) + a_2 \varepsilon_r(t) = w(t) \qquad (5.14)$$

where w(t) is the Gaussian white noise process with mean zero and strength Q(t). Thus,

$$w(t) = 0$$

$$w(t)w(t') = Q(t)\,\delta(t - t')$$

where Q(t) = intensity of white noise

$\delta(\cdot)$ = delta function.

Tobe and Sato [16] obtained the constants of the filter, a_1 and a_2, by matching the autocorrelation function of the filter response with that experimentally obtained. These are given in Table 5.1. Eq. (5.14) can be recast to,

$$\begin{Bmatrix} \dot{\varepsilon}_r \\ \ddot{\varepsilon}_r \end{Bmatrix} = \begin{bmatrix} 0 & 1 \\ -a_2 & -a_1 \end{bmatrix} \cdot \begin{Bmatrix} \varepsilon_r \\ \dot{\varepsilon}_r \end{Bmatrix} + \begin{Bmatrix} 0 \\ 1 \end{Bmatrix} w(t) \qquad (5.15)$$

5.6 Tooth Backlash

A clearance is provided between gear teeth so that they will roll together smoothly. This clearance is called backlash and is denoted by BL. In the backlash region, there is a loss of contact between mating gear teeth and thus the tooth load in the normal direction is zero. The backlash function f_{BL} is given by,

$$f_{BL} = \delta_n + \varepsilon \qquad \delta_n + \varepsilon > 0$$
$$= 0 \qquad -BL \leq \delta_n + \varepsilon \leq 0 \qquad (5.16)$$
$$= \delta_n + \varepsilon + BL \qquad \delta_n + \varepsilon < -BL$$

The force transmitted through the gears in the normal direction, F_n, is given by

$$F_n = k_t(t)\, f_{BL} + \bar{c}_t\, \dot{f}_{BL} \qquad (5.17)$$

The variation of F_n with respect to tooth stiffness is given in Fig. 5.3.

5.7 Augumented State Equations

As discussed earlier, the helical geared shafts system is driven by deterministic and filtered white noise inputs. Combining the system and filter equations (Equations 5.11, 5.15) using Eq. (5.12), the augumented state equations are obtained,

$$\begin{Bmatrix} \dot{z} \\ \ddot{z} \\ \dot{\varepsilon}_r \\ \ddot{\varepsilon}_r \end{Bmatrix} = \left[\begin{array}{c|c} [A_1(t)] & [A_r(t)] \\ \hline 0 & [A_f] \end{array}\right] \begin{Bmatrix} z \\ \dot{z} \\ \varepsilon_r \\ \dot{\varepsilon}_r \end{Bmatrix}$$
$$+ \{B(t)\} + \{G(t)\}\, w(t) \qquad (5.18)$$

where $[A_1(t)]$, $[A_r(t)]$, $[A_f]$, $\{B(t)\}$ and $\{G(t)\}$ are given in the Appendix III.

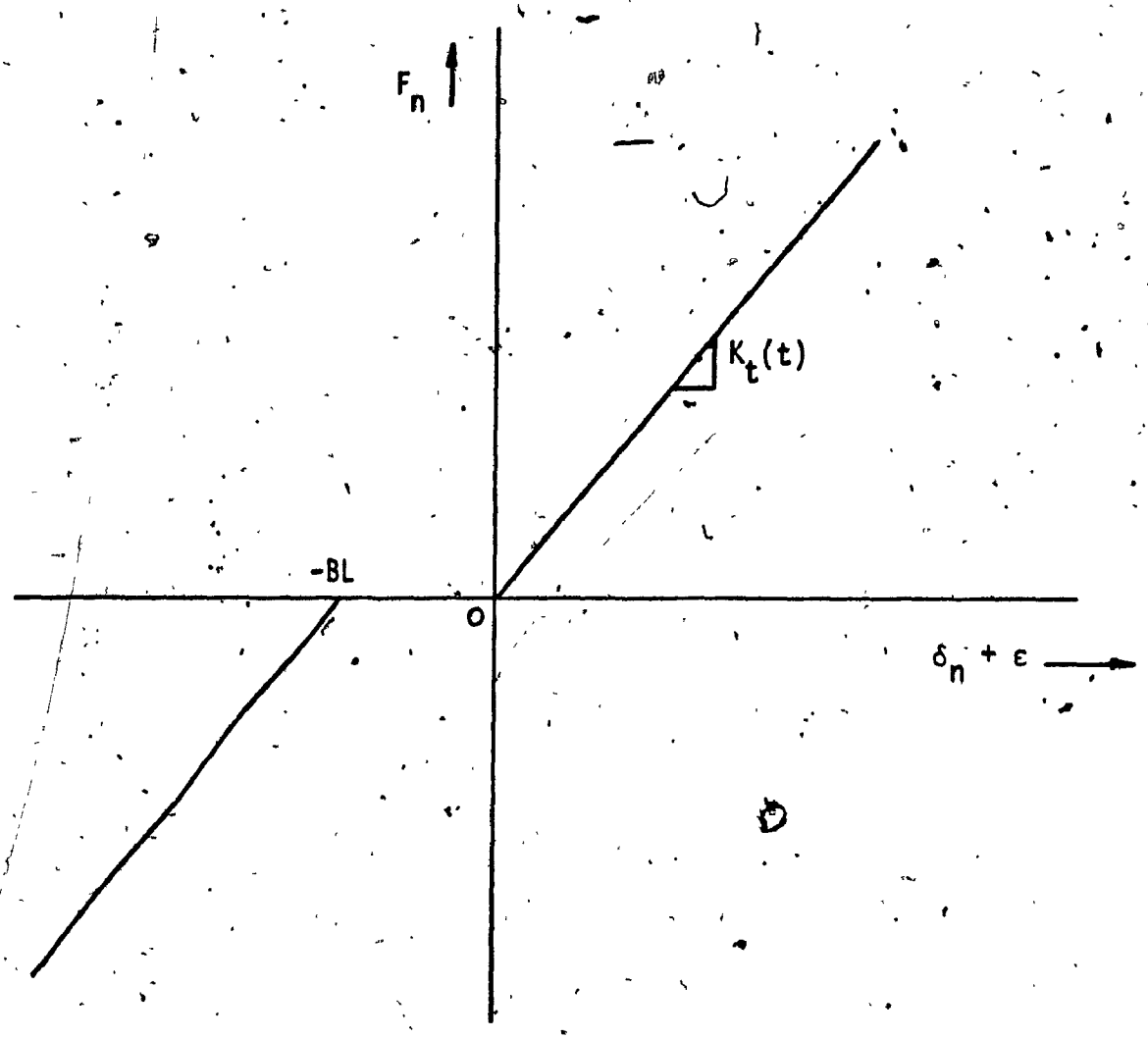

Fig. 5.3 Gear Tooth Backlash Model

The above equation can be put in the form,

$$\{\dot{x}(t)\} = [A(t)]\{x(t)\} + \{B(t)\} + \{G(t)\}\, w(t) \quad (5.19)$$

where $A(t) = \left[\begin{array}{c|c} [A_1(t)] & [A_r(t)] \\ \hline [0] & [A_f] \end{array}\right]$

and $x(t) = \begin{Bmatrix} z \\ \dot{z} \\ \varepsilon_r \\ \dot{\varepsilon}_r \end{Bmatrix}$

5.8 Solution Procedure

Even though the excitation is a stationary process, the system given by Eq. (5.19) is non-stationary because of its time varying, non-linear characteristics. It is therefore difficult to solve analytically. However, numerical solution of Eq. (5.19) can be obtained by the corresponding equivalent discrete-time system model,

$$x(t_{i+1}) = \phi(t_{i+1}, t_i)\, x(t_i) + b_d(t_i) + w_d(t_i) \quad (5.20)$$

where, the state transition matrix is given by

$$\phi(t_{i+1}, t_i) = \exp[A(t_{i+\frac{1}{2}})\ \Delta T]$$

and $\Delta T = t_{i+1} - t_i$

The Matrix Exponential technique, widely used in modern control theory, is adopted as an integration procedure for predicting the dynamic response of the system subjected to deterministic and filtered white noise inputs. This state space method is stable and accurate. It is also less

sensitive to an increase in the time step [74]. Truncation error for a given time interval can be determined, which in turn prescribes the number of terms to be taken to achieve the order of accuracy desired. Arumugam [98] used this method to obtain the dynamic tooth loads of a spur geared rotor system.

The discrete-time forcing vector in Eq. (5.22), $b_d(t_i)$ is given by

$$b_d(t_i) = \int_{t_i}^{t_{i+1}} \phi(t_{i+1}, \tau)\, B(\tau)\, d\tau \qquad (5.21)$$

The white Gaussian discrete-time stochastic process $w_d(t_i)$ is defined by

$$\langle w_d(t_i) \rangle = 0$$

$$\langle w_d(t_i)\, w_d^T(t_i) \rangle = Q_d(t_i) \qquad (5.22)$$

$$= \int_{t_i}^{t_{i+1}} \phi(t_{i+1},\tau)\, G(\tau) Q(\tau) G^T(\tau)\, \phi^T(t_{i+1},\tau)\, d\tau \qquad (5.23)$$

$$\langle w_d(t_i)\, w_d^T(t_j) \rangle = 0 \ , \ t_i \neq t_j \qquad (5.24)$$

If the time increment ΔT is chosen to be sufficiently small as compared to the time constants of the system, the vector $\{B(\tau)\}$ in Eq. (5.21) can be considered to be constant during that time increment and can be represented by $B(t_i)$, its value during the preceding instant. Bahar [74] shows that Eq (5.21) can be rewritten as

$$b_d(t_i) = \sum_{n=0}^{\infty} \frac{A(t_{i+\frac{1}{2}})^n (\Delta T)^{n+1}}{(n+1)!}\, B(t_i) \qquad (5.25)$$

$Q_d(t_i)$ in Eq. (5.23) is given by the trapezoidal rule,

$$Q_d(t_i) = 0.5\ \Delta T\ [G\ Q\ G^T + \phi(t_{i+1},t_i)\ G\ Q\ G^T \phi^T(t_{i+1},t_i)] \tag{5.26}$$

The mean and covariance propogation equations of the x(t) process defined by Eq. (5.20) are given by Maybeck [76].

$$m_x(t_{i+1}) = \phi(t_{i+1},t_i)\ m_x(t_i) + b_d(t_i) \tag{5.27}$$

$$P_{xx}(t_{i+1}) = \phi(t_{i+1},t_i)\ P_{xx}(t_i)\ \phi^T(t_{i+1},t_i) + Q_d(t_i) \tag{5.28}$$

where m_x = mean vector

P_{xx} = covariance matrix

Eq. (5.27) and (5.28) are recurrence relationships and hence starting from the initial conditons $m_x(t_o)$ and $P_{xx}(t_o)$ at time $t = t_o$, the states at other time instants can be computed by the method of time marching.

5.9 Numerical Results

The details of the geared shaft system used to obtain the numerical results are given in Table 5.1.

The natural frequencies and mode shapes of the system neglecting the backlash and assuming a constant value of tooth stiffness, $K_{tmax} = 0.8 \times 10^6$ N/m are given in Tables 5.2 and 5.3. The first and second modes are predominantly torsion of the driving shaft, while the third, fourth, fifth and seventh modes are predominantly torsion of the driven shafts. The sixth and eight modes are predominantly

Table 5.1

Details of the Geared Rotor System

a_1	0.11
a_2	0.102
BL	0.187×10^{-3} m
I_1	0.08485 Kg m^2
I_2	0.01142 Kg m^2
k_{x1}	0.8×10^6 N/m
k_{x2}	0.8×10^6 N/m
k_{y1}	0.24×10^6 N/m
k_{y2}	0.2×10^6 N/m
$k_{\theta 1}$, $k_{\theta 2}$	0.18×10^4 Nm/rad
$k_{\phi 1}$, $k_{\phi 2}$	0.8×10^4 Nm/rad
n	30
r_1	0.1 m
r_2	0.05 m
β	0-20
n	30
Q	$0.332 \times 10^{-6} m^2/s^3$
r_1	0.1 m
r_2	0.05 m
ϵ_{av}	6×10^{-4} m
β	$0-20^0$

Table 5.2

Natural Frequencies (Hz)

1	23.15
2	26.26
3	41.46
4	49.03
5	58.13
6	68.49
7	116.2
8	192.5

Table 5.3

Mode Shape $\begin{Bmatrix} y_1 \\ y_2 \\ \theta_1 \\ \theta_2 \\ x_1 \\ x_2 \\ \phi_1 \\ \phi_2 \end{Bmatrix}$

1st	2nd	3rd
-0.1008	0.7362x10^{-1}	-0.3862x10^{-1}
0.6044x10^{-3}	-0.1542	-0.9494x10^{-1}
1.0	1.0	-0.5181
0.1363x10^{-2}	-0.1713	1.0
0.2762x10^{-4}	-0.3785x10^{-2}	0.2557
0.2306x10^{-4}	-0.2934x10^{-2}	0.1943x10^{-1}
0.2176x10^{-3}	-0.2713x10^{-1}	0.1457
0.9808x10^{-4}	-0.1184x10^{-1}	0.4901x10^{-1}

4th	5th	6th
-0.4334x10^{-2}	-0.4334x10^{-2}	-0.2101x10^{-2}
-0.8948x10^{-2}	-0.8948x10^{-2}	-0.4188x10^{-2}
-0.5807x10^{-1}	-0.5807x10^{-1}	-0.2815x10^{-1}
1.0	1.0	-0.6216
-0.2812x10^{-2}	-0.2812x10^{-1}	-0.1093x10^{-2}
-0.1129	-0.1129	-0.4252x10^{-2}
0.8599x10^{-1}	0.8599x10^{-1}	1.0
0.1390x10^{-1}	0.1390x10^{-1}	0.1027x10^{-1}

7th	8th
0.1474x10^{-1}	0.118x10^{-2}
0.2794x10^{-1}	0.2204x10^{-2}
0.1974	0.1580x10^{-1}
1.0	0.6483x10^{-1}
0.5937x10^{-2}	0.4447x10^{-3}
0.1265x10^{-1}	0.8612x10^{-3}
0.2136	0.1301x10^{-1}
-0.3143	1.0

rotational (about the diametral axis) of the driving and driven shaft respectively.

The mean value of the dynamic response given by Eq. (5.27) in the flexural and torsional directions are obtained for a helix angle β of 20° and a speed of 2500 rpm (driving shaft). The deterministic component of the static transmission error, ε_{av}, exciting the system is assumed to have a magnitude of 6×10^{-4}m. Fig. 5.5 shows the flexural response (y - direction) of the shaft at the driving gear location. The response shows a fluctuation at the tooth mesh frequency superimposed on sinusoidal curve having a period of 0.037 s. Steady state is expected to be reached and maximum response is around 0.15 mm. The flexural response (y - direction) of the shaft in the driven gear location is shown in Fig. 5.6. The response exhibits a periodic variation at the tooth-mesh frequency superimposed on a variation with a period of about 0.043s. The maximum response is about 0.195 mm. The torsional response of the shaft (θ- direction) at the driving gear location is shown in Fig. 5.7. Steady state is expected to be reached and the maximum response is about 0.56×10^{-2} rad. The torsional response at the driven gear location is shown in Fig. 5.8. Steady state is expected to be reached with a maximum response of 0.51×10^{-2} rad.

The mean value of the dynamic response in the torsional and axial direction when the speed of the driving

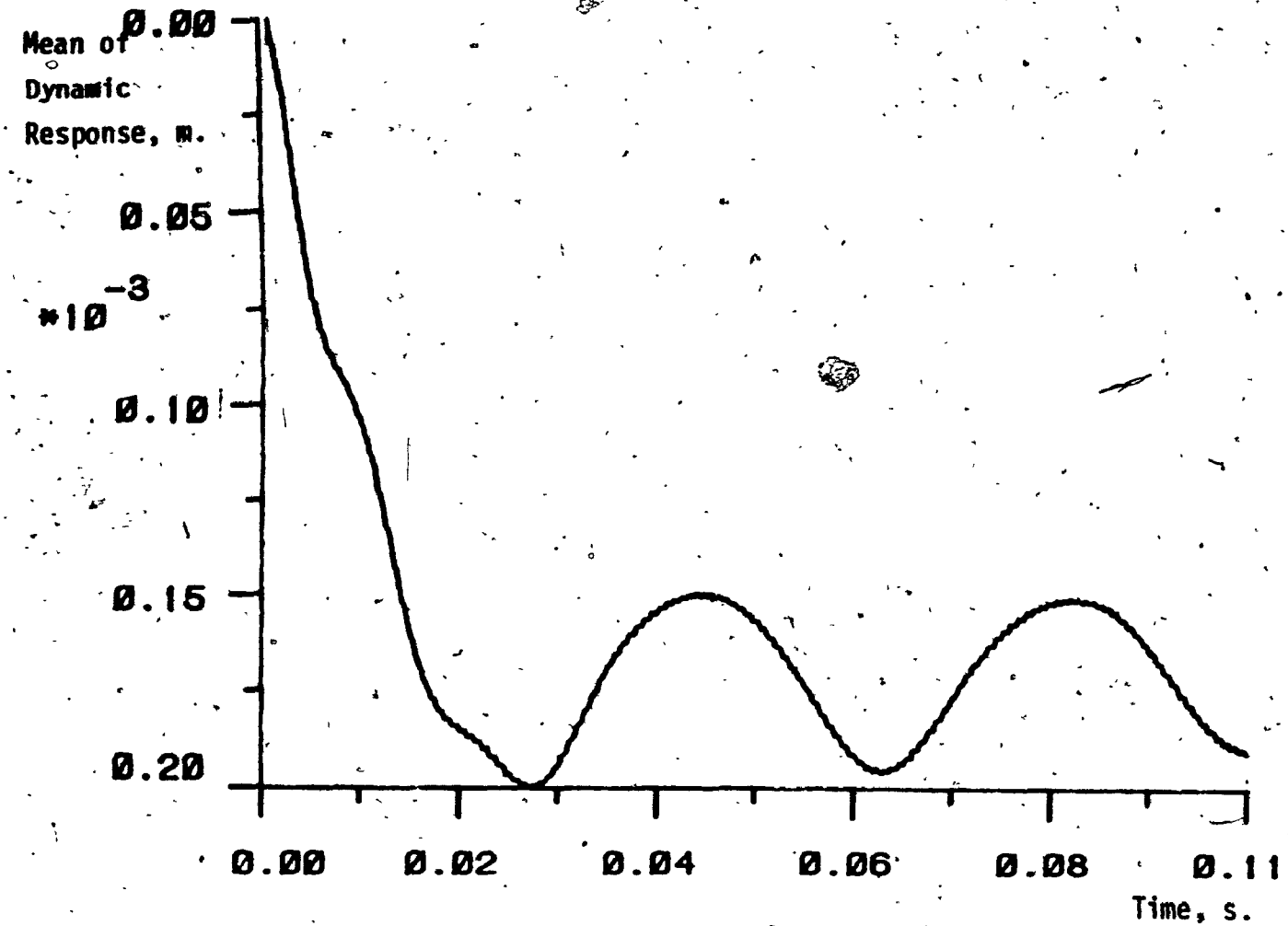

Fig. 5.4 Mean value of the dynamic response in the y-direction at the driving gear location (β=20°, RPM=2500)

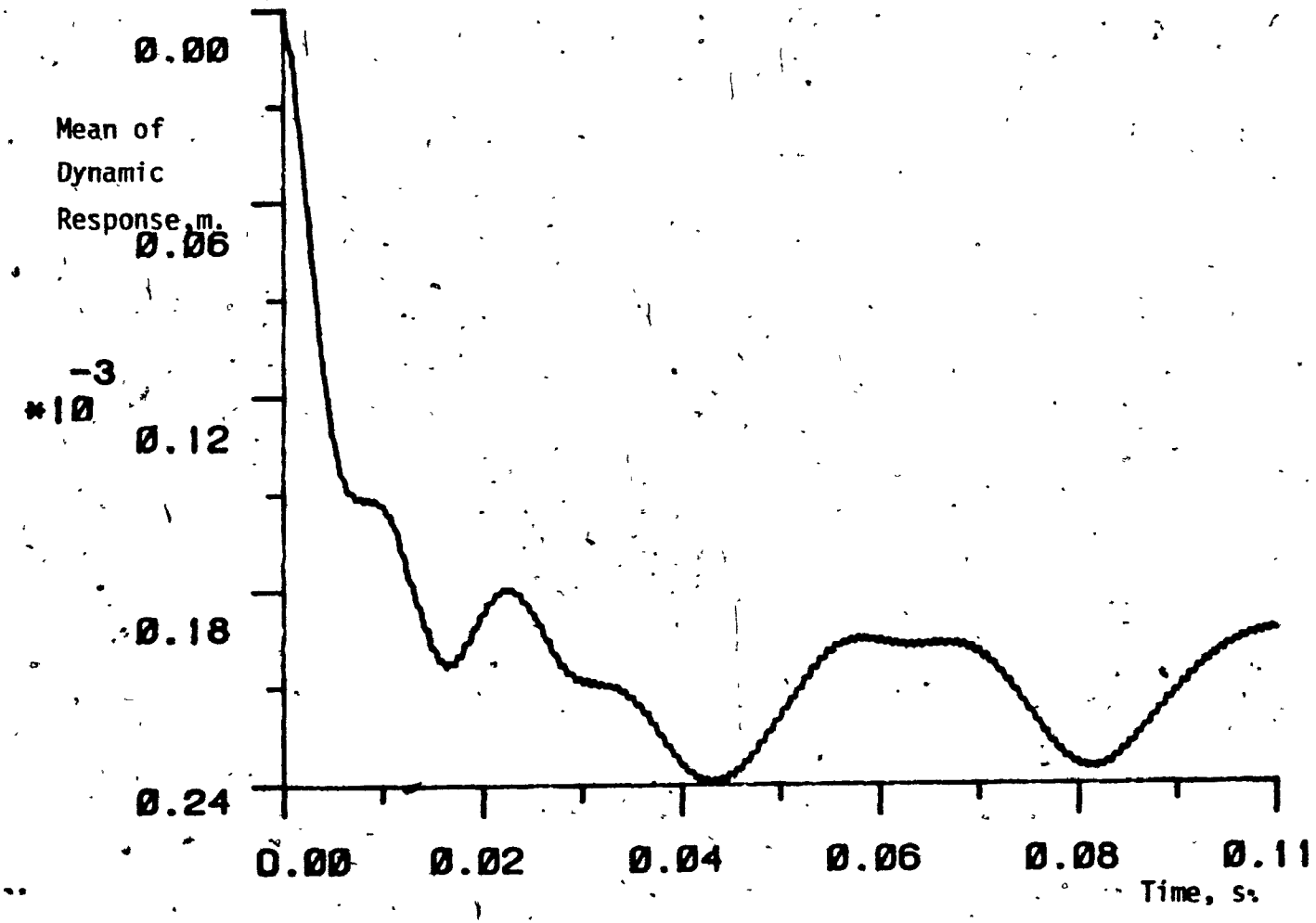

Fig. 5.5 Mean value of the dynamic response in the y-direction at the driven gear location (β=20°, RPM=2500)

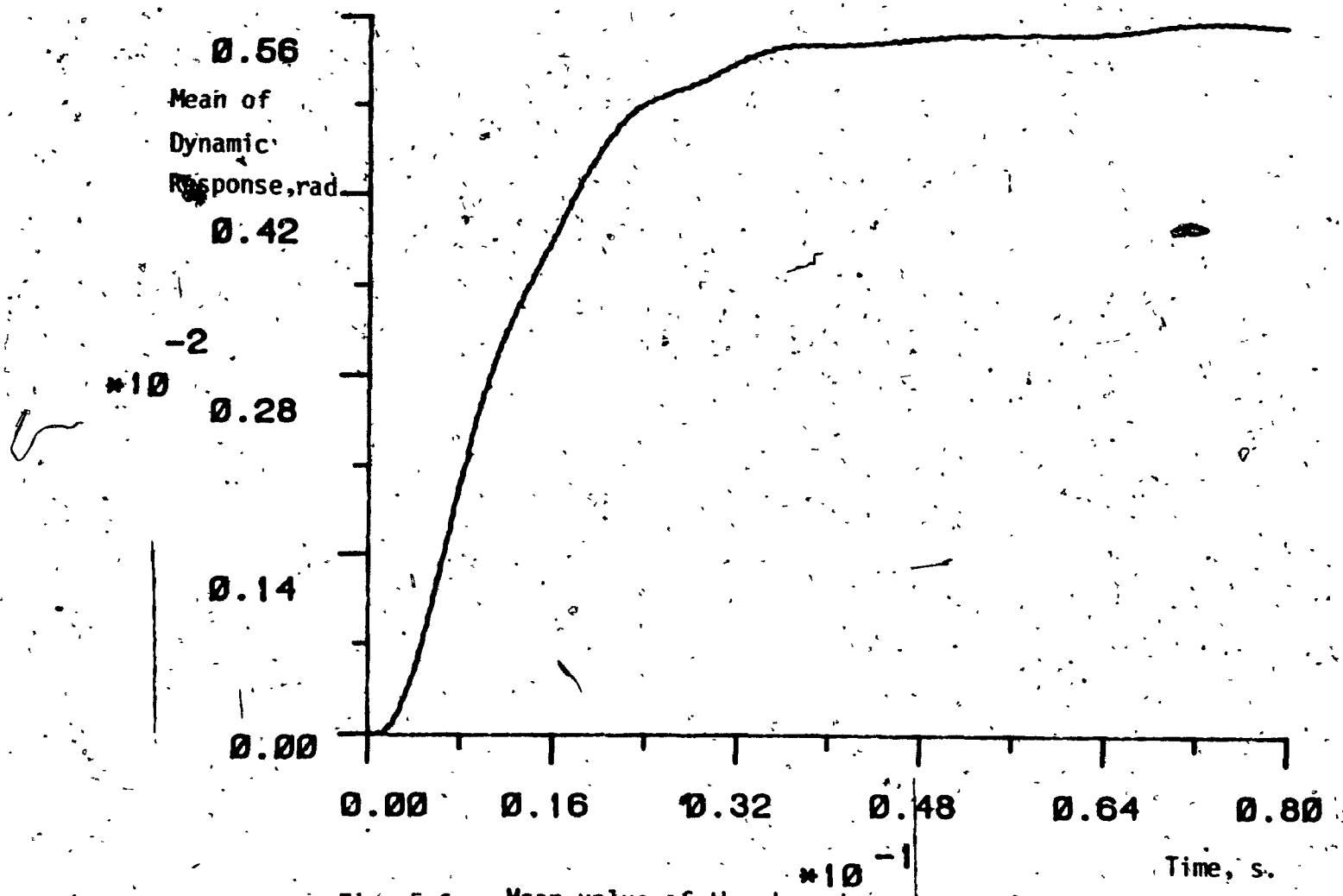

Fig. 5.6 Mean value of the dynamic response in the θ-direction at the driving gear location(β=20°, RPM=2500)

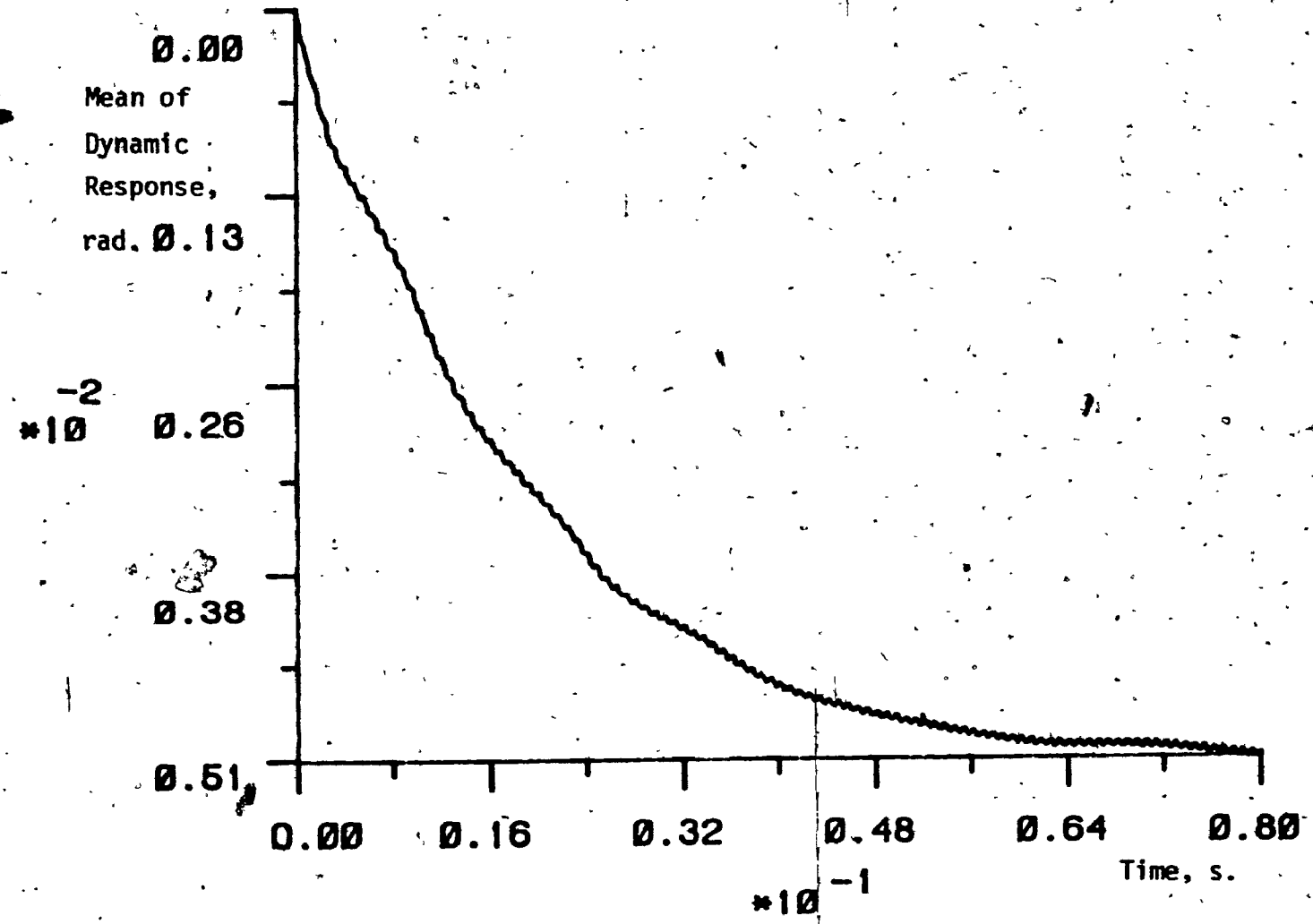

Fig. 5.7 Mean value of the dynamic response in the θ-direction at the driven gear location (β=20°, RPM=2500)

shaft is decreased to 500 rpm are obtained. Fig. 5.8 shows the torsional response at the driving gear location. Steady state is expected to be reached with a magnitude of about 0.03 rad. A small variation is seen at the tooth meshing frequency. Fig. 5.9 shows the torsional response at the driven gear location. Steady state is expected to be reached with a magnitude of about 0.025 rad. The axial response (x-direction) at the driving gear location is shown in Fig. 5.10. A peak of 0.09 mm is obtained and the period of the variation is about 0.025s.

The dynamic tooth load obtained from Eq. (5.17) is shown in Fig. 5.11 for a helix angle of 20° and speed (driving shaft) of 2500 rpm. The dyanamic load varies from -275 to 314 N with a variation at the tooth meshing frequency.

The variance of the dynamic response in the y- direction at the driving gear location of spur gear is obtained from Eq. (5.28) and is shown in Fig. 5.12. The variation shows a fluctuation with an increase in magnitude. This behavior was reported by Tobe and Sato [16], where the variance for a single degree of freedom geared shaft system subjected to a filtered white noise was obtained.

5.10 Summary

In this chapter, a complex model of a geared shaft system was analysed. The driving and driven shafts of the

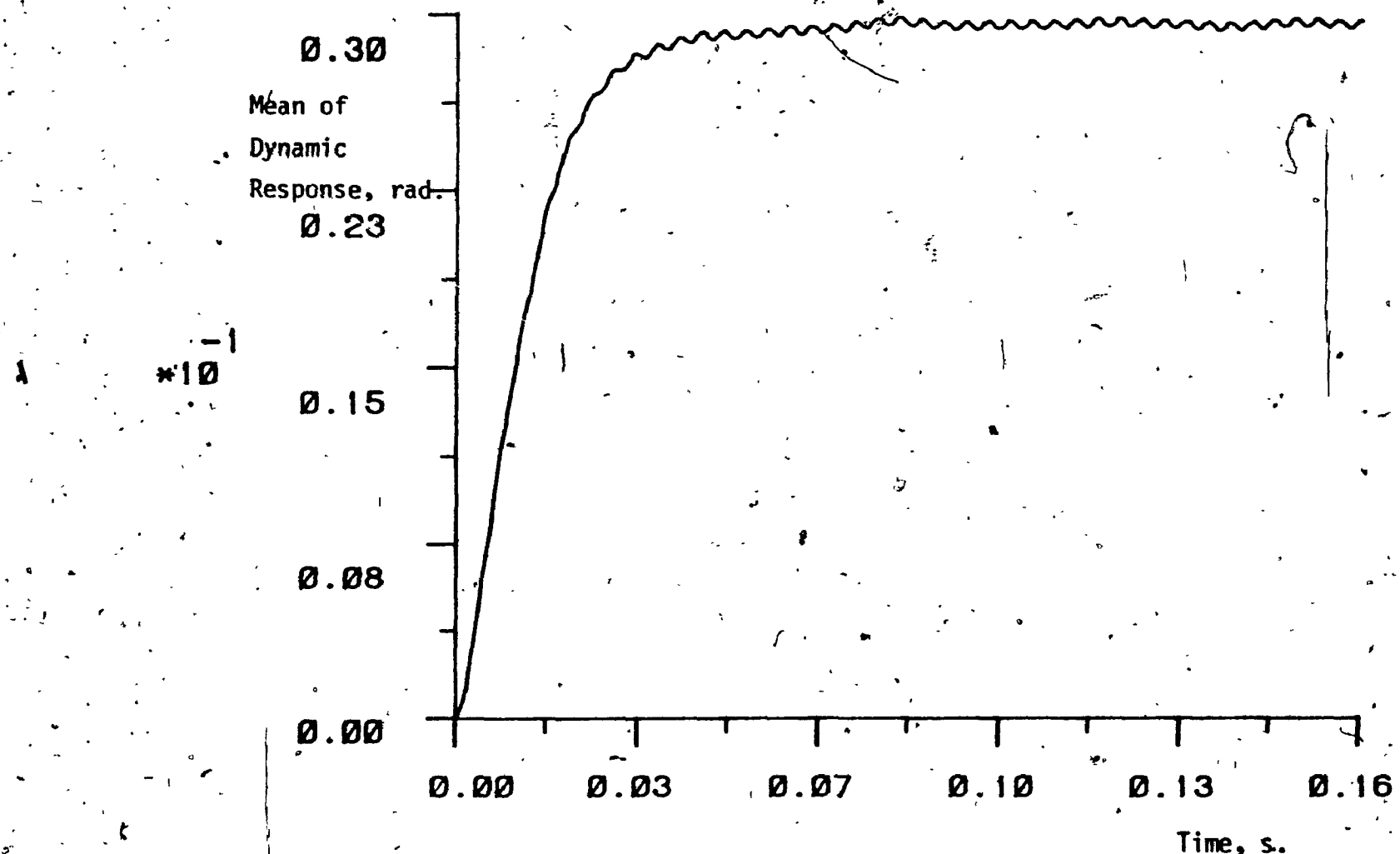

Fig. 5.8 Mean value of the dynamic response in the θ-direction at the driving gear location(β=20°, RPM=500)

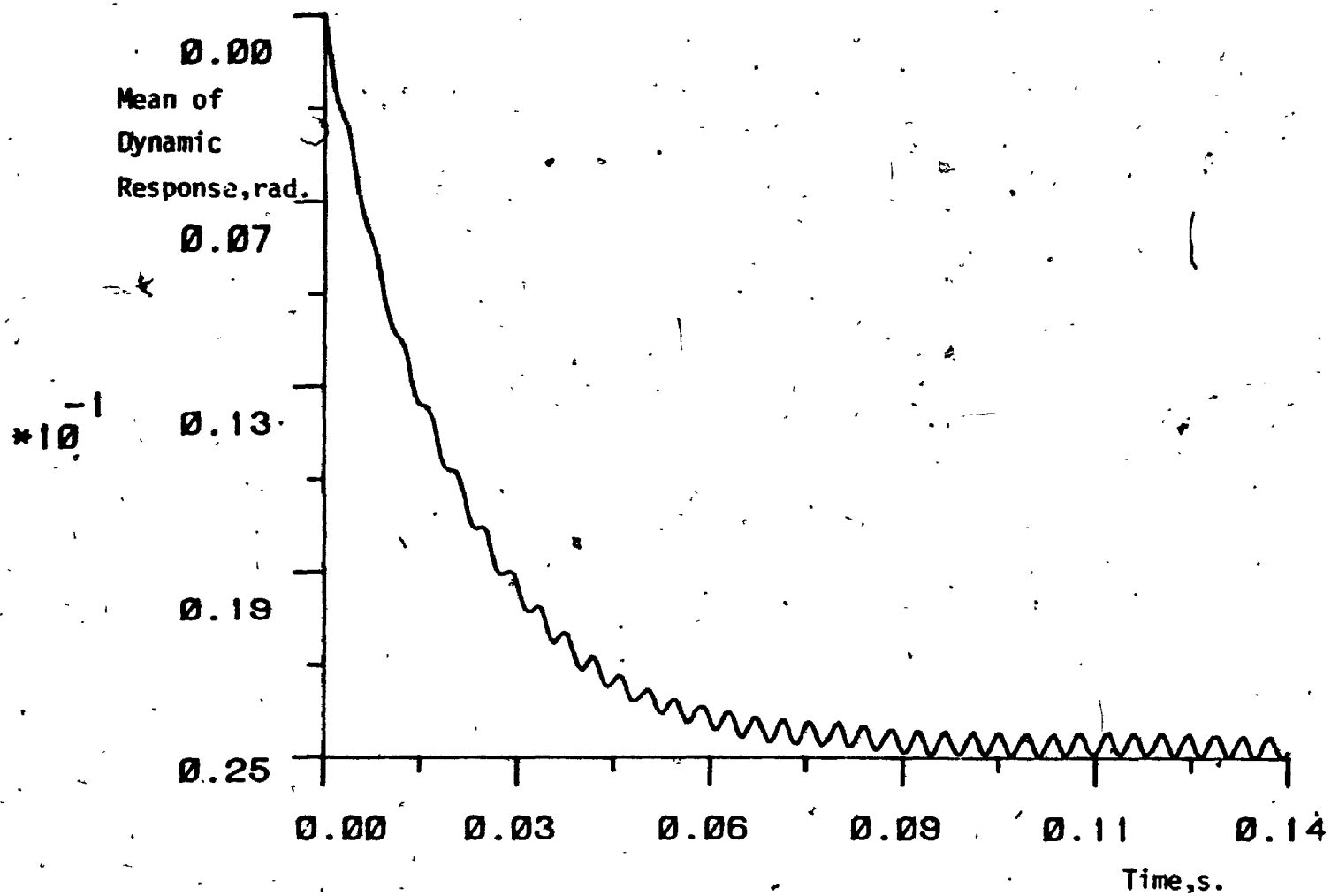

Fig. 5.9 Mean value of the dynamic response in the θ-direction at the driven gear location (β=20, RPM=2500)

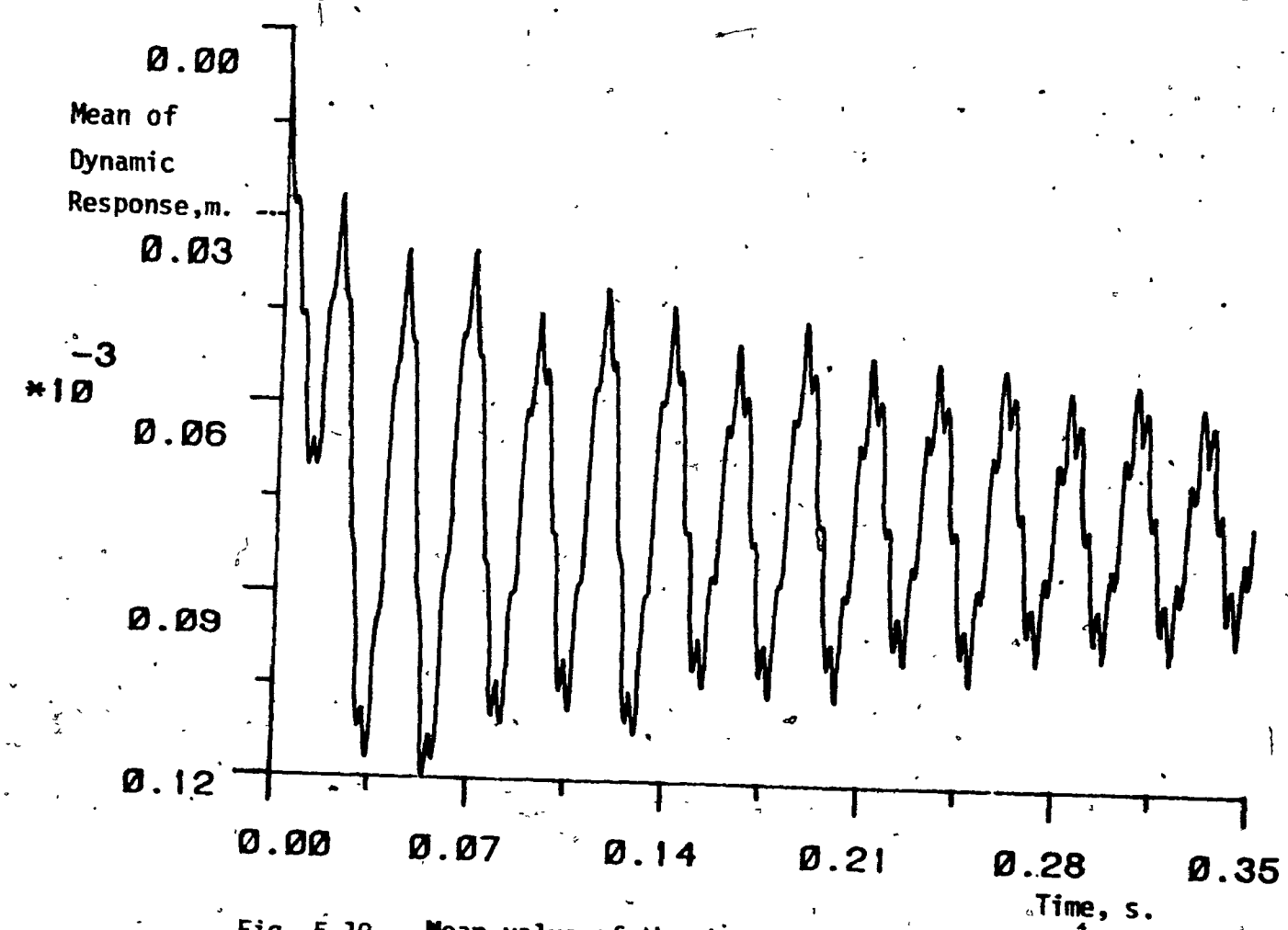

Fig. 5.10 Mean value of the dynamic response in the x-direction at the driving gear location (β=20°, RPM=500)

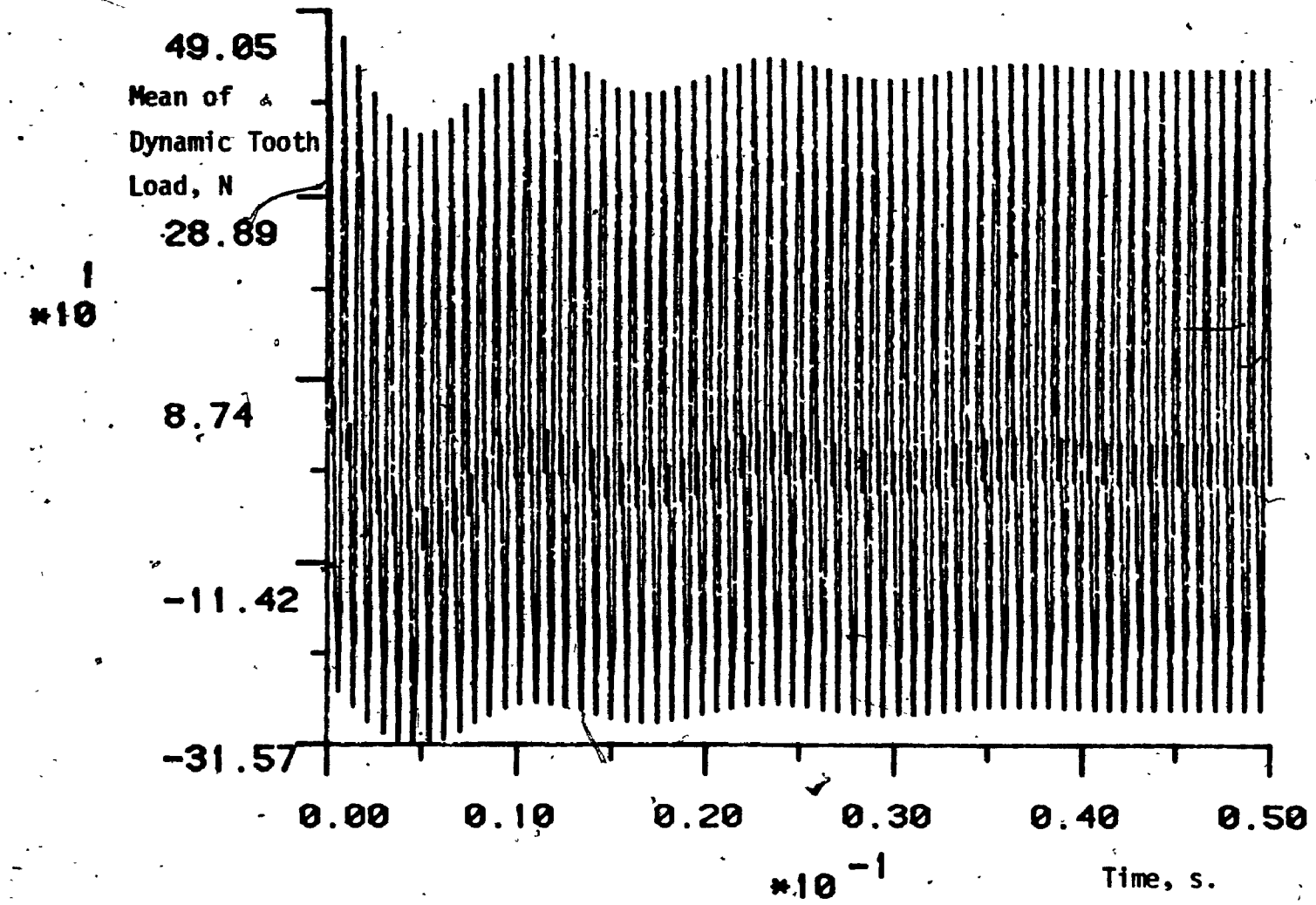

Fig. 5.11 Mean value of the dynamic tooth load vs. time (β=20°, RPM=2500)

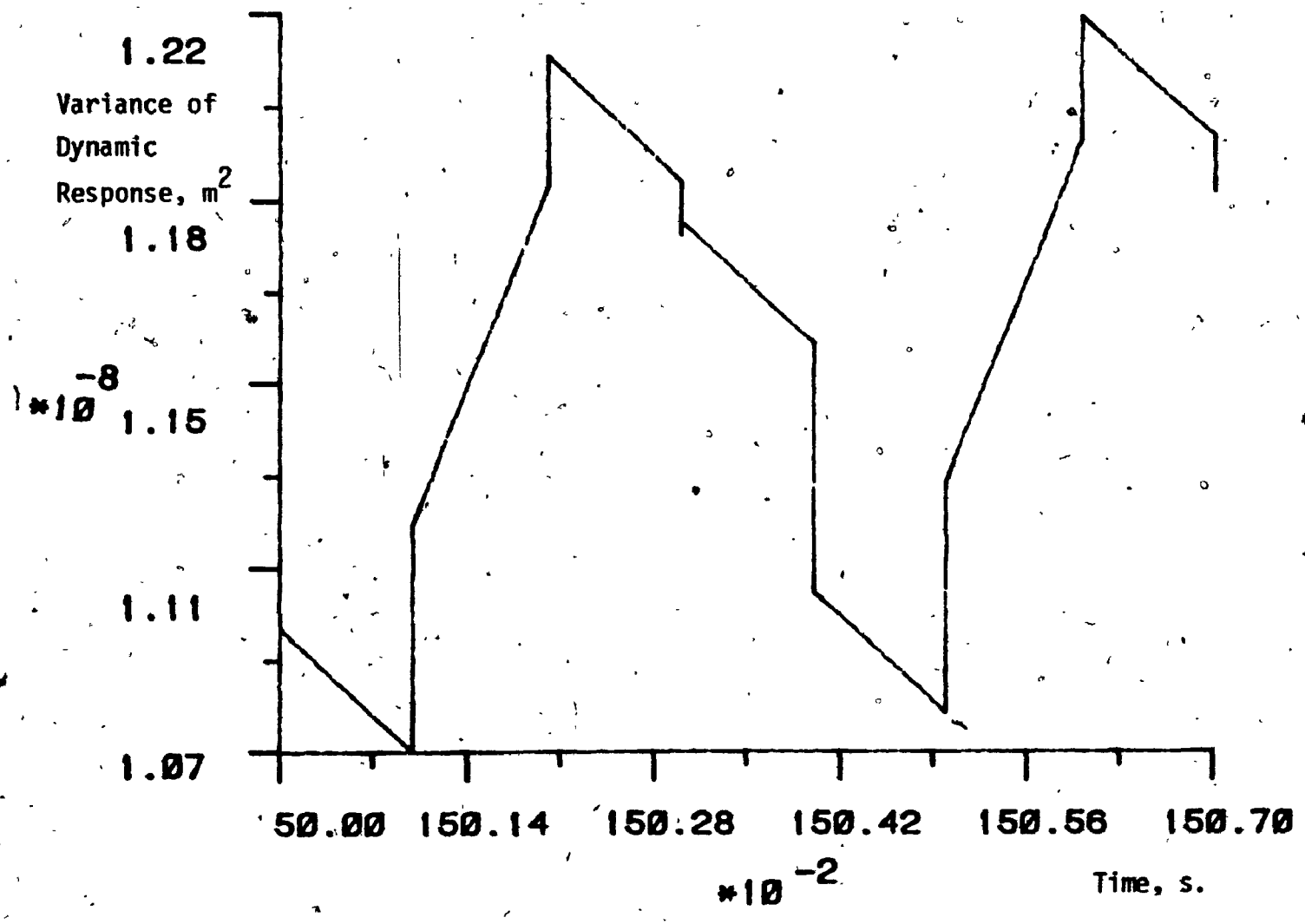

Fig. 5.12 Variance of the dynamic response in the y-direction at the driving gear location ($\beta=0^{\circ}$, RPM=2500)

system were coupled by helical gears. The coupling between the torsional, flexural, axial and rotational motions of the gears was considered. The time varying tooth stiffness represented by a trapezoidal variation. The backlash which results in the loss of contact between the mating gear teeth modelled using a non symmetric function. The excitation to the geared shaft system is considered in the form of a static transmission error which has two components, the deterministic component which can be considered to be having the frequency of tooth mesh, and a random component represented by the output of a linear filter, the input to which is a Gaussian white noise.

The mean of the dynamic response due to the deterministic input and also the variance of the dynamic response due to the random component are presented.

The vibration modes of the system corresponding to the lower natural frequencies (obtained by excluding the effect of backlash and variation in tooth stiffness) are found to be predominantly having torsional motion. The Matrix Exponential Method with piecewise linearisation is found to be effective in the numerical intergration of the non-linear equations of motion having deterministic and random inputs. This method is stable and accurate.

Stability analysis of a helical geared shaft system is discussed in the next chapter.

CHAPTER 6

Stability Analysis of a Helical Geared Shaft System

6.1 Introduction

In chapter 5, the dynamic response of a helical geared shaft system subjected to determinisitic and filtered white noise inputs was studied. In the analysis, the mesh stiffness of the helical gear pair had periodic variation as seen in Fig. 6.1. This variation in time results in a periodic parametric excitation to the dynamical helical geared shaft system. The usual item of interest in such problems are the boundaries of the instability regions. Instability eventually leads to unbounded response and may result in failure of the system.

6.2 Stability of Time Variant Systems

Stability of the equilibrium of linear and non linear systems has recieved considerable attention over the decades. There are several definitions of stability.

The most widely applied methods of determining the stability of linear systems are the direct method of Lyapunov [94, 95] and the Routh test [95]. The direct method of Lyapunov can also be used for non linear systems both time

invariant and time varying. For simple systems, construction of a Lyapunov function to check its stability may be simple, however, for complex systems with non-linearity and time varying parameters this procedure becomes quite tedious [95].

Linear systems exhibit forced or parametric resonance depending on the relationship between the exciting frequency and the natural frequency. Non-linear systems exhibit a combination resonance, in addition to the two kinds of resonance mentioned above. Mettler [97] gives a detailed classification of the different types of resonances.

It is the parametric resonance which is of importance in geared shaft systems due to the time varying tooth stiffness. Bolotin [63] studied the stability characteristics of a second order differential equations subject to parametric excitation. The equations of the the form,

$$\ddot{f} + \Omega^2 (1 + \alpha\phi(t)) f = 0 \qquad (6.1)$$

and is called a Mathieu-Hill Equation. Here $\phi(t)$ is a periodic function with a period $T = \frac{2\pi}{\theta}$ and α is a constant. He showed that if the periodic function $\phi(t)$ has a square wave variation,

$$\phi(t) = 1 \quad , \quad 0 < t < T/2$$

$$= -1 \quad , \quad T/2 < t < T$$

then the regions of unboundedly increasing solution (unstable) are separated from the regions of stability by the periodic solutions with periods of T and 2T. He also

showed that two solutions of identical periods bound the regions of instability and two solutions of different periods bound the region of stability.

Benton and Seireg [64] used the analysis of Bolotin to study the stability of a single degree of freedom pinion gear system. The periodic function in the Mathieu-Hill equation (6.1) represents the time varying tooth stiffness which is assumed to be of the square wave type. Iwatsubo [57] studied the stability of a four degree of freedom geared shaft system using Floquet theory. A square wave variation was assumed and the equations were put in the state-space form. The analysis of Bolotin discussed earlier, was used to obtain the boundaries of stable regions. Arumugam [98] obtained the instability regions for a spur geared rotor system using Floquet theory.

6.3 Mathematical Model

In this chapter, the stability of helical geared shaft systems is studied. The mathematical model of the helical geared shaft system of chapter 5 is extended including the inertia of the motor and dynamo and used for the stability analysis.

The equations of motion for the helical geared shaft system analysed is section 5.2 are given by Eq. (5.1 - 5.8). The equations of motion of the motor and dynamo are

given by

$$J_M \ddot{\theta}_M + K_{\theta 1}(\theta_M - \theta_1) + C_M \dot{\theta}_M = T_M \qquad (6.2)$$

$$J_M \ddot{\theta}_L + K_{\theta 2}(\theta_L - \theta_2) + C_L \dot{\theta}_L = -T_L \qquad (6.3)$$

Simplifying equations (5.1) - (5.8) and (6.2) and (6.3) using (5.9) and normalising gives,

$$\{\ddot{z}\} + [C_s]\{\dot{z}\} + [K_s]\{z\} = \{f(t)\}$$

The homogeneous equations of motion are recast into the state space form using $\{X_1\} = \{\frac{z}{\dot{z}}\}$ Eq. (6.4) then becomes,

$$\{\dot{X}_1\} = \left[\begin{array}{c|c} 0 & I \\ \hline -K_s & -C_s \end{array}\right] \{X_1\} \qquad (6.5)$$

The matrices $[K_s]$ and $[C_s]$ are given in Appendix IV.

The time varying tooth stiffness as discussed earlier, is a source of instability in geared shaft systems. For this particular study, the tooth stiffness is represented by a sinusoidal variation which is a first approximation of the trapezoidal variation considered in Chapter 5.

$$k(t) = k_{avg}(1 + \alpha \sin \omega_m t) \qquad (6.6)$$

where $\alpha = k_{var}/k_{avg}$

k_{var} = stiffness variation amplitude about average

k_{avg} = average stiffness which is average length of line of contact times stiffness per unit length for helical gears.

ω_m = tooth mesh frequency.

The sinusoidal variation of the tooth stiffness described by Eq. (6.6) is shown in Fig. 6.1.

6.4 Floquet Theory

Studies on stability of geared systems usually neglect the effects of backlash and gear errors. Although these assumptions are not generally true, it simplifies the complex stability analysis procedure.

The state equation (6.5) can be put in the form,

$$\{\dot{X}_1\} = [A_1(t)]\ \{X_1\} \tag{6.7}$$

where $[A_1(t)]$ is periodic due to the presence of the time varying stiffness in $[K_s]$. Let the period be T_m. Then,

$$A_1\ (t + T_m) = A_1(t) \tag{6.8}$$

where $T_m = 2\pi/\omega_{\text{tooth mesh}}$ (6.9)

Consider the equivalent discrete-time system model of Eq. (6.5),

$$X_1(t_{i+1}) = \phi(t_{i+1}, t_i)\ X_1\ (t_i) \tag{6.10}$$

which represents the state at time t_{i+1} in terms of that at t_i. If we start at the beginning of the mesh period, represented by t_0, the state at the end of the mesh period can be arrived at by successive application of Eq. (6.8). Thus,

$$X_1(T_m) = \phi\ (T_m\ ,\ t_0)\ X_1(t_0) \tag{6.11}$$

Hsu [67, 68] quotes the Floquet theory, according to which the overall state transition matrix, $\phi\ (T_m\ ,\ t_0)$, also known

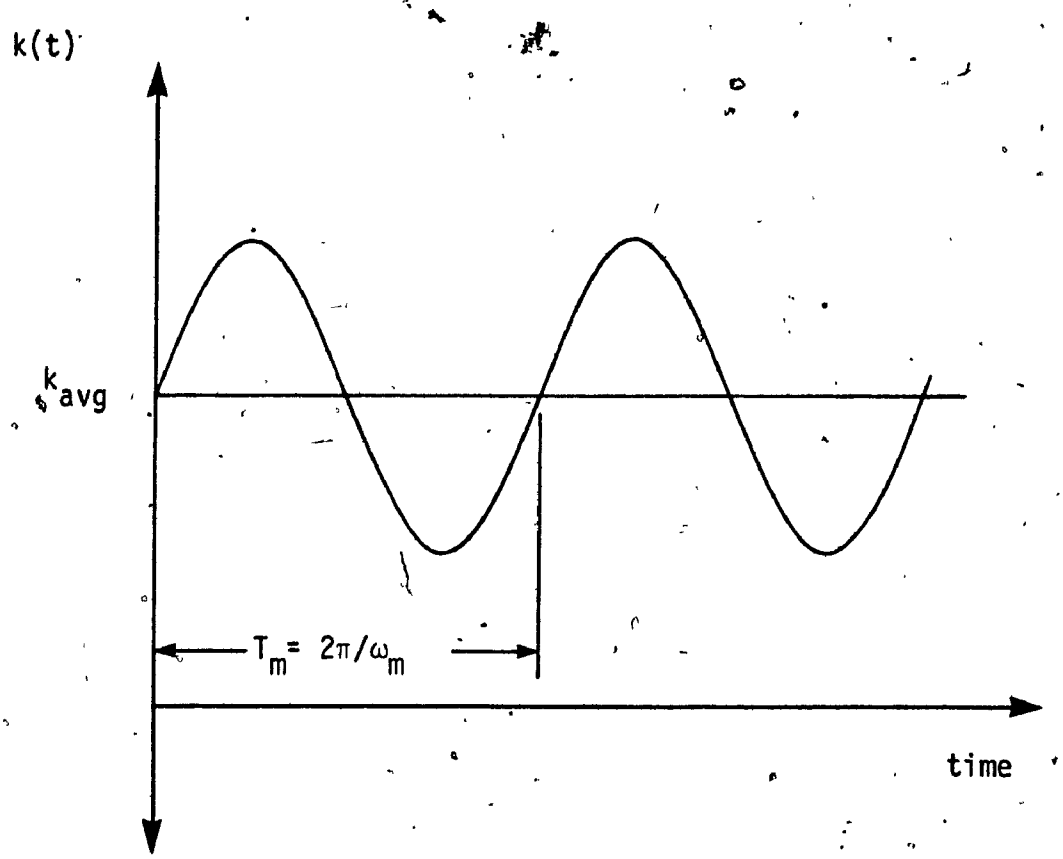

Fig. 6.1 Variation of tooth stiffness with time

as the "Growth Matrix" of the system governs its stability. The given system is asymptotically stable, if and only if, all the eigenvalues of the growth matrix have absolute values less then unity.

6.5 Numerical Results

The details of the geared shaft system used to obtain the numerical results are given in Table 5.1.

The regions of instability for sinusoidal variation [Eq. 6.6] with $\alpha = 1/3$ and damping ratio of 0.01 is shown in Fig. 6.2. The system is unstable at speeds of 4400 rpm of the driven shaft and also in the range 4820-4940 rpm. We see that when the value of ζ is increased to 0.05 with the same value of α, the instability is found to exist at 4000 rpm and in the range 4820 - 4940 rpm. The instabilities occur only in the range 4820-4940 rpm when ζ is increased to 0.1.

When the value of α, which determines the extent of variation in the tooth stiffness is increased from 1/3 to 1/2, there is a significant increase in the regions of instability as seen in Fig. 6.3. If $\zeta = 0.01$ the instability exists at 2200 rpm, 2410-2420 rpm, 2600 rpm, 3190-3250 rpm, 4630 rpm and 4680-4970 rpm. If the damping ratio ζ is increased to 0.05, the regions of instability decreases to between 3190-3250 rpm and 4680-4970 rpm, and remain the same when ζ is increased to 0.1.

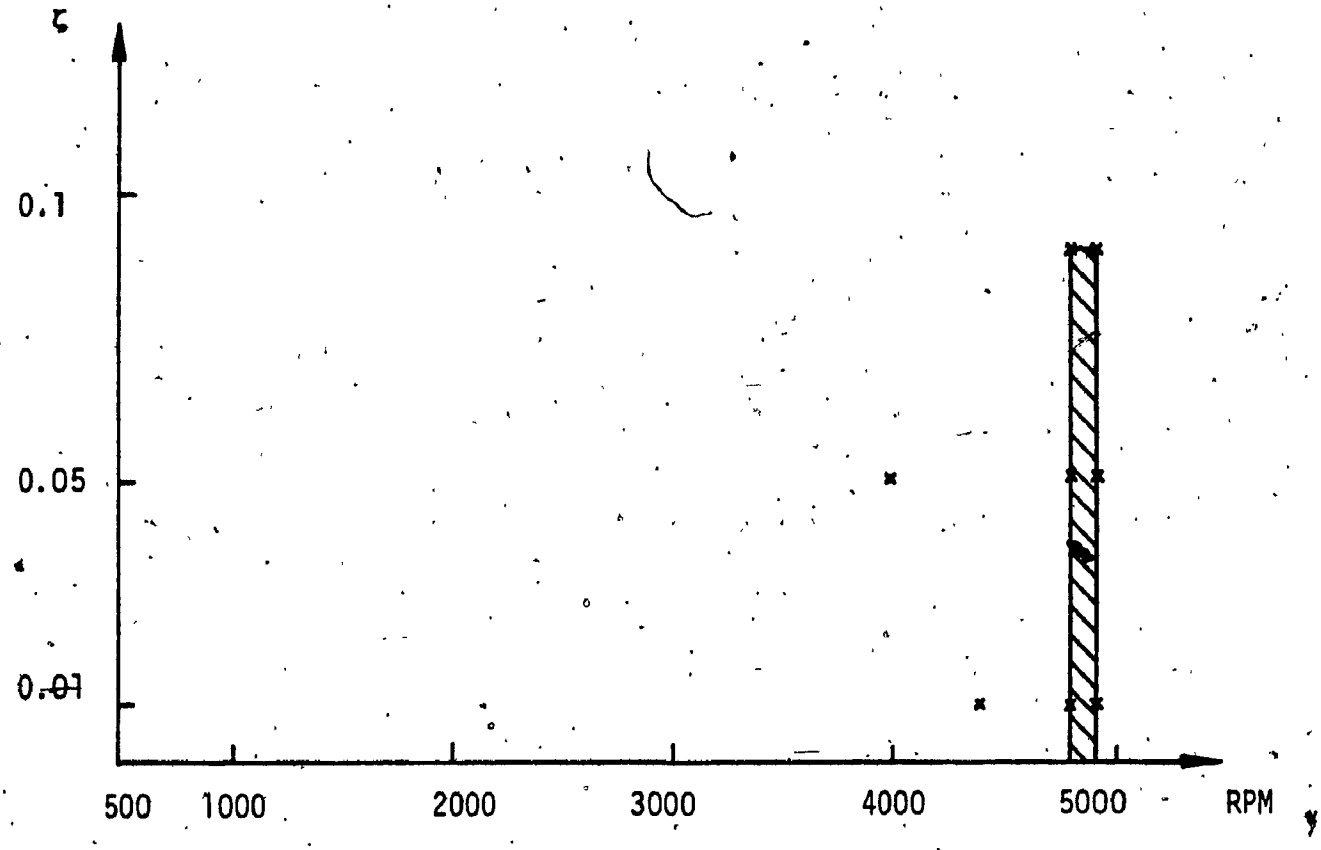

Fig. 6.2 Instability regions ($\alpha = 1/3$).

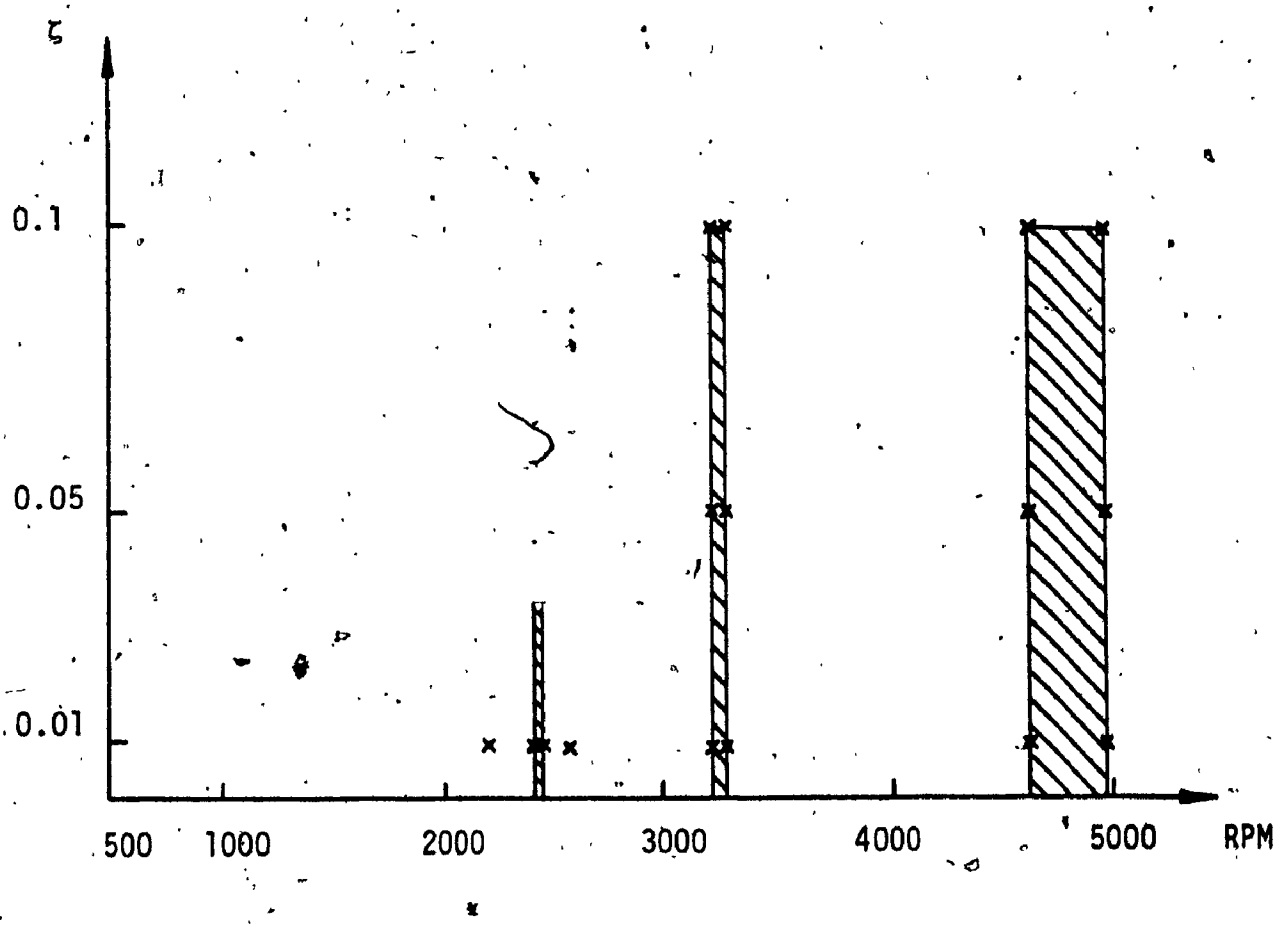

Fig. 6.3 Instability regions ($\alpha = 1/2$)

6.6 Summary

Instabilities in a geared rotor system occur due to periodic variation in the stiffness of the gear teeth. In this chapter, a helical geared shaft system was analysed to obtain the regions of instability. A sinusoidal variation is assumed for the tooth stiffness and Floquet theory is used to obtain the regions of instabilities for different degrees of variation and damping ratios.

The results show that for a certain degree of variation in tooth stiffness, the instability regions decrease with an increase in damping. We also see that for certain level of damping, the instability regions become much larger with an increase in the degree of variation in the tooth stiffness.

In the next chapter, experimental studies on the response of spur geared rotor system are carried out.

CHAPTER 7

Experimental Studies on the Response of Spur Geared Systems

7.1 Introduction

In chapter 2, the natural frequencies, mode shapes and dynamic response were determined analytically by solving the equations of motion for the lumped mass model of the geared shaft system and also numerically using finite element techniques. The equations of motion were solved using modal analysis.

In this chapter, the experimentally measured dynamic response is compared to the analytical solution. Also, the natural frequencies and mode shapes obtained from modal testing are compared with those obtained from the analytical solution.

7.2 Experimental Setup

An experimental facility was established in order to carry out a validation of the analytical model described in chapter 2. It consists of a motor driving a disk through a pair of gears, as shown in Figures 7.1 and 7.2. The driving and driven shafts are circular in cross section and are mounted on rolling contact bearings in cast iron pedestals.

Fig. 7.1 Experimental set-up of a spur geared rotor system (side view)

Fig. 7.2 Experimental set-up of a spur geared rotor system (front view)

The entire rotor system is mounted on a heavy steel frame which in turn is fastened to the floor. Fig. 7.3 shows a schematic representation of the geared rotor system. Table 7.1 gives the details of the experimental geared rotor system under study. The Structural Analysis System consisting of a Micronova MP/200 Microcomputer (with 12.5 MB Winchester disk and 2 disk drives), Tektronix 4010 Graphics Terminal and a Nicolet 660 B Dual Channel Fast Fourier Transform (FFT) analyser is shown in Fig. 7.4. A schematic diagram of the experimental facility is shown in Fig. 7.5.

7.3 Comparison of Analytical and Experimental Dynamic Response

7.3.1 Analytical Dynamic Response:

A simple lumped mass model of the actual geared shaft system, shown in Fig. 7.3. The equations of motion when excited by unbalances U_1 and U_2 in the driving and driven gears is given by,

$$[m]\{\ddot{q}\} + [c]\{\dot{q}\} + [k]\{q\} = \{f\} \qquad (7.1)$$

where

$$[m] = \begin{bmatrix} J_2 & & & & & 0 \\ & m_2 & & & & \\ & & I_2 & & & \\ & & & m_1 & & \\ & & & & I_1 & \\ 0 & & & & & J_1 \end{bmatrix}$$

TABLE 7.1

Details of the experimental setup

Motor	GEC, 5HP, 1720 rpm variable speed motor moment of inertia = 0.5 kgm^2
Driving Gear	Browning YC5660 , 10" PCD, 6 DP, 60 teeth, Moment of Inertia = 0.08485 kgm^2, Weight = 111.3 N
Driven Gear	Browning YSS630, 5" PCD, 6 DP, 30 teeth, Moment of Inertia = 0.0142 kgm^2, Weight = 60.13 N
Flexible Coupling	Browning FS5H Torsional Stiffness = 115 Nm/rad Weight = 38.3 N
Disk	Moment of Inertia = 0.0214 kgm^2
Unbalance	in driving gear = 2.01×10^{-3} kgm in driven gear = 1.125×10^{-3} kgm

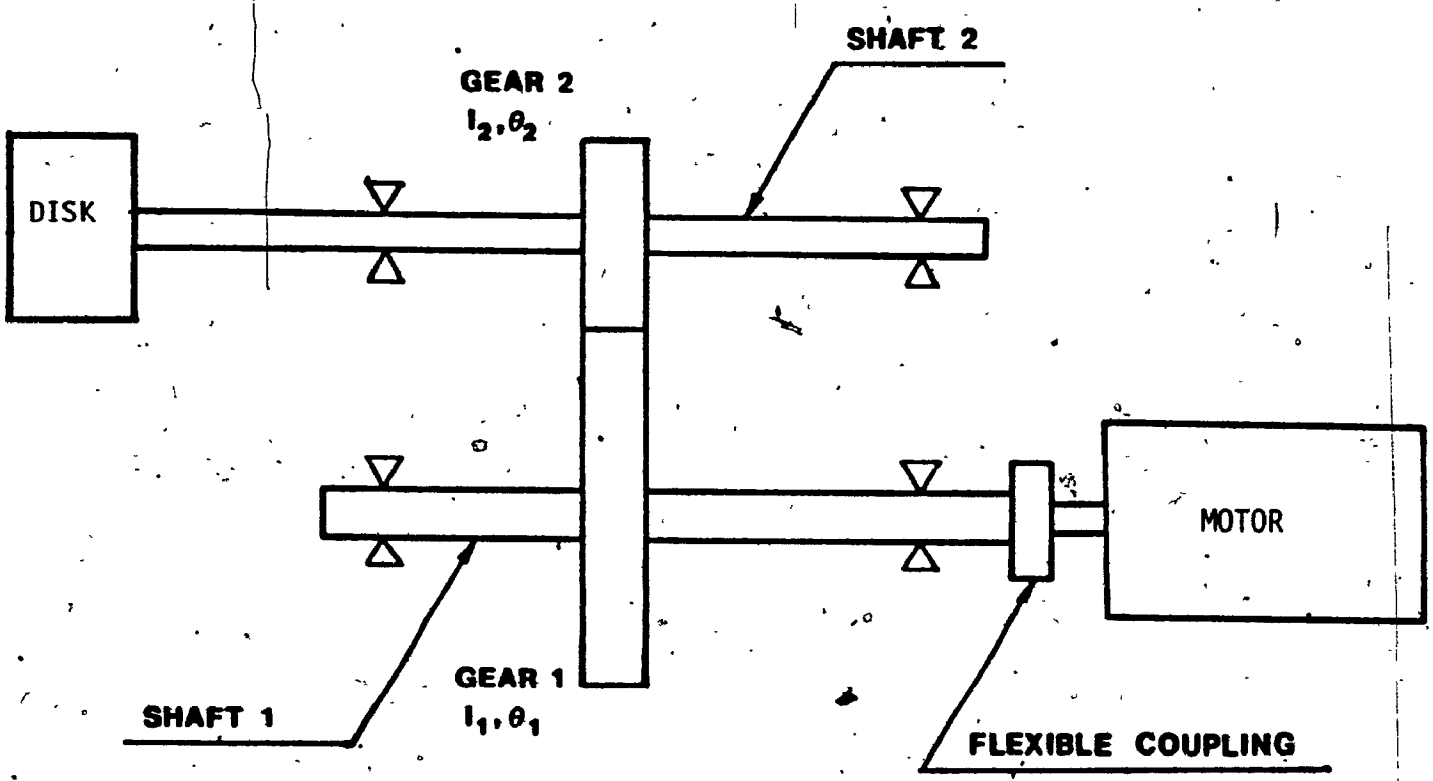

Fig. 7.3 Schematic representation of the experimental spúr geared rotor system

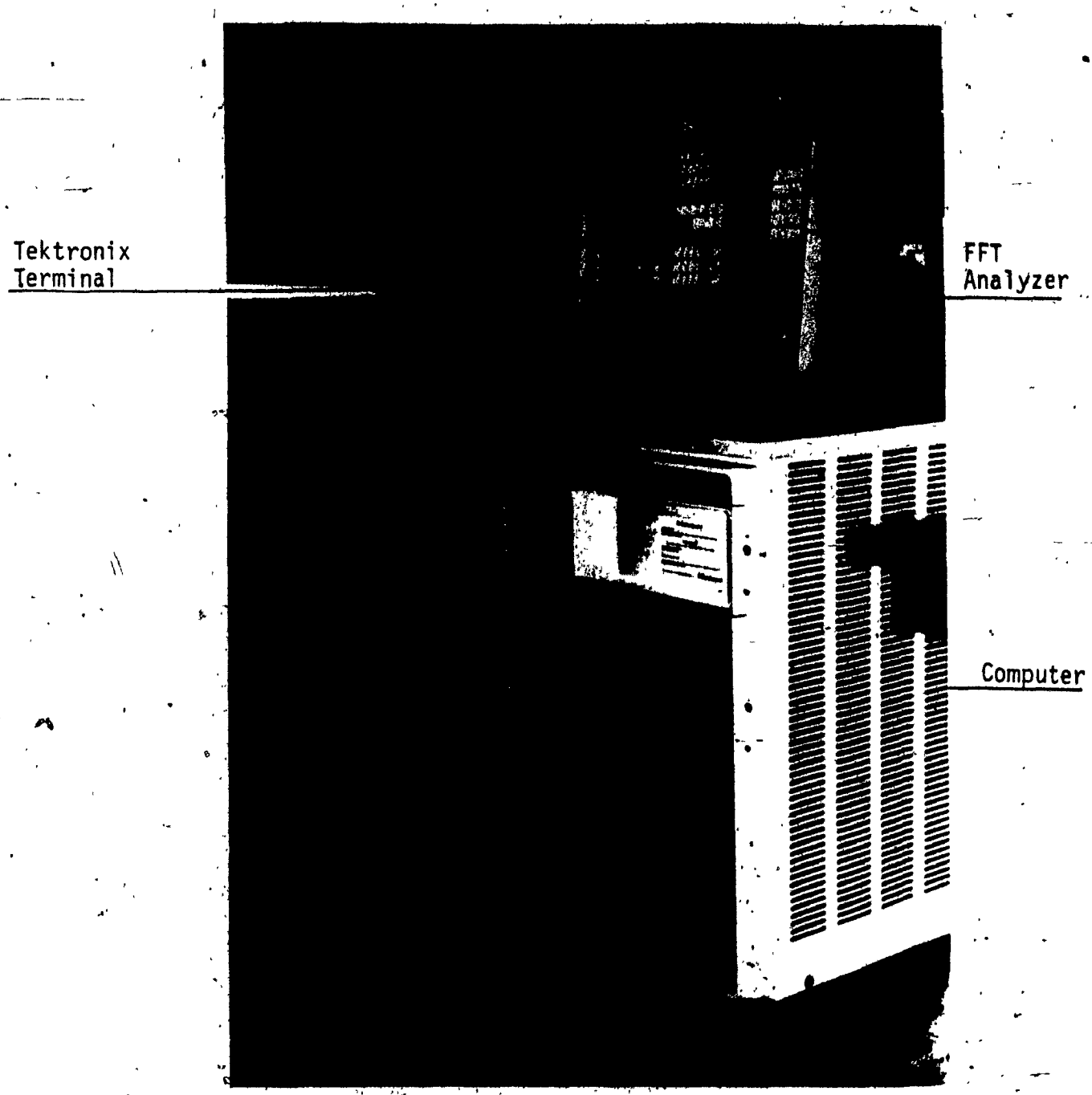

Fig. 7.4 Structural analysis system

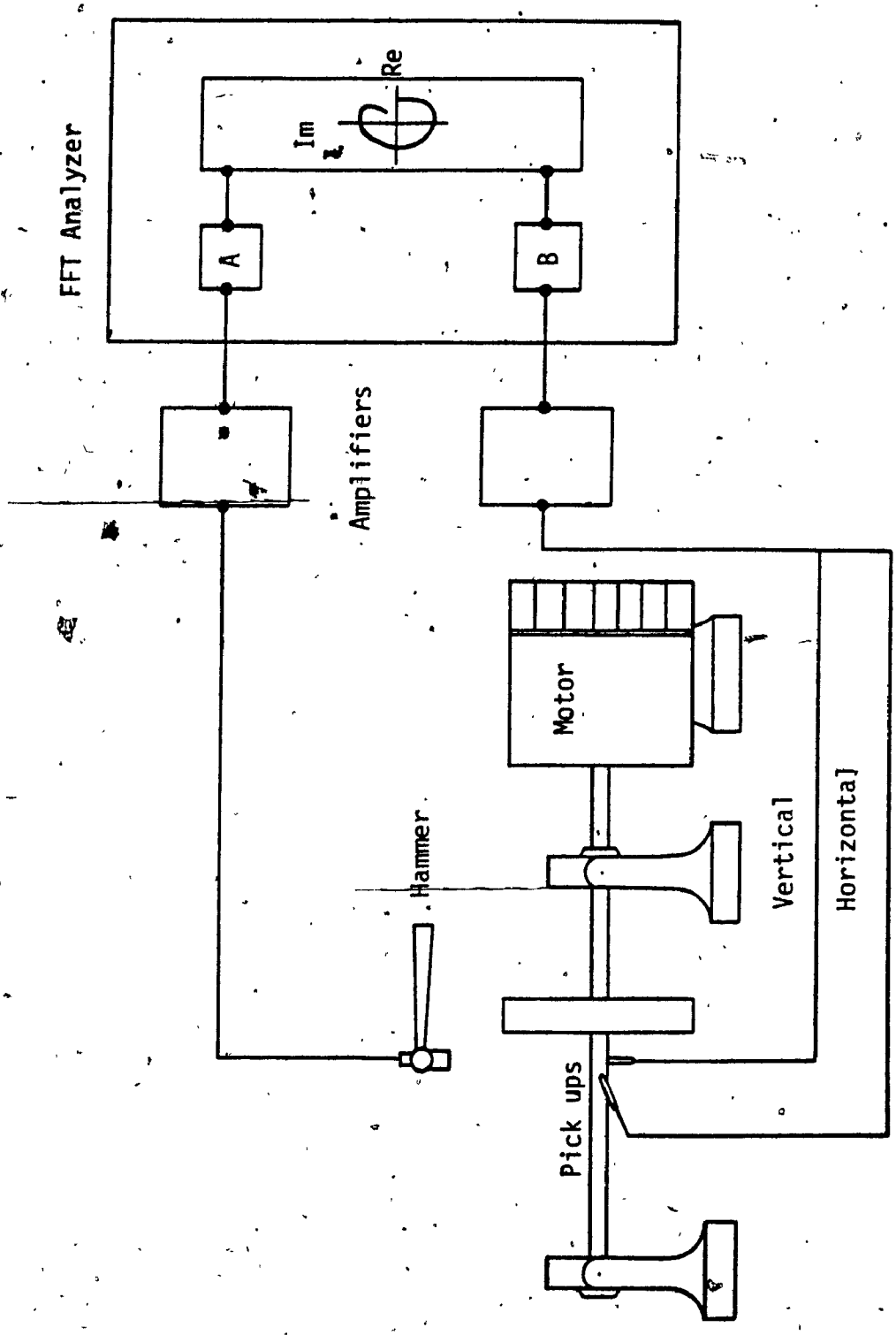

Fig. 7.5 Schematic diagram of the experimental facility (driven shaft not shown)

$$[k] = \begin{bmatrix} k_2 & 0 & -k_2 & 0 & 0 & 0 \\ 0 & k_{b2}+\bar{k}_t & \bar{k}_t r_2 & \bar{k}_t & \bar{k}_t r_1 & 0 \\ -k_2 & \bar{k}_t r_2 & k_2+\bar{k}_t r_2^2 & \bar{k}_t r_2 & \bar{k}_t r_1 r_2 & 0 \\ 0 & \bar{k}_t & \bar{k}_t r_2 & k_{b1}+\bar{k}_t & \bar{k}_t r_1 & 0 \\ 0 & \bar{k}_t r_1 & \bar{k}_t r_1 r_2 & \bar{k}_t r_1 & k_1+\bar{k}_t r_1^2 & -k_1 \\ 0 & 0 & 0 & 0 & -k_1 & k_1 \end{bmatrix}$$

$$\{q\} = \begin{Bmatrix} \theta_{xd} \\ y_2 \\ \theta_2 \\ y_1 \\ \theta_1 \\ \theta_{xm} \end{Bmatrix}$$

$$\{f\} = \begin{Bmatrix} 0 \\ U_2\omega_2^2 \sin(\theta_2+\theta_{f2}) \\ 0 \\ U_1\omega_1^2 \sin(\theta_1+\theta_{f1}) \\ 0 \\ 0 \end{Bmatrix}$$

Eq. (7.1) was derived on the theory of chapters 2-3. The time varying tooth stiffness, backlash and excitations other than those arising from unbalance are not considered.

The natural frequencies and mode shapes for the system defined by Eq. (7.1) is given in Table 7.2.

TABLE 7.2

Natural frequencies, Hz (RPM) 0-60 Hz.

1	0.0	(0.0)
2	4.38	(258.5)
3	19.40	(1164.)
4	26.92	(1615.)

Eigen Vectors

Mode shape : $\begin{Bmatrix} \theta_{xd} \\ y_2 \\ \theta_2 \\ y_1 \\ \theta_1 \\ \theta_{xm} \end{Bmatrix}$

1st Mode : $\begin{Bmatrix} 1.0 \\ 0.1281 \times 10^{-10} \\ 1.0 \\ 0.1052 \times 10^{-10} \\ -0.5 \\ -0.5 \end{Bmatrix}$

2nd Mode : $\begin{Bmatrix} 1.0 \\ -0.1759 \times 10^{-2} \\ 0.9958 \\ -0.1636 \times 10^{-2} \\ -0.4711 \\ 0.2302 \end{Bmatrix}$

3rd Mode : $\begin{Bmatrix} 1.0 \\ -0.05797 \\ 0.9139 \\ -0.1049 \\ 0.8258 \\ -0.01359 \end{Bmatrix}$

4th mode : $\begin{Bmatrix} 1.0 \\ -0.3144 \\ 0.8342 \\ 0.1643 \\ 0.7660 \\ -0.6493 \times 10^{-2} \end{Bmatrix}$

The response of the geared shaft sysem due to unbalance in the driving or driven gears is obtained using normal mode analysis. Modal damping of 3% is used for all the modes.

Fig. 7.6 shows the flexural response at the driving gear location due to unbalance in the driving and driven gears. When there is unbalance in the driving gear the response exhibits peaks at two of the natural frequencies within the frequency range, viz - 19.40 Hz (1164 rpm) and 26.92 Hz (1615 rpm). When there is unbalance in the driven gear however, the flexural response exhibits peaks at speeds which are gear ratio multiples of the system natural frequencies, viz - 9.7 Hz (582 rpm) and 13.46 Hz (807.5 rpm).

Fig. 7.7 shows the flexural response at the driven gear location due to unbalance in the driving and driven gears. We see a similar behaviour as in Fig. 7.5, except that the responses are much larger. In both Figures 7.6 and 7.7 there is a small peak observed at the natural frequency of 4.38 Hz or its gear ratio multiple.

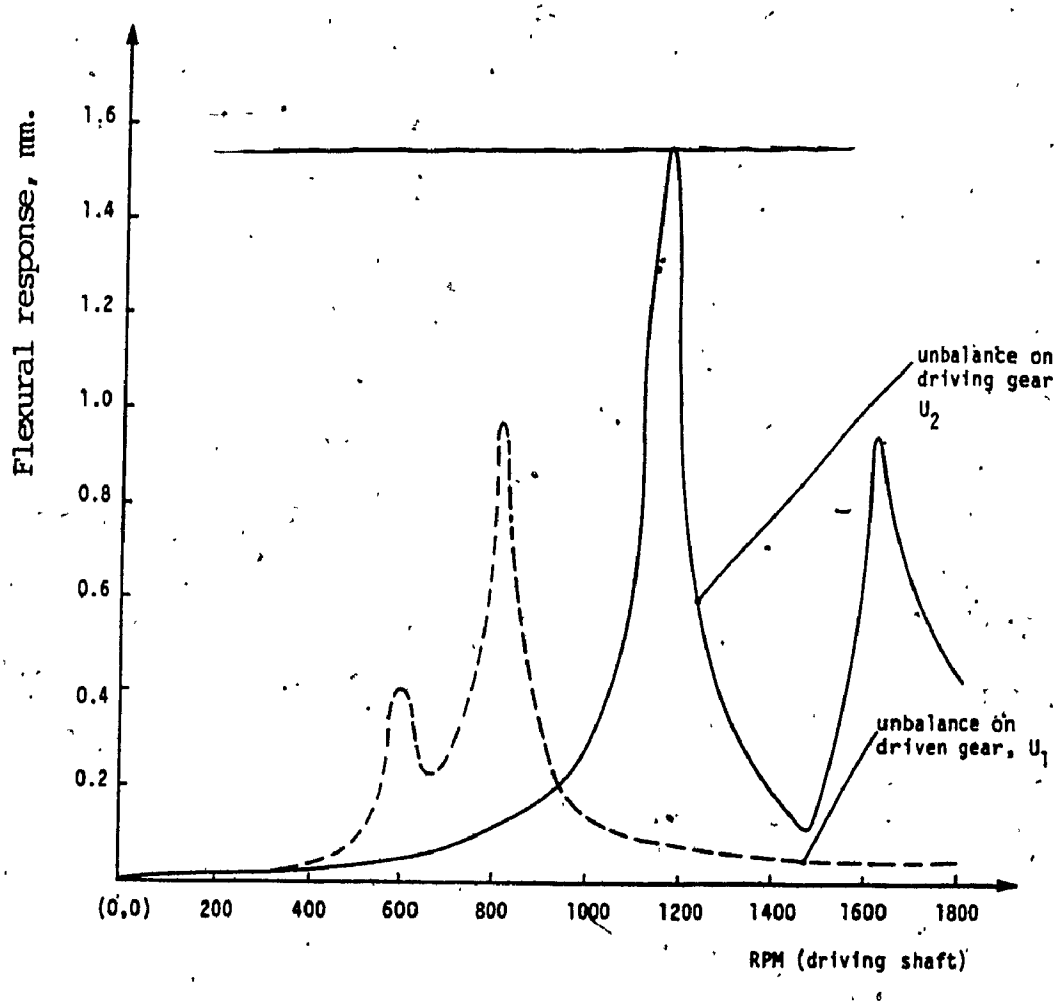

Fig. 7.6 Flexural response at the driving gear location due to unbalance in the gears

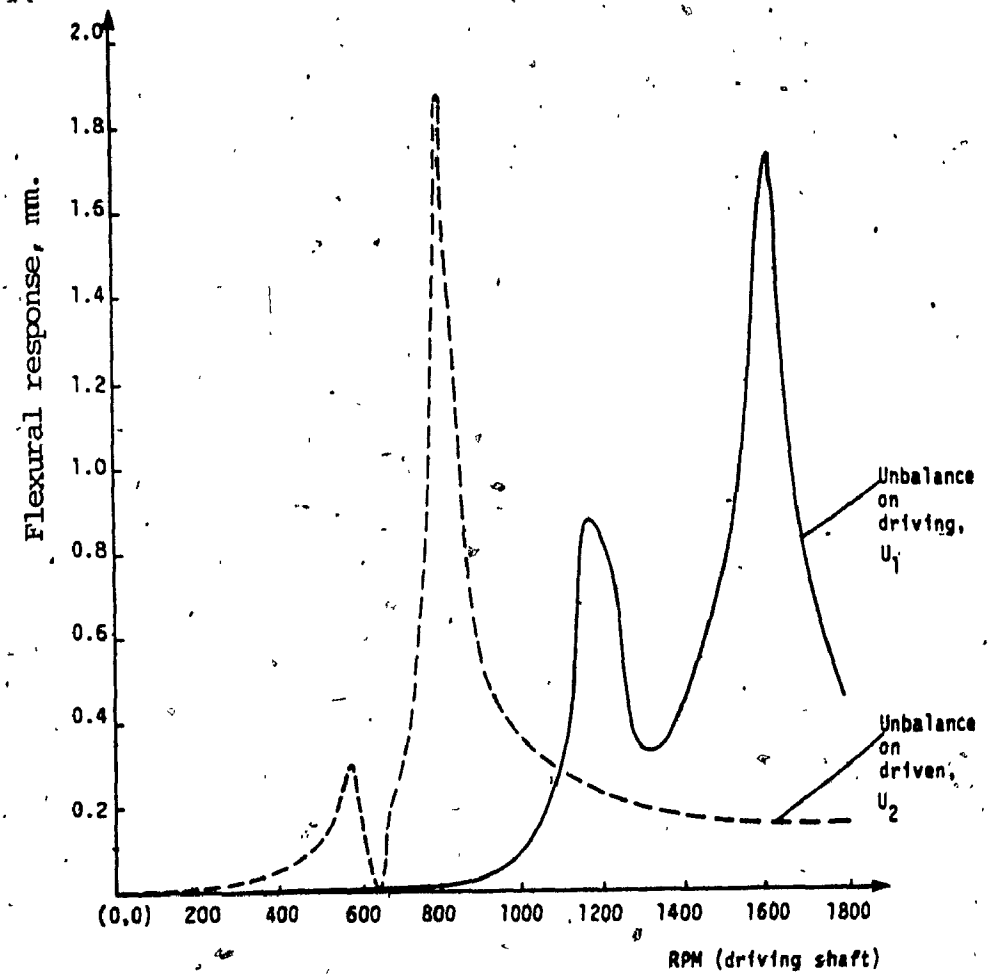

Fig. 7.7 Flexural response at the driven gear location due to unbalance in the gears

7.3.2 Experimental Dynamic Response

The geared shaft system under experimental investigation is driven by a variable speed motor. The speed of the driving side of the geared shaft system is measured by a digital tachometer. Two displacement measuring shielded sensors which operate on the eddy current principle are used to measure the dynamic response of the rotor in both the Z and Y directions at the gear locations. The sensors are mounted on two micrometer heads to enable precise adjustment of the gap between the sensors and the shaft surface. The dynamic response or whirl amplitude signals from the sensors, located along Z & Y directions, are amplified and fed to a FFT analyser.

The main objective in measuring the dynamic response is to observe whether there is a doubling of resonances as predicted by the analytical model. As discussed in chapter 2 and section 7.3.1, when there is unbalance in the driving and driven gears, the system experiences resonance not only at the system natural frequencies but also at the gear ratio multiples.

The amplitude of flexural response in the ~~z and x~~ directions at the driving gear locations for different speeds of the driving shaft is shown in Fig. 7.8 and Fig. 7.9. The

PAGE 234 OMITTED IN
PAGE NUMBERING.

PAGE 234 OMISE DANS
LA PAGINATION.

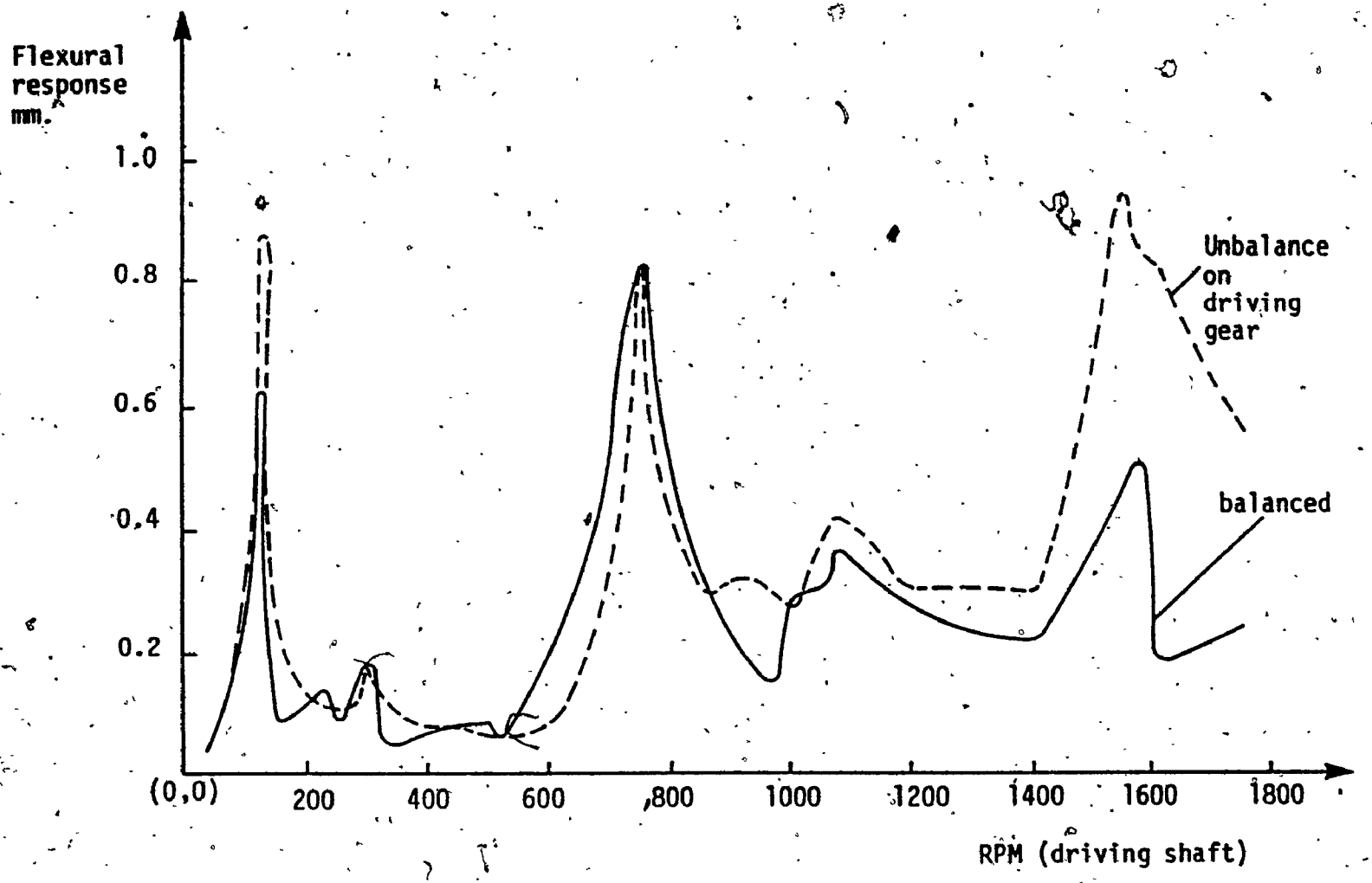

Fig. 7.8 Flexural response at the driving gear location in the z direction due to unbalance in the gears

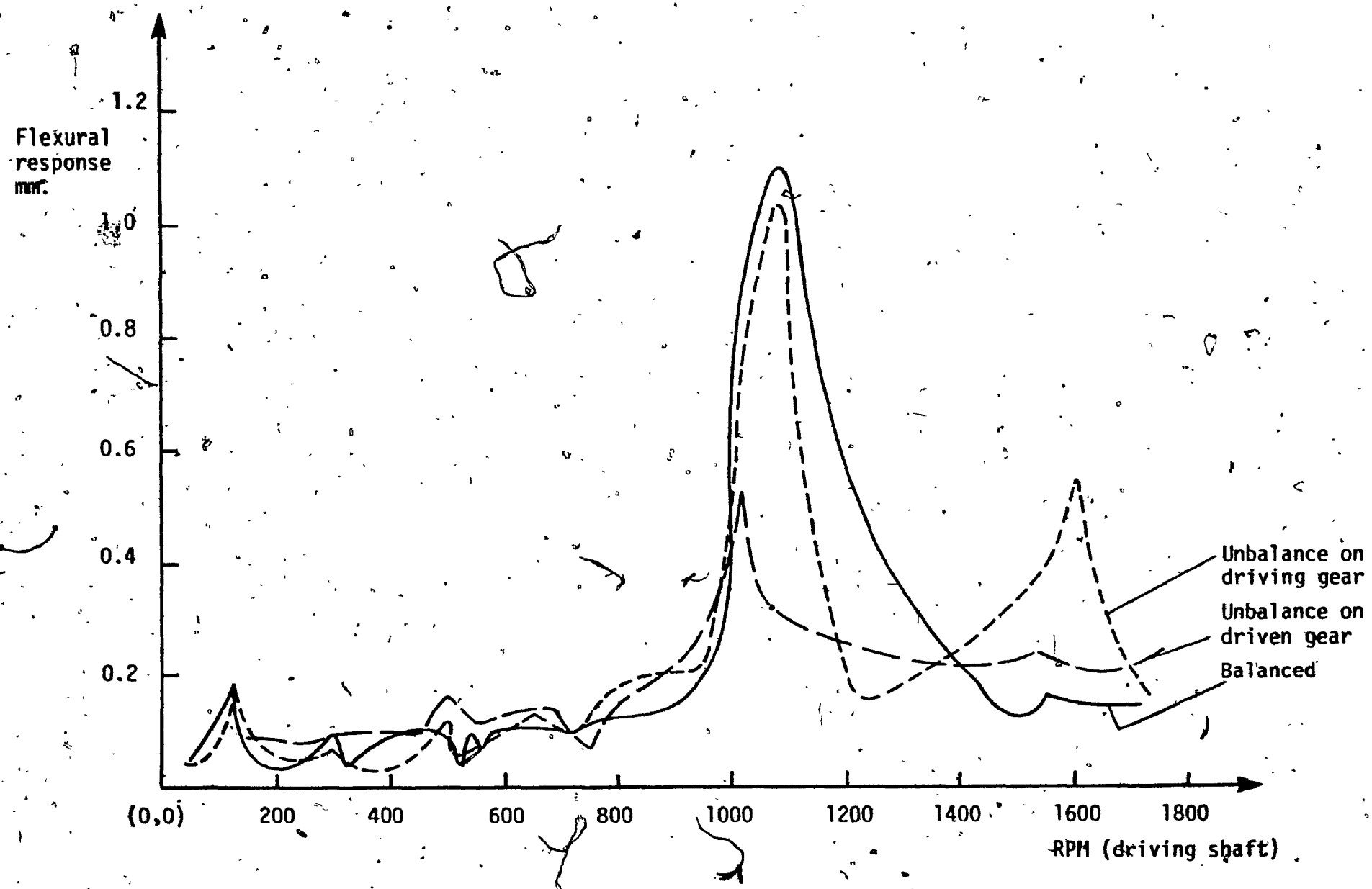

Fig. 7.9 Flexural response at the driving gear location in the x direction due to unbalance in the gears

plots show peaks at not only the analytically predicted natural frequencies but also at the gear ratio multiples. For instance, we see peaks at around 250 rpm (4.16 Hz.), 1075 rpm (17.9 Hz.) and 1550 rpm (25.8 Hz.) which are close to the analytically predicted natural frequencies [See Table 7.2] and also peaks at around 125 rpm (2.08 Hz.) 500 rpm (8.3 Hz.) and 766 rpm (12.7 Hz) which are gear ratio multiples of the system natural frequencies.

An exact comparison between the magnitude of the dynamic response between the analytical and experimental observations in not possible. This is because firstly, the driving side and driven side shafts were balanced separately. The magnitude and locations of the residual unbalance was not known accurately, therefore the unbalance used in the analytical model was not accurate, resulting in the discrepancy. Moreover, in an actual geared rotor system used for experimentation there are several other sources of error, the principal source being the static transmission error, as discussed in section 2.2. A measurement of this error and its introduction into the analytical model is therefore necessary. However, one of the objectives of this study has been to observe the doubling of system resonances for a torsion-flexural coupled system has been confirmed.

A similar phenomenon as seen in Figures 7.8 and 7.9 is found in Figures 7.10 and 7.11. Here, the flexural

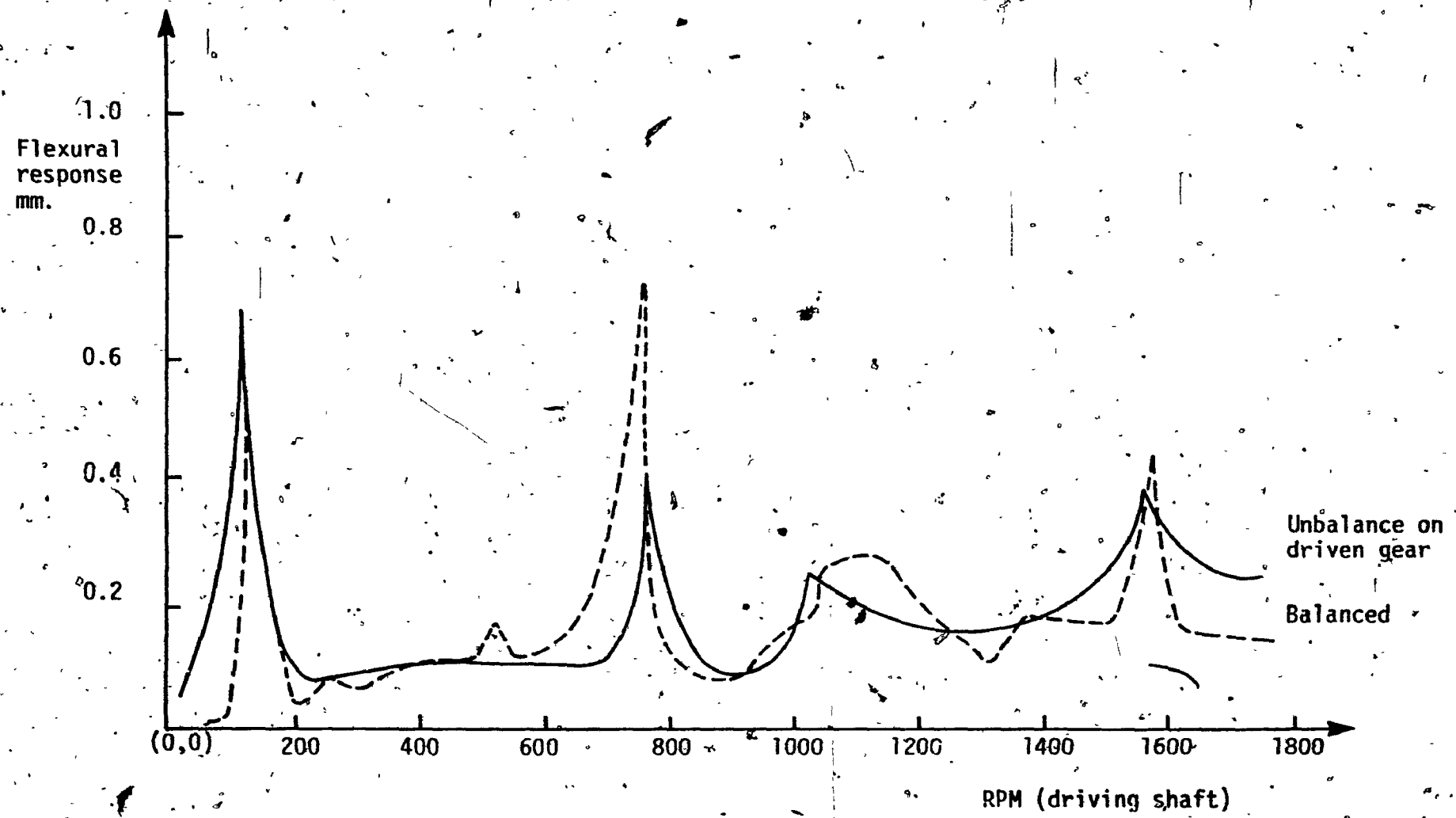

Fig. 7.10 Flexural response at the driven gear location in the z direction due to unbalance in the gears.

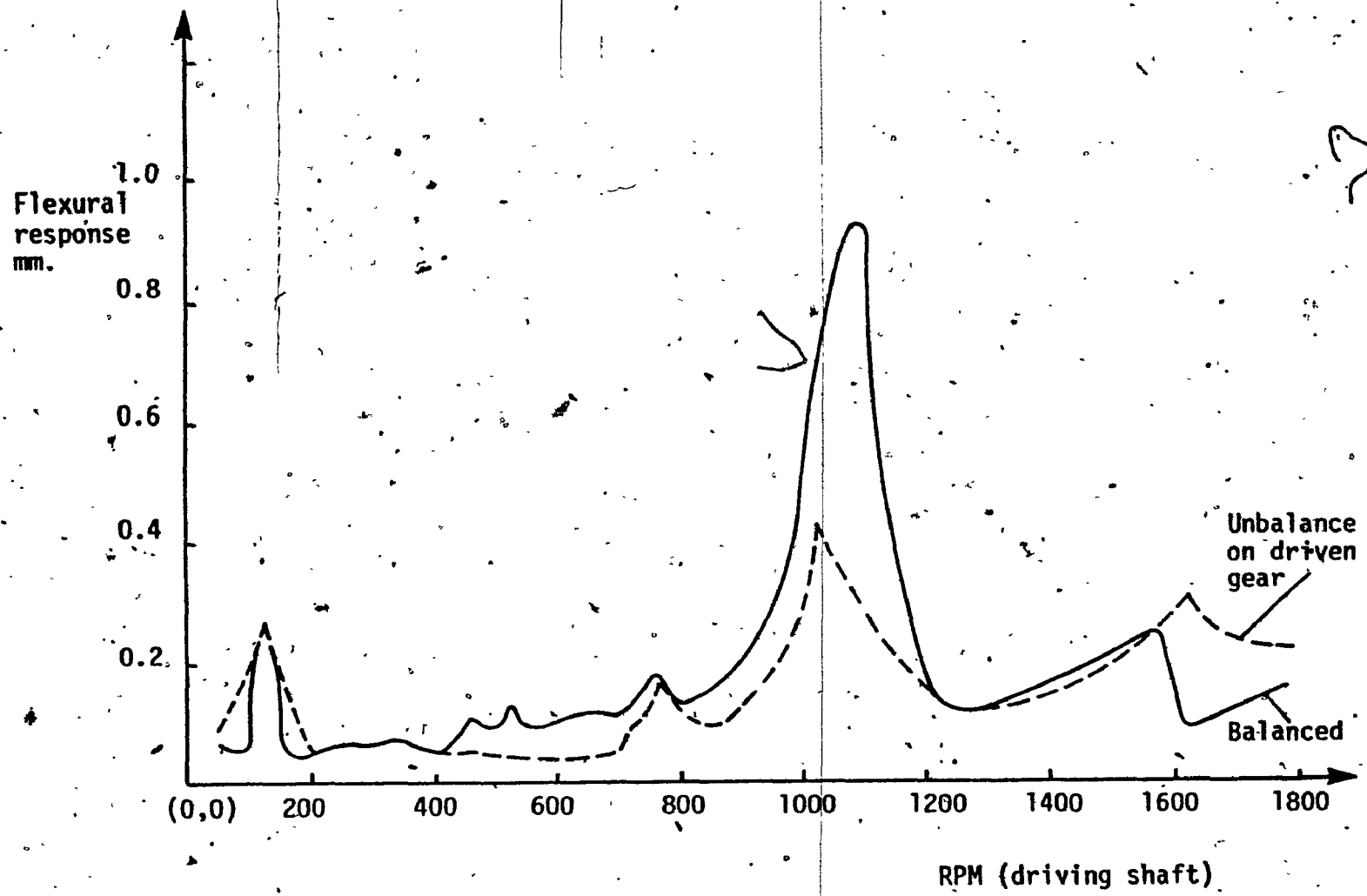

Fig. 7.11 Flexural response at the driven gear location in the x direction due to unbalance in the gears.

response is the Z and Y directions at the driven gear location is plotted with increasing speed of the driving shaft.

7.4 Modal Testing for a Spur Geared Rotor System

A dynamical system maybe described in two ways. One is the geometrical description using mass and stiffness matrices such as those obtained using finite element methods or lumped mass and stiffness properties. The other one is the modal description where the structure is defined using some of its gross properties such as natural frequencies, mode shapes, damping ratios etc. Modal analysis is a convenient tool to obtain the dynamic response of systems. Using experimentally obtained modal information in modal analysis will yield more realistic results for practical systems.

There are many applications of modal testing [96], however, in this chapter the requirements are

i) accurate estimates of natural frequency,

ii) descriptions of mode shapes using just sufficient detail and accuracy to permit their identification and correlation with those from the theoretical model.

The structural analysis system described in section

7.2 is used to carry out modal testing of the experimental spur geared rotor system setup. There are three basic steps associated with modal testing,

i) measurement of Transfer functions - experimental stage

ii) curve-fitting of mesasured transfer functions and extraction of modal parameters like natural frequencies, damping ratio, modal vectors, modal mass and modal stiffeness - Numerical analysis stage.

iii) establishment of the modal model-Modelling stage.

7.5 Frequency Response Functions for Non-Proportionally Damped Systems

Frequency response function is defined at a particular frequency as the ratio of the amplitude of the response to that of the force applied. Depending on the type of the response measured, it is called receptance, mobility or inertance of the system. The determination of the frequency response functions is the first step in modal testing and is important because the modal parameters are extracted from these functions using a curve fitting procedure. Consider a general system with non- proportional damping. The equations of motion are given by

$$[M]_{2N \times 2N} \{\dot{Q}\} + [K]_{2N \times 2N} \{Q\} = \{F\} \qquad (7.2)$$

where

$$[M] = \begin{bmatrix} 0 & m \\ m & c \end{bmatrix}$$

$$[K] = \begin{bmatrix} -m & 0 \\ 0 & k \end{bmatrix}$$

$$\{F\} = \left\{\begin{matrix} 0 \\ \hline f \end{matrix}\right\}_{2N \times 1} \quad \text{and} \quad \{Q\} = \left\{\begin{matrix} \dot{q} \\ \hline q \end{matrix}\right\}_{2N \times 1}$$

In Eq. (7.2), the first N equaitons express the identity,

$$[M]\ \{\dot{q}\} - [M]\ \{\dot{q}\} = \{0\} \tag{7.3}$$

Transforming the physical coordinates $\{Q\}$ into modal coordinates $\{p\}$ gives

$$\{Q\} = [\phi]\ \{p\} \tag{7.4}$$

where $[\phi]$ is the modal matrix. Substituting Eq. (7.4) in Eq. (7.2) and premultiplying throughout by $[\phi]^T$, the Eq. (7.2) becomes,

$$[\phi]^T\ [M]\ [\phi]\ \{\dot{p}\} + [\phi]^T\ [K]\ [\phi]\ \{p\} = [\phi]^T\ \{F\}$$

Let $[\mu] = [\phi]^T\ [M]\ [\phi]$

and $[\kappa] = [\phi]^T\ [K]\ [\phi]$ (7.5)

The complex eigen vectors $[\phi]$ are orthogonal to each other and hence the 2N number of uncoupled system equations

are obtained as follows

$$\mu_i \dot{p}_i + \kappa_i p_i = \mathcal{F}_i \qquad i = 1, 2, \ldots 2N$$

$$= \sum^{2N} \{\phi_i\}^T F_i \tag{7.6}$$

where μ_i and κ_i denote diagonal elements of $[\mu]$ and $[\kappa]$ respectively.

Consider the case of harmonic excitation at a point r on the shaft,

$$\{F\}^T = \{0, 0, 0, \ldots f_r, 0, 0\}e^{j\omega t} \tag{7.7}$$

where ω is the frequency of excitation. For steady state solution of the form, $p = \bar{p}\, e^{j\omega t}$, Eq. (7.6) becomes,

$$j\omega \mu_i \bar{p}_i + \kappa_i \bar{p}_i = \phi_{ri} f_r \tag{7.8}$$

which gives,

$$\bar{p}_i = \frac{\phi_{ri} f_r}{(j\omega\mu_i + \kappa_i)} \tag{7.9}$$

Now the response q_s, at point s is given by substituting Eq. (7.9) in Eq. (7.4),

$$q_s = \sum_{i=1}^{2N} \frac{\phi_{si}\phi_{ri}\, f_r}{(j\omega\mu_i + \kappa_i)} \tag{7.10}$$

which can be put in the form,

$$q_s = \sum_{i=1}^{2N} \frac{\phi_{si}\, \phi_{ri}\, f_r}{\mu_i\, (j\omega - \lambda_i)} \tag{7.11}$$

where

$$\lambda_i = -\frac{\kappa_i}{\mu_i} \tag{7.12}$$

Hence, the frequency response function $H_{sr}(j\omega)$ can be written as,

$$H_{sr}(\omega) = \frac{q_s}{f_r} = \sum_{i=1}^{2N} \frac{\psi_{ri}\ \psi_{si}}{\mu_i(j\omega-\lambda_i)} \qquad (7.13)$$

However, because the eigenvalues and eigenvectors occur in complex conjugate pairs, Eq. (7.13) can be rewritten [77], for a proportionally damped system as,

$$H_{sr}(\omega) = \sum_{i=1}^{2N} \frac{1}{\mu_i\ \lambda_i'} \left[\frac{\psi_{ri}\ \psi_{si}}{2j\ (j\omega-P_i)} - \frac{\psi^*_{ri}\ \psi^*_{si}}{2j\ (j\omega-P^*_i)} \right] \qquad (7.14)$$

where $\lambda_i' = \omega_i(1-\zeta_i^2)^{\frac{1}{2}}$

The pole for the ith mode P_i is defined as

$$P_i = -\zeta_i\omega_i + j\omega_i\ (1-\zeta_i^2)^{\frac{1}{2}}$$

P_i^* and ψ_i^* are complex conjugates of P_i and ψ_i respectively.

Equation (7.14) represents the frequency response function for a proportionally damped system. For a non-proportionally damped system, the frequency response function is given by

$$H_{sr}(\omega) = \frac{q_s(j\omega)}{f_r(j\omega)} = \sum_{i=1}^{2N} \left[\frac{\psi_{ri}\ \psi_{si}}{\mu_i(j\omega-P_i)} + \frac{\psi_{ri}^*\ \psi_{si}^*}{\mu_i^*(j\omega-P_i^*)} \right] \qquad (7.15)$$

The analytical form of the frequency response function is given by Eq. (7.15). Experimentally measured frequency response functions are fitted with this form using curve fitting procedures to extract the modal parameters.

7.6 Obtaining the Frequency Response Function

Experimental determination of modal parameters has usually been carried out on non rotating structures. These techniques can be also used for rotating structures such as a geared rotor system. The geared shaft system described in section 7.2 is subjected to modal testing. Eleven test points are prescribed, five on the driving shaft and six on the driven shaft. A schematic diagram of the geared shaft system with specified test points are shown in Fig. 7.12. The measurements are made both along the vertical and horizontal directions at any position along the rotor shaft using sensors mounted on a sliding block with micrometer heads. The sensors measure displacement and operate on the eddy current principle. An impulse hammer which has a force transducer to detect the magnitude of the force applied, is used to apply test force at points defined on the geared rotor system. The response signals from the displacement measuring sensor and the impulse hammer are fed into the FFT analyser. The FFT analyser then computes the Frequency Response function (FRF) from these two signals. Fig. 7.13 shows a NXN matrix of frequency response functions. Measuring the response at a fixed location and exciting each test point with the hammer yeilds one row of the FRF, which provides both the eigenvalues and eigenvectors of the system.

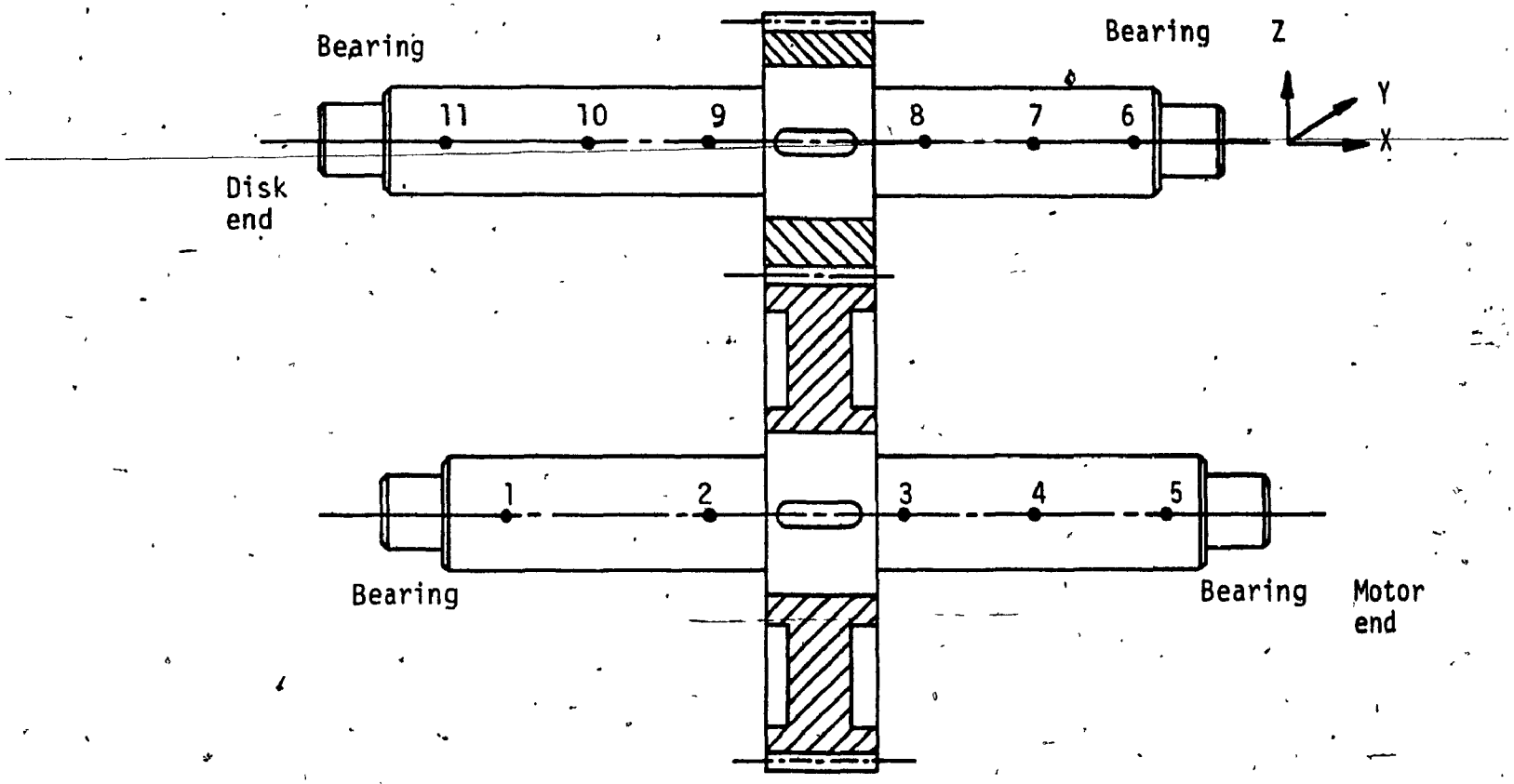

Fig. 7.12 Test points of the spur geared rotor system

$$H_{sr}^{A}(\omega) = \begin{bmatrix} H_{11} & H_{12} & \cdots & H_{1r} & \cdots & H_{1N} \\ H_{21} & H_{22} & & H_{2r} & & H_{2N} \\ \vdots & & & & & \\ H_{s1} & H_{s2} & & H_{s3} & & H_{sN} \\ \vdots & \vdots & & \vdots & & \vdots \\ H_{N1} & H_{N2} & & H_{Nr} & & H_{NN} \end{bmatrix}$$

Fig. 7.13 . Matrix of frequency response function

The magnitude of the impact is determined by the mass of the hammer head and the velocity with with it is moving when it hits the structure. The magnitude of the force is adjusted by varying the mass of the hammer head. The frequency range which is effectively excited by a hammer depends on the stiffness of the contacting surfaces and the mass of the impactor head. A typical impact force pulse and spectrum is shown in Fig. 7.14. The stiffer the contacting materials, the shorter will be the duration of the pulse and the higher will be the frequency range covered by the impact. Similarly, the lighter the impactor mass, the higher the effective frequency range. Generally a soft tip is used in order to inject all the input energy into the frequency range of interest, rather than use a stiffer tip which inputs energy outside the range of interest at the expense of those inside the range.

7.7 Modal Parameter Extraction

After the frequency response function is obtained, the next step consists of curve fitting it with a theoretical expression. The task basically involves finding the coefficients in a theoretical expression of the FRF that most closely matches the measured data. The coefficients are then directly related to the sought after modal parameters.

Most of the curve-fitting methods operate on the

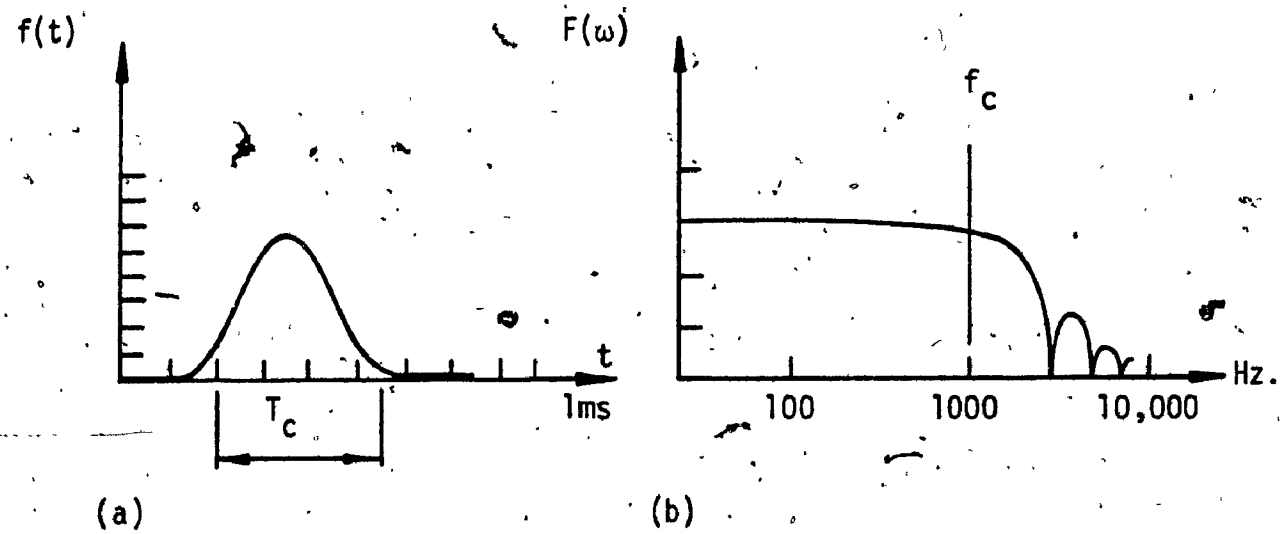

Fig. 7.14 Typical impact force pulse and spectrum [96]

(a) Time history
(b) Frequency spectrum

response chacterisitcs in the frequency domain, i.e. - the FRF itself, but there are other procedures that perfrom a curve fit in the time domain. The advantage of the frequency domain analyses is that the natural frequencies are clearly identified and the well developed FFT algorithms along with recent measurement techniques make it very fast.

There exists a number of curve fitting procedures, all of which share the same basic assumption: namely, that in the vicinity of a resonance the total response is dominated by the contribution of the mode whose natural frequency is closest. The methods vary as to whether they assume that all the response is attributed to that single mode or whether the other modes contributions are represented by a simple approximation.

7.7.1 The Peak-Pick SDOF Method

This is the simplest of the curve fitting methods and works well for structures whose FRF exhibit well separated modes. First individual resonance peaks are detected on the FRF plot (Fig. 7.15) and the frequency of maximum response taken as the natural frequency of that mode (ω_0). Secondly, the damping is determined from the sharpness of resonance and is given by

$$\zeta = \frac{1}{2}\left(\frac{\omega_2 - \omega_1}{\omega_0}\right) \qquad (7.16)$$

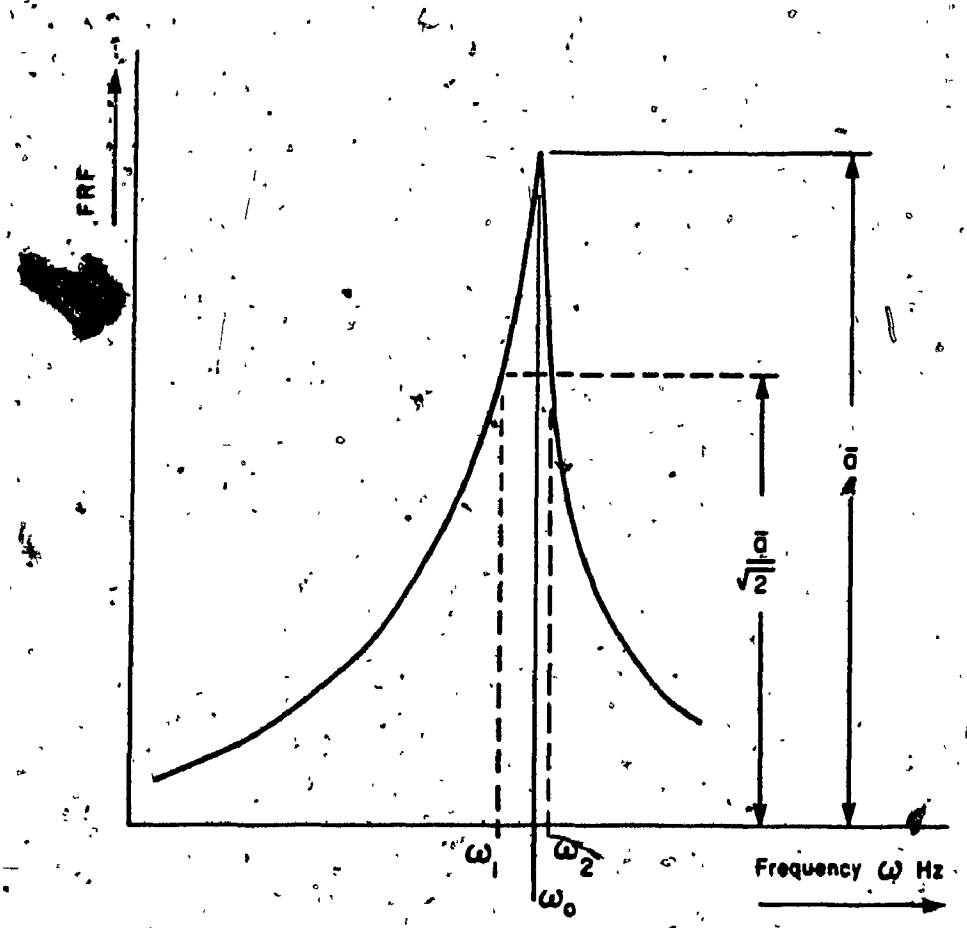

Fig. 7.15 FRF curve for a second order simple linear system

where ω_1 and ω_2 are frequencies at half power and ω_0 is the resonant frequency. To obtain the mode shape, the structure is excited at a natural frequency and the ratios of the amplitudes at various points on the structure are determined.

Peak pick method gives only a crude estimation of the modal parameters. A circle fit method, which is described next, gives a better estimation of the modal parameters.

7.7.2 Circle Fit SDOF Method

The circle fit method for extracting modal residues is based upon the use of the Nyquist plot of a transfer function. The following conditions are assumed:

1) The modes are weakly coupled in the frequency range where one mode is dominant.
2) The modes are lightly damped ($\zeta < 0.2$)

The FRF can be written from Eq. (7.14) for the dominant ith mode as;

$$H_i(j\omega) = \frac{1}{\mu_i \lambda_i} \left[\frac{\psi_{ri}\ \psi_{si}}{2j(j\omega - p_i)} \right] \qquad (7.17)$$

Let $\psi_{ri}\ \psi_{si} = R_r$, the complex residue. Consider the case of real residue of unit magnitude neglecting the imaginary component. Then, the real part of the FRF is found to be

$$\text{Re}\,[H_i(j\omega)] = \frac{\lambda_i' - \omega}{2\,[(\lambda_i'-\omega)^2 + (\zeta_i\omega_i)^2]} \qquad (7.18)$$

The imaginary part of the FRF is,

$$\text{Im}\,[H_i(j\omega)] = \frac{-\zeta_i\omega_i}{2[(\lambda_i'-\omega)^2 + (\zeta_i\omega_i)^2]} \qquad (7.19)$$

The real and imaginary parts of $H_i(j\omega)$ defined by Eqs. (7.18) and (7.19) form the following relationship,

$$\{\text{Re}\,[H_i(j\omega)]\}^2 + \{\text{Im}\,[H_i(j\omega)] - \frac{1}{4\zeta_i\omega_i}\}^2 = \left[\frac{1}{2\zeta_i\omega_i}\right]^2 \qquad (7.20)$$

Eq. (7.20) is the equation of a circle with its center on the imaginary axis at $(0, -\frac{1}{2\zeta_i\omega_i})$ and radius $\frac{1}{2\zeta_i\omega_i}$ This is shown in Fig. 7.16(a).

If we consider a complex residue R_r of the form,

$$R_r = ||R_r|| \exp(j\theta r)$$

then the diameter of the circle in 7.16(a) expands by a factor $||R_r||$ and the center of the circle rotates counter-clockwise by an angle θ_r from the imaginary axis as shown in Fig. 7.16(b).

Most of the errors in measurements are concentrated around the resonance region which affects the estimates of both damping and the modal constant. Also, even with clearly separated modes, it is often found that contribution of the neighbouring modes to the response of the mode being analysed is not insignificant. To deal with these limitations an iterative least square method which considers the contribution of other modes also can be used.

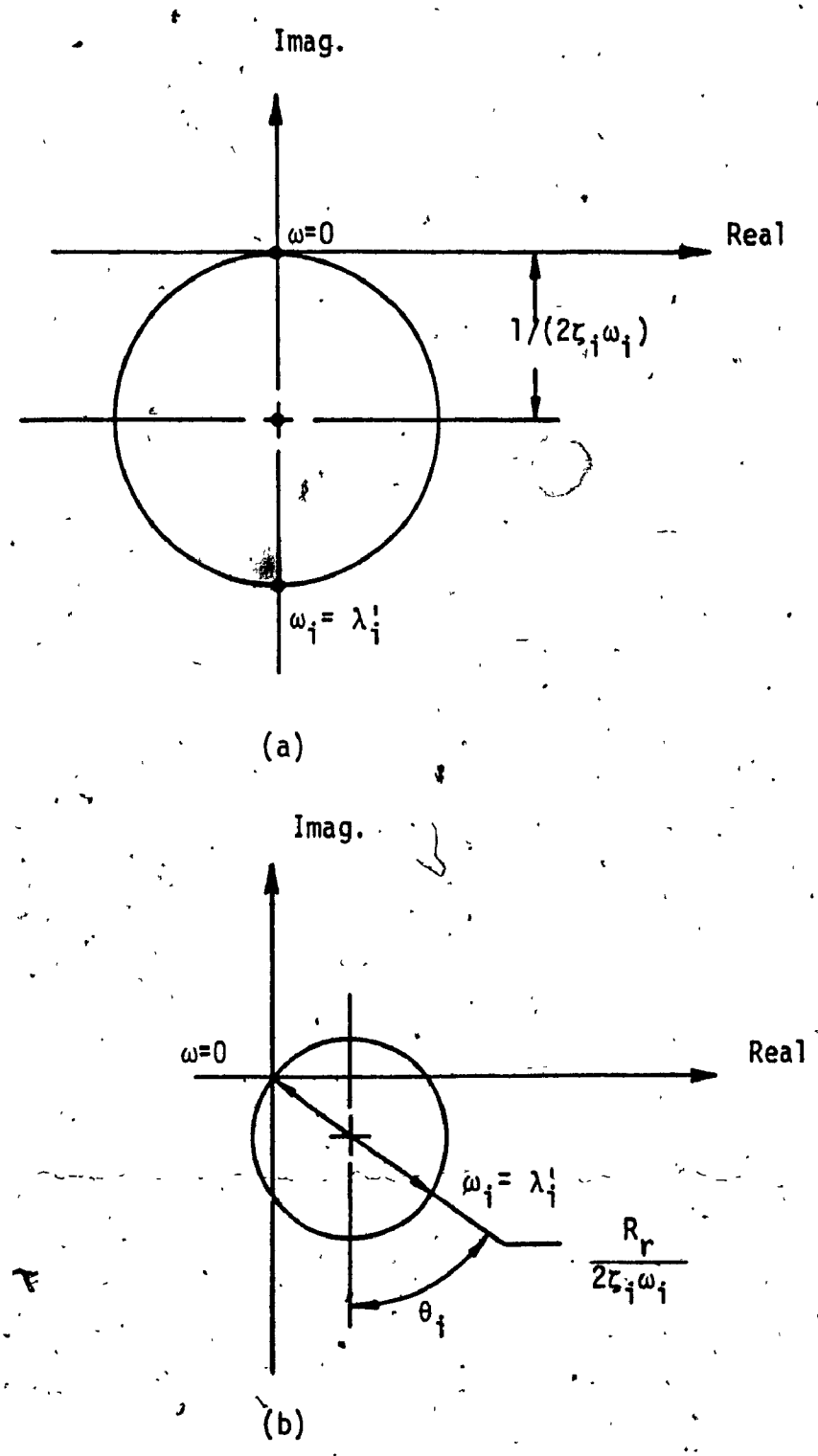

Fig. 7.16 Circle fit method

7.7.3 The Iterative Least Square (MDOF) Method

If the measured response is dominated by a single mode, SDOF methods described in section 7.7.1 and 7.7.2 are adequate. Otherwise a more sophisticated algorithm based on a Multidegree of Freedom (MDOF) model is necessary.

The complex modal parameters are identified by fitting the best curve between the measured FRF plot and the generated (or synthesised) plot from the analytical expression given by Eq. 7.15. The least square procedure is used as a criterion for the miminisation of error between the measured and the generated FRF plots. The criterion is

$$H^A_{sr}(\omega, \lambda_i, \phi_i) = H^M_{sr}(\omega) + E_p \qquad (7.21)$$

where H^A_{sr} is the generated FRF

H^M_{sr} is the measured FRF and

E_p is the error between them.

$$E_p = [H^A_{sr}(\omega, \lambda_i, \phi_i) - H^M_{sr}(\omega)]^2 \qquad (7.22)$$

Summing up the square of the error over "N" frequencies,

$$\sum_{p=1}^{N} E_p^2 = \sum_{p=1}^{N} [H^A_{sr}(\omega, \lambda_i, \phi_i) - H^M_{sr}(\omega)]^2 \qquad (7.23)$$

Differentiating Eq. (7.23) with respect to each unknown modal parameters in turn and setting the result to zero, gives a set of equations containing the unknown modal parameters.

H^A_{sr} is computed initially using modal parameters obtained from one of the SDOF methods. E_p is computed as the contribution of all other modes except the mode being measured. The results of this are used in an iterative loop to get more accurate results.

7.8 Results of the Modal Testing on a Spur Geared Rotor System

The frequency response plots are experimentally obtained as described in section 7.6, and these plots provide the natural frequencies of the system where we observe a peak in the amplitude plot and a change in the respective phase plot from 0^0 to 180^0. Since the operating speed of the driving gear is only around 1800 RPM, only the first four modes are considered. The experimental frequency response plots are obtained by measuring the response in the Z direction are the 7th test point, and exciting all the other test points in the Y and Z directions.

Some of the frequency response plots are shown in Figures 7.17 - 7.20. The system exhibits peaks at the natural frequencies, four of which lie in the range 0-30 Hz. They are given in Tables 7.3 - 7.6. The natural frequencies of the first three elastic modes compare quite well with the

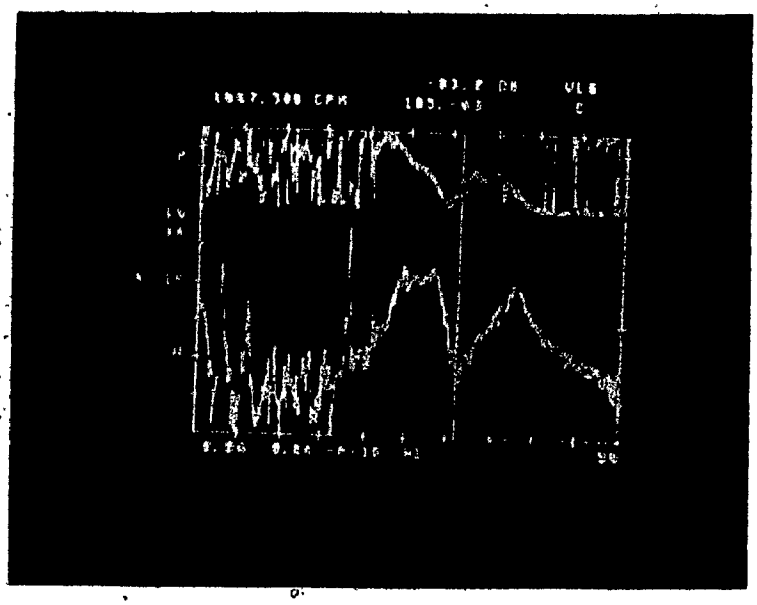

Fig. 7.17 Measured frequency response of the geared shaft system for measurement point 4Z+, driving point 7Z+, RPM=87

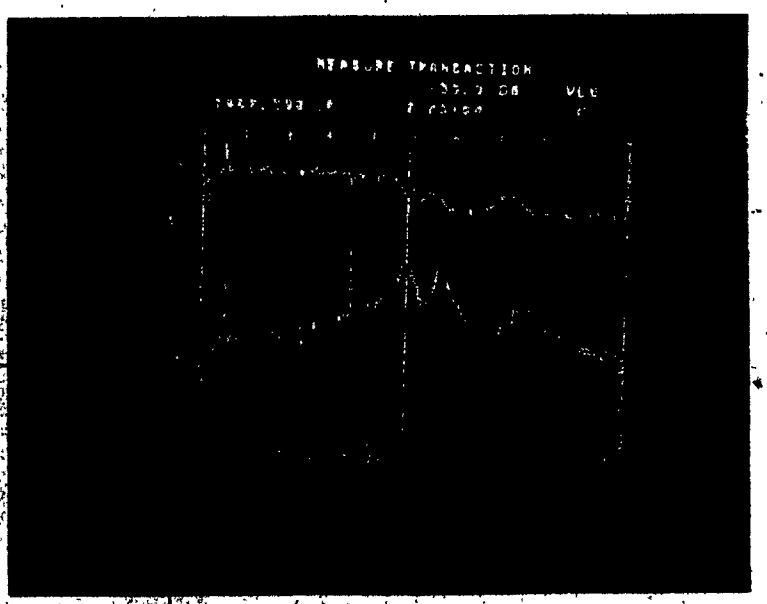

Fig. 7.18 Measured frequency response of the geared shaft system for measurement point 9Z+, driving point 7Z+, RPM=87

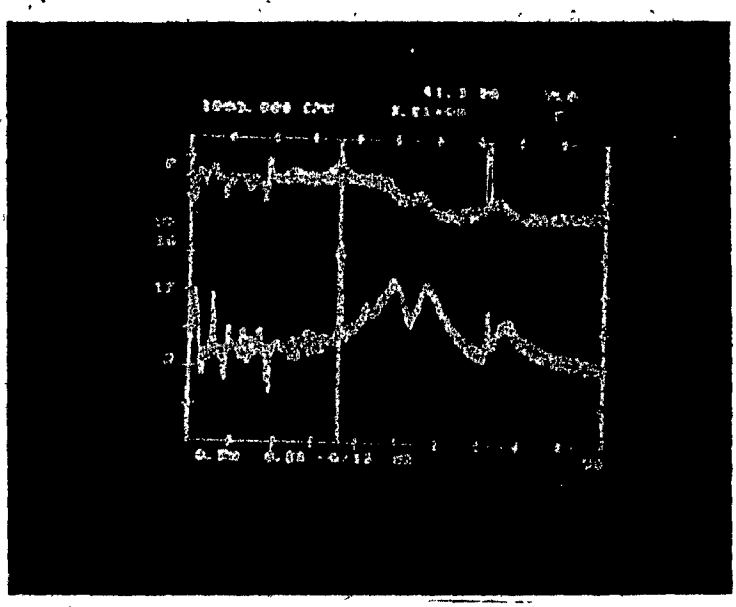

Fig. 7.19 Measured frequency response of the geared shaft system for measurement point 10Z+, driving point 7Z+, RPM=87

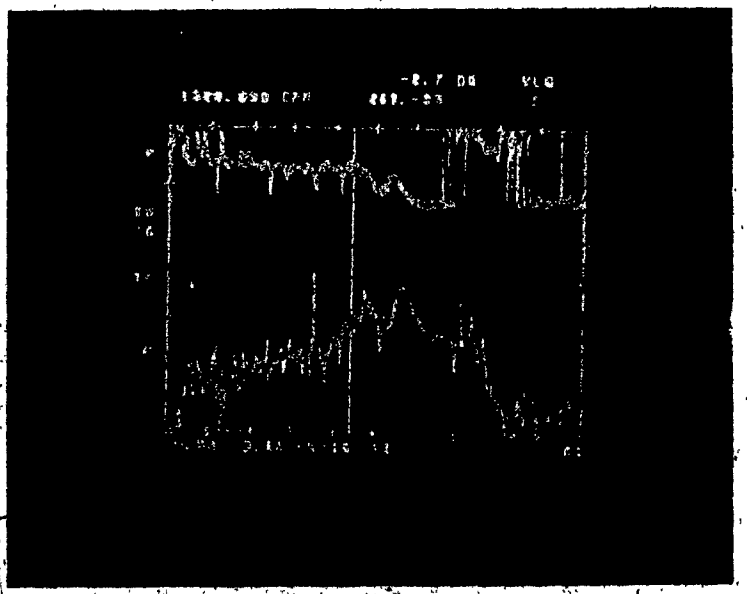

Fig. 7.20 Measured frequency response of the geared shaft system for measurement point 11Z+, driving point 7Z+, RPM=87

natural frequencies obtained from a simple lumped mass model of the geared rotor in rigid bearings given in Table 7.2.

The mode shapes for the first three elastic modes obtained experimentally are given in Figures 7.21 - 7.23. The motion of the two shafts comprising the geared shaft system is predominantly in the Z direction as seen in the figures. The modal parameters obtained from the modal testing are given in Tables 7.3 - 7.6. It can be seen from Table 7.3 - 7.6 and Table 7.2, that the natural frequencies from the experiments and the simple analytical model compare very well.

7.9 Summary

Experiments were carried out on a Spur Geared Rotor System. First, the unbalance response was obtained experimentally at the driving and driven gear locations and compared with that of the simple lumped mass analytical model. The flexural response at the driving and driven gears was experimentally measured and exhibited peaks not only at the system natural frequencies but also at the gear ratio multiples of the system natural frequencies when there is excitation from mass unbalance in both the gears. This phenomenon was observed in the analytical model (chapter 2). The peaks in

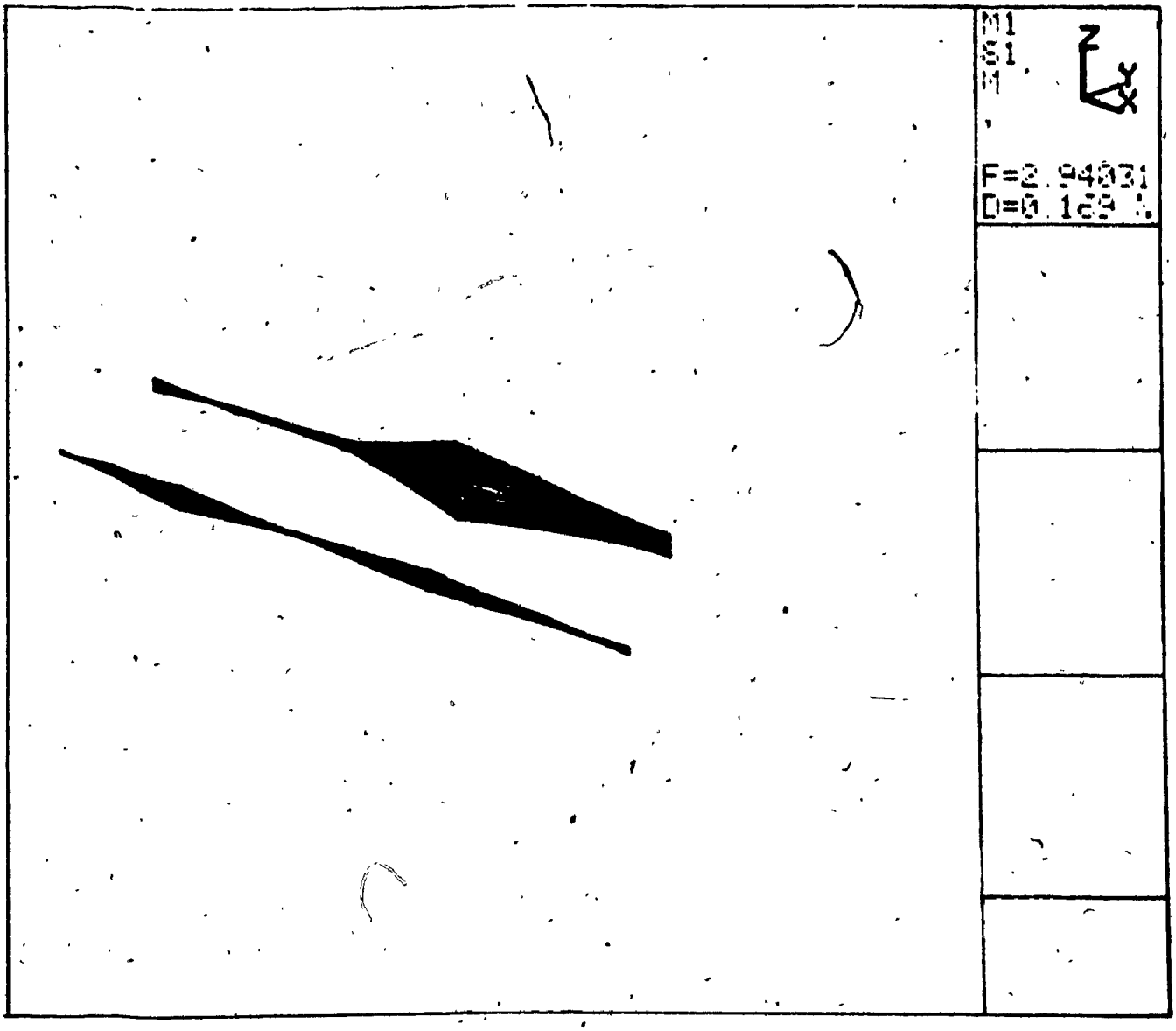

Fig. 7.21 First mode shape of the geared rotor system

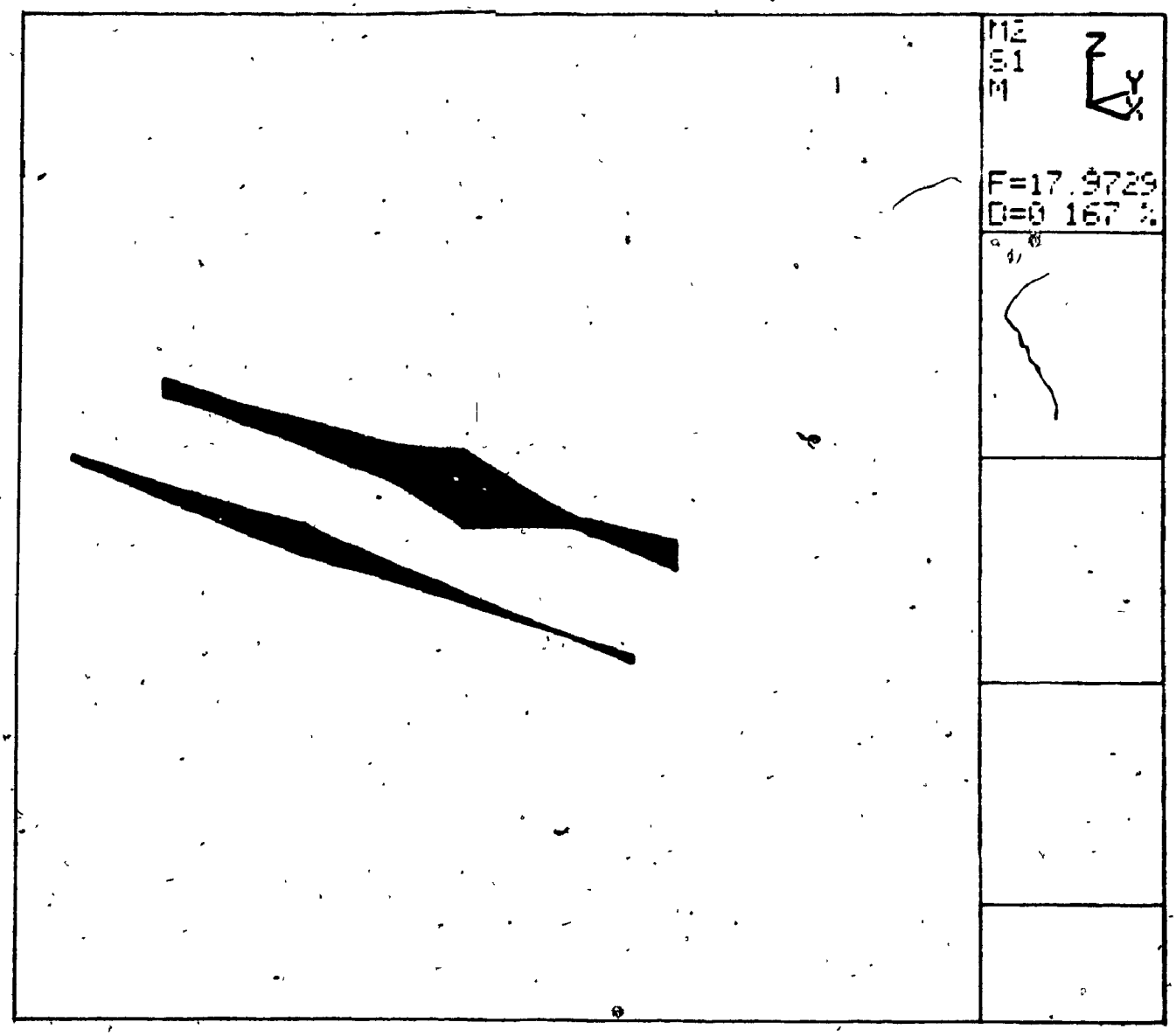

Fig. 7.22 Second mode shape of the geared rotor system

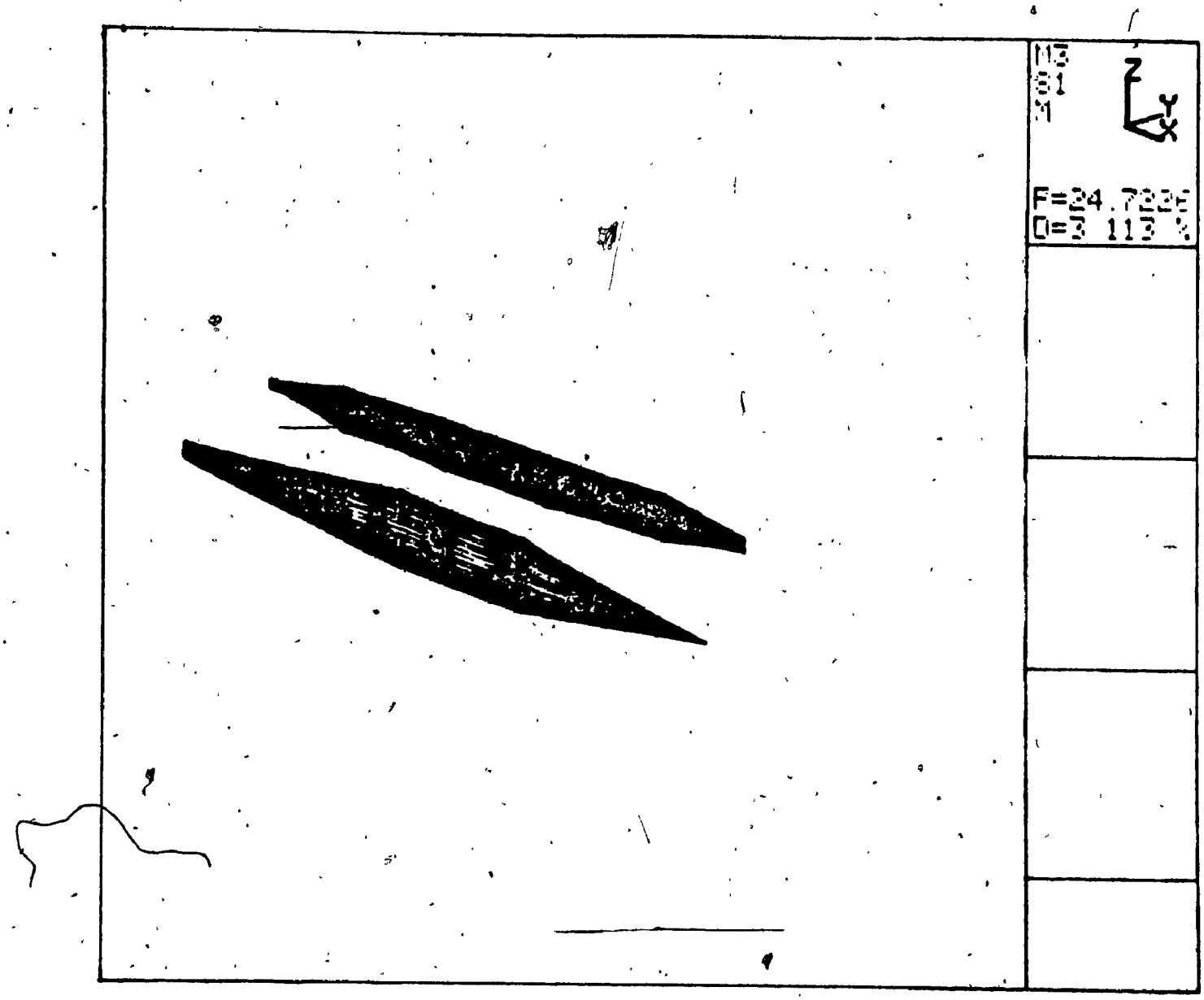

Fig. 7.23 Third mode shape of the geared rotor system

TABLE 7.3

Measured Modal Parameters of the Geared Rotor

Mode 1 Resonance Frequency: 2.94 Hz. Viscous Damping: 0.169%

Modal Mass: 1.84×10^{-3} Modal Stiffness: 0.63

RPM: 87

MEASURE PT	MEASURE DIR	DRIVING PT	DRIVING DIR	REAL	IMAG	MAG	PHASE
1	Z+	7	Z+	5.651E-02	6.371E-03	5.687E-02	6.4
2	Z+	7	Z+	-0.142E+00	-0.279E+00	0.313E+00	-116.9
3	Z+	7	Z+	-1.162E+02	3.724E-02	3.901E-02	107.9
4	Z+	7	Z+	6.485E-03	0.255E+00	0.256E+00	88.5
5	Z+	7	Z+	-4.574E-02	-5.760E-02	7.335E-02	-128.5
6	Z+	7	Z+	0.233E+00	0.181E+00	0.295E+00	37.8
7	Z+	7	Z+	0.457E+00	-0.126E+00	0.474E+00	-15.4
8	Z+	7	Z+	1.000E+00	-1.634E-07	1.000E+00	0.0
9	Z+	7	Z+	1.568E-02	-0.132E+00	0.133E+00	-83.2
10	Z+	7	Z+	-6.754E-02	-6.932E-02	9.696E-02	-134.3
11	Z+	7	Z+	0.173E+00	-5.894E-03	0.173E+00	-2.0

TABLE 7.4

Measured Modal Parameters of the Geared Rotor

Mode 2 Resonance Frequency: 17.9 Hz. Viscous Damping: 0.167%

Modal Mass: 2.97×10^{-4} Modal Stiffness: 3.79

RPM: 87

MEASURE PT	MEASURE DIR	DRIVING PT	DRIVING DIR	REAL	IMAG	MAG	PHASE
1	Z+	7	Z+	8.347E-02	-1.350E-02	8.456E-02	-9.2
2	Z+	7	Z+	0.186E+00	0.151E+00	0.240E+00	39.1
3	Z+	7	Z+	0.303E+00	0.286E+00	0.417E+00	43.4
4	Z+	7	Z+	0.171E+00	-3.656E-02	0.174E+00	-12.1
5	Z+	7	Z+	-9.316E-02	4.232E-02	0.102E+00	155.6
6	Z+	7	Z+	-0.118E+00	0.349E+00	0.369E+00	108.7
7	Z+	7	Z+	-3.379E-02	0.176E+00	0.188E+00	109.9
8	Z+	7	Z+	1.000E+00	0.000E+00	1.000E+00	0.0
9	Z+	7	Z+	0.120E+00	0.457E+00	0.472E+00	75.3
10	Z+	7	Z+	-3.204E-02	0.252E+00	0.254E+00	97.3
11	Z+	7	Z+	0.152E+00	0.203E+00	0.253E+00	53.2

TABLE 7.5

Measured Modal Parameters of the Geared Rotor

Mode 3 Resonance Frequency: 24.87 Hz. Viscous Damping: 3.113%

Modal Mass: 2.71×10^{-5} Modal Stiffness: 0.65

RPM: 87

MEASURE PT	MEASURE DIR	DRIVING PT	DRIVING DIR	REAL	IMAG	MAG	PHASE
1	Z+	7	Z+	0.236E+00	5.004E-02	0.241E+00	12.0
2	Z+	7	Z+	0.617E+00	0.147E+00	0.634E+00	13.4
3	Z+	7	Z+	1.000E+00	-1.164E-09	1.000E+00	0.0
4	Z+	7	Z+	0.912E+00	0.114E+00	0.919E+00	7.1
5	Z+	7	Z+	-3.329E-03	-8.150E-03	8.803E-03	-112.2
6	Z+	7	Z+	-0.180E+00	3.974E-02	0.185E+00	167.6
7	Z+	7	Z+	-0.347E+00	0.538E+00	0.640E+00	122.8
8	Z+	7	Z+	-0.681E+00	0.194E+00	0.708E+00	164.1
9	Z+	7	Z+	-0.504E+00	0.484E+00	0.699E+00	136.1
10	Z+	7	Z+	-0.106E+00	0.647E+00	0.656E+00	99.3
11	Z+	7	Z+	-0.138E+00	1.830E-02	0.139E+00	172.5

TABLE 7.6

Measured Modal Parameters of the Geared Rotor

Mode 4 Resonance Frequency: 28.89Hz. Viscous Damping: 3.42%

Modal Mass: 5.39×10^{-5} Modal Stiffness: 1.78

RPM: 87

MEASURE PT	MEASURE DIR	DRIVING PT	DRIVING DIR	REAL	IMAG	MAG	PHASE
1	Z+	7	Z+	0.538E+00	2.210E-03	0.538E+00	0.2
2	Z+	7	Z+	0.869E+00	0.192E+00	0.889E+00	12.5
3	Z+	7	Z+	1.000E+00	7.078E-08	1.000E+00	0.0
4	Z+	7	Z+	0.894E+00	-0.216E+00	0.919E+00	-13.6
5	Z+	7	Z+	0.379E+00	0.101E+00	0.392E+00	14.9
6	Z+	7	Z+	0.219E+00	-0.583E+00	0.623E+00	-69.4
7	Z+	7	Z+	0.444E+00	-0.711E+00	0.838E+00	-58.0
8	Z+	7	Z+	0.617E+00	-0.447E+00	0.762E+00	-35.9
9	Z+	7	Z+	0.599E+00	-0.738E+00	0.951E+00	-51.0
10	Z+	7	Z+	0.456E+00	-0.501E+00	0.677E+00	-47.7
11	Z+	7	Z+	0.336E+00	-0.311E+00	0.458E+00	-42.7

the experimental response also occured close to the analytically predicted values. The magnitude of the flexural response did not compare well because the driving and driven side shafts were balanced separately.

Modal testing was carried out on the same Spur Geared setup using the Structural Analysis System. The frequency response functions were obtained. The natural frequencies were identified and curve fitting was employed to obtain the modal parameters.

In the next chapter, conclusions of this investigation are presented and recommendations for future work are suggested.

CHAPTER 8

Conclusions and Recommendations

The dynamic behaviour of a geared rotor systems with spur or helical gearing was studied in this thesis.

The torsional-flexural coupling in a spur geared rotor system was considered and ignoring the effects of backlash and the time variation in tooth stiffness, a linear model was obtained. The natural frequencies, mode shapes and dynamic response were obtained by modal analysis. The excitations originating from within the geared shaft system such as deterministic and random components of the static transmission error and external sources such as random support excitations were considered. The analytical results were compared with those obtained from experiments.

The helical geared shaft system was analysed first using a linear model considering the torsional-flexural-axial -rotational coupling but ignoring the backlash and time variation in tooth stiffness. The natural frequencies, mode shapes and dynamic response to internal and external excitations described earlier, were obtained by normal mode analysis. The fatigue life of the gear carrying shafts was also obtained. Next, a complicated model of the helical geared

shaft system considering the time varying tooth stiffness and backlash is considered. The excitations to the geared shaft system are considered due to a static transmission error having deterministic and filtered white noise components. Filtered white noise is obtained by passing white noise through a linear filter. The mean and variance of the dynamic response are obtained. The response is obtained by piecewise linearisation and the Matrix Exponential Technique. The stability of the helical geared shaft system is also discussed.

An improved mathematical model of spur and helical geared rotors was obtained by considering gear mesh effects in the form of motion coupling, varying mesh stiffness and backlash. Finite beam elements were used to discretise the rotor system which is convenient and a good engineering approximation. The excitation to the system was considered in the form of a static transmission error having deterministic and random components.

8.1 Conclusions

The conclusions arrived on the basis of the results of this investigation in the different chapters of the thesis are summarised and given below.

1. The model proposed in this investigation and employed in subsequent analysis gave sufficiently accurate results to justify the use of this model for geared rotor systems. This statement is supported with results of chapters 2,3,5,6,7 and compared with references [11,54,98].

2. The geared shaft system experiences resonance not only at the system natural frequency but also at the gear ratio multiples when there is mass unbalance or geometrical eccentricity in both the gears as seen in Fig. 2.5. Analytical predictions of this phenomenon have been confirmed by the experimental results (Fig. 7.9).

3. The random support excitations can result in significant response at the gear locations as can be seen from a comparison of Figs. 3.8 and 3.11 giving the responses due to a static transmission error and a nominal random support excitation.

4. The simulation study carried out at 2500 rpm confirms the predictions on stability behaviour of the rotor system using Floquet theory (Refer Chapters 5 and 6).

5. A comparison of the results between the responses obtained using a linear model with modal analysis and the more complex time variant, non-linear model using numerical simulation shows that a linear model provides results of the same order of magnitude as the complex model (Refer Figs. 3.8 and 5.4).

6. The fatigue analysis shows that for nominal excitation levels, the shaft is subjected to high fluctuating stress levels which is evident from the need to take a high factor of safety as predicted by the analysis (Refer Chapter 4).

7. The regions of instability in the operation of a helical geared shaft system decreases with the increase in damping and hence damping can be used to control the regions of instability (Refer Chapter 6).

8. The torsional component of vibration is the most important in the operation of a helical geared shaft system as can be verified from Table 5.3.

The model of the gear mesh considered in this study neglects the effect of dynamic coupling because it is non-linear and of the second order of geometric eccentricity [52]. However, for higher excitation frequencies such as multiples of tooth meshing frequency, the dynamic coupling

terms may prove important. The finite beam elements in the analysis (except Section 2.7) are non-rotating, and thus gyroscopic forces are neglected. Gyroscopic forces are skew-symmetric and their effect on the system is important, however they are neglected in order to carry out simplified normal mode analysis.

8.2 Recommendations for Future Work

The effect of dynamic coupling in rotors could be considered in addition to the force coupling already considered. The effect of variation in input torque and a more accurate model for backlash [21] could be considered. The analysis in this investigation considered the rotor mounted on rigid or flexible rolling element bearings. The dynamic response of geared rotors on fluid film bearings or squeeze film bearings could be carried out. The actual excitations coming from the supports on which the geared shaft system is mounted may be non stationary and an analysis could be carried out to include this effect. The transient vibration of geared rotors during startup could be studied. Dynamic tooth loads could be measured experimentally, using strain gauges and comparison with analytical results could be made. The torsional-flexural-axial-rotational coupling in helical gears influences dynamic behaviour of the rotor system (Chapter 3), and experiments could be carried out to validate these effects.

REFERENCES

1. Mitchell, L.D., and Daws, J.W., "A Basic Approach to Gearbox Noise Prediction", Transactions of the SAE, Vol. 91, 1983, pp. 3366-3379.

2. Bradley, W.A., "Sound Gear Quality", Mechanical Engineering, Oct. 1972, pp. 31-36.

3. Chakraborty, J., and Hunashikati, H.G., "Determination of the Combined Stiffness of a Spur Gear System", ASME paper No. 74-DET-39.

4. Lewis, W., "Investigation of the Strength of Gear Teeth", Proceedings of the Engineers Club, Philadelphia, 1893, pp. 16-23.

5. Buckingham, E., "Dynamic Loads on Gear Teeth", ASME Research Publication, N.Y., 1931.

6. Tuplin, W.A., "Gear Tooth Stresses at High Speed", Proceedings of the Institution of Mechanical Engineers, Vol. 163, 1950, pp. 162-167.

7. Tuplin, W.A., "Dynamic Loads on Gear Teeth", Proceedings of the Insitution of Mechanical Engineers, 1958, pp. 24-30.

8. Reswick, J.B., "Dynamic Loads on Spur and Helical Teeth", Transactions ASME, Vol. 77, 1955, pp. 635-644.

9. Johnson, D.C., and Bishop, R.E.D., "A Note on the Excitation of Vibrating Systems by Gearing Errors", Journal of the Royal Aeronautical Society, Vol. 59, 1955, pp. 434-435.

10. Johnson, D.C., Excitation of Resonant Vibration by Gear Tooth meshing effects", Proceedings of the International Conference on Gearing, Institution of Mechanical Engineers, London, 1958, pp. 18-23.

11. Mahalingam, S. and Bishop, R.E.D., "Dynamic Loading of Gear Teeth", Journal of Sound and Vibration, 1974, pp. 179-189.

12. Cornell, R.W., and Westervelt, W.W., "Dynamic Tooth Loads and Stressing for High Contact Ratio Spur Gears", Journal of Mechanical Design, Transactions ASME, Vol. 100, Jan. 1978, pp. 69-76.

13. Mark, W.D., "Analysis of the Vibratory Excitation of Gear Systems; Basic Theory", Journal of the Accoustical Society of America, 63(5), May 1978, pp. 1409-1430.

14. Mark, W.D., "Analysis of the Vibratory Excitation of Gear Systems. II: Tooth error representations, approximations and application", Journal of the Acoustical Society of America, Vol 66, No. 6, Dec. 1979, pp. 1758-1787.

15. Remmers, E.P., "Gear Mesh Excitation Spectra for Arbitrary Tooth Spacing Errors, Load and Design Contact Ratio", Journal of Mechanical Design, Transactions ASME, Vol. 100, Oct. 1978, pp. 715-722.

16. Tobe, T. and Sato, K., "Statistical Analysis of Dynamic Loads on Spur Gear Teeth", Bulletin of the JSME, Vol. 20, No. 145, July 1977, pp. 882-889.

17. Tobe, T., Sato, K., and Takatsu, N., "Statistical Analysis of Dynamic Loads on Spur Gear Teeth (Effect of Shaft Stiffness)", Bulletin of the JSME, Vol. 19, No. 133, July 1976, pp. 808-813.

18. Wang, C.C., "Rotational Vibration with backlash: Part 1", Journal of Mechanical Design, Transactions ASME, Vol. 100, April 1978, pp. 363-373.

19. Wang, C.C., "Rotational Vibration with Backlash: Part 2", Journal of Mechanical Design, Transactions ASME, Vol. 103, April 1981, pp. 387-397.

20. Dubowsky, S., "On Predicting the Dynamic Effects of Clearances in One-Dimensional Closed Loop Systems", Journal of Engineering for Industry, Transactions ASME, Feb. 1974, pp. 324-329.

21. Azar, R.C., and Crossley, F.R.E., "Digital Simulation of Impact Phenomenon in Spur Gear Systems", Journal of Engineering for Industry, Transactions ASME, Vol. 99, No. 3, 1977, pp. 792-798.

22. Wang, D.C.H., and Sun, Z.S., "A Rotary Model for Spur Gear Dynamics", ASME Paper No. 85-DET-2.

23. Nakada, T., and Utagawa, M., "The Dyanmic Loads on Gear caused by Varying Elasticity of the Mating Teeth", Proceesings of the Sixth Japan National Congress for Applied Mechanics, 1956, pp. 493-497.

24. Harris, S.L., "Dynamic Load on the Teeth of Spur Gears", Proceedings of the Institution of Mechanical Engineers, Vol 172, 1958, pp. 87-100.

25. Attia, A.Y., "Dynamic Loading of Spur Gear Teeth", Journal of Engineering for Industry, Transactions ASME, Vol. 81, No. 1, 1959, pp. 1-9.

26. Gregory, R.W., Harris, S.L., and Munro, R.G., "Dynamic Behaviour of Spur Gears", Proceedings of the Institution of Mechanical Engineers, Vol. 172, 1958, pp. 87-100.

27. Utagawa, M., and Harada, T., "Dynamic Loads on Spur Gear Teeth having Pitch Erros at High Speed", Bulletin of JSME, Vol. 5, No. 18, 1962, pp. 374-380.

28. Ichimam, K., and Hirano, F., "Dynamic Behaviour of Heavily-Loaded Spur Gears", Journal of Engineering for Industry, Transactions ASME, May 1974, pp. 373-381.

29. Kasuba, R., and Evans, J.W., "An Extended Model for Determining Dynamic Loads in Spur Gearing", Journal of Mechanical Design, Transactions ASME, Vol. 103, April 1981, pp. 398-409.

30. Tobe, T., and Takatsu, N., "Dynamic Loads on Spur Gear Teeth caused by Teeth Impact", Bulletin of the JSME, Vol. 16, No. 96, June 1973, pp. 1031-1037.

31. Jeffcott, H.H., "The Lateral Vibrations of Loaded Shafts in the Neighbourhood of a Whirling Speed - The Effect of want of Balance", Phil. Mag., Series 6, Vol. 37, 1919, pp. 304.

32. Prohl, M.A., "A General Method for Calculating Critical Speeds of Flexible Rotors", Journal of Applied Mechanics, Transactions ASME, Vol. 12, 1945, pp. A-142 to A-148.

33. Myklestad, N.O., "A New Method for Calculating Natural Modes of Uncoupled Bending Vibration of Airplane Wings and other Types of Beams", Journal of Aeronautical Science, April 1944, pp. 153-162.

34. Bishop, R.E.D., and Gladwell, G.M.L., "The Receptances of Uniform and Non-uniform Rotating Shafts", Journal of Mechanical Engineering Science, Vol. 1, No. 1, 1959, pp. 78-91.

35. Green, R.B., "Gyroscopic Effects on the Critical Speeds of Flexible Rotors", Journal of Applied Mechanics, Dec. 1948, pp. 369-376.

36. Eshleman, R.L., and Eubanks, R.A., "On the Critical Speeds of a Continuous Rotor", Journal of Engineering for Industry, Transactions ASME, 91 (4B), Nov. 1969, pp. 1180-1188.

37. Tondl, A., "Some Problems of Rotor Dynamics", Chapman Hall, London, 1965.

38. Gunter, E.J., Choy, K.C., and Allaire, P.E., "Modal Analysis of Turbo-Rotors Using Planar Modes Theory", Journal of the Franklin Institute, Vol. 305, No. 4, April 1978.

39. Ruhl, R.L., "Dynamics of Distributed Parameter Rotor System: Transfer Matrix and Finite Element Techniques", Ph.D. dissertation, Cornell University, 1970.

40. Ruhl, R.L., and Booker, J.F., "A Finite Element Model for Distributed Parameter Turborotor Systems", Journal of Engineering for Industry, Trans. ASME, Feb. 1972, pp. 128-132.

41. Nelson, H.D., and McVaugh, J.M., "The Dynamics of Rotor-Bearing Systems using Finite Elements" Journal Engineering for Industry, Trans. ASME, Vol. 98, No. 2, May 1976, pp. 593-600.

42. Zorzi, E.S. and Nelson, H.D., "Finite Element Simulation of Rotor-Bearing Systems with Internal Damping", Journal of Engineering for Power, Trans. ASME, Vol. 99, No. 1, Jan. 1977, pp. 71-76.

43. Nelson, H.D., "A Finite Rotating Shaft Element Using Timoshenko Beam Theory", Journal of Mechanical Design, Trans. ASME, Vol. 102, Oct. 1980, pp. 793-803.

44. Zorzi, E.S., and Nelson, H.D., "The Dynamics of Rotor-Bearing Systems with Axial Torque - A Finite Element Approach", Journal of Mechanical Design, Transactions ASME, Vol. 102, Jan 1980, pp. 158-161.

45. Johnson, D.C., "Modes and Frequencies of Shafts Coupled by Straight Spur Gears", Journal of Mechanical Engineering Science, Vol. 4, No. 3, 1962, pp. 241-250.

46. Porter, B., "Critical Speeds of Torsional Oscillation of Geared Shaft Systems due to the Presence of Displacement Excitation", Journal of Applied Mechanics, Transactions of the ASME, March 1964, pp. 25-28.

47. Sankar, S., "On The Torsional Vibration of Branched Systems Using Extended Transfer Matrix Method", Journal of Mechanical Design, Transactions ASME, Vol. 101, No. 4, Oct. 1979, pp. 546-553.

48. Mitchell, L.D., "A New Branching Technique for the Static and Dynamic Analysis of Geared Systems", I Mech E Conference Publications, "Vibrations in Rotating Machinery", C 256/80, 1980, pp. 37-42.

49. Seireg, A., "Whirling of Shafts in Geared Systems", Journal of Engineering for Industry, Transactions ASME, May 1967, pp. 278-284.

50. Mitchell, L.D., and Mellen, D.M., "Torsional-Lateral Coupling in a Geared High Speed Rotor System", ASME Paper No. 75-DET-75.

51. Lund, J.W., "Critical Speeds, Stability and Response of a Geared Train of Rotors", Journal of Mechanical Design, July 1978, Vol. 100, pp. 535-539.

52. Daws, J.W., "An Analytical Investigation of Three-Dimensional Vibration in Gear-Coupled Rotor Systems", Ph.D. Dissertation, Virginia Polytechnic and State University, 1979.

53. David, J.W., and Mitchell, L.D., "Linear Dynamic Coupling in Geared Rotor Sytstems", ASME Paper No. 85-DET-11.

54. Iida,H., Tamura, A., Kikuch, K. and Agata, H., "Coupled Torsional Flexural Vibration of a Shaft in a Geared System of Rotors", Bulletin of the JSME, Vol. 23, No. 186, December 1980, pp. 2111-2117.

55. Iwatsubo, T., Arii, S., Kawai, R., "Coupled Lateral-Torsional Vibration of Rotor System Trained by Gears", Bulletin of the JSME, Feb. 1984, pp. 271-277, (Part 1. Analysis by Transfer matrix method).

56. Iida, H., and Tamura, A., "Coupled Torsional-Flexural Vibration of a Shaft in a Geared System", I Mech E Conference Publications, "Vibrations in Rotating Machinery", C 272/84, 1984, pp. 67-72.

57. Iwatsubo, T., Arii, S., Kawai, R., "The Coupled Lateral Torsional Vibration of a Geared Rotor System", I Mech E Conference Publications, C 265/84, 1984, pp. 59-66.

58. Hamad, B., and Seireg, A., "Simulation of Whirl Interaction in Pinion-Gear Systems Supported on Oil Film Bearings", Journal of Engineering for Power, Transactions ASME, Vol. 102, April 1980, pp. 508-510.

59. Wang, S.M., "Analysis of Non-Linear Transient Motion of a Geared Torsional", Journal of Engineering for Industry, Transactions ASME, Feb. 1974, pp. 51-59.

60. Kacukay, F., "Dynamic Behavior of High Speed Gears", I Mech E Conference Publications, "Vibrations in Rotating Machinery", C305/84, 1984, pp. 81-90.

61. Kiyono, S., Aida, T., and Fujii, Y., "Vibration of Helical Gears, Part 1 - Theoretical Analysis", Bulletin of the JSME, Vol. 21, No. 155, May 1978.

62. Kiyono, S., Aida, T. and Fujii, Y., "Vibration of Helical Gears, Part 2 - Experimental Investigation", Bulletin of the JSME, Vol. 21, No. 155, May 1978.

63. Bolotin, V.V., "The Dynamic Stability of Elastic Systems", Holden-Day, San Francisco, 1964.

64. Benton, M., and Seireg, A., "Simulation of Resonances and Instability Conditions in Pinion-Gear Systems", Journal of Mechanical Design, Transactions ASME, Vol. 100, Jan. 1978, pp. 26-32.

65. Tordion, G.V., and Gauvin, R., "Dynamic Stability of a Two-Stage Gear Train Under the Influence of Variable Meshing Stiffness", Journal of Engineering for Industry, Transactions ASME, Aug. 1977, pp. 785-791.

66. Benton, M., and Seireg, A., "Factors Influencing Instability and Resonances in Geared Systems", Journal of Mechanical Design, Transactions ASME, Vol. 103, 1981, pp. 372-378.

67. Hsu, C.S., "On Approximating a General Linear Periodic System", Journal of Mathematical Analysis and Applications, Vol. 45, 1974, pp. 234-251.

68. Hsu, C.S., "Impulsive Parametric Excitations: Theory", Journal of Applied Mechanics, Transactions ASME, June 1972, pp. 551-558.

69. Lund, J.W., "Response Characteristics of a Rotor with Flexible Damped Supports", Symposium of International Union of Theoretical and Applied Mechanics, Lyngby, Aug. 12-16, 1974, pp. 319-349.

70. Tessarzik, J.M., Chiang, T., and Badgley, R.H., "The Response of Rotating Machinery to External Random Vibration", Journal of Engineering for Industry, Trans. ASME, Vol. 96, No. 2, May 1974, pp. 477-489.

71. Subbiah, R., Bhat, R.B. and Sankar, T.S., "Response of Rotors Subjected to Random Support Excitations", Journal of Vibration, Acoustics, Stress and Reliability in Design, Oct. 1985, Vol. 107, pp. 453-459.

72. Bahar, L.Y. and Sinha, A.K., "Matrix Exponential Approach to Dynamic Response", Computers and Structures, Vol. 5, 1975, pp. 159-165.

73. Wilson, E.L., "A Computer Program for the Dynamic Stress Analysis of Underground Structures", Report No. 68-1, University of California at Berkeley, Berkeley, California, 1969.

74. Maybeck, P.S., "Stochastic Models, Estimation and Control", Vol. I, Academic Press, N.Y., 1977.

75. Bagci, C., "Fatique Design of Machine Element", The Shock and Vibration Digest (State-of-the-art review article), Vol. 14, No. 5, May 1982, pp. 3-11.

76. Bagci, C., "Computer-Aided Fatigue Design of Power Transmisssion Shafts Using Three-Dimensional Finite Shaft Element and Updated Mean Stress Diagram", Journal of Mechanisms, Transmissions and Automation in Design, Transactions ASME, Paper No. 85-DET-23.

77. Klosterman, A.L., "On the Experimental Determination and Use of Modal Representations of Dynamic Characteristics", Ph.D. Dissertation, University of Cincinnati, 1971.

78. Neriya, S.V., Bhat, R.B. and Sankar, T.S., "Effect of Coupled Torsional-Flexural Vibration of a Geared Shaft System of the Dynamic Tooth Load", Shock and Vibration Bulletin, June 1984.

79. Neriya, S.V., Bhat, R.B. and Sankar, T.S., "Coupled Torsional Vibration of a Geared Shaft System Using Finite Element Analysis", Shock and Vibration Bulletin, June 1985.

80. Neriya, S.V., Bhat, R.B., and Sankar, T.S., "Vibration of a Geared Train of Rotors with Torsional-Flexural Coupling", presented at the ASME Design Engineering Conference, Cincinnati, Ohio, Sept. 1985, Paper, No. 85-DET-124.

81. Neriya, S.V., Bhat, R.B., and Sankar, T.S., "Vibration of a Helical Geared Shaft System", Proceedings of the Ninth Machinery Dynamics Seminar, Montreal, Canada, Oct. 1986.

82. Neriya, S.V., Bhat, R.B., and Sankar, T.S., "Dynamic Response of a Geared Train of Rotors subjected to Random Support Excitations", Shock and Vibration Bulletin, January, 1987.

83. Neriya, S.V., Bhat, R.B., Sankar, T.S., "Dynamic Tooth Load and Response in a Torsion-Flexure Coupled Geared Shaft System due to Random Static Transmission Error", paper under review for publication in the Journal of Sound and Vibration.

84. Neriya, S.V., Bhat, R.B., Sankar, T.S., "Dynamic Response of a Helical Geared Shaft System subjected to Random Support Excitations", accepted for presentation at the IFTOMM Conference to be held in Sevilla, Spain, Sept. 1987.

85. Neriya, S.V. Bhat, R.B., Sankar, T.S., "On the Dyanmic Response of a Helical Geared Shaft System subjected to a Static Transmission Error in the form of Deterministic and Filtered White Noise Inputs", sent to the ASME Vibrations Conference to be held in Boston, Mass., Sept. 1987.

86. Eshleman, R.L., "Critical Speeds and Response of Flexible Rotor Systems", Flexible Rotor-Bearing System Dynamics, ASME, Vol. 1, 1972.

87. Thorkildsen, T., "Solution of a Distributed Mass and Unbalanced Rotor System Using a Consistent Mass Matrix Approach", MSE Engineering Report, Arizona State University, June 1972.

88. Przemieniecki, J.S., "Theory of Matrix Structural Analysis", McGraw-Hill, 1968, pp. 71, 295.

89. Meirovitch, L., "A New Method of Solution of the Eigenvalue Problem for Gyroscopic Systems", AIAA Journal, Vol. 12, No. 10. Oct. 1974.

90. Gerber, W., "Bestimmung der Zulossigen Spannungen in Eisen constructionen", A. Bayer Arch. Ing. Ver., 6, 1874.

91. Goodman, J., "Mechanics Applied to Engineering", Vol. 1, 9th. ed., Longsmans Green, London, 1930.

92. Soderberg, C.R., "Working Stress", Journal of Applied Mechanics, Transactions ASME, Vol. 57, No. 1, 1935, pp. A-106.

93. Shigley, J.E., "Mechanical Engineering Design", McGraw-Hill, Second Edition, 1972.

94. LaSalle, J., and Lefochetz, S., "Stability by Liapunovs Direct Method", Academic Press, New York, 1961.

95. Takahashi, Y., Rabins, M.J., Auslander, D.M., "Control and Dynamic Systems", Addison-Wesley Publishing Company, 1970.

96. Ewins, D.J., "Modal Testing: Theory and Practice", Research Studies Press Ltd., 1984.

97. Mettler, E., "Stability and Vibration Problems of Mechanical System Under Harmonic Excitation", Proceedings of the International Conference on Dynamic Stability of Structures, ed., Hermann, G., Pergamon Press, 1967.

98. Arumugam, S.K., "Simulation and Analysis of Dynamic Loads on Cylindrical Gears and an Improved Method for Fatigue Damage Assessment", Ph.D. Thesis, Concordia University, 1986.

99. Samaha, M.A., "Dynamic Response and Optimisation of a Railroad Freight Car under Periodic and Stochastic Excitations", D.Eng. Thesis, Concordia University, 1978.

APPENDIX I

MATRIX [α]

$$[\alpha]_{7x7} = \begin{bmatrix} 0 & 1 & 0 & 0 & 0 & 0 & 0 \\ 0 & 0 & 0 & 1 & 0 & 0 & 0 \\ 1 & 0 & 0 & 0 & 0 & 0 & 0 \\ 0 & 0 & 0 & 0 & 1 & 0 & 0 \\ 0 & 0 & 1 & 0 & 0 & 0 & 0 \\ 0 & 0 & 0 & 0 & 0 & 1 & 0 \\ 0 & 0 & 0 & 0 & 0 & 0 & 1 \end{bmatrix}$$

APPENDIX II

MEAN AND ALTERNATING COMPONENTS OF FORCE

Force in the normal direction

$$F_n = F_{ns} + F_{nd}$$

where F_{ns} = mean component of F_n

$= T_m/r_1$

and F_{nd} = alternating component of F_n

$= |A| \sin(\Omega_r t + \phi)$

where $|A| = e_{av} \sqrt{(\bar{k}_t)^2 + (\bar{c}_t \Omega_r)^2}$

$$\phi = \tan^{-1}\left(\frac{\bar{c}_t \Omega_r}{\bar{k}_t}\right)$$

The component of F_n in the directions of $\{y_1, y_2, \theta_1, \theta_2, x_1, x_2, \phi_1, \phi_2\}$ are

$$\begin{Bmatrix} y_1 \\ y_2 \\ \theta_1 \\ \theta_2 \\ x_1 \\ x_2 \\ \phi_1 \\ \phi_2 \end{Bmatrix} \xrightarrow{F_n} \begin{Bmatrix} \cos\beta \\ \cos\beta \\ r_1 \cos\beta \\ r_2 \cos\beta \\ \sin\beta \\ \sin\beta \\ r_1 \sin\beta \\ r_2 \sin\beta \end{Bmatrix}$$

APPENDIX III

MATRICES AND VECTORS

1) $[K] = [K_1] + [K]$

$$[K_1] = \begin{bmatrix} k_{y1}/m_1 & & & & & & \\ & k_{y2}/m_2 & & & & & \\ & & k_{\theta 1}/I_1 & & & & \\ & & & k_{\theta 2}/I_2 & & & \\ & & & & k_{x1}/m_1 & & \\ & & & & & k_{x2}/m_2 & \\ & & & & & & 2k\phi_1/I_1 \\ & & & & & & & 2k\phi_2/I_2 \end{bmatrix}$$

$$[K_2] = k_t(t)\,[L]$$

$$[L] = \begin{bmatrix} A_1 & A_2 & A_1r_1 & A_1r_2 & A_2 & A_2 & A_2r_1 & A_2r_2 \\ & A_1 & A_1r_1 & A_1r_2 & A_2 & A_2 & A_2r_1 & A_2r_2 \\ & & A_1r_1^2 & A_1r_1r_2 & A_2r_1 & A_2r_1 & A_2r_1^2 & A_2r_1r_2 \\ & & & A_1r_2^2 & A_2r_2 & A_2r_2 & A_2r_1r_2 & A_2r_2^2 \\ & & & & A_3 & A_3 & A_3r_1 & A_3r_2 \\ & & & & & A_3 & A_3r_1 & A_3r_2 \\ & & & & & & A_3r_1^2 & A_3r_1r_2 \\ & & & & & & & A_3r_2^2 \end{bmatrix}$$

Symmetric

$$\times \text{ diag } (1/m_1,\ 1/m_2,\ 1/I_1,\ 1/I_2,\ 1/m_1,\ 1/m_2,\ 2/I_1,\ 2/I_2)$$

where

$$A_1 = \cos^2 \beta$$

$$A_2 = \cos \beta \sin \beta$$

$$A_3 = \sin^2 \beta$$

2) $[C] = [C_1] + [C_2]$

$$[C_1] = \text{diag } [c_{y1}/m_1,\ c_{y2}/m_2,\ c_{\theta 1}/I_1,\ c_{\theta 2}/I_2,\ c_{x1}/m_1,\ c_{x2}/m_2,\ 2c_{\phi 1}/I_1,\ 2c_{\phi 2}/I_2]$$

$$[C_2] = \bar{c}_t [L]$$

3) $$[A_1(t)] = \left[\begin{array}{c|c} 0 & I \\ \hline -K & -C \end{array}\right]$$

4) $[A_r(t)]_{16x2} = \left[\begin{array}{c|c} 0 & 0 \\ \hline k_t(t)\{P\} & \bar{c}_t\{p\} \end{array}\right]$ for $\delta_n + \varepsilon > 0$

$\delta_n + \varepsilon < -BL$

where $\{P\}_{8xI} = \{\cos \beta/m_1, \cos \beta/m_2,$

$r_1 \cos \beta/I_1, r_2 \cos \beta/I_2, \sin \beta/m_1,$

$\sin \beta/m_2, 2r_1 \sin \beta/I_1, 2 r_2 \sin \beta/I_2\}^T$

$[A_r(t)] = 0$ for $-BL < \delta_n + \varepsilon < 0$

5) $[A_f] = \begin{bmatrix} 0 & 1 \\ -a_2 & -a_1 \end{bmatrix}$

6) $\{B(t)\} = \{0, 0, 0, 0, 0, 0, 0, 0, \{f_d(t)\}\}^T$

where $\{f_d(t)\}_{8x1} = +[k_t(t)\, \varepsilon_d(t) + \bar{c}_t\, \dot{\varepsilon}_d(t)]\, \{P\}$

$+ \left\{\begin{array}{c} 0 \\ \hline T_M/I_1 \\ -T_L/I_2 \\ \hline 0 \end{array}\right\}$, $\delta_n + \varepsilon > 0$

$= [k_t(t)\, \delta_n + \bar{c}_t\, \dot{\delta}_n]\, \{P\} + \left\{\begin{array}{c} 0 \\ \hline T_M/I_1 \\ -T_L/I_2 \\ \hline 0 \end{array}\right\}$, for $-BL < \delta_n + \varepsilon < 0$

$= -[k_t(t)\, (\varepsilon_d(t) + BL) + \bar{c}_t\, \dot{\varepsilon}_d(t)]\, \{P\} +$

$\left\{\begin{array}{c} 0 \\ \hline T_M/I_1 \\ -T_L/I_2 \\ \hline 0 \end{array}\right\}$

for $\delta_n + \varepsilon < -BL$

7) $\{G(t)\} = \{0, 0, 0, \ldots 0, 1\}^T$

APPENDIX IV.

Refer Appendix III for [K] and [C]

$$[K_s]_{10x10} = [K] + [K_{s1}]$$

$[K_{s1}]$ is a matrix with all zero entries except

$$K_{s1}(3, 9) = -k_{\theta 1}/I_1$$
$$K_{s1}(4, 10) = -k_{\theta 2}/I_2$$
$$K_{s1}(9, 3) = -k_{\theta 1}/J_M$$
$$K_{s1}(10, 4) = -k_{\theta 2}/J_L$$

Similarly,

$$[C_s]_{10x10} = [C] + [C_{s1}]$$

$$[C_{s1}] = \text{diag}\ (0, 0, 0, 0, 0, 0, 0, 0, C_M/J_M, C_L/J_L).$$